
Nuclear topology during cellular differentiation in mouse

Alessandro Brero



München 2004

Nuclear topology during cellular differentiation in mouse

Alessandro Brero

Dissertation
an der Fakultät für Biologie
der Ludwig-Maximilians-Universität
München

vorgelegt von
Alessandro Brero
aus Turin

München, den 29.6.2004

Erstgutachter: Prof. Dr. Thomas Cremer

Zweitgutachter: Prof. Dr. Heinrich Leonhardt

Tag der mündlichen Prüfung: 15.9.2004

Danksagung

Zunächst möchte ich mich bei meinem Doktorvater Thomas Cremer bedanken, formal, für die Betreuung der Doktorarbeit und persönlich, für den Raum mich entwickeln zu können. (Ob das gelungen ist mag dahingestellt sein, der Raum war zumindest vorhanden). Darüber hinaus bin ich Thomas für das wissenschaftliche und menschliche Umfeld dankbar, das nicht nur motivierend war, sondern letzten Endes auch dazu beigetragen hat, das ich keine Minute der vergangenen Jahre als „Arbeit“ empfunden habe (was für mich als von Natur aus „arbeitsscheuen“ Menschen nicht unwichtig war).

Very big thanks go out to Cristina Cardoso. Without you and the time spent in your lab, my thesis would certainly not be the same. Thanks for the inspiring and motivating environment and help. And of course to all the co-workers in Berlin at the Max-Delbrück-Center, who helped me a lot to get my stuff done; especially to Hariharan Easwaran for going through the text and for helping me a lot when I was in Berlin.

Ein großer Dank geht auch an Heinrich Leonhardt, nicht nur für die Übernahme der Zweitkorrektur und die konkreten Tipps für die Doktorarbeit, sondern auch für das persönliche Engagement und die fruchtbaren Diskussionen.

Ein großes Dankeschön auch an Marion Cremer, für das Korrekturlesen des Manuskripts, das die Qualität des vorliegenden Textes nicht unwesentlich verbessert hat und für die vielen wissenschaftlichen Diskussionen und netten Gespräche am Rande.

Bei Steffen Dietzel und Robert Mayer möchte ich mich herzlich für das Bereitstellen der embryonalen Stammzellen und der Makrophagen bedanken und „latürnich“ für ihre nette und kollegiale Zusammenarbeit.

I am also very grateful to Irina Solovei, for being a scientific role model and for your effective solutions, whenever there were problems; you really helped a lot.

Bei Isabel Jentsch möchte ich mich herzlich für die Karyotypisierung meiner Mäuschen bedanken.

Johann von Hase danke ich für seine Geduld mir beim Verstehen der 3D-RRD Software behilflich zu sein.

Ein kollektives „Grazie“ an alle übrigen Mitarbeiter der AG Cremer, die zur einer wirklich phänomenalen Arbeitsatmosphäre beigetragen haben. Im Einzelnen waren dies:

Nandy (tolle Diplomarbeit und in jeder Hinsicht bewundernswert), Roy (Holland at its best), Stefan (der Lottokönig von Untergiesing), Michaela (langjährige „Leidensgenossin“), Lothar (Ex-Banknachbar und „ergiebig“ Diskussionspartner), Andi („der Maradona von Kirchtrudering“), Joachim (mein persönlicher Lieblingsphysiker), Babett (wenn Not am Mann ist kann sie eine Diplomarbeit an einem WE schreiben...), Kathrin Teller (widerlegt problemlos ein berüchtigtes *Science* Paper), Katrin Küpper (hervorragender Farbgeschmack, und bei vielen Fragen eine richtig gute Hilfe), Claudia Weierich (2.-beste Köchin nach Mama), Claudia Heppberger (hat ein Pferd!), Roman (für mich einer der besten Espressotrinker überhaupt), Heiner (viele richtig gute Diskussionen, aus dem wird noch was), Dorothee (wenn ich mal nen Arzt brauche bist du die erste Wahl, es sei denn du entscheidest dich für Proktologie...), Dani (die andere Hälfte der „Bovine-Research-Force“), Heidi (viele praktische Tipps für den Laboralltag) und viele andere die zwischendrin mal da waren und Diplomarbeit gemacht haben wie Simone, Shaban, Tina, Kourosh...

Ein grosses Dankeschön gilt meiner Familie, allen voran meine Eltern, die mich während der zugegebenemassen langen, nicht enden wollenden Zeit der Doktorarbeit moralisch („quando hai finalmente finito?“)¹ als auch finanziell („mi devi 54€“)¹ unterstützt haben. Danke, auch an meinen Bruder Massi seiner Frau Dorothee und den kleinen David, der, obwohl grade eingeschult, dank meines „schlechten“ Einflusses eine intensive Begeisterung für „Apoptose“ entwickelt hat.

Last but not least danke ich Simone Barwisch für den emotionalen („bist oiwei no net fertig“)¹ und wissenschaftlichen („des ist doch total uninteressant“)¹ Rückhalt, sowie, dass Sie es trotz meiner temporären Unausstehlichkeit dennoch mit mir ausgehalten hat.

¹ Zitate sind natürlich ironisch gemeint!!!

Contents

ZUSAMMENFASSUNG	- 1 -
SUMMARY	- 3 -
ABBREVIATIONS	- 5 -
1 INTRODUCTION	- 6 -
1.1 GOALS OF THE STUDY	- 6 -
1.2 DIFFERENTIATION	- 7 -
1.2.1 A BRIEF OVERVIEW	- 7 -
1.2.2 DIFFERENTIATION AND NUCLEAR TOPOLOGY	- 10 -
1.2.3 <i>IN VITRO</i> DIFFERENTIATION SYSTEMS EMPLOYED IN THE PRESENT THESIS	- 12 -
Myogenesis	- 12 -
ES cell differentiation to macrophages	- 15 -
1.3 CHROMOSOME TERRITORIES	- 18 -
1.3.1 RADIAL DISTRIBUTION	- 19 -
1.3.2 SIDE-BY-SIDE DISTRIBUTION	- 22 -
1.4 EUCHROMATIN-HETEROCHROMATIN	- 26 -
1.4.1 PAST TO PRESENT: A BRIEF LOOK ON THE HISTORY OF CHROMATIN	- 27 -
1.4.2 PROTEINS AND CHROMATIN	- 29 -
1.4.3 RNA AND CHROMATIN	- 37 -
1.4.4 DNA METHYLATION AND CHROMATIN	- 38 -
Overview	- 38 -
Evolutionary aspects	- 39 -
Enzymes	- 39 -
Functional implications	- 41 -
Modes of action	- 46 -
The methyl-CpG binding domain (MBD) protein family	- 46 -
1.4.5 MOUSE PERICENTRIC HETEROCHROMATIN	- 50 -
2 METHODS	- 54 -
2.1 CELL CULTURE	- 54 -
2.1.1 BASIC CELL CULTURE	- 54 -
2.1.2 CELL CULTURE ON GLASS COVERSLEPS	- 55 -
2.1.3 ISOLATION OF PERIPHERAL LYMPHOCYTES	- 56 -
2.1.4 DIFFERENTIATION	- 57 -
The myoblast/myotube system	- 57 -
The ES cell/macrophage system	- 58 -
2.2 PREPARATION OF METAPHASE CHROMOSOMES (2D-FIXATION)	- 59 -
2.3 3D-FIXATION	- 61 -
2.4 IMMUNOFLUORESCENCE	- 62 -
2.5 FLUORESCENCE IN SITU HYBRIDIZATION (FISH)	- 64 -
2.5.1 PROBE GENERATION/AMPLIFICATION	- 64 -
Mouse major satellite specific probe	- 64 -

Mouse chromosome paint probes	- 66 -
2.5.2 PROBE LABELING	- 67 -
Label-DOP-PCR [<i>chromosome painting probes</i>]	- 68 -
Nick translation (NT) [<i>major satellite probe</i>]	- 69 -
2.5.3 FISH SETUP	- 70 -
Probe precipitation:	- 70 -
Hybridization	- 71 -
2.5.4 DETECTION	- 72 -
2.6 BRDU-LABELING	- 73 -
2.7 TRANSFECTION OF CELLS	- 74 -
2.7.1 CA ₃ (PO ₄) ₂ -METHOD	- 75 -
2.7.2 POLYFECT®-METHOD (QIAGEN)	- 75 -
2.8 COMBINATION OF FISH WITH TRANSFECTED CELLS AND IMMUNOFLUORESCENCE	- 76 -
2.9 MICROSCOPY	- 78 -
2.9.1 EPIFLUORESCENT MICROSCOPY	- 78 -
2.9.2 CONFOCAL-LASER-SCANNING-MICROSCOPY	- 79 -
Fixed specimens	- 79 -
<i>In vivo</i> observation	- 80 -
2.10 IMAGE PROCESSING	- 82 -
2.10.1 DOCUMENTATION	- 82 -
2.10.2 PIXEL SHIFT CORRECTION	- 82 -
2.10.3 3D-RECONSTRUCTION	- 84 -
2.11 VISUAL EVALUATIONS	- 84 -
2.12 AUTOMATED EVALUATIONS	- 88 -
2.12.1 RADIAL DISTRIBUTION ANALYSIS USING THE SOFTWARE 3D-RRD	- 88 -
2.12.2 ANGLES AND DISTANCES BETWEEN INTENSITY GRAVITY CENTERS USING IMAGEJ	- 91 -
2.12.3 CORRELATION ANALYSIS OF MECP2 EXPRESSION AND CHROMOCENTER CLUSTERING	- 94 -
3 RESULTS	- 98 -
3.1 DISTRIBUTION OF GENE DENSE AND GENE POOR CHROMOSOMES IN DIFFERENT MOUSE CELL TYPES AND DURING DIFFERENTIATION	- 98 -
3.1.1 CHOICE OF AN APPROPRIATE CHROMOSOME PAIR	- 98 -
3.1.2 3D-FISH	- 99 -
3.1.3 RADIAL DISTRIBUTION OF #11 AND #X CTs USING THE SOFTWARE 3D-RRD	- 101 -
3.1.4 RADIAL DISTRIBUTION OF #11 AND #X CTs USING THE SOFTWARE IMAGE J	- 107 -
3.1.5 SIDE-BY-SIDE DISTRIBUTION OF #X AND #11	- 109 -
Homologous distances and angles for #11 CTs	- 110 -
Distances and angles between #11 and #X	- 113 -
3.1.6 SUMMARY PART 1	- 116 -
3.2 ORGANIZATION OF PERICENTRIC HETEROCHROMATIN (CHROMOCENTERS) IN DIFFERENT MOUSE CELL TYPES AND DURING TERMINAL DIFFERENTIATION	- 117 -
3.2.1 NUMBER OF CHROMOCENTERS	- 117 -
3.2.2 INTRANUCLEAR DISTRIBUTION	- 125 -
Intranuclear distribution of chromocenters	- 126 -
Intranuclear distribution of pericentric heterochromatin	- 129 -
3.2.3 SUMMARY PART 2	- 133 -
3.3 THE ROLE OF MECP2 IN THE REORGANIZATION OF PERICENTRIC HETEROCHROMATIN	- 133 -
3.3.1 EXPRESSION OF ENDOGENOUS MECP2 INCREASES DURING MYOGENESIS	- 134 -

3.3.2	CORRELATION OF MECP2 EXPRESSION AND INCREASED HETEROCHROMATIN CLUSTERING	- 136 -
3.3.3	EFFECTS OF MECP2 OVEREXPRESSION DURING MYOBLAST DIFFERENTIATION	- 138 -
3.3.4	RESULTS OF IN VIVO ANALYSIS OF MECP2-YFP TRANSFECTED CELLS	- 140 -
3.3.5	SUMMARY PART 3	- 146 -
4	DISCUSSION	- 147 -
4.1	DISTRIBUTION OF GENE DENSE AND GENE POOR CHROMOSOMES IN DIFFERENT MOUSE CELL TYPES AND DURING TERMINAL DIFFERENTIATION	- 147 -
4.1.1	RADIAL DISTRIBUTION OF #11 AND #X CTS	- 147 -
	Hypothetical mechanisms	- 150 -
	Functional aspects	- 155 -
	Evaluation methods	- 156 -
	Conclusions and outlook	- 159 -
4.1.2	SIDE-BY-SIDE DISTRIBUTION OF #11 AND #X CTS	- 159 -
4.2	THE NUCLEAR ORGANIZATION OF PERICENTRIC HETEROCHROMATIN IN DIFFERENT CELL TYPES AND DURING TERMINAL DIFFERENTIATION	- 162 -
4.2.1	INTRANUCLEAR DISTRIBUTION	- 162 -
4.2.2	CLUSTERING	- 168 -
4.3	CONCLUDING REMARKS AND PROSPECTS	- 175 -
5	APPENDIX	- 178 -
5.1	MATERIALS	- 178 -
5.1.1	CHEMICALS AND ENZYMES	- 178 -
5.1.2	MEDIA, BUFFERS AND SOLUTIONS	- 181 -
5.2	EQUIPMENT AND SOFTWARE	- 183 -
5.2.1	GLASS, PLASTIC WARE AND OTHER IMPLEMENTS	- 183 -
5.2.2	VARIOUS TECHNICAL EQUIPMENT	- 184 -
5.2.3	OPTICS	- 184 -
5.2.4	SOFTWARE	- 186 -
5.3	SUPPLEMENTARY TABLES	- 187 -
5.4	SUPPLEMENTARY CD	- 190 -
6	LITERATURE	- 191 -
7	PUBLICATIONS	- 205 -
8	CURRICULUM VITAE	- 206 -

Zusammenfassung

Das zentrale Thema der vorliegenden Doktorarbeit war die Untersuchung der Zellkerntopologie im Verlauf zellulärer Differenzierung. Zu diesem Zweck wurden mehrere Zellsysteme der Maus verwendet, die eine Untersuchung von Zelltypen unterschiedlichen Differenzierungsniveaus ermöglichten. Unter anderem wurden zwei *in vitro* Differenzierungssysteme benutzt. In dem einen wurden embryonale Stammzellen (ES Zellen) der Maus zu Makrophagen differenziert, während im zweiten Modellsystem eine muskelspezifische Differenzierung von Myoblasten induziert wurde; im Verlauf dieser *in vitro* „Myogenese“ fusionieren Myoblasten miteinander und bilden vielkernige Myotuben. Zusätzlich wurden Maus Fibroblasten und Lymphozyten untersucht, u.a. um die Ergebnisse mit bereits publizierten Resultaten von Studien an menschlichen Zellen vergleichen zu können. Zwei Teilaspekte der Zellkernorganisation wurden beleuchtet: i) die radiale Verteilung genreicher und genarmer Chromosomen und ii) die räumliche Anordnung zentromerischen Heterochromatins.

In humanen Zellen, sowie in Zellen höherer Primaten und vom Huhn konnte gezeigt werden, dass Chromosometerritorien (CTs) von genreichen und genarmen Chromosomen eine unterschiedliche radiale Anordnung im Interphasekern aufweisen: während genreiche Chromosomen eher zentral liegen, sind genarme Chromosomen tendenziell in der Kernperipherie zu finden. Die im Rahmen dieser Arbeit durchgeführte Untersuchung der radialen Anordnung des genreichen Mauschromosoms #11 und des genarmen #X sollte vor allen Dingen zwei Fragen beantworten: 1) Finden sich bei Mäusen ebenfalls Gendichte-abhängige radiale CT-Verteilungen? 2.) Ändern sich die Verteilungen der untersuchten CTs im Verlauf der Differenzierung?

CTs in Interphasekernen wurden mittels Fluoreszenz *in situ* Hybridisierung (FISH) unter Verwendung chromosomenspezifischer Sonden visualisiert. Ihre radiale Verteilung wurde quantitativ mit Hilfe einer Computer-gestützten Auswertung bestimmt. Das genreiche Chromosom 11 zeigte eindeutig eine zentralere Lage als das genarme Chromosom X, das weiter zum Zellkernrand ausgerichtet war. Somit konnten die Ergebnisse bei Mensch, Primaten und Huhn auch bei der Maus bestätigt werden. Es fanden sich keine Hinweise für eine Veränderung dieser Verteilungen in Abhängigkeit zellulärer Differenzierung. Stattdessen schien das Ausmaß, wie stark die Verteilung von #11 von der von #X abwich mit der Zellkernform in den jeweiligen Zelltypen zu variieren. Zelltypen mit runderen Zellkernen wie Lymphozyten oder ES Zellen zeigten einen größeren Unterschied zwischen den beiden Verteilungen, als Myoblasten oder Makrophagen, die einen flacheren Zellkern aufwiesen. Eine entsprechende Beobachtung wurde bereits bei menschlichen Zellen beschrieben. Die Abstände, sowie die Winkel zwischen den Schwerpunkten homologer und heterologer Chromosomen sprachen ferner gegen eine Homologenassoziation der Chromosomen 11, als auch gegen jede andere Form einer deterministischen, nicht-zufälligen Anordnung homologer und heterologer CTs zueinander.

Es gab mehrere Gründe, die dafür sprachen perizentrisches Heterochromatin als Untersuchungsobjekt für die vorliegende Fragestellung zu verwenden. Zum einen umfasst es mit ~10% einen großen Teil des Mausgenoms. Ferner wurde des Öfteren und in unterschiedlichen Spezies gezeigt, dass es als epigenetischer Faktor an transkriptionellen „silencing“-Phänomenen beteiligt ist. Und schließlich wurde bereits in einigen Arbeiten über ein dynamisches Verhalten von perizentrischem Heterochromatin im Verlauf von Differenzierungsprozessen berichtet. Perizentrisches Heterochromatin, das aus vielen in Reihe angeordneten sog. „Major satellite“-Sequenzen besteht wurde mittels FISH über eine Satelliten-sequenzspezifische Sonde dargestellt. Perizentrisches Heterochromatin einzelner Chromosomen hat die Tendenz sich im Interphasekern zu größeren Aggregaten, den so genannten Chromozentren zusammenzulagern.

Im Rahmen der vorliegenden Arbeit konnte gezeigt werden, dass Anzahl und Größe der Chromozentren zelltypspezifische Unterschiede aufweisen und dass im Verlauf terminaler Differenzierung die Anzahl der Chromozentren signifikant abnimmt, während die Größe der Heterochromatin-Cluster entsprechend zunimmt. In Anbetracht der Tatsache, dass eine ähnliche Zusammenlagerung zentromerischer Regionen in differenzierenden Zellen der Ratte und des Menschen beobachtet wurde (Chaly and Munro 1996; Beil et al. 2002), liegt die Vermutung nahe, dass die Verringerung der Cluster-Anzahl bzw. ihre Vergrößerung eine charakteristische Eigenschaft terminal differenzierter Zellen darstellt. Die Mehrzahl der Chromozentren stand unmittelbar in Kontakt mit der Zellkernperipherie, während ein kleinerer, variabler Anteil Kontakt zu einem oder mehreren Nukleoli hatte. Nur ein sehr kleiner Anteil befand sich im so genannten „internen Zellkernkompartiment“, also ohne Verbindung zur Kernperipherie oder einem Nukleolus. Eine quantitative Auswertung zur Ermittlung der radialen Verteilung ergab, dass perizentrisches Heterochromatin in Lymphozyten am periphersten angeordnet ist, gefolgt von ES Zellen. In den übrigen Zelltypen waren die Verteilungen ähnlich und mehr zur Zellkernmitte orientiert. Da perizentrisches Heterochromatin charakteristischerweise eine hohe Anzahl an methylierten Cytosinen aufweist (Miller et al. 1974) und beschrieben wurde, dass die Konzentration des an methyliertem Cytosin bindenden Proteins MeCP2 dort erhöht ist (Lewis et al. 1992), bot es sich an zu untersuchen, ob und inwieweit sich beide Parameter im Verlauf der Differenzierung ändern. Beide Parameter wurden mittels Immunfluoreszenz bestimmt. Während der terminalen Differenzierung von Myoblasten zu Myotuben konnte sowohl eine verstärkte DNA-Methylierung in der perizentrischen Region als auch eine verstärkte Expression von MeCP2 beobachtet werden. Mittels transient transfizierter Myoblasten, die eine fluoreszente Version von MeCP2 (MeCP2-YFP) exprimierten, konnte ferner gezeigt werden, dass die Aggregation von perizentrischem Heterochromatin artifiziell, also ohne Differenzierung, nur durch Überexpression von MeCP2 induzierbar ist. Dieses Ergebnis legt den Schluss nahe, dass MeCP2 ursächlich am verstärkten Zusammenlagern perizentrischen Heterochromatins während der terminalen Differenzierung beteiligt ist. Eine Lebendzell-Beobachtung MeCP2-YFP exprimierender Myoblasten ergab ferner, dass das Fusionieren der Heterochromatincluster während der gesamten Interphase stattfindet (G1, S und G2).

Im Rahmen der vorliegenden Doktorarbeit konnte somit sowohl Kontinuität als auch Dynamik in der Zellkerntopologie während zellulärer Differenzierung nachgewiesen werden. Mit der Gendichte-abhängigen Verteilung der CTs 11 und X, zeigte sich ein stabiles Verteilungsmuster, das trotz Differenzierung erhalten blieb und im Kontext äquivalenter Ergebnisse in anderen Spezies für ein evolutionär konserviertes Verteilungsmuster spricht. Mit dem Phänomen der Aggregation perizentrischen Heterochromatins konnte andererseits eine dynamische Reorganisation von Chromatin nachgewiesen werden, die gerichtet und reproduzierbar mit terminaler Differenzierung einherging. In Anbetracht des epigenetischen Potentials von perizentrischem Heterochromatin (Fisher and Merckenschlager 2002) erscheint ein funktioneller Zusammenhang zwischen dessen topologischer Reorganisation und dem Differenzierungsprozess wahrscheinlich. Die Identifizierung von MeCP2 als ein Schlüsselfaktor bei der Aggregation von perizentrischem Heterochromatin während der Differenzierung bietet zudem neue experimentelle Ansatzpunkte um nach einem funktionellen Zusammenhang zwischen Zellkernarchitektur und Differenzierung und Entwicklung zu suchen.

Summary

The purpose of the present thesis was to investigate nuclear topology during cellular differentiation. Several mouse cell cultures were analyzed including cell types representing distinct differentiation stages. I utilized two *in vitro* differentiation systems, one where embryonic stem (ES) cells were induced to terminally differentiate to macrophages, while in the second, cultured myoblasts were differentiated to myotubes; during this *in vitro* myogenesis myoblasts fuse and generate polynucleated syncytial myotubes. Additionally I investigated mouse fibroblasts and lymphocytes, in order to compare my results with published data on human cells. Two aspects of nuclear organization were highlighted: i) the radial distribution of gene dense and gene poor chromosomes and ii) the organization of pericentric heterochromatin.

Chromosome territories (CTs) of gene dense and gene poor chromosomes have been shown to distribute differentially in interphase nuclei of various species including man (Croft et al. 1999), higher primates (Tanabe et al. 2002) and chicken (Habermann et al. 2001); while gene dense chromosomes are found more centrally, gene poor chromosomes have the tendency to lie more at the nuclear periphery. By analyzing the radial distribution of gene dense mouse chromosome 11 and gene poor chromosome X I sought to answer two main questions: 1.) Is there the gene density related radial distribution of CTs conserved in mouse? 2.) Does the radial distribution of these CTs change upon differentiation?

These questions were answered using a fluorescence *in situ* hybridization (FISH) approach with chromosome-specific probes visualizing complete CTs and a quantitative evaluation software. Gene dense #11 CTs were found more towards the nuclear center, while gene poor #X CTs were distributed more at the periphery. Thus, the results in human, primates and chicken could be confirmed in mouse. Moreover, no indications for a differentiation-dependent change in the distribution of the analyzed chromosomes were found. Instead, the degree of difference between the radial distributions of #11 and #X appeared to vary substantially between cell types according to the nuclear shape. Cell types like lymphocytes or ES cells where the nucleus had a more spherical shape showed a clearer difference between both CT distributions than those with a flat shaped nucleus like myoblasts or macrophages, which is consistent with observations in human cells. According to interhomolog and -heterolog distances and angles between CT gravity centers, there was no evidence for a homologous association of #11 CTs as well as for any other kind of a non-random, deterministic side-by-side distribution of #11 and #X CTs.

Pericentric heterochromatin appeared as a suited object of investigation for the present thesis for several reasons. First, comprising ~10% of the mouse genome it represents a substantial part of chromatin in the nucleus. Secondly, it has been reported to convey transcriptional silencing as an epigenetic modifier of transcriptional activity in several species and finally various reports have described a dynamic behavior of pericentric heterochromatin during differentiation. Pericentric heterochromatin, which consists of tandem repeats of the so-called major satellite sequence was visualized by FISH with a satellite specific probe. Pericentric heterochromatin of individual chromosomes tends to aggregate in the interphase nucleus building so-called chromocenters. In the present thesis, I could show that the number and size of chromocenters is cell type specific and that the number of pericentric heterochromatin cluster is significantly reduced during terminal differentiation, concomitantly with an increase of chromocenter size. Considering data on centromere clustering in differentiating rat and human cells (Chaly and Munro 1996; Beil et al. 2002) the present findings suggest that the reduction in number and the increase in size of pericentric heterochromatin cluster is a hallmark of terminally differentiated cells. The analysis of the intranuclear distribution of chromocenters revealed that the majority of chromocenters is abutting the nuclear pe-

riphery, with a variable intermediate fraction contacting one or more nucleoli. Only a very small fraction resided in the so-called interior nuclear compartment, i.e. without contacts to both the periphery and a nucleolus. A quantitative analysis of the radial distribution of pericentric heterochromatin in the various cell types revealed a significantly more peripheral location in lymphocytes, followed by ES cells, while in all other analyzed cell types the distribution was similar and more internal.

Since pericentric heterochromatin is characterized by an intense methylation of cytosines (Miller et al. 1974) and was described to be enriched for the **methyl-CpG binding protein** MeCP2 (Lewis et al. 1992), I was interested whether levels of DNA methylation and of endogenous MeCP2 would change during differentiation. Both parameters were determined using an immunofluorescence approach. In both cases, I found a substantial increase during terminal differentiation of myoblasts to myotubes. Using a transient transfection strategy with a fluorescently tagged MeCP2 derivative (MeCP2-YFP), I could moreover show that the increased clustering of pericentric heterochromatin could be artificially induced in myoblast in the absence of differentiation by overexpression of MeCP2. This result strongly suggests that MeCP2 is causally involved in the phenomenon of pericentric heterochromatin clustering during terminal differentiation. *In vivo* time-lapse analysis of MeCP2-YFP transfected myoblasts revealed that fusion of chromocenters occurs during all interphase stages (G1, S and G2).

In conclusion, the present thesis revealed both, continuity and dynamics of nuclear topology during cellular differentiation. On the one hand, the gene-density-related radial distribution of #11 and #X CTs represented a stable organizational motif that remained unaffected by cellular differentiation. In fact, this finding corroborates the idea of an evolutionary conserved distribution pattern of CTs. On the other hand, the clustering of pericentric heterochromatin during terminal differentiation denoted a dynamic and reproducible reorganization that, considering the epigenetic potential of pericentric heterochromatin, is likely to be of functional importance for cellular differentiation. The identification of MeCP2 as a key player in the clustering process of pericentric heterochromatin offers new starting points for investigating the functional relevance of nuclear architecture during differentiation and development.

Abbreviations

'	Minutes
"	Seconds
°C	Degree Centigrade
3D-RRD	Three dimensional relative radial distance (software for distribution analysis)
BSA	Bovine serum albumine
CLSM	Confocal laser scanning microscope
cm	centimeter
CT	Chromosome territory
DNP	Dinitrophenyl-group
ES cell	Embryonic stem cell
EtOH	Ethanol
gARR	Global average relative radius = average distance of a segmented fluorescence object over a whole set of nuclei
GC	Fluorescence intensity gravity center
h	hours
HDAC	Histone deacetylase
HEBS	HEPES Buffered Saline
HMT	Histone methyltransferase
iARR	Individual average relative radius = average distance of a segmented fluorescence object within an individual nucleus
KS	Kolmogoroff Smirnov
NE	Nuclear envelope
PBS	Phosphate buffered saline
PEV	Position effect variegation
rpm	Rounds per minute
RT	Room temperature
RTT	Rett syndrome
SSC	Sodium chloride sodium citrate
WCP	Whole chromosome painting (probe)

1 Introduction

1.1 Goals of the study

The main purpose of the present thesis was to investigate nuclear architecture in the light of cellular differentiation. The reason for choosing differentiation as an experimental system was that one could expect large-scale changes on a transcriptional level responsible for commitment, cell cycle exit and finally for establishment of the cell type specific function. Consequently detecting a reorganization of the higher order chromatin arrangement correlating with these major transcriptional changes during differentiation would be helpful to detect topological principles that might have functional implications in terms of an epigenetic modification of expression profiles. Yet, I was not only interested in a reorganization of chromatin during differentiation, but also in stable distributional motifs, i.e. in arrangements that would remain unchanged in spite of extensive modifications of transcriptional programs. Such stable arrangements of chromatin present in different cell types independent of cellular commitment and specialization could define a basic nuclear order essential for proper nuclear functions *per se*.

As objects of investigation, I have chosen several different mouse cell types exhibiting very distinct cellular functions. Lymphocytes and fibroblasts were used as there was already substantial data available for human cells with which the obtained results could have been compared in order to address questions concerning the evolutionary conservation of nuclear topology. Moreover, I have employed two different mouse *in vitro* differentiation systems including embryonic stem cells differentiating to macrophages as well as myoblasts to myotubes. A big advantage of such differentiation systems is that that differentiated cells can be compared with their actual precursors, avoiding possible artifacts that can arise if different cell lineages are compared with each other that might substantially deviate in important characteristics such as karyotype, gender, genetic background of the donor animal etc.

Choosing mouse as experimental system offered the advantage that embryonic stem cells could be analyzed, while concomitantly many different DNA probes and antibodies were available, including a complete set of whole chromosome painting probes (WCP) for the mouse chromosome complement, which could be used to visualize specifically entire chromosome territories. Moreover, there is vast amount of database-information available including DNA sequences. Finally, many studies on nuclear architecture and chromatin organization have been performed in mouse, which provided the opportunity to compare and relate obtained results with data from the literature.

The nucleus consists of many structural and/or functional subcompartments, which define "nuclear architecture" by their relative and/or absolute spatial arrangement. Because nuclear architecture as a whole, with all its facets can certainly not be analyzed within the limited time-frame of a PhD thesis I focused on the topology of two important subcompartments: (1) chromosome territories and (2) pericentric heterochromatin. (1) Chromosome territories (CTs) are the coherent spatial entities made up by chromatin belonging to one specific chromosome. In humans (Croft et al. 1999), chicken (Habermann et al. 2001) and higher primates (Tanabe et al. 2002) it has been shown that CTs are distributed radially in a non-random fashion with gene dense chromosomes located in the interior, and gene poor at the periphery. One goal of this study was to test whether this differential radial distribution is conserved in mouse, and whether the distribution is affected during differentiation. (2) Pericentric heterochromatin has long been known to convey transcriptional silencing, as originally revealed by eye-color variegating phenotypes in the fruit fly *Drosophila melanogaster*, a phenomenon known as position effect variegation (PEV) (reviewed in e.g. (Schotta et al. 2003)). Since its involvement in epigenetic silencing was also shown for mammalian cells (reviewed in e.g. (Fisher and Merckenschlager 2002)), it appeared conceiv-

able that its topology might play a role in resetting transcriptional programs during differentiation, which was decisive to include it as object of investigation in the present thesis.

In the following three chapters, I want to introduce the three main topics that were central for this work. (1) I will try to outline some relevant aspects of cellular differentiation and present the differentiation systems that have been utilized. (2) Next, I will summarize some current opinions concerning the topology of CTs, and finally (3) I will try to sketch the current view concerning the characterization of chromatin according to modifications of its DNA and protein constituents.

1.2 Differentiation

1.2.1 A brief overview

The term **differentiation** is used on the one hand to describe the diversification of pathways during embryonic development, whereas on a single-cell level it is used describing the process of cell “maturation” (Muller 1999). In any case, it defines the process that leads to cellular specialization. During evolution, differentiation has proven as a successful strategy of multicellular organisms to develop specialized functions, be it on a cellular level as producing gametes or on a multicellular scale building tissues and organs. Differentiation in multicellular organisms can be very simple comprising only two different cell types, as in some green algae and slime molds (citations in (Schlichting 2003)) but can reach up to 200 different cell types as in vertebrates (Slack 2001). Although differentiation is thought to be intimately correlated with the evolution of multicellularity, important driving mechanisms as plasticity of gene expression are already present in unicellular organisms (Schlichting 2003). Yeasts and bacteria for example are able to react to changing environmental conditions by altering their transcriptional programs, which represents a mode of adaptation that can even be accompanied by morphological changes; the fungus *Candida albicans* for instance has two modes of growths a round budding growth and hyphal one depending on environmental conditions (Schlichting 2003). The fixation of originally plastic/dynamic transcription programs within a group of cell of a multicellular organism could have been a driving force in the evolution of organisms with differentiated cell types (Schlichting 2003). However, the reason(s) and the exact mode for the evolution of differentiation are still obscure. In any case the utilization of differentiation as a basic principle in the construction plan of multicellular organisms must have represented a decisive selective advantage, considering that so many extant organisms are making use of it.

The first step for an omnipotent cell on its track to differentiation is developmental **commitment**. This only vaguely defined term is usually used to describe cells or embryonic tissue that becomes restricted in its developmental fate. A comprehensive description of this topic can be found in “Essential Developmental Biology” by Jonathan Slack: Commitment to a specific differentiation pathway is defined by the expression of a certain combination of developmentally relevant genes. Historically commitment was explained by two operational definitions: **specification** and **determination**. Embryonic cells or tissues were termed to be “**specified**” to a specific structure if they were able to autonomously develop into that structure if explanted from the embryo, i.e. lacking their positional context. Cells or tissues were defined as irreversibly committed or **determined** if they differentiated to preset structures even if they were artificially placed in a completely different context within the developing embryo. Experimentally this was demonstrated in grafting experiments where embryonic tissue with a known and predictable fate was transplanted from its “normal” position within the embryo, to another, where it still developed into the determined structure irrespective of the altered cellular surrounding ((Slack 2001) p.63-64). Due to the lack of a stringently defined terminology, the term “commitment” is sometimes also used to describe a state of “terminal

determination”, i.e. a “...*final, irreversible programming of a particular cell type. ...*” (Muller 1999).

An end point of differentiation is reached when a certain profile of expressed genes conveying a cell's specific function is no longer subdued to large-scale changes, which is also often correlated with a characteristic morphological shape. Often, yet not always such a terminal differentiation state is accompanied by a loss of proliferation capacity, a state that is termed **postmitotic**. This “end point” is referred to as **terminal differentiation** and it implies that the cell fate is irreversibly fixed, i.e. the cellular function cannot be changed any more. However, the absoluteness of the term “terminal” is actually misleading, as there are many examples for a **de-differentiation** and/or **trans-differentiation** of cells, where “terminally” differentiated cells can actually lose characteristic features of the differentiated state and switch to a distinct cell type with its according expression profile. A well-known “naturally” occurring example is the regeneration capacity of urodele amphibians, which upon injury are able to re-build limb structures. After amputation cells at the cut extremity actively dedifferentiate, proliferate building the so-called regeneration blastema, which includes pluripotent precursor cells, which finally redifferentiate again, thereby rebuilding a completely functional new limb. In an *in vitro* approach, McGann et al. have recently shown a similar potential for mammalian myotubes as a reaction to incubation with newt regeneration extracts (McGann et al. 2001). Similar to the situation in newts myotube nuclei showed cell cycle reentry as revealed by BrdU incorporation, a nucleotide analog that is incorporated into the DNA of cells in S-phase. Cell cycle reentry had previously been shown to be inducible in mammalian myotubes by expression of the large T antigen from the SV40 virus (Lujvidin et al. 1990) and by myoseverin, a microtubule binding protein (Rosania et al. 2000). Both treatments of myotubes with newt regeneration extract and with myoseverin caused fission of polynucleated mouse myotubes, generating mononucleated single cells that were capable to proliferate. These experiments clearly showed that even in mammals terminal differentiation does not necessarily mean that the cells are ultimately incapable to react to cues that might deeply affect its fate and make it change its function. Moreover, there is an ongoing discussion concerning trans-differentiation of adult stem cells in mammals, although the existence of such adult stem cell plasticity is still heavily debated (reviewed e.g. in (Camargo et al. 2004)).

Finally it should be noted that plant cells behave differently as compared to animal cells as somatic differentiated cells apparently retain their totipotency as under favorable conditions even a single explanted cell is able to rebuild a complete new organism ((Wolpert et al. 1999), p 243-244).

Developmental potency and the mechanism of differentiation in animal cells has been a focus of embryology from the late 19th century onwards (reviewed e.g. in (Wilmot et al. 2000)). An initial hypothesis was brought up by Roux and Weismann, who proposed that upon cellular differentiation the genome of cells would be changed in such a way that only those portions would be retained that were essential for the respective cell function, i.e. that substantial parts that were not needed for a specific cell type would be physically lost¹. Consequently, any differentiation would be inevitably connected with a loss of totipotency. By destroying one of two cells of an early frog embryo with a hot needle Roux showed that totipotency was indeed lost from the two cell stage onwards, as his manipulated embryo developed only to one half. It were the groundbreaking experiments of Driesch on sea urchin and Spemann using salamander that contradicted Roux's results, as they showed that individualized cells of 4

¹ It should be noted that at that time the chemical basis of genes was still not known. In fact, the chromosome theory of heredity had still not been established; this theory proposed and propagated mainly by Boveri and Sutton finally linked phenotypes and the factors described by Mendel with chromosomes.

and 2 cell stages respectively retained the potential to develop into complete organisms. Apparently the remnants of the destroyed blastomere in Roux's embryo had handicapped the actually totipotent sister cell to develop the second half of the organism. In following studies Loeb and Spemann showed that totipotency in sea urchins and salamander was actually retained until the 16 cell stage (Wilmut et al. 2000). In the light of these early embryologic studies, the first nuclear transfer experiments came into play in order to enlighten the question on the totipotency of differentiated nuclei. This sort of experiments, that was already proposed by Spemann himself finally culminated in the end of the 20th century in the generation of mammalian clones obtained from transferring nuclei of terminally differentiated cells into enucleated oocytes. Briggs and King in the 50s of the 20th century were the first who generated living tadpoles from enucleated *Rana pipiens* oocytes in which they had transferred nuclei from a blastula stage (8 000-16 000 cells) by micromanipulation (Briggs and King 1952). Using cells from the intestinal epithelium of *Xenopus* tadpoles Gurdon and Uehlinger went even a step further in respect to the differentiation state of the donor cell used for the nuclear transfer (Gurdon and Uehlinger 1966). They could show that such transferred nuclei were able to sustain the development of adult frogs. In sheep Wilmut and Campbell finally could prove that actually nuclei of even terminally differentiated cells, as mammary gland cells were able to govern embryonic development to term, i.e. to a viable organism (Wilmut et al. 1997). Moreover, their results showed that the principle of nuclear totipotency was also valid for mammals. Recently it has been shown that nuclei of neurons as the prime example of a terminally differentiated cell type are likewise capable to support embryonic development after NT (Eggan et al. 2004). Although this progression of experiments convincingly shows that nuclei do not lose their totipotent capacity during differentiation, the usually very low success rate of nuclear transfer experiments to create viable offspring indicates that the modification of the donor nucleus via cytoplasmic factors of the oocyte is a complex and difficult process. Indeed once a nucleus is transferred, the complete set of genes that was previously used to define the donor's cell fate and function has to be reset, expressing a repertoire of genes necessary for embryonic development. Establishing, maintaining and eventually changing complete expression profiles of cells is thought to be governed by so-called epigenetic mechanisms. Such mechanisms are thought to be responsible for the distinct heritable identities of cells belonging to different lineages in one organism although they actually possess the same material on the genetic/sequence level, hence the term epi-(=above/outside) genetic. Epigenetic mechanisms have been described to act by very different means, and an exhaustive definition of the phenomenon has still to be reached. Some of these mechanisms have been shown to act on the chromatin level by methylation of DNA or of chromatin constituents like the core histones or even by the composition of histone variants and non-histone proteins (described in detail in 1.4). Other epigenetic mechanisms have been proposed to act on a more global, topological scale as through the specific position of genes within the nucleus relative to functional nuclear subcompartment as nucleoli, heterochromatin, splicing compartments etc. (reviewed e.g. in (Cremer and Cremer 2001; Fisher and Merckenschlager 2002; Spector 2003)). It is exactly this resetting or **reprogramming** of the epigenetic state of a differentiated donor cell that appears to be one of the major difficulties of cloning by nuclear transfer. An "erasure" of epigenetic marks, which might conflict with the correct spatio-temporal expression of developmentally relevant genes, should happen before the embryonic genome is activated, i.e. before embryonic gene expression has to take over the coordination of further development. In different species, this happens at different stages (Shi et al. 2003). The difference in time available for reprogramming could be one reason for the varying success rates in cloning of different animals. In bovine for example, where genome activation happens at the 8-16 cell stage, the generation of viable offspring is much higher than in mouse cells, where embryonic transcriptions starts already at the 2 cell stage (Shi et al. 2003), where consequently the time for a successful reprogramming is substantially less.

The increasing commitment of a cell by epigenetic means might also explain the generally reduced developmental potential of differentiated cells if used as nuclear donors as compared to less committed cells like embryonic stem cells or blastomeres.

In terms of evolution of differentiation epigenetic mechanisms are hypothesized to have played a role in the “fixation” of a given transcriptional program by which the primarily plastic or reversible response of cells engaged in an early multicellular organisms might have been restricted or canalized, thereby giving rise to a constitutive and therefore differentiated cell type (Schlichting 2003).

Besides having a fundamental impact for basic research, a detailed understanding of cellular differentiation represents an important prerequisite for many clinical applications like cell replacement therapies. Such approaches, as far away they might yet appear, imply the possibility to alleviate degenerative diseases like muscular dystrophies or such that are caused by loss of neuronal cells like Parkinson’s Disease. Important questions en route to such applications are: (1) How can embryonic stem cells effectively be brought to differentiate along specific pathways? (2) How big is the risk of tumor formation, once stem cells are grafted into a recipient? (3) Which kind of adult stem cells are suited for cell transplantations? (4) Are there possibilities of retrodifferentiation and/or transdifferentiation of endogenous cells that could replace such that were lost in the course of a disease? Increasing the knowledge on cellular differentiation will hopefully open new opportunities to bring this clinical potential forward but will also help to discriminate between realistic and legitimate chances and unrealistic “salvation promises”.

1.2.2 Differentiation and nuclear topology

An important question of developmental biology is how cell identity is maintained. The constancy of transcriptional programs is crucial for terminally differentiated cells to keep up their specific functionality, as well as for committed cells in order to perpetuate the information concerning their terminal fate during proliferation. The latter is known as **cell heredity** and is as the former thought to be based on a cellular property designated as “epigenetic **cellular memory**” (Muller 1999). Polycomb group and trithorax group proteins are thought to play a crucial role in an evolutionary conserved mechanism conveying epigenetic memory by establishing, maintaining and dynamically regulating transcriptional programs (reviewed e.g. in (Orlando 2003)). An increasing body of evidence argues that chromatin modifications like DNA methylation, utilization of histone variants, modification of core histones, especially at N-terminal tail domains, as well as the composition of chromatin constituents in general is involved in setting transcriptional programs, thus determining cellular memory. Besides mechanisms that work on the chromatin level, more and more findings point at nuclear topology as an additional epigenetic constituent of cellular memory. Both transcriptional activation and gene silencing have been shown to correlate with specific topographic motifs of nuclear architecture, although a definite proof for a causal involvement is yet still missing.

Several studies arguing for an implication of nuclear architecture on gene activation report a looping of actively transcribed regions from the main body of the chromosome, where it actually belongs. In human fibroblasts, for example Volpi et al. showed an increased protrusion of chromatin loops harboring the MHC II gene cluster upon transcriptional activation induced by interferon- γ (Volpi et al. 2000). Another cluster of developmentally co-regulated genes that was shown to be arranged according to its transcriptional activation state is the epidermal differentiation complex (EDC). Williams et al. showed that in human keratinocytes, where these genes are actively transcribed, the cluster could be found significantly more often outside of the corresponding chromosome 1 territories than in lymphoblasts, which do not show expression of EDC genes (Williams et al. 2002). In both studies, the regions under investigation

were quite large and contained a number of genes with an identical temporal regulation. Whether such large-scale looping might also affect single transcribed genes has still to be elucidated. Another kind of spatial nuclear reorganization was described during erythroid differentiation of murine erythroleukemia (MEL) cells. Here Francastel et al. (Francastel et al. 2001) showed first of all that the small subunit of the transcriptional activator NF-E2, which is important for globin gene expression, relocates from pericentric heterochromatin to an euchromatic compartment, where the larger subunit is localized so that a functional transcription factor is reconstituted. Secondly they observed a relocation of the β -globin gene (-cluster) from heterochromatin¹ to a non-heterochromatic region. Since both redistributions occurred prior to transcriptional activation, their results suggest a causal involvement of transcription factor and gene topology in gene regulation. Martou and colleagues observed that the gene *Plc β 3*, which is up-regulated during mouse Purkinje development was relocated towards the nuclear interior upon activation, while a constitutively transcribed gene in this cell type retained its radial position (Martou et al. 2002).

Many studies focusing on nuclear topology and gene silencing during differentiation found a crucial involvement of heterochromatic regions especially at centromeric and pericentric sites. One of the first studies arguing for an effect of nuclear topology on gene silencing was dealing with the expression of an eye color gene during compound eye development in *Drosophila*. Similar to the classical form of position effect variegation (PEV), which is caused by heterochromatic silencing of a gene in *cis*, i.e. by adjacent heterochromatin on the same chromosome, Dernburg et al. described a *trans*-silencing effect (Dernburg et al. 1996) caused by a heterochromatin block inserted in one copy of the *brown* eye pigment gene of *Drosophila*. They could show that through homologous association of the mutated gene carrying the insertion with the intact copy and due to a stochastic association of the inserted heterochromatic region with centromeric heterochromatin, the intact copy was dragged to the centromeric region and silenced due to the transcriptionally non-permissive environment exerted by centromeric heterochromatin. Fisher and colleagues presented several examples demonstrating that inactive genes in cycling human and murine B-lymphocytes were mostly associated with centromeric/pericentric heterochromatin (Brown et al. 1997; Brown et al. 2001). Moreover, they noticed that this association was not present in quiescent cells, but was rather established upon mitogenic stimulation (Brown et al. 1999). Additionally they could show that during T cell development the association of two differentiation-dependent silenced genes (*Rag* and *TdT*) with pericentric heterochromatin was only present if the genes were heritably, i.e. irreversibly shut off (Brown et al. 1999). Because the repositioning appeared as a delayed consequence of transcriptional inactivation and was not present in an immature T cell line that was able to re-express both genes the authors argued that repositioning might rather have a function in establishing a stably repressed state, than causing silencing *per se*. Another interesting example for an epigenetic effect of pericentric heterochromatin on differentiation-dependent transcriptional control was provided by the work of Skok et al., who showed that upon transition of biallelic to monoallelic expression of immunoglobulin genes in activated mouse B-lymphocytes, non expressed genes were recruited to pericentric heterochromatin (Skok et al. 2001). Kosak et al. found that upon differentiation of hematopoietic progenitors to pro B-cells immunoglobulin loci *IgH* and *Ig κ* were redistributed from a peripheral location to a more central position (Kosak et al. 2002). Since this reorganization preceded transcription and recombination of V(D)J gene segments the authors proposed that this spatial rearrangement might represent a prerequisite for B-cell maturation, in that the genes have to be placed in a transcription/recombination competent compartment. In a study on developing T cells Grogan et al. demonstrated that after activation of naive CD4⁺

¹ Defined by intense DAPI staining and/or by FISH with a major satellite specific probe visualizing pericentric heterochromatin.

T cells under different conditions, which generates the two T-helper subsets Th1 and Th2 with complementary cytokine expression profiles (γ -IFN⁺ / IL-4⁻ or γ -IFN⁻ / IL-4⁺), those cytokines which were heritably silenced were relocated to pericentric heterochromatin (Grogan et al. 2001). This redistribution was only accomplished after several cell divisions after which the cells lose the ability to revert the expression profile and hence their capacity to change subset identity. In a very recent study, Su et al. could demonstrate a repositioning of the mouse terminal transferase gene *Dnmt*, which they found to relocate towards pericentric heterochromatin after stimulation of thymocyte maturation, whereupon the gene is silenced (Su et al. 2004). Interestingly they found that the repositioning coincided with deacetylation of histones H3 at lysine 9 and preceded methylation of H3 at lysine 9 and demethylation of H3 at lysine 4; whereas the latter two modifications are known to correlate with transcriptionally inactive chromatin, the former is characteristic for transcriptionally competent chromatin (see chapter 1.4.2 p. 33). These findings exemplify how nuclear topology and chromatin modifications might act coordinately as epigenetic modulators of transcription.

1.2.3 In vitro differentiation systems employed in the present thesis

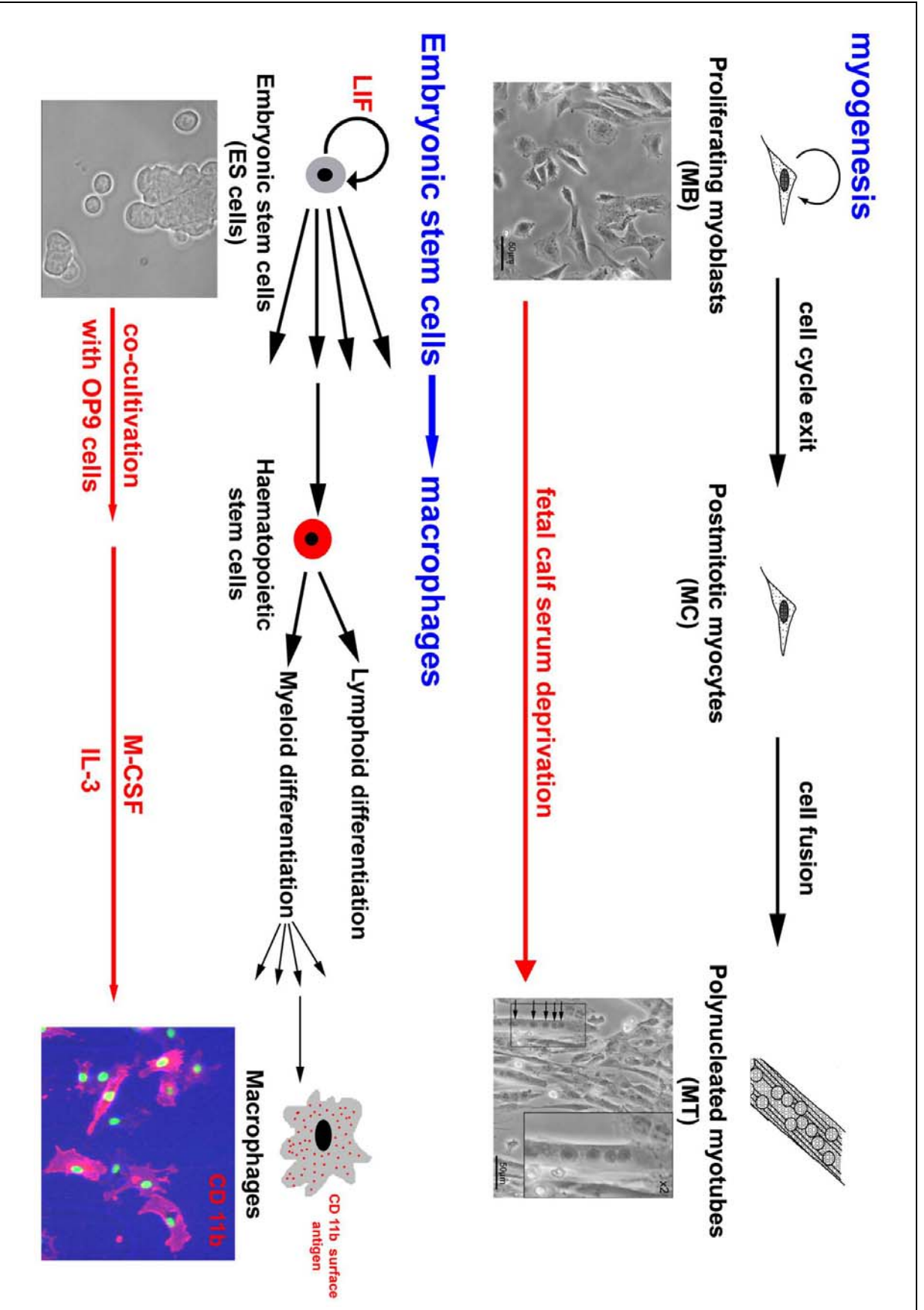
These many examples showing a potential implication of centromeric/pericentric heterochromatin in gene regulation during cellular differentiation were an important motivation for the present thesis to investigate the large-scale topology of centromeric/pericentric heterochromatin during differentiation in mouse. For that purpose, I have chosen two different *in vitro* differentiation models.

Figure 1.1 outlines coarsely the differentiation systems used: myogenesis and the differentiation of embryonic stem (ES) cells to macrophages. In the following, a brief introduction of both differentiation pathways is given considering relevant aspects of the situation *in vivo* and *in vitro*.

Myogenesis

In vitro myogenesis is regarded as a qualified system to study muscle development as it recapitulates all important differentiation steps including proliferation, commitment, migration, cell cycle withdrawal, fusion of cells leading to the formation of polynucleated syncytial myotubes and contraction. A big advantage as a model to study cellular differentiation is that the handling is very easy and that there is no need for special differentiation relevant factors like cytokines or hormones as for many other *in vitro* systems, which can be very expensive or if not commercially available time consuming and laborious to generate.

Figure 1.1: Utilized in vitro differentiation systems. Myogenesis: myoblasts (MB) are cultured in standard mediums like F-10 or DMEM supplemented with 20% fetal calf serum. Differentiation is induced by fetal calf serum deprivation, either by using serum less medium or by using horse serum instead (Lawson and Purslow 2000). After 1-2 days cells become elongated and begin to align along their length. During that period, muscle specific genes start to be expressed and cells usually exit the cell cycle becoming so-called postmitotic myocytes (MC). After 3 days, single cells start to fuse and the first polynucleated syncytial myotubes (MT) appear. Continued cultivation leads to an increase myotube size by additional fusion events. Eventually after prolonged cultivation (~10d), myotubes show spontaneous contractions. **ES cell/macrophage differentiation:** ES cells are cultivated in the presence of the leukemia inhibitory factor (LIF) that prevents differentiation and thus preserves the pluripotent state. Note that the cell line used (EB5) does not need cultivation on inactivated feeder cells as other ES cell lines do. In a first commitment step ES cells are differentiated to hematopoietic precursors (similar to hematopoietic stem cells in the embryo) by co-cultivation with OP9 stromal cells. These non-adherent cells can be harvested and induced to differentiate to macrophages by applying the cytokines macrophage colony-stimulating factor (M-CSF) and interleukin 3 (IL-3). Macrophages can be identified by the expression of the surface antigen Cd11b (red) and by its typical morphology. Nuclei in the epifluorescence image illustrating macrophages appear green since ES cells used for differentiation were stably transfected with a histone H2B-GFP construct. Further details on cell culturing can be found at 2.1.4.



Myoblasts can be prepared either from skeletal muscle directly (Irintchev et al. 1997) or one can use cell lines, which are available for several different species including humans. Proliferating myogenic myoblasts are maintained by cultivation in standard media containing usual or somewhat elevated levels of fetal calf serum (FCS: 10-20%). Differentiation can be readily induced by FCS deprivation. Removal of FCS is thought to prevent the activity of yet unidentified growth factors that might counteract terminal differentiation by sustaining proliferation. 1-2 days after applying the differentiation medium the cell culture changes its appearance dramatically; the cell shape is transformed from fibroblast-like to elongated spindles, while the cells start to align in a parallel fashion. At this stage, the majority of myoblasts has exited the cell cycle, which can be monitored by lack of BrdU incorporation, a dTTP precursor analog that is incorporated in cycling cells during DNA replication. Moreover muscle specific genes like myosin heavy/light chain, tropomyosin etc. are been turned on. Approximately 3 days after applying FCS deprived medium, the first polynucleated syncytial myotubes can be seen in the culture, which are created by fusion of mononucleated myocytes. If the culture is carried on by applying fresh differentiation medium approx. all 2 days the fusion process continues generating larger myotubes with an increasing number of nuclei. After an extended period of culturing for more than a week myotubes eventually show spontaneous contraction, which demonstrates that *in vitro* differentiation effectively yields functional muscle precursor.

Myogenesis **in vivo** is one of the best-characterized examples for the development of a specific tissue in vertebrates. In the following a brief overview concerning some important molecular aspects on myogenesis is given that however is naturally far from being exhaustive. A group of four myogenic regulatory factors (MRFs) plays a central role in muscle development: MyoD, Myf5, myogenin and MRF4. The myogenic potential of all four proteins was initially characterized by their ability to convert non-myogenic cell types like fibroblasts to myotube forming cells by ectopic expression (Sabourin and Rudnicki 2000). All four proteins belong to the superfamily of basic helix-loop-helix (bHLH) transcription factors, whereby the basic domain interacts with DNA, while the HLH domain is important for dimerization. Transcription factor activity is usually achieved by heterodimerization with ubiquitously expressed bHLH E proteins, upon which DNA is bound in a sequence specific manner targeting the so-called E-box motif. Many muscle specific genes harbor such an E-box in their promoter/enhancer regions and can thus be activated by MRFs. The gene of the cell cycle inhibitor p21 contains also an E-box, which is targeted by myogenin, which in cultured myoblasts is induced by FCS deprivation that in turn induces cell cycle withdrawal and terminal differentiation. Cell cycle exit is thought to involve p21 dependent inhibition of cyclin dependent kinases (CDKs), leading to hypophosphorylation and hence activation of the retinoblastom protein (pRb) ((Moran et al. 2002) and citations therein). pRb on the other hand is known to interact with E2F proteins thereby impeding the G1-S transition, keeping cells in a non-proliferative state (Harbour and Dean 2000).

A negative regulation of MRFs is achieved on the dimerization level via interactions with HLH proteins, like the Id factors or Twist, which lack the DNA binding domain or with Mist1 a bHLH protein that lacks the transactivation domain, which is necessary for promoting transcription (reviewed e.g. in (Sabourin and Rudnicki 2000)).

Initially it was thought that MyoD and Myf5 are redundant constituents of the same differentiation pathway, since MyoD^{-/-} mice were viable and showed normal muscle development, but increased levels of Myf5. Similarly Myf5^{-/-} mice showed a normal muscle development, although they died soon after birth due to severe rib defects (see citations in (Sabourin and Rudnicki 2000)). According to this idea double knock out mice died at birth showing a complete lack of skeletal myoblasts and muscles. However, a closer molecular characterization of all 4 MRFs especially concerning their temporo-spatial expression pattern during embryo-

genesis revealed a hierarchical mode of action. MyoD and Myf5 are considered as primary MRFs as they are required for the determination step to the myogenic lineage. In fact, both genes are expressed already in proliferating myoblasts. During embryonic muscle development it has been shown that MyoD and Myf5 play non-identical roles as they have a distinct spatial and temporal expression pattern (see citations in (Sabourin and Rudnicki 2000)). Myogenin and MRF4 have been shown to act downstream of MyoD and Myf5. While myogenin^{-/-} mice developed myoblasts but lacked completely myofibers, MRF4^{-/-} animals had normal musculature, but increased myogenin levels, arguing for a compensation of MRF4 by myogenin (see citations in (Sabourin and Rudnicki 2000)).

MRFs have a broad spectrum of interaction partners including components of the basal transcription machinery or cell cycle controlling proteins like pRb, which is an important cell cycle inhibitor. The fine-tuning between muscle differentiation and cell cycle regulation is further revealed by the inhibiting effect of growth promoting factors on the myogenic potential of myoblasts *in vitro*. Especially onco-/proto-oncogenes, like c-Jun, c-myc or viral proteins like adenoviral E1A or large T antigen of SV40 have been shown to negatively affect differentiation (see citations in (Sabourin and Rudnicki 2000)). E1A and large T were shown to even induce reversal of terminal differentiation in C2C12 myotubes, as myotube nuclei reentered the cell cycle as revealed by DNA replication (Cardoso et al. 1993; Crescenzi et al. 1995). MyoD seems moreover to interact with chromatin remodeling factors like p300/CBP and the histone deacetylase PCAF (see citations in (Sabourin and Rudnicki 2000)).

Similar to neuronal cells myofibers, consisting of many myotubes can exist over the whole life span of an organism. In case of injury however, so-called satellite cells sitting beneath the basal lamina adjacent to muscle fibers can be induced to undergo myogenic differentiation and fuse to existing myotubes or form new ones, respectively. It should be stressed that satellite cells are not equivalent to cultured myoblasts. Actually those myogenic “stem” cells are considered quiescent and do not express any of the four MRFs. Upon injury MyoD and Myf5 is rapidly turned on and cells start to proliferate. Later on myogenin and MRF4 are expressed and induce terminal differentiation (reviewed in (Sabourin and Rudnicki 2000)).

ES cell differentiation to macrophages

In contrast to *in vitro* myogenesis, which represents a quite short differentiation path in terms of mitotic divisions and commitment steps, the differentiation of mouse ES cells to macrophages, the second model used in the present thesis, represents a “long” and intricate differentiation pathway. Using this model was insofar attractive as extremely different cell types in terms of commitment could be compared: a pluripotent cell, undetermined and provided with all differentiation possibilities on the one side and a terminally differentiated postmitotic cell with a determined cellular function on the other. Figure 1.2 summarizes the differentiation options of pluripotent stem cells into the various lineages. Murine ES cells, which were the first to be isolated, have been generated either from the epiblast stage or earlier (reviewed in (Prelle et al. 1999)). **In vivo** in a first major commitment step embryonic stem cells differentiate to multi-/pluripotent¹ hematopoietic stem cells (HSCs), which give rise to immune cells, blood cells, tissue-specific macrophages and dendritic cells. (figure 1.3). In the embryo, hematopoiesis is accomplished by so-called primitive HSCs, which first appear extra-embryonically in the yolk sac in so-called blood islands. It should be added that the demands on the repertoire of hematopoietic cells in an embryo/fetus is markedly different from the

¹ The term “pluripotent” is commonly used to describe hematopoietic stem cells, although only a differentiation potential into hematopoietic cells is assured. So actually the term multipotent would be more appropriate, not considering a transdifferentiation potential, that is at present heavily debated (Camargo et al. 2004).

adult. The early embryo for example lacks lymphocytes and primitive erythrocytes express specific globins with a higher O₂ affinity, in order to secure O₂ transfer from the maternal blood. At later stages HSCs can be found in a mesodermal region called aorta-gonad-mesonephros (AGM) and then in the fetal liver.

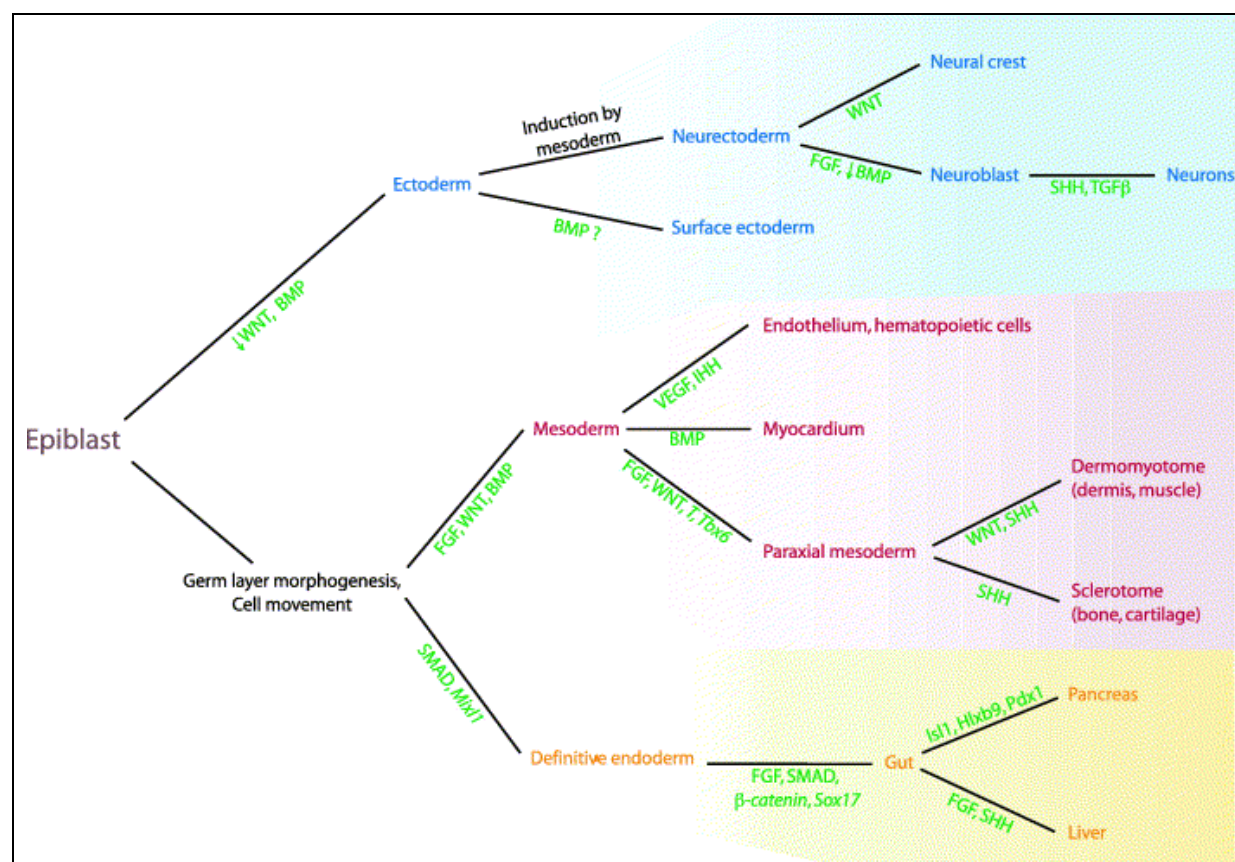


Figure 1.2: “Specification and differentiation of germ layer derivatives in mouse embryos”. Taken from (Loebel et al. 2003): “Ectodermal (blue), mesodermal (red), and definitive endodermal (orange) lineages derived from the epiblast (brown) are shown, with the signaling pathways and transcription factors indicated in green. The question mark signifies the lack of direct evidence for involvement of BMP4 in surface ectoderm differentiation in mouse embryos.” The epiblast represents the inner cell mass after the division into the primitive endoderm, which gives only rise to extraembryonic structures, while the primitive ectoderm or epiblast will develop into the embryo proper. Note that ES cells are isolated from epiblast cells or earlier embryonic stages (reviewed in (Prele et al. 1999)).

At present it is still a matter of debate when, where and how during ontogenesis the definitive HSCs, i.e. those which will be present in the adult animal are created (discussed in (Kyba and Daley 2003)). In the adult mammal hematopoietic stem cells reside in the bone marrow of the larger bones (Slack 2001), where they are imbedded within connective tissue, the so-called stroma. Stromal cells represent an important factor in creating a “microenvironment” that via its variable composition of soluble growth and differentiation factors regulates the further differentiation of HSCs into the various hematopoietic cells, according to the particular demands. HSCs make up just 1/10⁵ of all cells in the bone marrow, which contains many immature hematopoietic precursor cells. HSCs are thought to be quiescent or at least to cycle very slowly (Szilvassy 2003) and are capable of self-renewal, which is an important property in order to cope with the life long demands for vast amounts of hematopoietic cells. Upon external stimuli, they can generate committed precursors of the various lineages in order to supply the organism with the necessary amounts and types of hematopoietic cells.

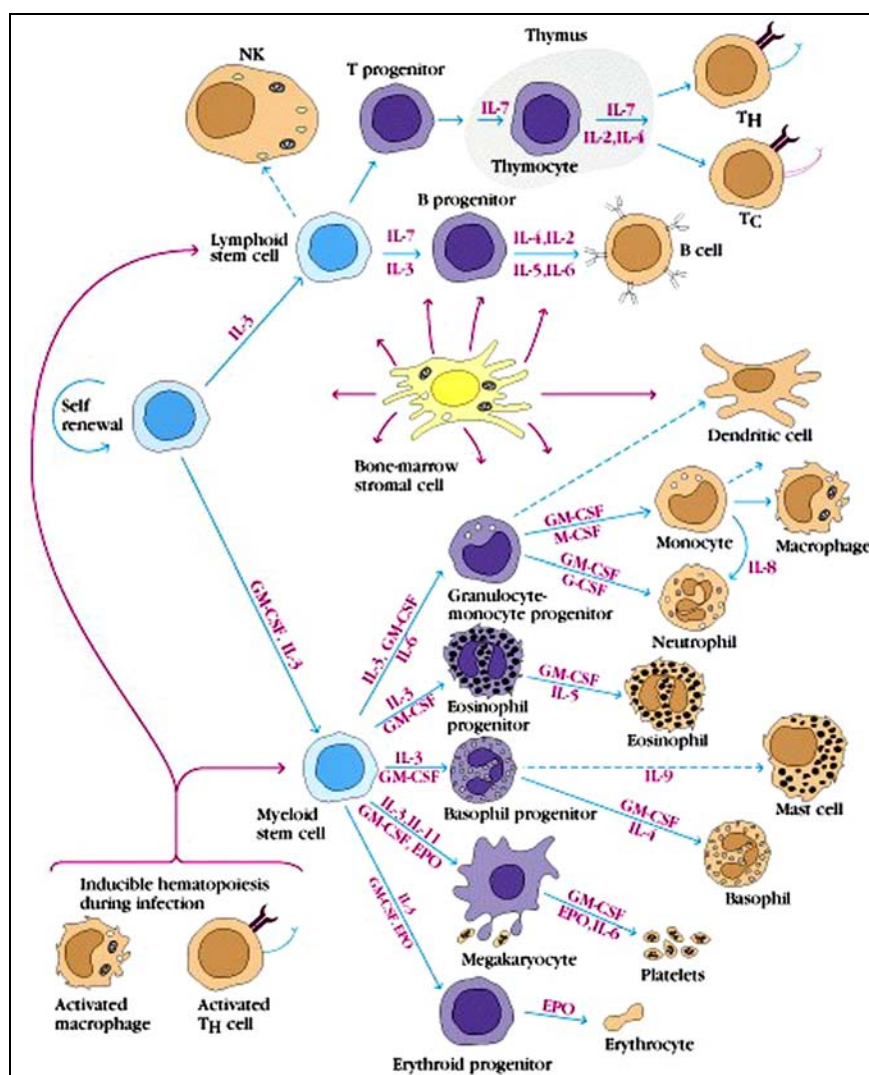


Figure 1.3: Taken from <http://tutor.lscf.ucsb.edu/instdev/sears/immunology/chapter02/hematopoiesis.htm> ©Duane W. Sears. Shown is a proposed genealogy of hematopoietic cells. Pluri-/multipotent stem cells are shown in blue, progenitor cells are highlighted in purple, stromal cell in yellow and differentiated cells in brown. Cytokines promoting a specific transition (blue arrow) are written in purple. Purple arrows represent cytokine secretion. T_H = T helper cell, T_C = cytotoxic T cell.

However, it has to be added that regulation of hematopoiesis is accomplished not only at the level of HSCs, but also at the level of more committed cells, which allows a faster response to fluctuating requirements. HSCs differentiate into at least **eight** different lineages (Szilvassy 2003). At first a dichotomous separation takes place, yielding a lymphoid and a myeloid lineage. Lymphoid committed cells develop to B and T-lymphocytes. The latter can develop either to cytotoxic $CD8^+$ cells or to $CD4^+$ T-helper, which can differentiate further comprising two subsets $Th1$ and $Th2$. Upon antigen activation, B-lymphocytes can differentiate terminally to plasma cells. Myeloid committed cells can differentiate to the three granulocyte lineages (basophil, neutrophil, and eosinophil), to erythrocytes, to megakaryocytes which generate platelets and to monocytes. The latter can float in peripheral blood and infiltrate different tissues thereby differentiating to tissue-specific macrophages including osteoclasts (bone), histiocytes (connective tissue), microglia (CNS), Langerhans cells (epidermis) and others.

An important role in hematopoietic differentiation is played by cytokines, which are fairly small, usually secreted and soluble proteins that among other functions can have cell growth, survival and differentiation inducing effects on HSCs as well as on hematopoietic precursor cells. More than 20 such hematopoietic cytokines are known, of which the colony stimulating factors (CSFs) have been studied most extensively (reviewed in (Barreda et al. 2004)). These were named after their potential to direct differentiation of hematopoietic progenitor cells growing as a colony in a semi solid agar medium towards a specific lineage (Walbot and Holder 1987). Depending on the developmental background of a responsive cell type as well as on the combination of present CSFs the effects can be different. Interleukin-3 (IL-3, multi-CSF) appears to be important in stimulating the proliferation of HSCs and its derivatives. The granulocyte macrophage colony-stimulating factor (GM-CSF) appears to act in combination with granulocyte colony-stimulating factor (G-CSF), macrophage colony-stimulating

factor (M-CSF) and erythropoietin (EPO). IL-3, GM-CSF, and EPO are important in stimulating the proliferation of HSCs and its derivatives. The granulocyte macrophage colony-stimulating factor (GM-CSF) appears to act in combination with granulocyte colony-stimulating factor (G-CSF), macrophage colony-stimulating factor (M-CSF) and erythropoietin (EPO). IL-3, GM-CSF, and EPO are important in stimulating the proliferation of HSCs and its derivatives. The granulocyte macrophage colony-stimulating factor (GM-CSF) appears to act in combination with granulocyte colony-stimulating factor (G-CSF), macrophage colony-stimulating factor (M-CSF) and erythropoietin (EPO).

factor (M-CSF) or erythropoietin, in promoting the proliferation and differentiation along the granulocyte, macrophage or erythroid lineage.

In vitro the differentiation of ES cells to HSCs is all but trivial. In fact, it appears that *in vitro* ES cell differentiation prefers the embryonic/yolk sac mode of differentiation, generating cells resembling rather primitive HSCs (Kyba and Daley 2003). This assumption comes from the findings that ES cell-derived HSC-like cells, which are capable to differentiate into myeloid and lymphoid lineages, do not engraft mice whose bone marrow has been destroyed. This engrafting potential is considered as an important characteristic of adult/definitive HSCs. Recently it has been shown that already a small modification in the transcription repertoire of hematopoietic precursor cells generated from ES cells, namely an ectopic expression of the homeotic gene *HoxB4*, was sufficient to convey engrafting capability (see citations in (Kyba and Daley 2003)). The most successful way to generate HSC-like cells with myeloid and lymphoid differentiation capacity was found to be the co-cultivation of ES cells with the stromal cell line OP9, which is derived from the bone marrow of mice, deficient M-CSF (Nakano et al. 1994). M-CSF is thought to have an inhibitory effect on ES cell differentiation to lineages other than macrophages and thus the lack of it appears to be responsible for the generation of HSC-like cells with lymphoid differentiation potential. Those HSC-like cells can then be induced to differentiate at a high percentage to macrophages by applying a combination of IL-3 and M-CSF (see also *Methods*).

Increasing the basic understanding on hematopoietic differentiation of ES cells has an important clinical impact as using ES cells derived HSCs for cell replacement therapies would offer several advances compared to conventional sources as bone marrow or chord blood (reviewed in (Kyba and Daley 2003)). One advantage would be that it would offer the possibility of a nearly unlimited supply, whereas bone marrow donors are still a limiting factor. Moreover, ES cell derived HSCs are thought to represent a more immature state compared to bone marrow HSCs. This is supposed to cause less age related problems as the accumulation of various defects, lower long-term survival or greater incidence of graft-vs-host disease, which have been observed for aged bone marrow. Furthermore, co-transplantation of iso-genic hematopoietic stem cells with other grafts would provide the possibility to enhance tolerance after transplantation, or at least to reduce the level of immunosuppression.

Yet there are certainly many obstacles that have to be overcome before it will be possible to use ES cell derived hematopoietic progenitors in replacement therapies, one of the most substantial being the lack of capacity to engraft bone marrow of the recipient.

1.3 Chromosome territories

Since its first description in 1831 by Brown (Brown 1831), the cell nucleus has been fascinating many generations of researchers, last but not least since at the turn of the century increasing evidence arose that it harbored the structures apparently involved in heredity. The term “chromosome” dates back to a review paper by Wilhelm Waldeyer from 1888, who introduced it to name those light microscopic threadlike structures in the nucleus, which became visible during mitosis and which had been shown to split during “karyokinesis” (see (Cremer and Cremer 1988) and citations therein).

It were the ground breaking studies of Sutton and Boveri, that led to the so-called “Sutton-Boveri chromosome hypothesis” or “chromosome theory of heredity”, which combined Mendel’s laws of heredity with chromosome behavior during meiosis (see (Martins 1999) and ci-

tations therein). The ideas of individuality and continuity of chromosomes¹ as proposed by Boveri and Rabl were accepted only slowly in the beginning of the 20th century and were still paralleled by a perception of complete disassembly of chromosomes during interphase and reassembly during mitosis as described by Hertwig (Cremer and Cremer 1988). The actual organization of chromosomes within the interphase nucleus, has since then been the matter of manifold speculations. A model with a high impact was proposed by Carl Rabl (Rabl 1885), who suggested a polar orientation of chromosomes with centromeres at one pole of the nucleus and telomeres at the other, resulting from the orientation of chromosomes at anaphase. This arrangement could be confirmed for various organisms including *Drosophila melanogaster's* polytene chromosomes (Hochstrasser et al. 1986), fission yeast (Funabiki et al. 1993), and various plants (Avivi and Feldman 1980; Abranches et al. 1998), but seems not to account for mammals (Manuelidis and Borden 1988; Weimer et al. 1992; Vourc'h et al. 1993; Cerda et al. 1999). It was not before the 70's of the 20th century, long after experiments by Avery (1944) had proven that DNA was the actual compound carrying and propagating genetic information, that experimental data was provided indicating a territorial organization of chromosomes. Irradiation experiments using UV microbeams damaging only parts of an interphase nucleus, combined with [³H]thymidine labeling of damaged DNA, revealed that DNA repair was restricted to only a few chromosomes as visualized by autoradiography of subsequent mitoses. These findings argued strongly for an organization of chromosomes as separate non-intermingling entities (Zorn et al. 1979). A direct evidence for the existence of chromosome territories (CTs) was finally provided in the mid 80's of last century using in situ hybridization techniques. Utilizing labeled human genomic DNA as a probe on hybrid cell lines bearing one or several human chromosomes (Manuelidis 1985; Schardin et al. 1985) visualized well-defined domains. After it became possible to generate chromosome specific painting probes the territorial organization of chromosomes could be confirmed on cultured cells (Lichter et al. 1988), as well as on tissue sections (Borden and Manuelidis 1988). Meanwhile examples for a territorial organization of interphase chromosomes have been shown for many different organisms (e.g. mouse (Mahy et al. 2002), higher primates (Tanabe et al. 2002), chicken (Habermann et al. 2001), marsupials (Rens et al. 2003) and Hydra (Alexandrova et al. 2003)), including plants (Fransz et al. 2002) and yeasts (Loidl 2003). Interestingly already before the idea that chromosomes consisted of territorial entities was completely accepted various groups had already started to ask whether interphase chromosomes would be arranged in a random fashion or whether they followed some kind of topological organization principle (see following chapters). Two main aspects of a non-random distribution of CTs were usually considered: (1) the radial distribution and (2) the side-by-side distribution. The radial distribution describes the relative distance of chromosome territories to the nuclear center, while the side-by-side distribution includes chromosome neighborhoods and relative constellations of CTs. A frequently investigated non-random side-by-side distribution is the association of homologous chromosomes.

1.3.1 Radial distribution

The first studies proposing a non-random radial distribution of CTs in interphase nuclei were actually investigating metaphase spread preparations from mitotic cells. A common idea was that the relative distribution of chromosomes in interphase nuclei would be conserved at least to some extent during mitosis, despite the obvious reorganizations due to chromosome condensation, spindle alignment etc. Concordant results between mitotic and interphase studies

¹ The idea that chromosomes were constantly existing entities also during interphase, though not visible, and that different chromosomes were not equivalent but qualitatively different were heavily debated arguments at that time.

concerning the distribution of the inactive X chromosomes and the long arm of #Y, as well as findings showing that radiation induced translocation chromosomes tended to lie close together in mitotic spreads supported this supposition (see (Hens et al. 1982) and citations therein). An additional drawback of these studies was that they dealt with artifact prone preparation techniques like colcemide treatment to increase the frequency of mitotic cells or hypotonic cell swelling to improve chromosome spreading. Nevertheless, some conclusions were drawn out of these investigations that could at least partially be confirmed later using methods capable to visualize CTs directly in interphase nuclei (see below). In two independent studies using spread preparations of human fibroblasts it was shown that mitotic chromosomes were arranged in a size-related fashion (Hens et al. 1982; Wollenberg et al. 1982). By measuring the distances between centromeres and the center of the mitotic spread and between centromeres of homologous and heterologous chromosomes both groups could demonstrate a preferential localization of human #1-#12 and #X on the periphery of the spread and a more interior position for #13-#22 and Y. Accordingly, they suggested a size-related radial distribution also in interphase nuclei with larger chromosomes localizing more peripheral, smaller ones more in the nuclear interior. Both observed slight deviations from this general rule mostly pronounced for #1 being more internal and #18 being more peripheral than other similar sized chromosomes. Hens et al. found additionally a significant correlation between the position of chromosomes in the mitotic spread and their replication timing, with earlier replicating chromosomes being more internal. After also considering data on gene density, although quite poor at that time, they concluded that "...smaller, earlier replicating, gene-dense chromosomes are preferentially found near the metaphase plate center, surrounded by longer chromosomes which finish their replication rather late during S phase" (Hens et al. 1982). As a functional implication for their findings, they suggest the "bodyguard" hypothesis, originally described by Hsu (Hsu 1975), which reasons that gene dense chromatin in the nuclear interior is protected by gene poor chromatin at the nuclear periphery against all kinds of DNA damaging agents from the cytoplasm (see 4.1.1.2 for discussion). These early findings on mitotic spread preparations were later confirmed by in situ hybridization techniques visualizing CTs in interphase nuclei (Boyle et al. 2001; Cremer et al. 2001; Bolzer et al. submitted).

In two studies, which utilized electron microscopy, the spatial distribution of mitotic chromosomes was analyzed *in situ* (Mosgoller et al. 1991; Leitch et al. 1994). Compared to earlier works on mitotic spreads this had the advantage to be free from artifacts caused by colcemide treatment and hypotonic swelling. Mosgoller et al. described a correlation between the chromosome size and the distance of centromeres to the center of the mitotic figure, with larger chromosomes being more peripheral and smaller being more central (Mosgoller et al. 1991). Similar results were obtained in a study by Leitch et al., who could confirm a significant more internal location for #Y and #18 and a more peripheral for #6, but failed to detect significant deviations for chromosomes 1, 2, 3, 9, 16 and 17 (Leitch et al. 1994).

In the last few years, an increasing number of studies have accumulated evidence for a non-random radial distribution of CTs by assessing interphase nuclei directly utilizing FISH with chromosome specific painting probes. Croft et al from W. Bickmore's group showed that the similar sized human chromosomes 18 and 19 are positioned differentially in several cell types including lymphoblasts and lymphocytes, with the gene dense #19 (22.3 genes/Mbp)¹ being localized more internal and #18 (4.4 genes/Mbp)¹ more peripheral (Croft et al. 1999). Boyle et al. also from the same group expanded this investigation determining the radial distribution of all human chromosomes (Boyle et al. 2001). They could show that in lymphoblasts and fibroblasts there was a general tendency for each chromosome to have a ra-

¹ Gene density was calculated from the chromosome size and number of annotated genes from the *Ensembl* database (<http://www.ensembl.org>). Last update: January 2004).

dial position according to its gene density, with gene poor chromosomes located more at the periphery and gene dense more in the interior. In fibroblasts however, Bridger et al. from Bickmore's group reported a cell cycle dependent anomaly of this gene-density-related radial distribution. While in cycling fibroblasts the gene poor #18 CTs were found at the periphery, thus equaling the situation in lymphocytes and lymphoblasts, in quiescent cells #18 was apparently repositioned to the nuclear center and thus was distributed as the gene rich #19 (Bridger et al. 1998). In a similar study, Cremer et al. confirmed the results concerning a gene-density-related radial distribution of CTs in human lymphocytes, but failed to reproduce these results in fibroblasts, where we found a size-related distribution of CTs instead, with smaller chromosomes being more centrally located and larger ones more peripherally (Cremer et al. 2001). A. Bolzer from the group of T. Cremer showed recently that this size correlated distribution is independent from the cell cycle stage, thus clearly contradicting the results of Bridger et al. mentioned above (Bolzer et al. submitted). The reason for these conflicting observations has yet to be resolved.

A size-related distribution had previously been demonstrated by Sun et al. in human fibroblasts by investigating the radial distribution of subtelomeric q-arm regions of nine different chromosomes (Sun et al. 2000). Recently Rens and colleagues could demonstrate a size-related distribution in the marsupial potoroo, which has only $2n=12$ (female) chromosomes (male=13) with remarkable differences in the chromosomes size (Rens et al. 2003). Their finding argues for an evolutionary conservation of a size-related radial CT distribution, although the influence of gene density could not be assessed, since there was no data available.

A basic question is how and to which extent gene content and/or DNA content influence the radial position of CTs in different cell types. Concerning the size-related distribution in human fibroblasts it should be pointed out that the set of big chromosomes that Cremer et al. found to be more peripheral contains not only the largest chromosomes, but at the same time exhibits a markedly reduced gene density (6.5 genes/Mbp) compared to the set of small chromosomes (13 genes/Mbp). Therefore, the observed differences in the radial distributions could also be contributed to the difference in gene density. On the other hand the internal position of #18 and #Y in fibroblasts and amniotic fluid cells is hard to explain if gene density solely would be the driving force in determining the radial position of CTs. The radial distribution of #18 and #Y as described by Cremer et al. is a good example to bring this controversy to mind: in fibroblasts both chromosomes are internal accordant to their size just as the other small chromosomes, while in lymphocytes they are located at the periphery and thus positioned as the other gene poor chromosomes.

In a recent study by the Cremer group the radial distribution of human #18 and #19 was analyzed in a number of different normal and malignant cell types (Cremer et al. 2003). They showed that the general difference in the radial distribution of #18 and #19 remained valid in various normal and malignant cell types even if the chromosomes were involved in translocations. In the colon carcinoma cell line SW 480, for example #19 chromatin showed an internal position although it was involved in translocations with #5 and #8, which are known to be located peripherally (Boyle et al. 2001). This finding argues clearly for an intrinsic property of gene rich chromatin to localize more internally. In contrast, in the Hodgkin-derived tumor cell line HDLM-2 #19 chromatin, which is involved in translocations with the more peripheral #2 and #9, exhibits an external shift of the #19 material compared to the progenitor cell line lacking the rearrangements.

In chicken cells, Habermann et al. could show a clear-cut difference in the radial distribution of gene dense microchromosomes and gene poor macrochromosomes. Using 3D-FISH with probes sets specific for large (#1-#5 & #Z), intermediate (#6-#10) and small/microchromosomes he could show that large and intermediate chromosomes localized significantly more peripheral and microchromosomes more internal. This size-related distri-

bution was concomitantly gene-density-related, since the small microchromosomes have a gene density that is on average 2-4 times higher than that in macrochromosomes. This concomitance of a small chromosome size and a high gene density, similar to the human probes sets used by Cremer et al. (Cremer et al. 2001) did not allow to answer the question concerning the involvement of gene density vs. chromosome size in determining the radial position of CTs.

Tanabe et al. expanded the studies by Croft et al. (Croft et al. 1999) by investigating the radial distribution of chromatin homologous to human #18 and #19 in lymphoblastoid cells of seven higher primate species, whose last common ancestor with humans dated back more than 30 million years ago (Tanabe et al. 2002). Their intention was to test the degree of evolutionary conservation of this distributional motif originally found in humans. They could show that the more internal location of #19 and the more external location of #18 were indeed conserved in all investigated primate species. This finding was especially astonishing, since some of the analyzed species, such as gibbons have a substantially rearranged karyotype including multiple translocations of the analyzed chromatin material. Chromatin homologous to human #19 for example was located internally despite being translocated on the rather large gibbon chromosomes 10, 14 and 16, which according to the idea of a chromosome size-related distribution should be localized more peripherally. Additionally the authors provide evidence that supplementary heterochromatic blocks influence the radial position of adjacent chromatin by “dragging” it further to the periphery.

The emerging picture concerning the radial distribution of CTs clearly shows a correlation with gene density that seems to be evolutionary conserved as the results in higher primates in chicken indicate. Findings in interphase nuclei as well as in mitotic cells have additionally shown that chromosome size apparently influences the distribution. To which extent and how gene density and/or chromosome size play role in organizing CTs within the interphase nucleus is still controversial. A model trying to consolidate the apparently conflicting data is proposed in the discussion chapter.

1.3.2 Side-by-side distribution

The perception of an ordered distribution of CTs in interphase nuclei does not only include the possibility of a non-random radial organization, but also of a non-random side-by-side distribution of CTs, i.e. where the relative position of individual CTs is a reproducible constant. An intensely studied example of such a predetermined intranuclear distribution of CTs is the phenomenon of homologous association. To date such a pairing of chromosomes in interphase nuclei has been shown in several diploid cell types of diptera (including *Drosophila melanogaster*) and in polytene chromosomes of salivary gland cells of such species. Possible functions of this neighboring of homologous sequences include (i) transvection, which is defined as a mutual supplementation of gene activity of heteroalleles, (ii) pairing dependent gene silencing and (iii) pairing dependent trans-inactivation, where heterochromatic silencing in cis can have a dominant effect on an associated wt allele in trans (see (Henikoff 1997) and citations therein). Diploid cells of *S. cerevisiae* (budding yeast) have also been shown to exhibit association of homologues via multiple interstitial interactions (Burgess et al. 1999). As a possible reason for somatic pairing in budding yeast it was proposed that inter-homologue recombinational DNA repair in G1 and G0 cells could thus be enabled, thereby bypassing the lack of sister chromatids as repair templates (Kleckner and Weiner 1993). Although the majority of available data in mammalian cells argues against somatic pairing as a general phenomenon there are a few controversially discussed studies supporting the idea of homologous association in some exceptional cases.

Arnoldus et al. for example could show a cell type specific association of the pericentromeric region of human chromosome 1 in cerebellar neurons, but not of the pericentromeric region of #7 (Arnoldus et al. 1989). In a subsequent study on human brain tissue, involving probes specific for the centromeric regions of chromosomes 1, 6, 7, 10, 11, 17, 18, X and Y the authors found an increased frequency of somatic pairing for #17 (Arnoldus et al. 1991). Williams et al. also found this association in prostate tissue, plus an additional association of the centromeric region of #9 (Williams et al. 1995).

Using centromeric probes for human chromosome 15, Lewis et al. demonstrated somatic pairing of centromeres/p-arms in human leukocytes as well as in malignant leukemia and lymphoma cells but could not reproduce this finding in amniotic fluid cells, uterine cervical tissue and tissue fibroblasts, consequently suggesting a cell type specificity (Lewis et al. 1993) of the observed phenomenon. Since chromosome 15 is known to carry NOR sequences involved in nucleolus formation and since the visualized regions were frequently associated with nucleoli, the observed association was suspected to result from a neighboring association of homologues at a nucleolus.

LaSalle and Lalande found a similar association of the centromeric regions of #15 in lymphocytes, although only during late S-phase (LaSalle and Lalande 1996). Since the adjacent imprinted region involved in Prader-Willi (PWS) and in Angelman syndrome (AS) showed an even closer association than the centromeric region, they concluded that this cell cycle specific "kissing" as they called it could play a role in a replication dependent maintenance mechanism for the imprint in the respective region. A similar result was obtained for an imprinted region on mouse chromosome 7, where a transient association was observed in fibroblasts during S-phase (Riesselmann and Haaf 1999). It must be added that the results of LaLande and LaSalle are not undisputable. In the human myeloid leukemia cell line HL 60 for example Nogami et al. could not reproduce the results of LaLande and LaSalle (Nogami et al. 2000). Although an association of this region was observed in late S-phase, no difference was found between the centromeric regions and the imprinted regions. Clearly contradictory results were obtained by K. Teller in the group of T. Cremer, in spite of using the same experimental setting as LaSalle and Lalande's (Teller 2003 855). She showed that #15 centromeric regions were located closer to each other than the imprinted regions during late S-phase, and not vice versa as described by LaSalle and Lalande. This was an important finding as it debilitated LaSalle's and Lalande's argument that the observed association was specifically driven by the imprinted regions and could not be the result of the nucleolar associations of the NORs on #15 as previously proposed by Lewis et al. (Lewis et al. 1993). Furthermore she could also demonstrate that in cells from PWS patients lacking the imprinted segments the distance between the centromeric regions did still decrease at late S-phase, while LaSalle and Lalande found the distance between the centromeric regions to be stable in such cells. Finally LaSalle and Lalande strengthened their hypothesis by demonstrating another late S-phase specific association for the imprinted region on #11, which is a chromosome without an NOR, thereby reinforcing their argument for an independency of the phenomenon from NOR regions. Kathrin Teller on the other hand observed even a slight increase of the distance between these regions on #11 during late S-phase.

Applying FISH with whole chromosome painting (WCP) probes Chandley et al. demonstrated an association of homologous chromosomes 3, 7, 8, 13, 17 and 21 in human Sertoli cells, which was absent in cycling peripheral lymphocytes¹. #X and #Y did not exhibit somatic pairing (Chandley et al. 1996) in either cell type. Though the reason for such a somatic pairing of homologous chromosomes remains enigmatic the authors propose a potential role in transcriptional regulation similar to that described in mouse Sertoli cells where nucleolar activity

¹ Homologous chromosomes were regarded as associated either if there was only one WCP signal present or if the CT signals were less than 1 CT-diameter apart.

was shown to depend on the association behavior of NOR bearing chromosomes (Haaf et al. 1990). The experiments of Chandley et al. using WCP probes are the most reasonable ones if *homologous association* or *somatic pairing* as a phenomenon involving the complete chromosome and not just a specific region has to be assessed. It should be kept in mind, that all other studies mentioned so far investigated the association behavior of centromeric regions (Arnoldus et al. 1989; Arnoldus et al. 1991; Lewis et al. 1993; Williams et al. 1995; LaSalle and Lalande 1996). Since such regions usually contain satellite repeats, which are known to cluster (Comings 1980; Haaf and Schmid 1989; Alcobia et al. 2000), the results obtained by analyzing only centromeric regions have to be questioned as potentially biased.

Although there are examples for homologous association as those just described, most studies performed with mammalian cells failed to evidence somatic pairing of homologous chromosomes. In a study by Lesko et al. on human T-lymphocytes (Lesko et al. 1995) for instance, the analysis of #7, #11 and #17 centromeric regions revealed no indication for a somatic pairing, although Arnoldus et al. had formerly described an association for #17 centromere sequences in cerebellar neurons (Arnoldus et al. 1991). Performing FISH with centromeric probes for #1 and #15 in human lymphocytes, fibroblasts and amniotic fluid cells, Emmerich et al. could not find a specific homologous association or relative positioning of the analyzed regions (Emmerich et al. 1989) which is conflicting with the results of Lewis et al. who did describe an association for #15 centromeres in lymphocytes (Lewis et al. 1993).

Also investigating centromeric regions but this time of #18 and #X in amniotic fluid cells and fibroblasts/fibroblastoid cells Popp et al. found a statistically significant internal location of the #18 probe, which accords with the results obtained later using WCP probes (see above and (Cremer et al. 2001), but could not show any specific homologous association of these regions.

Ferguson and Ward used centromere-specific probes for chromosome 1, 2, 5, 7, 9, 10, 11, 12, 17, and 20 in human T-lymphocytes and were also unable to observe homologous pairing of the visualized regions.

Vourc'h et al. probing mouse subsatellite regions of #X, #8 and #11 in lymphocytes point out that their data does not support any specific homologous association (Vourc'h et al. 1993).

In a study by Alcobia et al. where they performed FISH with centromere-specific probes visualizing all human chromosomes in fibroblasts and hematopoietic cells, they observed an association of homologous sequences in less than 2% of all analyzed cells, which clearly argues against a somatic pairing (Alcobia et al. 2000).

In contrast to all the studies mentioned so far Habermann et al. demonstrated a lack of somatic pairing using whole chromosome specific painting probes for individual chicken macrochromosomes in fibroblasts and neuronal cells (Habermann et al. 2001). These results are especially meaningful as they exclude also a sequence specific somatic pairing, which is not possible if only specific chromosomal regions are visualized. In a similar approach Cremer et al. could rule out homologous associations between human chromosomes 18 and 19 in lymphocytes and fibroblasts as well as between centromeric regions of #1, #3, #4, #7, #8, #15, #17, #18 and #Y in amniotic fluid cells (Cremer et al. 2001). Bolzer et al went even a step further by visualizing all 46 chromosomes simultaneously in male human fibroblasts using a combinatorial labeled WCP probe set (Bolzer et al. submitted). Their data presented a highly variable position of homologous and heterologous CTs.

Nagele et al. argued as well against a somatic pairing of homologous chromosomes both in mitotic (Nagele et al. 1995) as well as in quiescent cells (Nagele et al. 1999), but in the same time favoring another kind of non-random side-by-side distribution that goes even further than the phenomenon of homologous association. They proposed an arrangement of chromosomes in which all homologues would be topologically separated according to their parental origin (see below).

Taken together in mammalian/vertebrate cells a general pairing of homologous chromosomes along their complete length similar to many cell types in *Drosophila* seems not to be very likely. Nevertheless, it cannot be ruled out that transient and/or cell type specific associations of homologous regions especially of centromeric regions take place, which might have important functional implications.

Besides a somatic pairing of homologous chromosomes, several other non-random side-by-side distributions of CTs have been proposed for mammalian cells, some of which are presently discussed very controversially.

Nagele et al. for example presented a vehemently debated hypothesis concerning the organization of human chromosomes in the prometaphase rosette (Nagele et al. 1995). Applying FISH with WCP probes for #7, #8, and #16 and centromeric probes for #1, #9 and #X on prometaphase stages of human fibroblasts they showed that all analyzed homologous chromosomes were separated by an average angle of 144°-166°. Since they did never observe an angle smaller than 90° they concluded that homologous chromosomes would be arranged on separate halves of the rosette possibly according to their parental origin. Moreover, the arrangements between both halves appeared to be organized in an antiparallel fashion as revealed by the arrangement of several sets of heterologous chromosome pairs. The finding that #X and #16 were found to be associated both in rosettes and in interphase nuclei, let them assume that the side-by-side organization in prometaphase would be maintained during mitosis until the subsequent interphase.

This concept was additionally supported by several subsequent studies, one of which showed a similar prometaphase arrangement for homologous chromosomes 7, 11, 21 and 22 and a tripartition of rosettes in triploid cells (Nagele et al. 1998). This line of evidence was backed up by the results of Koss et al., who showed that in the majority of human bronchial cell nuclei chromosome 1, X and 7 homologues were separated by angles between 148° and 157°, which were almost identical to those described by Nagele et al. in prometaphase rosettes of human fibroblasts (Koss 1998). Investigating quiescent human fibroblasts Nagele et al. described a non-random positioning of chromosomes 7, 8 and 16 in diploid and of #Y in triploid cells and demonstrated a preferential juxtaposition of #11 and #8 in prometaphase rosettes as well as in interphase nuclei, confirming the idea of a distributional continuity between both cell cycle stages (Nagele et al. 1999). As a possible mechanism to ensure a reproducible positioning of chromosomes over several mitotic cycles Nagele et al. suggest a permanent association of chromosomes over the whole cell cycle (Nagele et al. 1995). Such a continuous association of chromosomes appears very unlikely as shown in an *in vivo* bleaching study by Walter et al. (Walter et al. 2003). HeLa cells having fluorescently labeled chromatin by incorporation of a histone H2B-GFP fusion protein were bleached, such that only a small but coherent fluorescent region was left. Following mitosis, this formerly coherent entity was redistributed into several separated patches, clearly arguing against a stable association of chromosomes during subsequent cell cycles.

Findings contradictory to those of Nagele et al. concerning the organization of the prometaphase rosette (Nagele et al. 1995) were presented by Allison and Nestor, who analyzed the relative positions of all human chromosomes in different mitotic stages of primary lymphocytes and fibroblast cell lines using FISH with chromosome specific centromere and painting probes. In all three analyzed cell types inclusive the one used by Nagele et al. the relative positions of homologous chromosomes appeared to be random. The measured angles were as often smaller than 90° as they were larger, which is clearly inconsistent with the results of Nagele et al.. Similarly Bolzer et al. could show a random side-by-side orientation of homologous chromosomes in prometaphase rosettes of human fibroblasts by using an M-FISH approach (Speicher et al. 1996), visualizing all chromosomes simultaneously (Bolzer et al. submitted).

Another important type of a non-random side-by-side distribution that was proposed in a functional context is the preferential association of chromosomes known to be involved in translocations that are frequently observed in cancerogenesis. Applying FISH with WCP probes Parada et al. demonstrated an association of two translocated chromosomes involving #12, #14 and #15 material in a mouse lymphoma cell line (Parada et al. 2002). Interestingly in splenocytes and other cell types lacking this rearrangement, “normal” chromosomes 12, 14 and 15 were found frequently in a triplet cluster, suggesting a conservation of the relative positioning of these chromosomes between cells with and without rearrangements. They also found non-random spatial positioning of these chromosomes at mitotic stages of lymphoma cells and splenocytes, indicative that a non-random side-by-side distribution might be propagated through successive cell divisions, as proposed in the model by Nagele et al. (Nagele et al. 1995). Roix et al. investigated specifically the distribution of genes that are known to be frequently involved in lymphomas and found a statistically significant correlation between the translocation frequencies observed in the respective B-cell cancers and the spatial proximity of these genes in normal lymphoblasts (Roix et al. 2003). They concluded that the spatial proximity of specific genes, which results from a higher order compartmentalization of the nucleus contributes to the high incidence of translocations observed in certain types of malignant cells. The observed cell type specificity of the phenomenon is suggested to be due to alternative arrangements of the respective sequences. Utilizing an M-FISH approach, thereby visualizing all 46 human chromosomes simultaneously, Cornforth et al. investigated the relative interphase position of chromosomes by irradiating lymphocytes and analyzing the frequencies of translocation products. The idea behind this experimental set up is that the spatial proximity between two chromosomes can be deduced from the frequency of translocation events between them. Their results support a general randomness in the side-by-side positioning of all autosomes except for a small group of chromosomes exhibiting an increased clustering. This deviation was explainable by the non-random radial distribution of a group of chromosomes (1, 16, 17, 19 and 22), which had been previously described to be located more in the nuclear interior (Boyle et al. 2001).

Alcobia et al. presented indications for a non-random, cell type specific association of human centromeric regions in chromocenters¹. Using FISH with centromere probes for individual chromosomes they found that chromocenters were composed of non-random combinations of specific chromosomes and that the compositional pattern varied in a cell type specific manner between myeloid cells, lymphoid cells and fibroblasts (Alcobia et al. 2000).

Taken together, a predetermined positioning of chromosomes in the interphase nucleus of mammalian cells appears very unlikely, most convincingly shown by the high variability of the side-by-side distribution of CTs observed in most of the analyzed cell types. Nevertheless, the present data leaves enough space for cell type specific and/or transient associations of specific sequences that might have functional implications in terms of a transcriptional/topological relation or that might be involved in the formation of potentially carcinogenic translocations.

1.4 Euchromatin-heterochromatin

In the following, a coarse sketch of the chromatin field is attempted. Regarding the limited time and space of the present thesis, it will be not more than a low resolution map of an ex-

¹ Chromocenters are clusters of centromeric heterochromatin belonging to different chromosomes. The term dates back to a work by Baccarini in 1908, who used it to name big aggregates of “chromatin”, which he mainly found in differentiated tissue of the Maltese mushroom *Cynomorium coccineum* L. (Baccarini 1908).

tremely vast area that is constantly growing at an elevated pace. The high frequency of new findings in this scientific field is reflected by the short time periods between the publication of new review articles that, due to the bulk of new information, focuses on rather restricted chromatin aspects, such as on one specific modification of one specific histone at one position etc.. Concerning the abundance of new results in this field, it should also be added that many of the current findings and their interpretations still have to be considered as preliminary. One example illustrating the complexity of chromatin diversification and the limitations that can be sometimes posed by antibody specificity used to investigate such chromatin modes regards the methylation of histone H3 at lysine residues. Antibodies initially raised against methylated peptides resembling the lysine 9 position of histone H3 did not discriminate between differential methylation statuses, especially between the di- and tri-methylated histones and consequently were unable to resolve distinct methylation pattern. Additionally these antibodies recognized similar motifs at other histone H3 and H4 positions, additionally reducing their specificity (Perez-Burgos et al. 2004). Since this cross reactivity regarded epitopes with different biological consequences in respect to transcriptional regulation, many results obtained by applying these antibodies had to be reconsidered in the light of these new circumstances.

In the following, I will try to outline the present transition in the characterization of chromatin, from the traditional dualistic concept of eu- and heterochromatin as introduced by Heitz in the 20's of the 20th century to the molecular definition of chromatin according to its components and in relation to its functional implications. Therefore, I will introduce some of the most relevant protein components and its modifications as well as the phenomenon of DNA methylation and some of its associated proteins. Finally, I want to briefly sketch the basic properties of centromeric/pericentric heterochromatin since it presented an important object of investigation in the present thesis.

1.4.1 Past to present: a brief look on the history of chromatin

In 1928 Heitz introduced the terms “heterochromatin” and “euchromatin”, which he used according to the existing terms “heterochromosome” and “euchromosome” to describe chromosome portions which remained in a mitotic, condensed state in the interphase nucleus as revealed by staining with carmine acetic acid and light microscopy (Heitz 1928). However, the discrimination of differentially stained nuclear entities was described already decades before. In fact, already 1882 Flemming had described nuclear structures, which he had made visible using aniline dyes and which he consequently named “chromatin”, derived from the Greek word for color (Flemming 1882). The observation that chromatin would build thread-like structures before cell division¹ moreover prompted him to name the process “mitosis” following the Greek term for thread. In the beginning of the 20th century Heidenhain described a tissue-specific appearance of nuclear structures which he had visualized utilizing basic and acidic dyes (Heidenhain 1907).

The particularity of “heterochromatin” as described by Heitz was that these chromosome portions, which he visualized by carmine acetic acid in fixed (ethanol:acet. acid 2:1) moss thallus cells would not become invisible after mitosis as the rest of mitotic chromosomes did, but instead remained visible in the interphase nucleus. This phenomenon had been described before for the sex chromosomes in some animal species and had been termed “heteropyknose” (Heitz 1928). Although it was speculated that compared to euchromatin, heterochromatin would represent a more condensed state, equivalent to that of mitotic chromosomes, there were effectively no clues on the physical nature of this intensely stainable nuclear chromo-

¹ Similar observations of this phenomenon were described before by Schneider, Bütschli and Strassburger, but without staining of the specimen (Cremer 1985).

some regions. Experiments using radioactively labeled thymidine analogs to visualize replicated DNA, together with photometric measurements of Feulgen stained nuclei in grasshopper and rye revealed that heterochromatin contained 2-3 times more DNA per unit area, which supported the initial idea of a higher density of heterochromatin (Lima De Faria 1959). Electron microscopic approaches are also able to discriminate between denser chromatin localized at the nuclear periphery and around nucleoli and less dense chromatin distributed in between, but to what extent these structures are equivalent to heterochromatin and euchromatin as defined by light microscopic means is still unresolved.

In terms of genetic activity, Heitz suggested that heterochromatin should be inert as it corresponded to a conformation equivalent to divisional chromatin, which was postulated to be inactive according to ideas of Boveri and Roux (cited in (Brown 1966)). This was later substantiated by findings in *Drosophila*, showing that loss of the mostly heterochromatic Y chromosome did not affect normal fly development, except for the sterility of affected flies (see {Brown, 1966 #877}).

In the following decades, the dualistic principle of eu- and heterochromatin was beginning to become too narrow to suffice the dynamic properties chromatin appeared to have. Instead of a structural or morphological definition of chromatin a more dynamic one was proposed, defining chromatin rather as a "...state, than a substance..."¹. The term "facultative" heterochromatinization introduced 1966 by Brown implements the idea that "...all chromosome regions are potentially capable of becoming heterochromatic..."¹ {Brown, 1966 #877}. 1961 Grundmann and Stein formulated (translated from German): "...In the past 20 years the definition of this chromatin dualism has become more and more difficult. ..., the necessity of a subdivision in eu- and heterochromatin at all has become controversial. ... So today, the difference between eu- and heterochromatin as a mere variation of states has been clearly recognized. ..." (Grundmann and Stein 1961). Today more than 40 years later the terms eu- and heterochromatin are still in use, actually they can be found in every textbook dealing with chromatin; clear definitions though are still absent. A current approach is to expand the concept of the originally dichotomous subdivision of chromatin, in order to define chromatin states on a molecular level. An important breakthrough for this to develop was the disclosure of the fundamental structure of chromatin, the nucleosome. This smallest chromatin subunit is a nucleo-protein complex consisting of four different so-called core histones (present in two sets) with DNA wrapped helically around it (reviewed in (Olins and Olins 2003); see below). Based on this groundwork many studies have demonstrated an intriguing modifiability of this basic chromatin unit in terms of covalent modifications. The observation that these modifications can be present in various combinations, having distinct effects on nuclear functions plus the findings that various histone variants are utilized in a site and cell function dependent manner led to a model called the "histone code hypothesis" (Strahl and Allis 2000). The idea behind it is that a combination of specific chromatin modifications is used by a nuclear "translation apparatus" composed of specific "effector" protein and protein complexes that interpret this "code" influencing various nuclear functions, such as transcription, replication or mitosis.

Besides such a variability concerning histone composition and modification also DNA methylation and its interacting proteins have been shown to contribute to the definition of functionally distinct chromatin states. The so-called non-histone proteins like HP1, polycomb or trithorax group proteins (see below) constitute another level of chromatin characterization. Together with histones, histone modifications and DNA methylation they constitute an interdependent network that is responsible for fine tuning specific functional chromatin states.

¹ Quatations taken from (Brown 1966).

1.4.2 Proteins and chromatin

The nucleosome, the “basic” unit of chromatin, is composed of an octamer built by the 4 different core histones, H2A, H2B, H3 and H4 each present in two copies, around which a 146bp long stretch of DNA is coiled, equaling ~1.7 left-handed superhelical turns (Grigoryev 2004). Longer DNA stretches isolated under low salt conditions have been shown to consist of linearly aligned nucleosomes with a variable DNA linker inbetween ranging from 10-90bp (Richmond and Davey 2003). Using electron microscopy it has been demonstrated that such isolated nucleosome arrays arrange in a “beads-on-a-string” conformation (Olins and Olins 1974) also known as the 10 or 11nm fiber¹. At or near the DNA entry-exit site of the histone octamer the linker DNA can be optionally associated with so-called linker histones like H1 or related proteins. Binding of linker histones was shown to be essential for a further compaction of the “beads-on-a-string” structure *in vitro*, which results in a mixture of higher order conformations, of which the most compact form is a so-called solenoid structure or 30nm fiber¹ (Horn and Peterson 2002). It has to be added though, that this first level of higher order organization of chromatin has not yet been evidenced to exist *in vivo*. Especially if it exists as an orderly superhelical structure extending over long stretches or rather represents an irregular array of alternating condensed and open states is still a matter of debate (see e.g. (Horn and Peterson 2002)). Higher order structure beyond the 30nm fiber is even more obscure, although some concrete candidate models as the loop domain model are currently discussed (see e.g. (Cook 2001)).

The fact that histones can be modified by covalently bound chemical groups is actually known since the 60s of the 20th century; in fact Allfrey et al. demonstrated already 1964 that histone acetylation influenced transcriptional activity *in vitro* (Allfrey et al. 1964). Lately however it has become clear how manifold the modifications actually can be. Besides an elevated number of modifying chemical groups, there are numerous amino acid residues mainly at the N terminal ends of histones acting as potential acceptors. These N-terminal “tails” are remarkably rich in positively charged amino acids like lysine or arginine, which interact with the DNA backbone as well as with core regions of nucleosomes, thereby leading to chromatin compaction. These residues are often affected by covalent modifications resulting in an alteration of the net charge of the tails and hence to a change of their interaction capacity. It has been shown that some functional groups can be present in multiple copies on one single amino acid, which additionally increases the complexity of possible histone modifications. In summary, such modifications can be present on different amino acids, on different histones including distinct functional groups and some of them at a varying degree. This manifoldness that allows many different combinatorial labeling themes of chromatin, together with the fact that many specific modifications have been shown to convey distinct nuclear function led to the formulation of the so-called “histone code hypothesis” (Strahl and Allis 2000). As already noted above, the idea is that concrete combinations of histone modifications are specifically “translated” by effector complexes in the context of various nuclear functions including replication, transcription, mitosis, DNA repair etc. It should be added though, that the functions of many of these chromatin alterations are still not resolved. On the other hand, acetylation and methylation have been studied very extensively, and were shown to act in an intricate combinatorial way exerting a regulatory influence on transcription. In the following, the histone modifications known to date are shortly introduced.

Modifications of histones are mainly found in the N-terminus, which in contrast to the central part is said to lack a structured conformation (van Holde et al. 1995). **Acetylation** and methylation of histones was already described in the 60s of the 20th century (Allfrey et al. 1964). The modification of histones with acetyl groups affects lysines at the N-terminus of histones

¹ The value refers to the diameter of the structure.

H3 and H4 and is accomplished in a dynamic fashion by enzymes termed histone acetyltransferases (HATs) and histone deacetylases (HDACs). Acetylation has long been considered to favor transcription by “opening” chromatin via neutralization of the lysines’ and arginines’ positive charges, thus weakening the potential interaction of the histone tails with the negative charges of the DNA backbone and with core histones, thereby preventing a tight packaging of chromatin. This chromatin opening is supposed to increase the DNA binding probability of factors that are relevant for transcription. Phosphorylation of histone serine residues is thought to act similarly, but beyond neutralizing positive charges, phosphate groups actually introduce additional negative charges, which could open chromatin via repulsive forces towards negatively charged phosphates on the DNA backbone. Besides this role in relaxing the condensation state of chromatin by a charge-dependent mechanism, acetylated lysines have been shown to be specifically bound by proteins harboring a conserved motif called the bromodomain (reviewed e.g. in (Strahl and Allis 2000)). What is more, acetylated amino acids at different positions of H3 or H4 have been demonstrated to interact specifically with different bromodomain containing proteins, arguing that histone modifications act position and context specific, which strongly supports the histone code model (see citations in (Iizuka and Smith 2003)). According to a data base query (Jenuwein and Allis 2001), more than 75 bromodomain proteins are estimated to exist in humans, including members of various protein families like transcription factors or chromatin remodeling complexes (Jenuwein and Allis 2001). This high incidence of bromodomain bearing proteins argues for a high binding specificity of such effector proteins (Jenuwein and Allis 2001), that probably depends on the amino acid context of the acetylated lysine, i.e. its position within the histone, the histone type, modifications of adjacent amino acids etc.. In addition to its involvement in transcriptional regulation histone acetylation has been shown to play a role in DNA double strand break repair (see citations in (Iizuka and Smith 2003)). Histone deposition and chromatin assembly during S-phase is a further nuclear function where histone acetylation might play a role, as in *Drosophila* specifically acetylated lysine residues of histone H4 have been shown to associate with a chromatin assembly complex called RCAF (see citations in (Iizuka and Smith 2003)).

In contrast to acetylation and phosphorylation, **methylation** of histones does not greatly affect the charge of the modified amino acid (Strahl and Allis 2000). Methylation affects mainly N-terminal lysines (Lachner et al. 2003) and arginines (Stallcup 2001) of histones H3 and H4. An important observation already in the 60s of the 20th century was that single lysine residues in histones could carry one two or three methyl groups (reviewed in (DeLange and Smith 1971)). However, only recently it has been demonstrated that the degree of methylation has biological implications in terms of transcriptional regulation (Santos-Rosa et al. 2002). Histone methylation has been found to be associated with both transcriptional activation and silencing. Lysines at position 4 and 36 of histone H3 as well as arginine methylations appear to be implicated in transcriptional activity, while lysine 9 and 27 on H3, as well as lysine 20 on H4 appear to be involved with silencing (Peters et al. 2003). The decision whether a methylated lysine interacts with effector complexes that either stimulate or repress transcription is apparently dependent on the position of the modified amino acid, the degree of methylation as well as on the combination with other modified amino acids. In a recent paper by Su et al., they describe a detailed temporal change in combinatorial histone modifications accompanying the heritable silencing of the *Dnmt* gene during thymocyte maturation (Su et al. 2004). The authors show that upon inactivation of the *Dnmt* gene the promoter region is initially deacetylated at H3K9 (K=one letter amino acid code for lysine; H3=histone H3), as well as demethylated on H3K4; i.e. in a first step the modifications that are associated with transcriptional activity are removed. This is followed by an extended methylation of histone H3 at lysine 9, which is considered a hallmark of silent chromatin. The spreading of these modifications roughly 10kb up- and downstream of the promoter region appeared to be cor-

related with the heritability of the transcriptional repression. In general transcriptionally permissive euchromatic regions are thought to be mono- or di-methylated at the “repressive” residues K9 and K27 on H3, while constitutive heterochromatin like pericentric regions are enriched in H3K9 tri- and H3K27 monomethylation (Peters et al. 2003) and as shown recently in H4K20 tri-methylation (Kourmouli et al. 2004; Schotta et al. 2004). H3K4 in *Saccharomyces cerevisiae* is found to be di-methylated in active and inactive euchromatic genes, while the tri-methylated state is found exclusively in actively transcribed genes (Santos-Rosa et al. 2002). It should be noted that differential enzymes are involved in setting the methylation marks in eu- and heterochromatin. Mammalian G9a for example has been shown to be important for global di-methylation of H3K9 in euchromatin, while Suv39h1/2 are mainly responsible for setting the tri-methylated marks on H3K9 (Peters et al. 2003; Rice et al. 2003). Much more lysine HMTases or potential HMTases bearing the characteristic and evolutionary conserved SET domain¹ are known in mammals to date, though most of them still lack a detailed characterization (Lachner and Jenuwein 2002). Lysine methylation appears to be also involved in cellular/transcriptional memory, a phenomenon, which describes the maintenance of a cell type specific transcription program during development. Polycomb-group (Pc-G) proteins and trithorax-group (trx-G) proteins are important players in cellular memory involved either in heritable gene silencing or in keeping a transcriptionally permissive state, with several members having a histone methyltransferase (HMTase) activity (reviewed e.g. in (Orlando 2003; Pirrotta et al. 2003)). The Pc-G protein [E(z)] (*enhancer of zeste*) for example shows specificity for H3K9 and K27 di-, tri-methylation, i.e. for repressive positions. Trx-G HMTases on the other hand have been shown to either dimethylate H3K4, a transcriptionally stimulating residue, or to combinatorially methylate H3K4, H3K9 and H4K20, thereby recruiting a coactivator and preventing the binding of repressive proteins like HP1 (see citations in (Lachner et al. 2003)). X-inactivation in female mammals, the probably most prominent example for the formation of facultative heterochromatin is also correlated with a specific set of lysine methylations that is distinct from constitutive heterochromatin. Investigations with highly specific antibodies have revealed that the inactive X (X_i) is highly enriched for tri-methylated H3K27, while K9 is mainly di-methylated (Plath et al. 2003). This lack of apparent H3K9 tri-methylation could also explain the lack of HP1 α and β at the inactive X chromosome (Cowell et al. 2002; Peters et al. 2002). In contrast, in constitutive heterochromatin like at pericentric sites histone H3 is mainly tri-methylated at K9 and monomethylated at K27 (Peters et al. 2003). Apart from the lysines mentioned above, which are all situated at the N-terminal tail domain, H3K79 is a “methylatable” lysine residue that lies within the histone core domain. In budding yeast it was shown to be involved in silencing at telomeres, at the silent mating-type loci, as well as of rDNA genes (see citations in (Iizuka and Smith 2003)). Interestingly this residue is modified by an HMTase (Dot1), which lacks the characteristic SET domain. Whether H3K79 methylation is enriched in eu- or heterochromatin is still a matter of debate (Ng et al. 2003). Recent findings in *Neurospora crassa*, *Arabidopsis thaliana* (see citations in (Lachner et al. 2003)) and in mice pericentric satellite regions (Lehnertz et al. 2003)) have suggested that H3K9 methylation could trigger DNA methylation. However, findings by Fuks et al. argue for the existence of dependence also in the opposite direction, as he could demonstrate the recruitment of an HMTase activity by MeCP2, which is a protein that binds specifically to methylated CpGs in the DNA (Fuks et al. 2003). Most probable histone and DNA methylation affect each other mutually (Geiman and Robertson 2002). In contrast to acetylation and phosphorylation, no enzyme has yet been detected that is able to remove methyl groups from modified histones.

¹ “SET” is derived from the following methyltransferases bearing such a motif: Su(var)3-9, a suppressor of PEV in *Drosophila*, Enhancer of zeste, a Polycomb-group protein, and Trithorax, a trithorax-group protein

Although clipping of the modified tail could account for a “radical” removing of the modification, histone replacement appears to be the mechanism that is used to “get rid” of methyl marks. In *Drosophila*, Ahmad and Henikoff could show that the histone variant H3.3 is used in a replication independent fashion to replace the major H3 variant at various loci including actively transcribed rDNA genes (Ahmad and Henikoff 2002). In a subsequent study from the laboratory of Henikoff, McKittrick et al. showed that H3.3 is relatively enriched in histone modifications, which favor transcriptional stimulation (McKittrick et al. 2004), whereas H3 was relatively enriched for “silent” modifications. The lack of a direct and dynamic mechanism to remove the methyl mark via an enzymatic reaction could be interpreted that histone methylation represents a rather long-term epigenetic regulator.

Phosphorylation as a covalent modification has been shown to occur mainly at serine residues of histones H1 and H3. It appears to be associated with chromatin condensation during mitosis, as well as with chromatin relaxation during transcriptional stimulation (Iizuka and Smith 2003). This apparent antagonism between condensation and decondensation caused by the same functional group can be explained as noted above for lysine methylation, by selective effects depending on the position of the modified residue as well as on the combination with other histone modifications, which allows the recruitment of different sets of effector proteins. Phosphorylation of serine 10 of histone H3 has been shown to correlate with the activation of the so-called immediate-early genes (*c-fos*, *c-jun*, *c-myc*), which are important for cell cycle re-entry of quiescent mammalian cells (Strahl and Allis 2000). As already noted H3S10 phosphorylation is supposed to play a role in dosage compensation in *Drosophila*, in combination with acetylation of H4 residues (Strahl and Allis 2000). Transcriptional stimulation via H3S10 is thought to be exerted by an interaction with histone acetyl transferases (see citations in (Iizuka and Smith 2003)). A possible switch between on-off states of genes could be accomplished via a H3S10 phosphorylation-H3K9 methylation mechanism, since transcriptionally stimulating and repressing marks on both positions appear to be mutually inhibiting (Jenuwein and Allis 2001). An alternative concept to the histone code hypothesis concerning transcriptional activation through histone-phosphorylation has been suggested from studies in *Tetrahymena*, where the authors found that a local increase of negative charges in the linker histone H1 increased the dissociation rate from chromatin, which could increase chromatin decondensation thereby causing augmentation of transcription levels (see citations in (Iizuka and Smith 2003)). Whether this so-called “charge patch” mechanisms does also account for core histone modifications, and to what extent it acts alternatively or additionally to histone code defined mechanisms is still a matter of ongoing investigation. H3S10 and H3S28 phosphorylation has been shown to correlate with mitotic chromosome condensation in various species (see citations in (Berger 2001)). Mutational analyses in *Tetrahymena* argue strongly that H3S10 phosphorylation plays a pivotal role for proper mitosis (see citations in (Berger 2001)). Mechanistic details though concerning the implication of histone phosphorylation in chromatin condensation are still not known. A further line of action for histone phosphorylation seems to be DNA-damage repair. It has been shown that the histone variant H2AX, which represents ~11% of chromatin bound H2A proteins (West and Bonner 1980) is phosphorylated at a C-terminal serine residue as a response to double strand breaks (DSBs), giving rise to the so-called γ -H2AX form (Redon et al. 2002). This histone modification was shown to be crucial for the recruitment of proteins involved in DSB repair (see citations in (Iizuka and Smith 2003)).

Although **ubiquitination** of proteins is a well-studied phenomenon involved in cellular protein degradation, its role as histone modifier is still not very well understood. Its major targets seem to be lysine residues on histone H2A and H2B (van Holde et al. 1995). Both, an involvement in transcriptional silencing as well as in activation have been reported. In budding yeast ubiquitination of H2BK123 was shown to be required for H3K4 methylation as well as for H3K79 methylation by Dot1 (see above), the latter arguing for an indirect participation in

gene silencing. In *Drosophila*, on the other hand ubiquitination of histone H1 by the coactivator TAFII250, a subunit of the transcription factor TFIID, was shown to correlate with transcriptional activation (Pham and Sauer 2000).

Just recently a new histone modifying molecule was reported to be associated with transcriptional silencing, **SUMO**. The **small ubiquitin-related modifier** (SUMO) had previously been described as a non-histone tag, where it is thought to be involved in various cellular functions including protein-protein interactions and protein localization. SUMOylation of histone H4 (the exact position of the accepting amino acid has not yet been determined) was shown to mediate transcriptional repression via HDAC and HP1 γ recruitment (Shiio and Eisenman 2003).

A histone modification that is often not included in the concept of the “histone code” is **poly(ADP-ribosylation)**, as its function initially appeared to be restricted to the detection and signaling of DNA damages (Rouleau et al. 2004). The modification, which is not only restricted to histone proteins but also occurs on other nuclear proteins like HMG (high mobility group) proteins, lamins, topoisomerases and others, is targeted to glutamate residues (γ -carboxyl group) and affects mainly histones H1, H2A and H2B. As indicated by the name a long ADP-ribose polymer is added to the relevant amino acids utilizing NAD⁺ as ADP-ribose donor; those polymers can comprise up to 200 units and can be linear or branched. The consequence of adding many negatively charged ADP-ribose molecules, is that the affected chromatin components like histones lose their affinity to bind DNA and consequently dissociate (Rouleau et al. 2004). Thus an important function that has been assigned to poly(ADP-ribosylation) is to relax/open chromatin, which is an important prerequisite for many nuclear functions such as DNA repair, replication, transcription, recombination etc. (Rouleau et al. 2004). Poly(ADP-ribosylation) is a dynamic process that is accomplished by poly(ADP-ribose) polymerases (PARPs) and can be reverted by poly(ADP-ribose) glycohydrolase (PARG). Apart from a covalent modification of histones with poly(ADP-ribose), auto poly(ADP-ribosylation) of PARP has been suggested to act in a histone shuffling mechanism via non-covalent interactions with unbound histones. The proposed mechanism implies that histones, which are released from sites of DNA repair, replication or transcription, are sequestered at the poly(ADP-ribose) through electrostatic interactions of the positively charged histones with the negative charges of the ADP-ribose polymer; for the reconstitution of chromatin, sequestered histones could be released again by PARG dependent cleavage of the polymer. Site specificity of this process could be accomplished via specific cues for PARP activation as has been shown to happen at DNA strand breaks (see (Rouleau et al. 2004) for a discussion of the model).

This brief overview illustrates how manifold and complicated combinatorial histone modifications can actually be. Considering additionally the utilization of histone variants (see below) it appears conceivable that a histone code of this kind could indeed be responsible for a fine tuning of gene regulation. The stability of some histone modifications like methylation marks could account for stable epigenetic labels, which are necessary not only for permanent silencing of genes during development and differentiation, but also of mobile genetic elements in order to assure genome integrity. On the other hand, the histone code appears sufficiently dynamic to allow switches of transcriptional programs necessary to change transcriptional programs during differentiation, as apparently revealed by the Pc-G/Tx-G system.

Linker histones play a crucial role in establishing/stabilizing the next level of higher order chromatin structure beyond the beads-on-a-string conformation. Although they share no sequence or structural homology to core histones they were named so according to their isolation along with the core histones (see citations in (Kornberg and Lorch 1999)). *In vivo* linker histones are usually found at a stoichiometry of ~1:1 per nucleosome (Hansen 2002). *In vitro* the presence of linker histones is essential for the formation of the 30nm or solenoid struc-

ture (van Holde et al. 1995), although the existence of such a regular solenoid *in vivo* is still controversially debated, just as are further structural details concerning a higher order conformation (Adkins et al. 2004). Linker histones as well as core histones (except H4) are present as protein families comprising variant and invariant forms, with some of the variants exerting specific functions (discussed later) (Brown 2001). In mammals there are 6 somatic linker/H1 histones and two germ line specific variants (see citations in (Alami et al. 2003)). Linker histone proteins usually have a short N-terminal and a long C-terminal tail that harbors many positively charged amino acids, like lysines and arginines. The central globular domain associates with the nucleosome, whereas the interactions can be at various sites (Adkins et al. 2004). Linker histones localize near the entry/exit site of the DNA at the nucleosome, thereby comprising a structure referred to as the “chromatosome”, which includes an additional variable stretch (10-90bp) of linker DNA. As revealed by *in vitro* studies on nucleosomal arrays, high salt concentrations appear to be sufficient for the formation of higher order structures including solenoid stretches and associations of individual oligonucleosomes. In the presence of linker histones however, condensation appears more complete achieving a maximally folded state also at lower salt concentrations (see citations in (Hansen 2002) and (Horn and Peterson 2002)), thus suggesting a stabilizing mode of action. The capacity for higher order folding thus appears to be inherent in the nucleosomal structure with a high concentration of cations enabling a tighter packing through neutralization of negative charges on the DNA backbone. Linker histone binding appears, moreover, to reduce the sliding capability of histone octamers *in vitro*, which *in vivo* might be important to increase accessibility of promoter or enhancer sequences (see citations in (Adkins et al. 2004)) for appropriate proteins. A dynamic implication of histone H1 in transcriptional regulation was demonstrated in *Tetrahymena*, where it was shown that upon phosphorylation of H1 its dissociation from the DNA was increased, thereby phenocopying¹ a loss of H1 (Dou et al. 2002). H1 appears also to contribute to the histone code since it was shown that ubiquitination by the coactivator TAFII250 in *Drosophila* correlates with transcriptional activation (Pham and Sauer 2000) (see also above).

As already mentioned, higher organisms exhibit non-allelic isotypes of all histones except for H4, so-called **histone variants**, which are encoded by separate genes (reviewed e.g. in (Brown 2001)). These can code for identical proteins, for slightly altered ones or as in some cases for highly divergent ones. In the following, a few of the better-understood examples for histones H1, H2A and H3 are presented. **Linker histones** especially in mammals show a high number of variant genes. In mice at least eight different H1 genes are known. Besides six somatic forms, named H1a-e and H1⁰ (also referred to as replacement linker histone (Alami et al. 2003)) two germ line specific variants are known, one in the male, H1t (for testis) and one in the female H1oo (for oocytes). From *in vitro* studies it has been suggested that H1t induces relaxation/opening of chromatin, which is hypothesized to facilitate recombination during meiosis or the removal of histone during sperm maturation since in mature spermatids histones are replaced by protamines (Walbot and Holder 1987). However, mice lacking H1t showed normal viability and fertility, arguing for the existence of a compensation mechanism. Similarly, knockouts of each of the six somatic H1 isotypes revealed no aberrant phenotype, although the individual H1 variants are expressed in a tissue and development/differentiation specific manner (Brown 2001). This argues that the loss of one isotype can apparently be compensated by another; at all developmental stages and in all tissues. On the other hand, a triple knockout of H1c-e caused a reduced H1/nucleosome ratio of 1:2 instead of 1:1 resulting in embryonic death (see citations in (Brown 2001)). Following this finding, it could be argued that linker histone variants might be important to maintain a cor-

¹ phenocopying=resulting in the same phenotype

rect stoichiometric balance, but are in effect functionally redundant. Yet, Alami et al. observed subtle changes in the transcriptional activity of a reporter transgene upon selective loss of individual H1 isotypes (Alami et al. 2003). The authors used mice carrying transgenic reporters that exhibited variegated expression due to position effects exerted by the integration site. Upon loss of individual H1 isotypes, the authors observed subtle changes in the expression pattern that depending on the lost histone variant was either enhanced or attenuated. According to this finding, the authors proposed that H1 isotype composition might represent a transcriptional fine-tuning mechanism. Similar properties of individual H1 variants were proposed by another group, which used a chromatin immunoprecipitation approach with H1 isotype specific antibodies and found a selective enrichment of specific isotypes at actively transcribed or inactive genes (Parseghian et al. 2000).

H1⁰ is the most divergent H1 variant (~60% compared to H1a) and is mainly expressed in terminally differentiated cells (van Holde et al. 1995). The avian homolog H5 is believed to play an important role in the heterochromatinization of avian erythrocytes, which finally leads to a complete cessation of transcription (van Holde et al. 1995), although apparently other proteins are involved (Grigoryev and Woodcock 1993). It has been shown that if H1⁰ is overexpressed in cultured cells the steady state level of RNA polymerase II (pol II) transcripts is reduced, supporting the view that it is involved in transcriptional attenuation (see citations in (Brown 2001)). Overexpression of H1c on the other hand was shown to lead to a dramatic increase of pol II transcripts, although not in all cells (see (Brown 2001)).

A clear-cut example for a transcriptional control by the specific utilization of variant H1 proteins is the regulation of the 5S rRNA genes during *Xenopus* embryogenesis. Here the developmentally regulated expression of an oocyte 5S rRNA vs. an adult form was shown to be switched upon expression of adult H1 that replaced the early stage H1M variant and selectively impeded transcription factor binding and consequently transcription from the oocyte locus. In contrast to the oocyte 5S rRNA gene, the adult gene showed a higher binding affinity to the transcription factor than to the adult H1 isotype (discussed in (Brown 2001)), and was consequently transcribed.

An important histone variant of **H3** that is found from yeast to mammals is CenpA, which is localized predominantly in centromeric regions (Brown 2001). A big part of its carboxy terminus shows more than 60% sequence identity to H3 while its N-terminus comprising 47 amino acids is not related to H3. Translation of CenpA mRNA has been shown to be co-regulated with the replication timing of centromeric regions during mid/late S-phase (Brown 2001), and this translation timing turned out to be critical for its correct sub-chromosomal targeting (see citations in (Brown 2001)). CenpA was demonstrated to be essential for mammalian development since knock out mice died early during embryogenesis (Howman et al. 2000). CenpA deficient embryos showed severe defects in the organization of centromeres as well as in chromosome segregation.

Another important H3 variant is H3.3. As already noted above, in contrast to H3, H3.3 can be deposited independently of S-phase since it has been demonstrated to become enriched in nuclei of non-replicating cells (see citations in (Ahmad and Henikoff 2002)). Studies in *Drosophila* have shown that the H3.3 variant, which varies only in 4 amino acids from the bulk H3 is enriched for covalent modifications that according to the histone code model are associated with transcriptional activity (McKittrick et al. 2004). H3.3 could well be involved in a mechanism to remove transcriptionally repressive histone H3 methyl marks by replacing modified H3 since so far no enzymes have been detected that can de-methylate modified histones.

In humans, a set of 16 individual genes codes for histone **H2A** variants. Ten of those, which are electrophoretically irresolvable, are summarized as the H2A1 variants. Six H2A1 variants have identical sequence, while the other four deviate in 3-4 amino acids. One isotype having a proline residue replaced by methionine and therefore exhibiting an aberrant electrophoretic

mobility is termed H2A2¹. The majority of chromatin incorporates H2A1 and H2A2 isotypes. Additional five variants, including macroH2A1, macroH2A2, H2AZ, H2AX and H2ABbd show marked differences as compared to the bulk H2A (Redon et al. 2002). The variant H2ABbd was detected only recently (Chadwick and Willard 2001). It shares only 48% identity with the major H2A isotype and its main characteristics are that it is absent from the inactive X chromosomes and that it colocalizes with acetylated histone H4 (K12) suggesting an implication in transcriptional activation.

H2AZ is found from yeast to mammals as an essential histone isoform sharing 59% identity with histone H2A. In mice, it represents ~4% of the complete H2A pool (West and Bonner 1980). Though its function *in vivo* has yet to be determined, *in vitro* it has been shown that H2AZ can modulate folding of nucleosomal arrays into higher order structures (Brown 2001). Rangasamy et al. showed that H2AZ is not expressed in mouse ES cells and that transcription is turned on after the onset of differentiation. Moreover, they showed that H2AZ is first targeted to pericentric heterochromatin followed by other genomic regions, but excluded from the inactive X (Rangasamy et al. 2003). The authors propose that H2AZ might represent a signal for a discrimination of constitutive and facultative heterochromatin during early development.

MacroH2A1 (mH2A1) and macroH2A2 (mH2A2) proteins represent special kinds of histone variants. Their size is almost thrice that of their “default” counterpart (van Holde et al. 1995). Moreover they possess a C-terminal part, that makes up more than 50% (~25 kDa) of the protein and which shares no similarity to any given histone sequence (Brown 2001). In fact, it has been suggested that mH2A could represent a fusion between histone H2A (the N-terminus exhibits 64% sequence identity to the major isotype) and another protein of yet unknown identity (van Holde et al. 1995). In a recent paper describing the crystallographic structure of macroH2A it was proposed that the large C-terminal part could harbor poly(ADP-ribosylation) activity (discussed in (Ladurner 2003)). If this would prove true, mH2A would bear two functions, a chromatin constituent on the one hand and concomitantly an enzyme, possibly involved in chromatin modification on the other. As revealed by immunofluorescence macroH2A localizes predominantly at the inactive X-chromosome both in interphase and in mitotic cells. Its localization is apparently dependent on Xist RNA (see citations in (Brown 2001)). Based on the observation that macro H2A is also found at other regions apart from X_i, together with the fact that it was also found in chickens, which lack X inactivation, it was interpreted that it could be also involved in a more general mode of transcriptional silencing (Costanzi and Pehrson 1998).

The histone variant H2AX makes up ~11% of the complete H2A protein in mice. It shows high conservation to H2A, but has a prolonged C-terminal bearing two serine residues, which are phosphorylated upon DNA double strand breaks (DSBs), although the second to a lesser extent (Redon et al. 2002). As described above, this DNA damage dependent covalent modification resulting in the so-called γ -H2AX form plays a fundamental role in the recruitment of proteins involved in DSB repair. It should be added, though, that H2AX was found to be not essential, i.e. mice lacking H2AX are viable. However, both knock out mice and cells were hypersensitive to DSB inducing agents (see citations in (Iizuka and Smith 2003)). Experiments with irradiated nuclei have revealed that γ -H2AX marked chromatin forms foci in the interphase nucleus at the position of the irradiation and that a stretch containing approximately 20MB of DNA is affected by the modification. Within that stretch however not all H2AX histones turned out to be modified (see citations in (Redon et al. 2002)).

In conclusion, the existence of such a plentitude of histone variants, many of which appear to be evolutionary conserved together with the observation that many of them exhibit distinct spatio-temporal expression profiles and/or subchromosomal specificity that correlates with

¹ The various histone genes are termed H2A A, H2A B etc. (see also (Redon et al. 2002) figure 1).

distinct nuclear functions strongly argues that the histone isotype composition of chromatin is a further constituent in defining an epigenetic state.

Beyond the association of DNA with histones, which builds the “ground floor” of, allegorically speaking, the “chromatin skyscraper”, myriads of other proteins participate in building the nucleoprotein particle we refer to as chromatin. An important characteristic of chromatin is that its composition changes dynamically according to functional demands. The group of **chromatin-associated proteins** is actually a very heterogeneous group including as diverse proteins as enzymes, high mobility group proteins, transcription factors or scaffold and/or matrix proteins (van Holde et al. 1995). The latter group is not very stringently defined and comprises proteins that are supposed to be involved in a higher order chromatin structure in meta- (scaffold) and/or interphase (matrix) chromosomes.

1.4.3 RNA and chromatin

Apart from the highly variable composition of chromatin concerning its protein constituents, an additional structural as well as functional constituent of chromatin has attracted much attention during the last decade: non-coding RNAs. RoX1/2 (**RNA on the X**), for example are two X-chromosomal non coding transcripts involved in dosage compensation in *Drosophila*, which are responsible for the formation and spreading of a chromatin remodeling complex called MSL along the male X chromosome (see (Andersen and Panning 2003)). This nucleoprotein complex coats the whole X chromosome in male flies and is responsible for creating hyperactive chromatin, supposedly via histone modifications, which is thought to be responsible for the elevated transcription levels (reviewed in (Andersen and Panning 2003)).

In a similar way, dosage compensation is achieved in mammals with the difference that the second X chromosome in females is (largely) silenced via the Xist non-coding RNA. A second non-coding RNA Tsix representing the reverse transcript of the Xist gene appears to be important for the choice of the X that will be silenced. In extraembryonic tissue of mice Xist and Tsix are inversely imprinted, with Xist being only expressed from the paternal X and Tsix only from the maternal, thereby skewing inactivation, resulting in an exclusive silencing of the paternal homolog (see citations in (Andersen and Panning 2003)).

Another example where non-coding RNA was found to play a critical role for the functional and structural integrity of chromatin is at pericentric heterochromatin in yeast and mice. In both cases bi-directional and thus complementary transcripts from pericentric satellite regions (outer repeat in yeast, major satellite in mice) have been observed (reviewed in (Maison and Almouzni 2004)). A current model for the formation of heterochromatin via RNA in *S. pombe* is that non-coding satellite transcripts are processed by the RNAi machinery, generating smaller fragments, so-called siRNAs (small interfering RNAs) which in turn could recruit a histone H3K9 methyltransferase. Histone H3K9 methylation would then create a binding site for Swi 6 (a homolog of HP1) which, possibly in a spreading mechanism, could nucleate the formation of heterochromatin (see (Maison and Almouzni 2004)). In *S. pombe*, the RNAi machinery has been shown to be additionally involved in silencing of the mating type locus and in centromere function (Maison and Almouzni 2004). In mice, non-coding RNA was shown to be essential for the recruitment of HP1 to pericentric regions, arguing strongly for an implication of these RNAs in centromeric organization (Maison et al. 2002). Since RNA transcripts from the major satellite region were detected in mouse cells (Lehnertz et al. 2003), it appears conceivable that similar to *S. pombe* also in mouse an siRNA dependent mechanism might be responsible for the formation/maintenance of pericentric constitutive heterochromatin.

Beyond the level of protein and RNA composition, another level for a structural and/or functional characterization of chromatin is the DNA itself, which can be site-specifically modified via covalently bound methyl groups.

1.4.4 DNA methylation and chromatin

Since a substantial part of the present thesis focuses on the methyl-CpG-binding protein **MeCP2** and its role in nuclear architecture a short introduction into the vast field of DNA methylation is attempted. A special emphasis is put on the role of proteins that are thought to be directly involved in translating DNA methylation marks, the so-called **methyl-CpG-binding domain** or **MBD** proteins. In the light of the huge amount of information that has been accumulated in the field, including manifold implications of DNA methylation, e.g. in transcriptional regulation, cancer, imprinting development etc., the following outline cannot be more than a basic introduction of the phenomenon. For an in depth study of individual aspects I will refer to appropriate reviews or original articles.

Overview

The modification of nucleotides in the DNA by covalently bound methyl groups was already described in the late 40s, beginning 50s of the 20th century. In the 60s it was proposed that DNA methylation might be involved in a protection mechanism i) against the integration of foreign DNA or ii) in rendering host DNA resistant to DNAses directed against foreign DNA (Srinivasan and Borek 1964). The latter idea evolved probably in parallel with the discovery of bacterial restriction enzymes, which were thought to protect methylated bacterial host DNA from “invading” bacterial and viral DNA (reviewed in (Arber and Linn 1969)) by specific digestion of the “parasitic” unmodified DNA. It was not before 1975 though that methylation of DNA in mammals was suggested to be connected with transcriptional regulation (see citations in (Jaenisch and Bird 2003)). DNA methylation is found in many different organisms including prokaryotes, fungi, plants and animals (Hendrich and Tweedie 2003), where it can serve different functions. Methyl groups in the DNA are found at cytosines at the C⁵ position yielding 5-methyl cytosine (5mC) or at adenines at N⁶ resulting in N⁶-methyladenine (6mA), whereas the latter is mainly found in prokaryotic genomes. As already noted, methylation of DNA in bacteria is involved in a protection mechanism in which restriction endonucleases digest specifically foreign DNA by discriminating invader DNA from host DNA via their substrate specificity for unmodified sequences. In higher eukaryotes the majority of methylated bases are cytosines, with only some species showing low levels of methylated adenines (see (Doerfler 1983)). Methylation of eukaryotic DNA varies widely, from undetectable as in budding/fission yeast, nematodes or in adult *Drosophila* flies over intermediate levels in mammals (2-8 mol%) to high levels, reaching ~50 mol% in higher plants (see citations in (Doerfler 1983)). In humans, approximately one percent of all DNA bases are expected to be 5mC (Kriaucionis and Bird 2003). The sequence context in which methylated bases are found in eukaryotes varies also considerably. In mammals, for example methylation is mainly found in CpG doublets, with this “mini”-palindrome being methylated on both strands. In fact 60-90% of CpGs are methylated in mammalian genomes with the exception of so-called CpG islands, which are stretches of ~1kb that frequently coincide with promoter regions (Hendrich and Tweedie 2003). These sequences, which are thought to be involved in transcriptional regulation, comprise ~1% of the mammalian genome. Exceptions of the rule that CpG islands are generally unmethylated are silenced genes on the inactive X-chromosome and at imprinted loci, i.e. where depending on the parental origin one homolog allele is silenced. In contrast to mammals, in fungi methylation within a non-CpG context is rather the norm than an exception, while in plants besides CpGs also CpNpG sequences are frequently found to be methylated (Hendrich and Tweedie 2003).

Evolutionary aspects

From an evolutionary point of view DNA methylation is thought to represent an ancient mechanism, as the catalytic domain of DNA methyltransferases (Dnmts), the enzymes responsible for adding methyl groups, appears to be conserved from prokaryotes to humans (Hendrich and Tweedie 2003). However, in the course of genome evolution there must have been adaptations concerning how methyl marks were eventually utilized, since in different taxa DNA methylation appears to be involved in different functions. While in prokaryotes and fungi methylation appears mainly to serve protection needs of the host genome (see citations in (Hendrich and Tweedie 2003)), in higher eukaryotes transcriptional silencing seems to be the main purpose (reviewed e.g. in (Geiman and Robertson 2002; Robertson 2002; Jaenisch and Bird 2003)). Different aspects of transcriptional silencing are presently discussed to be associated with DNA methylation. Among these are repression of selfish DNA elements in order to secure genome integrity¹, reduction of transcriptional noise, developmental regulation of gene expression, as well as silencing of imprinted genes and of genes on the inactive X-chromosome in female mammals. A major change concerning the genomic organization as well as the extent of DNA methylation is thought to have occurred at the origin of vertebrate evolution (Tweedie et al. 1997). This idea is based on the observations that in invertebrates DNA methylation, if present at all, affects only a minor part of the genome and is organized in patches, with alternating stretches of methylation-free and methylated regions. In contrast to this fractional organization, DNA methylation in vertebrates is global, i.e. distributed over the whole genome. Furthermore, methylated DNA in non-vertebrates does not necessarily correlate with transposable elements or other functional chromosomal regions. In vertebrates DNA methylation appears to be highly organized, as it is enriched in centromeric regions and at other repeat containing sites as well as at transposable elements, while it is largely absent at CpG islands (Robertson 2002). Moreover whereas in vertebrates DNA methylation is supposed to be associated with transcriptional regulation, in invertebrates this is apparently not the case, since no correlation was found between transcription and methylation, neither for house keeping genes, nor for tissue-specific genes (Tweedie et al. 1997).

In the following, I will mainly focus on the situation in mammals to describe the enzymes involved in DNA methylation and to introduce some examples where methylation plays a significant role in cellular/nuclear functions.

Enzymes

DNA methylation represents a postsynthetic modification, i.e. nucleotides are modified after they have been incorporated into DNA. In respect to their substrate, two different kinds of DNA methyltransferases (Dnmts) are distinguished: 1.) Maintenance Dnmts show a higher affinity for hemimethylated DNA, i.e. DNA where only one strand of the CpG palindrome is modified. Hemimethylated DNA results from the replication of methylated regions. *De novo* Dnmts in contrast add methyl groups to completely unmethylated DNA. In both cases the methyl-group donor is S-adenosyl-L-methionin (SAM). The three main, catalytically active Dnmts in mammals are Dnmt1 as maintenance methyltransferase and Dnmt3a and 3b as *de novo* methylating enzymes. **Dnmt2** is expressed ubiquitously at low levels, but although it exhibits the highest conservation of all Dnmts between different species, so far it could not be shown to possess catalytic activity (Robertson 2002). *Dnmt2* knock out mice consequently showed no aberrant phenotype (see (Robertson 2002)). **Dnmt1** was shown to be essential for development, since null mice died at mid-gestation (Robertson 2002). Interestingly *Dnmt1*^{-/-} ES cells were viable and showed normal morphology and a 5mC level that was still

¹ ...which is in effect also some sort of host genome protection.

30% of that in wild type cells, suggesting some compensatory methylation maintenance activity (Robertson 2002). Across various mammalian species the N-terminus of Dnmt1 appears to be rather variable, while the catalytic C-terminus is more conserved (Margot et al. 2000). The intracellular distribution of Dnmt1 has been described to be diffuse nucleoplasmic during G1 and G2, while the enzyme accumulates in replication foci, sites of actively replicated DNA, during S-phase, (Leonhardt et al. 1992). Recent results however suggest a modification of this view, since it could be shown that Dnmt1 actually remains at sites of late replicating chromatin throughout G2 and M-phase and is only released in the subsequent G1, where it distributes homogeneously within the nucleoplasm (Easwaran 2003). Since Dnmt1 mRNA has also been found in low proliferative tissue, where only few cells are suspected to be actually replicating DNA, it has been proposed that Dnmt1 might exert an additional function beyond methylating hemimethylated DNA during S-phase (see citations in (Robertson 2002)). In fact, several splicing isoforms of Dnmt1 have been found that could account for additional functions. **Dnmt1b** for example, is a 16 amino acids longer splicing isoform in humans (2 amino acids longer in mice) that has been shown to be catalytically active *in vitro*. Its abundance however as well as its biological function still has to be determined (see (Robertson 2002)). Dnmt1o and Dnmt1p are two sex-specific isoforms. **Dnmt1o** (o=oocytes) has a shorter N-terminal end and accumulates specifically during oocyte growth. In preimplantation embryos Dnmt1o is the only present Dnmt1 variant, and localizes in the cytoplasm, except for the 8 cell stage where it is transiently relocated into the nucleus (Carlson et al. 1992; Cardoso and Leonhardt 1999). Since knock out female but not male mice were infertile, with embryos from k.o. females showing defective methylation pattern at imprinted loci, the current idea is that Dnmt1o and especially its nuclear localization at the 8 cell stage is important for maintaining imprints (discussed in (Robertson 2002)). During mouse preimplantation development, while the genome is globally demethylated, Dnmt1o appears to be responsible for keeping a retrotransposable element (IAP=intracisternal A-type particle) methylated and thus silent, (Gaudet et al. 2004). Silencing of such mobile elements is thought to be crucial to prevent potential mutagenesis by transposition.

Dnmt1p (p=pachytene) is a larger splice isoform and its mRNA was detected exclusively in pachytene spermatocytes. Whether the transcript is translated at all and how the precise expression pattern looks like is still controversially discussed (see (Robertson 2002)). The same isoform however was found to be specifically transcribed and translated in differentiated myotubes, at the expense of the ubiquitously expressed Dnmt1, which was shown to be downregulated upon differentiation (Aguirre-Arteta et al. 2000). Since myotube nuclei show no DNA replication, this isoform supposedly serves a function that is independent of DNA synthesis.

The *de novo* methylating enzymes Dnmt3a and b are supposed to be responsible of methylation of the embryonic genome after implantation, i.e. after the parental genomes have been demethylated (Jaenisch and Bird 2003). **Dnmt3a** and Dnmt3b were demonstrated to be catalytically active *in vitro* as well as *in vivo* and transcripts were found in ES cells, in the early embryo as well as in adult tissue and in tumor cells (reviewed in (Robertson 2002)). In contrast to Dnmt1, Dnmt3a was found to be distributed as focal structures inside the nucleus in a cell cycle-independent fashion. *Dnmt3a* knock out ES cell lines appeared to be normal concerning their *de novo* methylation potential and null mice developed inconspicuously until birth, but showed shortly after undergrowth and died by 4 weeks of age. **Dnmt3b**, which has only little sequence homology to Dnmt3a in its N-terminal end was shown to be catalytically active *in vitro* and *in vivo*. Moreover, its expression compared to Dnmt3a is low in most tissues, but high in testis, so that an implication in methylation during spermatogenesis has been proposed. Its localization in centromeric regions in ES cells and the observation that mutant *Dnmt3b*^{-/-} cells exhibit a significantly decreased methylation of minor satellite repeats, suggested an involvement in centromeric satellite methylation. Dnmt3b appears to be more

important for embryonic development than Dnmt3a, since no viable null mice were retained. Mutations in *Dnmt3b* in humans cause the so-called ICF syndrome, where pericentric repeats show also hypomethylation (see (Robertson 2002) and below). Other than Dnmt3a several splicing isoforms were found for Dnmt3b. The eight variants described in mouse and the five in humans are expressed in a tissue specific manner, yet not all of them appear to be catalytically active. **Dnmt3L** is a separately coded protein that lacks the catalytic motif. It colocalizes with Dnmt3a and b and was found to be highly expressed in mouse embryos and testis (Robertson 2002). *Dnmt3L* null mice show methylation defects at maternal imprints but otherwise a normal genome wide methylation pattern, which suggests that Dnmt3L is involved in the establishment of maternal imprints, probably by recruiting Dnmt3a or b to target loci, either directly or indirectly (see (Robertson 2002)).

Although many enzymes have been described, that can actually add methyl groups, only little is known about DNA demethylases. The existence of such enzymes however is almost assured since active demethylation of the paternal genome during preimplantation development has been evidenced (Mayer et al. 2000). Similarly, there must be demethylases, which can remove imprints in the course of germ cell development, in order to set the novel parental identity. Candidate enzymes for DNA demethylation include on the one hand glycosylases, which in effect resemble a “base excision DNA repair activity” where the methylated cytosines are removed, resulting in an abasic site and single strand breaks that have to be consecutively repaired (Jost et al. 2001; Vairapandi 2004). Another proposed mechanism includes direct demethylation of 5mC, via the methylated CpG binding protein MBD2 (Bhattacharya et al. 1999). Since MBD2 has also been reported to be involved in 5mC dependent transcriptional repression (Hendrich and Tweedie 2003), it was proposed that it might exert a dual, promoter-specific role as a repressor through binding of 5mC on the one hand and as an activator through active DNA demethylation on the other (Detich et al. 2002). The demethylase activity of MBD2 however is not undisputed (see (Vairapandi 2004)).

Functional implications

DNA methylation in mammals is involved in many different nuclear functions including transcriptional regulation of individual genes, imprinting, X-inactivation, genome stability and preventing the spread of potentially “parasitic” DNA elements like transposable sequences. Furthermore, DNA methylation appears to be involved in several pathological situations including cancer and other, more specific diseases like Rett syndrome or ICF syndrome. In the following, I want to sketch a few examples depicting the role of DNA methylation in various biological settings.

DNA methylation during development

As already noted DNA methylation levels change dramatically in two situations during development: i) in the early embryo and ii) during gametogenesis (reviewed in (Reik et al. 2001)). The occurrence of major changes in the nuclear methylation levels are sometimes referred to as “reprogramming” (Reik et al. 2001), which is a term that is also often used in the context of resetting the epigenome¹ of nuclei which are “transferred” in the course of cloning experiments (reviewed e.g. in (Shi et al. 2001)). In the mouse, it has been shown that primordial germ cells are highly methylated with similar levels as somatic cells. During early embryonic development (E13-14) a genome wide demethylation in germ cell nuclei starts including the

¹ The “epigenome“ in a less strict sense is a collective term for all kinds of epigenetic modifications of the genome that have a hereditary informational impact that is independent of its sequence. DNA methylation, histone modifications and chromatin composition are all constituents of the epigenome. In a stricter sense, the epigenome defines only the DNA methylation pattern within the genome.

differentially methylated regions (DMRs) of imprinted genes. Though the mechanism has still to be elucidated, an active mechanism appears probable, since fusion of embryonic germ cell lines with somatic cells leads to a dominant demethylation of the respective somatic sequences. This demethylation takes place when germ cells have already entered the gonads. Hereafter the germ cells enter mitotic (male) or meiotic (female) arrest. Remethylation of male germ cells takes place several days later still in the embryo (E15-16), while female remethylation is accomplished after birth, during oocyte growth. Mature germ cells finally exhibit a similar methylation level as somatic cells but possess the sex specific imprints. Besides being important to reset parental imprints this “reprogramming” was suggested to be important to remove additional epigenetic marks (Reik et al. 2001). Moreover, the prolonged demethylated state of oocytes could reduce the risk of mutations of methylated cytosines by deamination events (see (Reik et al. 2001)). Once the oocyte is fertilized, a demethylation wave of the parental genomes takes place¹. The paternal genome is rapidly demethylated during the first 6-8 hours after fertilization, before replication of pronuclei starts. Demethylation of the paternal genome was demonstrated to be an active process, since it was not reliant on DNA replication (Mayer et al. 2000). Demethylation of the maternal genome in contrast resembles a passive mechanism, accomplished by a lack of maintenance methyltransferase activity. Dnmt1o (see above) the only methyltransferase present in the early developing embryo is retained in the cytoplasm until the blastocyst stage and is only transiently relocated into nuclei at the 8 cell stage (Carlson et al. 1992; Cardoso and Leonhardt 1999). This short interplay of Dnmt1o was shown to be necessary for methylation maintenance of imprinted regions (see (Reik et al. 2001)) and for the silencing of a retrotransposable IAP sequence (Gaudet et al. 2004). How methylation maintenance at DMRs is accomplished before and after this stage is at present not known, but *de novo* methylation by Dnmt3a and/or 3b has been suggested (Reik et al. 2001). After implantation of the blastocyst, *de novo* methylation is thought to be performed by Dnmt3a and 3b (see above). While these just described de- and remethylation events represent the situation in mouse, it should be kept in mind that the timing of both processes can vary in other species (Reik et al. 2001). Demethylation during early development is thought to be crucial for the erasure of acquired epigenetic marks, but an additional role in resetting transcriptional programs for embryonic development are currently discussed. This idea is further strengthened by observations that development can go awry if “reprogramming” of the nucleus is not performed properly. Such a faulty or incomplete reprogramming is thought to be the cause for the impaired development of reconstituted embryos, cloned by nuclear transfer (reviewed e.g. in (Shi et al. 2001)). The developmental potential of transferred nuclei has been shown to be poorest if somatic, differentiated cells are used as donors. Studies investigating epigenetic modifications of such transferred nuclei have revealed that the genomic methylation status was often aberrant (Dean et al. 2001; Jaenisch and Bird 2003) and that imprints were often incorrect (Humpherys et al. 2001; Jaenisch and Bird 2003). The observation that less differentiated cells like ES cells usually confer a greater developmental potential than somatic cells at an advanced differentiation state, might be explained by the greater similarity between the epigenome of ES cells and that of nuclei of early embryonic cells.

DNA methylation and imprinting

Differentially methylated regions (DMRs), i.e. where only one of both alleles is methylated are often found near imprinted genes. Imprinted genes are expressed exclusively or predominantly from either the paternal or the maternal allele. Methylation is often but not always

¹ It should be added that first protamines, which serve sperm DNA packaging are removed and substituted by histones before genome wide demethylation (Reik et al. 2001).

associated with the silent copy. Methylation at the DMR2 region near the *H19* gene, for example, results in silencing of the *H19* gene. Concomitantly methylation prevents binding of the insulator protein CTCF, which enables an enhancer region downstream of the *H19* gene to exert a transcriptionally stimulating activity on the *Igf2* gene, which lies upstream of the DMR resulting in its transcription. This exemplifies how methylation can actually regulate two differentially imprinted genes at the same time (Lewin 2004). Imprinting is found mainly in eutherian mammals but several imprinted genes have also been described for several marsupials (see citations in (John and Surani 2000)). The evolution of imprinting is thought to be intimately correlated with the development of a placenta for the “internally” developing embryo in eutherian mammals. It is supposed to resemble the competition of maternal and paternal genes for motherly resources; since several imprinted genes are expressed in the brain, the increased expansion of the neocortex in the course of mammalian evolution is also discussed as an evolutionary force for imprinting (John and Surani 2000). In humans, approximately 60 imprinted genes are known and a total of ~100 are estimated to exist to date (Lucifero et al. 2004).

DNA methylation and X-inactivation

Besides imprinting another mammalian phenomenon where DNA methylation is involved in allelic silencing, is the so-called X-inactivation of the supernumeral X-chromosome in females. Though the establishment of X inactivation does not appear to rely on DNA methylation, maintenance of the inactive state is dependent on the continuous activity of Dnmt1 and hence on methylation marks set on the inactive X (Xi) (see citations in (Jaenisch and Bird 2003)). The widespread methylation of CpG islands is thought to represent a rather late event in the course of inactivation (see (Riggs 2002)). The importance of 5mC for sustaining the silenced state of genes on the inactive X, was demonstrated by applying the methylation inhibitor and cytidine analog 5-azacytidine, which led to reactivation of formerly silenced genes (see (Riggs 2002)). The promoter of *Xist* RNA, a non-coding RNA that covers the inactive X, and which is essential for X inactivation, is methylated on the active X chromosome, thereby reinforcing the active state. It should be added that besides DNA methylation, histone modifications as deacetylation of histone H4 and methylation of lysines 9 and 27 on histone H3 are important constituents of the inactive X that might synergistically cooperate with DNA methylation marks to stably maintain either silent or active states. Several observations support the view of interdependence between DNA methylation and histone modifications. Methylated DNA binding proteins like MeCP2 have been shown to recruit histone deacetylases and methyltransferases (Jones et al. 1998; Nan et al. 1998; Fuks et al. 2003). Dnmt1 has been shown to associate with a histone deacetylase and thus to promote histone deacetylation (Riggs 2002). In *Neurospora crassa*, methylation was found to depend on histone H3K9 methylation (Tamaru and Selker 2001). Intriguingly skewed inactivation of the paternal X chromosome in marsupials and in extraembryonic tissue of mice appears to be independent of DNA methylation (John and Surani 2000).

DNA methylation and environmental influences

While during development, imprinting or X-inactivation the methylation of DNA resembles a scheduled, programmatic event, several examples have been demonstrated where DNA methylation can change dynamically upon environmental influences. Vernalization of plants for example, where flowering is promoted by a long period of low temperature, has been shown to be regulated by a gene whose activity is controlled by DNA methylation (see citations in (Jaenisch and Bird 2003) and (Sheldon et al. 2000)). Accordingly, it could be shown that low temperatures induced global hypomethylation. Ageing with its many different environmental influences was demonstrated to correlate with both, hypo- and hypermethylation of DNA. In-

creasing hypomethylation was shown in aging mice as well as in mouse fibroblasts during continuous culturing (see (Jaenisch and Bird 2003)). In tissues of aging humans, in contrast specific genes appeared to gain methylation marks (see (Jaenisch and Bird 2003)). It has been suggested that age related local DNA hypermethylation could increase cancer risk by methylation and silencing of tumorsuppressor genes (Jaenisch and Bird 2003) (see below). An increasing body of evidence points at diet as an influential factor for DNA methylation. A methyl deficient diet for instance was shown in rats to result in liver cancer and associated with hypomethylation and increased expression of oncogenes, although a definite causal implication has not yet been evidenced (discussed in (Jaenisch and Bird 2003)). To test directly the influence of methyl-donor supplemented diet on the activity of methylation-dependent gene expression, mice carrying the *agouti viable yellow* alleles were investigated. These alleles cause a variegated color phenotype depending on the stochastic expression pattern of a retroviral element (IAP=intracisternal A-type particle). IAP is expressed if non-methylated which leads to a yellow fur color, obesity and age related tumor formation. If pregnant yellow (IAP is transcribed) mice were fed with methyl donors supplemented food a larger percentage of the offspring showed a normal, wild type fur color, indicating that the specific diet composition had altered the methylation state, resulting in silencing of IAP (reviewed in (Jaenisch and Bird 2003)). Furthermore a reduced methylation state of IAP in yellow mice was reported to be transmitted to the progeny. These intriguing findings exemplifies how environmentally acquired modifications of the epigenome can have long term phenotypic consequences, which can actually be inherited; an aspect that could play a major role for the predisposition of age related diseases such as cancer.

DNA methylation and diseases

Several pathological situations have been correlated with dysfunctions within the DNA methylation system. ICF (immunodeficiency, centromere instability, facial anomalies) syndrome for example is caused by mutations in the *de novo* methyltransferase *Dnmt3b* (discussed in (Robertson 2002)). Affected individuals exhibit severe immunodeficiencies, including lack of several immunoglobulin isotypes, facial dysmorphisms, neurological and intestinal impairments and a delayed development. Hypomethylation of juxta-centromeric satellite repeats of specific chromosomes were found to correlate with an elongation of these heterochromatic regions and with an increased involvement in chromosomal aberrations.

A further genetic disease related to DNA methylation is Rett syndrome, a neurological disorder, where affected children, loose acquired speech and motor skills and develop neuropathological symptoms like ataxia, autism and seizures. The syndrome is caused by mutations in the gene for the methylated-CpG-binding protein MeCP2 (for details, see chapter on MBD proteins).

DNA methylation in cancer has been a topic for more than 20 years (reviewed in (Feinberg and Tycko 2004)) and is one of the most intensely studied topics in the field of DNA methylation research (Riggs 2002). The main themes thought to be relevant are global hypo- and local hypermethylation (Jaenisch and Bird 2003). Genomic **hypomethylation**, which was actually the first DNA methylation aberration observed in cancerous cells (see (Feinberg and Tycko 2004 1002)), could act via unscheduled activation of oncogenes thereby leading to uncontrolled proliferation. Moreover it has been suggested that hypomethylation at centromeric repeats might lead to alterations in chromatin structure and hence to an increased chromosomal instability (Feinberg and Tycko 2004) similar as described for ICF patients (see above). The first direct demonstration that global hypomethylation is causally involved in the formation tumors was recently provided by Gaudet et al., who could show that mice with a hypo-

morphic Dnmt1 allele¹, besides exhibiting reduced CpG levels and karyotypic anomalies, developed aggressive T cell lymphomas (Gaudet et al. 2003). A further mode of action how hypomethylation could increase cancer incidence could be the activation of silenced transposable elements like LINE-1², which has been shown to be hypomethylated in colorectal cancer tissue (see (Feinberg and Tycko 2004)). Once activated it could induce chromosomal rearrangements. Another example for cancer induction caused by hypomethylation is the human papilloma virus (HPV). In the latent state, its genome is hypermethylated while in the active state in cervical cancer it is progressively hypomethylated (see (Feinberg and Tycko 2004)). Local **hypermethylation** of tumor suppressor (TS) genes is meanwhile a well-accepted concept how DNA methylation deficiencies could contribute to the formation of cancer (Baylin and Bestor 2002; Feinberg and Tycko 2004). The first TS gene ever described, the retinoblastoma protein, was shown to be methylated in a various number of tumors (see (Feinberg and Tycko 2004)). Yet, the idea that silencing of TS genes by DNA methylation is the primary cause for tumor generation remains heavily debated, especially since there are experimental indications that additional epigenetic factors like histone modifications might be involved in the silencing of TS genes (discussed in (Feinberg and Tycko 2004)). Therefore, it has been proposed that DNA methylation might help in maintaining or reinforcing silencing, rather than initiating it. Hypermethylation of tumor suppressor genes could also increase the risk of point mutations by deamination of CpGs, resulting in a genetic rather than an epigenetic basis of tumor generation (discussed in (Jaenisch and Bird 2003)). Other genetic alterations that are favored by cytosine methylation are an increased susceptibility to an UV-light spectrum present in the sunlight leading to CC→TT transitions and an increased susceptibility to the tobacco carcinogen benzo(a)pyrene diol epoxide, which results in G→T transversions (see citations in (Jones and Baylin 2002)).

Recapitulating one can imagine different scenarios how TS function could be lost due to DNA methylation defects: i) hypermethylation of CpG islands at TS promoter sequences, impeding transcription factor binding, ii) loss of heterozygosity (LOH) due to increased levels of chromosome rearrangements at hypomethylated sites and iii) mutations at hypermethylated sites in TS genes by a) spontaneous deamination, b) UV-induced mutation and c) mutations induced by chemical carcinogens.

Changes in global or in specific methylation pattern can eventually affect imprinted genes that are specifically controlled by differentially methylated regions (DMRs). Consequently, loss or gain of methylation marks at DMRs can result in a loss of imprinting (LOI). Increased methylation at the maternal DMR2 (see above), which is normally unmethylated was shown to occur in Wilms tumor (see (Feinberg and Tycko 2004)). This LOI led to silencing of the *H19* gene and to activation of *Igf2*, resulting in a two fold higher concentration of Igf2. Apart from tumor cells, LOI was also found in non-neoplastic tissue surrounding the tumors. According to this finding, it was suggested that epigenetic alterations might represent a gate-keeper function, since they were the first traceable changes before transformation. In Beckwith-Wiedemann syndrome, it was shown that hypermethylation at DMR2 correlates with the risk to develop Wilms tumors. Interestingly LOI at the *Igf2* locus in colorectal cancer appears to be correlated with hypomethylation at *Igf2* and not with hypermethylation at *H19* as in Wilms tumor, underscoring the fact that epigenetic imbalances *per se*, no matter how they arise, are involved in cancerogenesis (Feinberg and Tycko 2004). As a matter of fact

¹ Dnmt1 expression is only 10% of that in wild type mice

² Long interspersed nuclear element 1 is a repetitive sequence, derived from a transposable element that comprises ~17% (!) of the human genome. Though most copies are degenerated and thus inactive, some are thought to retain their transposable potential. Therefore, methylation is crucial for keeping them in a silent state (Suter et al. 2004).

recent clinical trials applying “epigenetic chemotherapy” by using 5-azacytidine as DNA methylation inhibitor (see (Yang et al. 2003)) in order to reactivate TS genes are controversially discussed, since their global mode of operation might also have adverse effects like the activation of oncogenes (see (Gaudet et al. 2003), but (Yang et al. 2003)).

Modes of action

The precise mode of action how DNA methylation modulates transcription is far from being understood. In fact different mechanism could account for controlling gene expression at different loci. Though DNA methylation in general has been associated with transcriptional silencing, in several examples methylation has been shown to induce expression, as demonstrated for Igf2 locus, where methylation prevents binding of CTCF, which results in a positive enhancer function (see above). Methylation of CpGs near promoter regions is thought to act by at least two different mechanisms. One possibility is that methylation of specific target sites simply abolishes binding of transcription factors or transcriptional activators by sterical hindrance. Another option is that specific adaptors bind to methylated regions, which can then trigger different kinds of downstream responses. In mammals, there are five known methyl-CpG-binding proteins. Four of them, MeCP2, MBD1, MBD2 and MBD4 are constituents of the MBD protein family all of which share the conserved methyl-CpG-binding domain (MBD) (Hendrich and Bird 1998) (figure 1.4). While MeCP2, MBD1 and MBD2 have been shown to act as transcriptional repressors, MBD4 appears to be involved in reducing the mutational risk from potential C→T transitions, which result from deamination of 5mC. A fifth member of the MBD family, MBD3 does not bind to methylated DNA (Hendrich and Tweedie 2003), but is a constituent of the NuRD (nucleosome remodeling and histone deacetylation) corepressor complex. A further, recently detected 5mC-binding protein is Kaiso, which shows no sequence conservation with MBD proteins, but which functions also as a transcriptional repressor (Prokhortchouk et al. 2001). In contrast to MBDs, Kaiso appears to bind in a sequence specific manner at sequences containing two symmetrically methylated CpGs.

The methyl-CpG binding domain (MBD) protein family

As already noted, in mammals the MBD family comprises five members: MBD1-4 and MeCP2. MBD2 and 3 are highly conserved between each other, having the same genomic structure except for their intron length (Hendrich and Tweedie 2003). Since homologous ESTs for MBD2/3 were also found in invertebrates, it is thought to represent the ancestral form from which all other family members have been derived (Hendrich and Tweedie 2003). The increase in number of 5mC binding proteins from invertebrates to vertebrates is believed to have paralleled the increase in DNA methylation (see above), such that cells could better cope with methylation dependent silencing on the one hand, but also with the increased mutational risk emerging from spontaneous deamination on the other (Hendrich and Tweedie 2003).

In mammals, **MBD3** does not bind to methylated CpGs due to two amino acid substitutions within the MBD (see (Hendrich and Tweedie 2003)). Other vertebrates however, like frogs, the fugu fish or zebrafish have two MBD3 forms, one of which retains a 5mC binding ability. MBD3 in mammals is a constituent of the NuRD corepressor complex. NuRD is found in many organisms including plants and plays an important role in transcriptional silencing via histone deacetylases. Constituents of the NuRD complex have been shown to be essential for embryonic development. The function of MBD3 within the multiprotein complex however has still to be resolved. **MBD2** interacts with the NuRD complex thereby constituting the MeCP1 complex (methyl-CpG-binding protein), which was actually the first methyl CpG binding activity isolated in mammals (Meehan et al. 1989). In spite of the many potential binding sites of MBD2 it does not appear to act as a global transcriptional repressor.

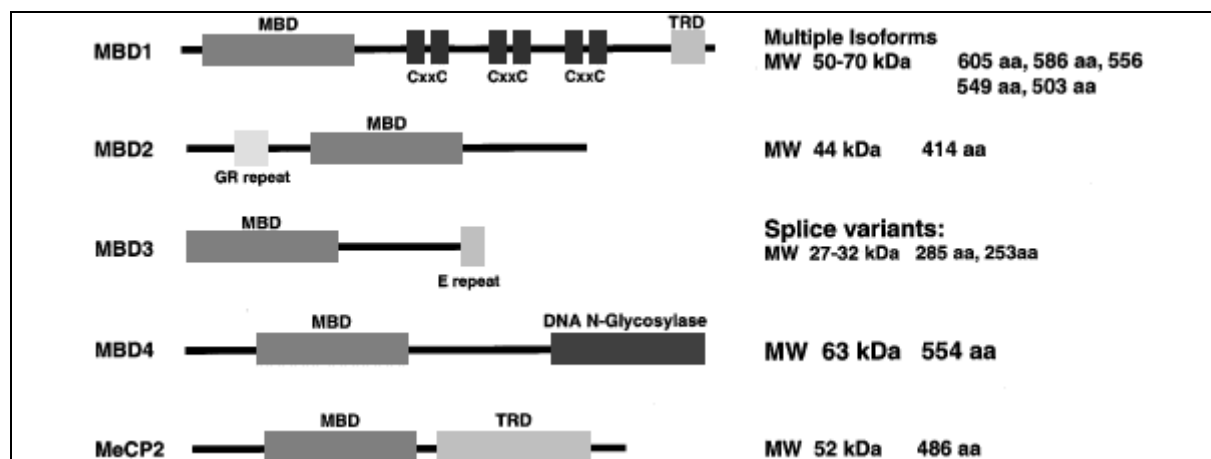


Figure 1.4: MBD family members (taken from (Wade 2001)). aa=amino acids CXXC=cystein rich motif (one letter amino acid code: C=cystein, X=any), E=glutamate, GR=glycine-arginine, kDa=kiloDalton, MBD=methyl-CpG binding domain, MW=molecular weight, TRD=transcriptional repression domain. Only the isoform MBD2a is shown (see text). TRDs in MBD1 and MeCP2 show no sequence similarities (Wade 2001).

In fact only one target gene of MBD2 has been described up to now, which is *Irf4* during T cell differentiation. Here loss of MBD2 has been shown to correlate with a leaky instead of a complete repression. Consequently it has been hypothesized that MBD2 (as well as MeCP2, see below), might rather act in fine tuning transcriptional control by reducing transcriptional noise at genes which actually are already shut off (Hendrich and Tweedie 2003). Alternatively, the lack of a global de-repression of methylated genes upon MBD2 loss could be explained by redundancy among MBD family members (Hendrich and Tweedie 2003). Studies abrogating several MBD proteins at the same time will help to enlighten this question. An interesting phenotype of MBD2 *-/-* mice is that affected female animals neglect their offspring due to an unknown neurological effect (Kriaucionis and Bird 2003). MBD2b, is an isoform, which is generated by using an alternative translation start codon generating a protein that lacks 140 N-terminal amino acids. Surprisingly it has been reported to possess a demethylase activity (Bhattacharya et al. 1999). In gene reporter assays, it was even demonstrated to act as a transcriptional activator (Detich et al. 2002). Thus it has been proposed that MBD2 could act as both, a transcriptional repressor as well as a stimulator. The function-determining factors though still have to be elucidated. It should be added though, that other groups could not reproduce the demethylase activity of MBD2b yet. Consequently, the existence of this activity is still controversially discussed (see (Wade 2001)).

MBD1 is unique among the transcriptionally repressive MBDs, since it can suppress transcription from both methylated as well as unmethylated promoters in transient transfection assays (Hendrich and Tweedie 2003). The latter appears to depend on multiple cystein rich CXXC motifs (C=cystein; see figure 1.4). Its repression potential seems to act via the recruitment of HDAC activity (Hendrich and Tweedie 2003). Similar to MBD2, MBD1 *-/-* mice exhibit also neurological deficiencies, as they show a reduced neuronal differentiation and have defects in spatial learning as well as in hippocampus long-term potentiation (Hendrich and Tweedie 2003).

MBD4 is the only member within the MBD family that is not involved in transcriptional regulation. Instead, it appears to be implicated in reducing the mutational risk that is immanent in genomes with high methylation levels, by transitions of 5mC \rightarrow T via deamination. This transition poses a bigger problem for the DNA repair machinery than C \rightarrow U transitions, which results from the deamination of unmethylated cytosines, since it results in G-T mismatches, in which the mismatched base (G or T) cannot readily be identified. In contrast, uracil in G-U mismatches can easily be pinpointed as the “wrong” base, since it is not a constituent of

DNA. Accordingly, MBD4 possesses a C-terminal glycosylase moiety (figure 1.4) that can specifically remove Ts from G-T mismatches (Hendrich and Tweedie 2003). In fact, its preferred substrate is 5mCpG/TpG, i.e. the deamination product of the 5mCpG/5mCpG dinucleotide (see citations in (Hendrich and Tweedie 2003)). In a transient transfection assay MBD4^{-/-} cells showed a 3.3 fold increase in C→T transitions compared to wild type cells (see citations in (Hendrich and Tweedie 2003)), which supports the idea of MBD4 being a mutation attenuator.

Since **MeCP2** was the first methyl-CpG binding protein to be cloned and the second methylated DNA binding activity to be isolated after MeCP1, it is often referred to as the founder member of the MBD family. A single methylated CpG dinucleotide has been shown to be sufficient for binding (Lewis et al. 1992). In transient transfection assays with methylated gene reporter in *Xenopus* and in mice it was demonstrated that MeCP2 functions as a transcriptional repressor, via interaction with the Sin3 corepressor complex, which contains histone deacetylases (Jones et al. 1998; Nan et al. 1998). A ~100 amino acids containing transcriptional repression domain (TRD) in the middle of the protein (figure 1.4) has been shown to be critical for transcriptional silencing. Apart from the recruitment of HDACs, MeCP2 has been associated with a histone methyltransferase activity specifically modifying histones H3 at lysine 9, which is known to represent a transcriptionally repressive chromatin label (Fuks et al. 2003). Moreover Georgel et al. have shown that MeCP2 can induce a compaction of oligonucleosomes *in vitro*, which could additionally suppress transcription *in vivo* through a dense chromatin conformation that is incompatible with the binding of factors relevant for transcriptional activation (Georgel et al. 2003). With the idea in mind that MeCP2 might act as a global transcription repressor, it was very surprising that an expression profiling analysis comparing MeCP2 null mice with normal animals revealed only subtle changes in the mRNA profiles of brain tissues (Tudor et al. 2002). This finding paralleled the observations in MBD2^{-/-} mice (see above). Possible reasons for this finding could be either that other MBD proteins can compensate for the loss of MeCP2, or that the changes in transcription levels induced by MeCP2 deficiency are so small that they are undetectable with current microarray technology. This supports the rationale that MBD repressors might rather act as reducers of transcriptional noise than to shut down active genes (Hendrich and Tweedie 2003). On the other hand it could well be that MeCP2 represses genes in a tissue and/or time specific fashion. Matarazzo et al. for example using a proteomic approach found substantial differences in protein expression pattern between MeCP2 deficient mice and wild type mice (Matarazzo and Ronnett 2004). Importantly, they showed that the degree of differences varied depending on the analyzed tissue (olfactory epithelium vs. olfactory bulb) and the age of the animals (2 vs. 4 weeks after birth). Apart from a potential global effect, MeCP2 has recently been linked to the regulation of two specific target genes. The genes of *Hairy2a* in *Xenopus* (Stancheva et al. 2003) and *BDNF* in rat (Chen et al. 2003) and mice (Martinowich et al. 2003), both proteins that are involved in neuronal development and differentiation, have methylated promoters with bound MeCP2, which is released upon transcriptional activation. MeCP2 is expressed ubiquitously in many tissues of humans, rats and mice, although at a variable level. In human and mouse brain for example MeCP2 appears to be absent in glia but is expressed in neurons (Shahbazian et al. 2002). Several lines of evidence argue that MeCP2 expression increases during neuronal maturation and differentiation. Shahbazian et al. for instance found that in human and mouse MeCP2 is first expressed in ontogenetically older brain structures (Shahbazian et al. 2002). Jung et al. showed that in rat neurons MeCP2 expression increases (Jung et al. 2003) during differentiation, both *in vivo* and *in vitro*. Mullaney et al. could additionally provide support that MeCP2 expression correlates with synaptogenesis in rat brain (Mullaney et al. 2004). In the mouse olfactory system Ronnett and co-workers found a postnatal increase of MeCP2 expression in olfactory neurons before terminal differentiation and synaptogenesis (Cohen et al. 2003). In human brain tissue Balmer et al. demonstrated

that MeCP2 expression increased with age and that enhanced MeCP2 level correlated with the utilization of an alternative polyadenylation site of the MeCP2 mRNA (Balmer et al. 2003). According to its substrate specificity, MeCP2 localizes mainly at heavily methylated regions. In mouse nuclei, for example MeCP2 intensely decorates pericentric heterochromatin (Lewis et al. 1992) (see chapter about pericentric heterochromatin). In human cells, however the intranuclear distribution of MeCP2 was found to deviate from the pattern in mouse, in that it did not strictly colocalize with methylated DNA, pericentric satellite sequences or heterochromatic regions (visualized by intense DAPI staining) (Koch and Stratling 2004). Intriguingly the authors found an additional binding affinity of MeCP2 for TpG dinucleotides and proposed a sequence specific binding defined by adjacent sequences. By using an immunoprecipitation approach, they revealed an association of MeCP2 with retrotransposable elements, especially with Alu sequences, and with putative matrix attachment regions (MARs). In this respect, it should be added that the MeCP2 homolog in chicken (named ARBP) was originally isolated as a MAR binding activity (von Kries et al. 1991), even before rat MeCP2 was actually described for the first time (Lewis et al. 1992), although its homology to the rat protein was realized only later (Weitzel et al. 1997). Interestingly ARBP/MeCP2 binding in chicken appears to be not dependent of CpG methylation (Weitzel et al. 1997). Since the results in human cells were obtained using a breast cancer cell line (MCF7), it will be interesting to investigate further human cell types including primary cells, to elucidate the nature of the deviating binding specificity between human and mouse cells.

Two very recent studies have reported a second MeCP2 splicing isoform, which yields a protein with a slightly different N-terminal end, due to the utilization of an alternative translation start codon (Kriaucionis and Bird 2004; Mnatzakanian et al. 2004). Surprisingly this new MeCP2 isoform mRNA appears to be much more abundant in different analyzed mouse and human tissues than the originally described isoform. As revealed by fluorescently tagged fusion proteins, both isoforms show the same subnuclear distribution in cultured mouse cells (Kriaucionis and Bird 2004). An antibody raised against the "old" isoform was shown to recognize also the novel variant (Kriaucionis and Bird 2004). Consequently, in previous immunocytochemical studies most probably both isoforms have been visualized. The differences between both isoforms are only subtle, with the new protein having a 12 (human) and 17 (mouse) amino acids longer N-terminus followed by a divergent stretch of 9 amino acids. Since neither the MBD nor the TRD are affected by the changes, both proteins are anticipated to be functionally equivalent. However, functional assays are indispensable to obtain definite proof.

As already noted, MeCP2 expression in neurons appears to be correlated with differentiation and maturation. Its implication in neuronal function is further supported via its involvement in a human neuropathological disease, termed Rett syndrome (RTT). The syndrome was originally described in 1966 by the Austrian pediatrician Andreas Rett, but its genetic basis was revealed only recently (Amir et al. 1999). At least 80% of Rett syndrome cases are caused by spontaneous mutations in the *MeCP2* gene (Kriaucionis and Bird 2003), which is localized on Xq28 (Amir et al. 1999). It is the second most frequent form of female mental retardation after Down syndrome, and its incidence is approximately two fold higher than phenylketonuria (Jellinger 2003). RTT is diagnosed in 1:10000-1:22000 female births, with affected girls being heterozygous for the *MeCP2* mutation (Kriaucionis and Bird 2003); consequently the phenotype is caused by the ~50% of cells which do not express functional protein, due to random inactivation of the X chromosome containing the wild type copy of *MeCP2*. Affected children develop normally during the first 6-18 month, but then lose already acquired speech and motor skills. The regression includes seizures, ataxia, autism, intermittent hyperventilation as well as stereotypic hand movements (Kriaucionis and Bird 2003). After an initial rapid deterioration the state apparently stabilizes and in spite of further life threatening symptoms like arrhythmia or gastrointestinal dysfunctions patients can actually survive into adolescence or

even adulthood (see citations in (Jellinger 2003)). RTT patients exhibit a reduced brain size and weight, which is not due to neuron loss but rather to a reduced neuron size, including a reduced arborization of dendrites (see citations in (Jung et al. 2003)). Males carrying an equivalent mutation as affected females show a more severe phenotype and usually die before 2 years of age (Kriaucionis and Bird 2003). Most mutations found in RTT patients are located within the functional domains, i.e. within the MBD and TRD of MECP2, but several mutations have also been found in the C-terminal region, where until recently no concrete function could be assigned to. Recently it was shown that the C-terminal domain of MeCP2 is crucial to compact oligonucleosomes into dense higher order conformations *in vitro* (Georgel et al. 2003). Interestingly this activity was found to be independent of the methylation of CpGs of the oligonucleosomal arrays, which parallels the findings in human and chicken cells where MeCP2 binding was as well found at non-methylated sites (see above) (Weitzel et al. 1997; Koch and Stratling 2004). In a study by Buschdorf and Stratling the C-terminal domain of MeCP2 was found to specifically bind to the Group II WW domain found in the splicing factors FBP and HYPIC (Buschdorf and Stratling 2004). Although the functional role of this association has yet to be unraveled, various mutations within this C-terminal region were shown to correlate with the RTT phenotype. In mouse models for RTT, animals carrying mutations in the C-terminus generally exhibit a less severe phenotype than those with a null mutation (Shahbazian et al. 2002). Mice where MeCP2 was conditionally knocked out only in the brain yielded the same phenotype as those where the whole animal was affected, suggesting that the observable phenotype is largely due to a failure of proper brain development (discussed in (Kriaucionis and Bird 2003)). Apart from RTT, MeCP2 mutations have also been found in other neurological disorders such as some non-specific X-linked mental retardations, in Angelman syndrome and in autism (Kriaucionis and Bird 2003).

In conclusion, Rett syndrome illustrates that not only the establishment and the maintenance of methylation marks is pivotal for a normal development as shown by the phenotypes caused by loss of Dnmt functions (see above), but that also the correct interpretation of methyl marks is a critical prerequisite for normal ontogeny, especially for the development of neurological structures.

1.4.5 Mouse pericentric heterochromatin

All mouse chromosomes are acro- or telocentric, i.e. the centromere is located at the very end of the chromosome. The chromosome end where the primary constriction¹ is situated consists of telomeric TTAGGG hexanucleotide repeats, which are directly neighboring the centromeric region that consists of minor satellite repeats. Adjacent to this centromeric site lies a large pericentric region comprised of major satellite repeats (figure 1.5). Telomeric repeats are estimated to extend over a region of 20-60 kb/telomere (Garagna et al. 2002), which is markedly longer than in humans, where it was determined to be between 2 and 15 kb (Martens et al. 2000; Barwisch 2003). The centromeric region was reported to comprise 250-500 kb/chromosome (Garagna et al. 2002). It consists of tandem arrays of the so-called minor satellite, a 120bp sequence that sums up to ~1% of the mouse genome. The name was chosen in contrast to the 234bp major satellite sequence, which makes up 10% (!) of the murine genome (Mitchell 1996).

¹ The term "primary constriction" is usually used as a synonym for the centromere as the microtubule attachment region for the mitotic spindle, alluding to its microscopic appearance (see (Mitchell 1996)).

Interestingly neither the minor nor the major satellite could be detected on the Y chromosome, suggesting that the sequence *per se* appears not to be the determining factor in organizing a functional centromere (see (Mitchell 1996))¹. *In situ* hybridization experiments with

major and minor satellite specific probes have revealed that the major satellite region is more distant from the primary constriction than the minor satellite repeat (Joseph et al. 1989), hence the term “pericentric” or “pericentromeric”. Minor satellite sequences contain conserved sequence motifs called CENP-B boxes, originally characterized in human alphoid repeats, which are assumed to bind CENP-B proteins. CENP-B proteins are believed to be implicated in the formation of higher order structures at the centromere, although their functional necessity has still not been resolved (discussed in (Mitchell 1996)). Already 1974 Miller et al. showed that satellite sequences in the mouse (and

human) were enriched in methylated cytosines (Miller et al. 1974). Indeed 40% of genomic 5mCs are contained in the pericentric region (see (Lewis et al. 1992)). Accordingly several 5mC binding proteins like MeCP2 (Lewis et al. 1992), MBD1, MBD2 and MBD4 (Hendrich and Bird 1998) have been found to be concentrated in pericentric heterochromatin. Further hallmarks of pericentric heterochromatin are the presence of specific histone modifications, including tri-methylation of H3K9 (Peters et al. 2003), mono-methylation of H3K27 (Peters et al. 2003) and tri-methylation of H4K20 (Kourmouli et al. 2004; Schotta et al. 2004). At the same time specific histone modifications like methylation of H3K4 (Peters et al. 2003) or acetylation of histone H4 (Maison and Almouzni 2004) are underrepresented in pericentric regions.

Other enriched protein constituents at pericentric heterochromatin are HP1 α and β^2 (Taddei et al. 1999), which are apparently targeted by tri-methylated histone H3 at lysine 9 (Lachner et al. 2001). Via HP1 acting as adaptors many other proteins can indirectly be associated with pericentric sites, such as the tumoursuppressor pRb, the histone H3K9 histone methyltransferase Suv39h, the lamin B receptor and many others (reviewed in (Singh and Georgatos 2003)). An intriguing finding was that both complementary strands of the major satellite sequence are actively transcribed (Rudert et al. 1995; Lehnertz et al. 2003). In fact it could

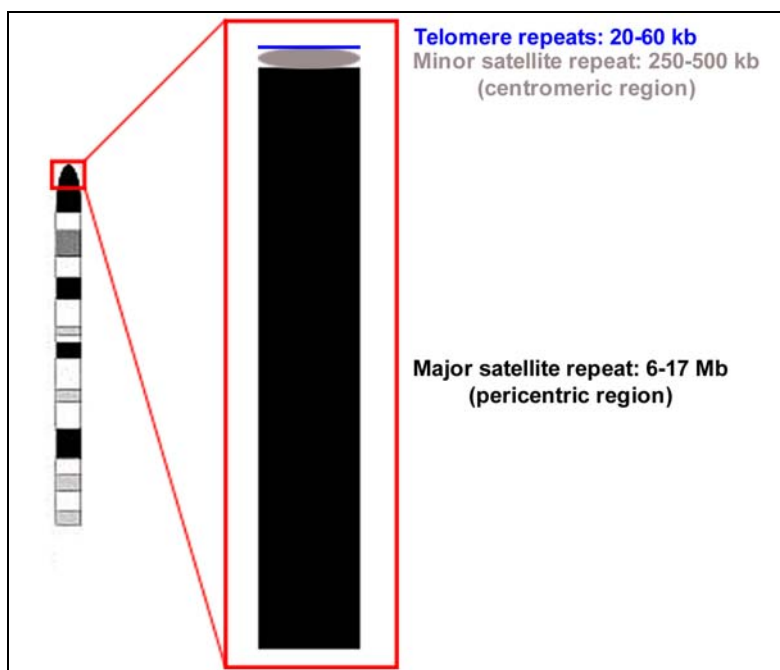


Figure 1.5: Organization of mouse centromeric region. The sketch illustrates the organization of repeats at the mouse primary constriction. The relative extent of the individual regions are drawn to scale, using mean values. The magnitudes for the respective regions are taken from (Garagna et al. 2002).

¹ This idea is further supported by the observations that mouse chromosomes can be stably maintained in somatic cell hybrids with human cells, despite the lack of sequence homology between mouse and human centromeric repeats (see (Mitchell 1996)).

² HP1 α appears to be exclusively found in pericentric regions while some HP1 β is also present in euchromatic regions, while HP1 γ is found in hetero- as well as in euchromatic compartments (discussed in (Maison and Almouzni 2004)).

be demonstrated that HP1 binding critically depends on the presence of RNA (Maison et al. 2002), though the exact mode of action is still unresolved.

A current model how the composition of pericentric heterochromatin could be accomplished, is that major satellite transcripts recruit Suv39h the histone methyltransferase responsible for tri-methylation of H3K9 via an RNAi (RNA interference) dependent mechanism¹. Tri-methylated H3K9 then specifically targets HP1 α and β to pericentric sites, which could facilitate tri-methylation of H4K20 via the specific Suv4-20h HMTase (discussed in (Schotta et al. 2004)). Since HP1 associates with Suv39h, thus propagating the generation of additional HP1 binding sites, a self-sustaining feedback loop is established which secures stability of the heterochromatic state (Maison and Almouzni 2004).

Another recently described property of nucleosomes at pericentric sites is the enrichment of the histone isoform H2AZ, which was shown to be specifically targeted to pericentric heterochromatin upon ES cell differentiation during early mammalian development (Rangasamy et al. 2003). According to its absence at the inactive X-chromosome, it has been suggested to be an early discrimination mark for constitutive versus facultative heterochromatin.

It has become increasingly accepted that the highly specific chromatin status at pericentric sites concerning DNA methylation, histone and non-histone composition/modification is of functional importance. Besides having an important role in chromosome segregation and hence in genome stability (Peters et al. 2001; Taddei et al. 2001), several studies have revealed an implication of pericentric heterochromatin in transcriptional silencing. Several examples therefor have already been described in chapter 1.2.2, which is about epigenetic mechanisms regulating transcription during differentiation. Table 1.1 summarizes some recent studies demonstrating a participation of mouse pericentric heterochromatin in controlling gene activity.

All these examples show a clear-cut correlation between pericentric heterochromatin proximity and gene silencing and suggest a role as an epigenetic modifier of transcription. Given the large-scale changes of expression pattern during differentiation and considering previous observations describing a dynamic behavior of centromeric regions during neuronal development (Manuelidis 1985), the investigation of pericentric heterochromatin topology during cellular differentiation appeared as an ideal starting point to look for a reorganization of nuclear architecture against the background of epigenetic relevance.

¹ Studies in *S. pombe* have suggested that first small-interfering RNAs (siRNAs) are generated from dsRNA formed by transcripts of the repetitive elements by an RNA specific nuclease. These siRNAs appear to associate with RNAi effector proteins, which are targeted to specific sites by complementary binding of siRNAs either to nascent transcripts or to the target DNA itself (reviewed in (Grewal and Rice 2004)). These effector proteins are then thought to recruit specific histone modifying activities, such as H3K9 HMTases.

Study	Observations
(Brown et al. 1997; Brown et al. 1999)	Several inactive genes are associated with pericentric heterochromatin in cycling B-lymphocytes, but not in resting cells.
(Brown et al. 2001)	α - and β -globin loci are separated from pericentric heterochromatin regions in erythroblasts, where they are expressed. In lymphocytes, where the genes are not active, β -globin is associated with pericentric heterochromatin, while α -globin is not.
(Brown et al. 1999)	Genes that are heritably silenced during T-cell development (<i>Rag</i> and <i>TdT</i>) are repositioned to pericentric heterochromatin domains
(Skok et al. 2001)	During the transition from biallelic to monoallelic expression, silenced immunoglobulin genes are recruited to pericentric heterochromatin.
(Grogan et al. 2001)	During T-cell development cytokine genes which are heritably shut off are repositioned to pericentric heterochromatin.
(Francastel et al. 1999)	A functional enhancer counteracts silencing of a transgene by preventing its localization at pericentric heterochromatin.
(Francastel et al. 2001)	During erythroid differentiation of MEL cells β -globin genes are relocated from pericentric heterochromatin to an euchromatic compartment. Moreover, the subunit of a transcriptional activator, critically involved in differentiation and globin gene expression, is repositioned from pericentric heterochromatin to a euchromatic compartment, thereby associating with another subunit, thus generating a functional heterodimer.

Table 1.1: The table summarizes some recent studies, which demonstrate an influence of pericentric heterochromatin on transcriptional control. The results presented in the quoted publications are described in more detail in chapter 1.2.2.

2 Methods

2.1 Cell culture

2.1.1 Basic cell culture

Following different mouse cell types were studied in the various experiments:

- Myoblasts Pmi28
- Myotubes derived from Pmi28 myoblasts
- Myoblasts C2C12
- Myotubes derived from C2C12 myoblasts
- Primary lymphocytes from peripheral blood
- Embryonic fibroblasts
- Embryonic stem cells EB5¹ (H2B-GFP), stably transfected, expressing a Histone H2B-GFP fusion protein
- Macrophages derived from EB5 (H2B-GFP) embryonic stem cells

Table 5.1 in *Supplementary Material* summarizes the most important parameters of the different cell types including source, growth conditions, split rates etc.. Standard cell culture techniques were used as described in (Celis 1994) or (Spector et al. 1998). The most important steps are summarized in the following; note that all cultivated cells were adherent, lymphocytes were only collected and immediately fixed without any further cultivation.

Materials:	
• 1xPBS (Mg ⁺⁺ -, Ca ⁺⁺ -free)	• Cetrifuge
• Cryo vials (2ml)	• Waterbath, 37°C
• Growth media (see table 5.1 in <i>Supplementary materials</i>)	• Cooling box
• Liquid nitrogen tank with racks	• Cryo box
• Meliseptol	• Laminar flow cabinet
• Sterile tissue culture flasks (25cm ² , 75cm ²) or petri dishes (∅35mm, ∅100mm)	• Freezing medium (10% DMSO in appropriate complete medium for respective cell type)
• Trypsin/EDTA (0.05%/0.02%)	• Sterile 50ml/15ml tubes

Methods
<i>Cell freezing</i>
➤ Cells are grown until ~70% confluence. One 75cm ² flask is used to freeze two vials, each containing 1.5ml of cell suspension.
➤ Cells are washed twice, using 1xPBS (37°C) to remove medium which would inactivate trypsin.
➤ 2ml 1xTrypsin per flask are applied and cells are incubated at RT or 37°C for a few minutes.
➤ Cell detachment is monitored using an inverted phase contrast microscope and can be accelerated by striking against the flask side.
➤ Cells are harvested into a 50ml or 15ml tube using the appropriate growth medium.
➤ Cell suspension is spun down for 10' at 10 000rpm.

¹ EB5 (H2B-GFP) cells were cultivated and differentiated by R. Mayer and S. Dietzel in the group of T. Cremer. EB5 (H2B-GFP) cells were established and provided by Timm Schroeder from the Institute for Clinical Molecular Biology and Tumour Genetics, GSF in Munich. The expression vector pCAG-IP and EB5 cells that were used to generate the cell line, were originally made available by H. Niwa from the RIKEN Center for Developmental Biology, Kobe.

- Supernatant is removed and the cells are resuspended in freezing medium, using 3ml per 75cm² flask.
- Cell suspension is aliquoted in 1.5ml portions per cryo vial (precooled on ice).
- In a pre-cooling step, cells are incubated for 24h at -80°C in an isopropanol-containing box, which enables a mild cooling of ~1°C per minute.
- Vials are placed in a “cryo box” within a rack and stored in a liquid nitrogen tank.

Cell thawing

- Cryo vials are briefly thawed in a 37°C water bath and plated in a 25cm² cell culture flask using fresh preheated (37°C) complete medium.
- After several hours or the next day, the medium is changed. Too long incubations of cells with medium still containing residues of DMSO have to be avoided.

Cell passaging

- Cells are cultivated in 25cm² or 75cm² cell culture flasks with a filter cap for CO₂ adaption.
- Cells are washed twice using preheated (37°C), autoclaved 1xPBS (Mg⁺⁺- and Ca⁺⁺-free).
- 1ml/2ml 1xTrypsin are applied per 25cm² /75cm² culture flask.
- Cells are incubated at RT or 37°C for a few minutes
- Detachment of cells is monitored using an inverted phase contrast microscope. Detachment can be promoted by striking against the flask side
- Adequate growth medium is used to stop Trypsin activity and the cell suspension is diluted appropriately (see Table 1 in *Supplementary Materials*)

All cell culture work was done under sterile conditions using a laminar airflow cabinet. All items that were placed inside were disinfected using Meliseptol®. Opening of bottles and caps was done over a flame using a Bunsen burner. Cells were grown at 37°C, 5% CO₂ in a humidified atmosphere.

2.1.2 Cell culture on glass coverslips

Cell culture was performed as described in 2.1.1, with the exception that glass coverslips were used instead of plastic flasks. Coverslips of different sizes were utilized, though for most experiments 20x20mm and 76x26mm were preferred. The latter were etched at one end using hydrofluoric acid in order to generate a frosted surface, so that notes could be written on. Moreover, 23x23mm photoetched coverslips were used, which feature 520 alphanumeric coded squares for the relocation of individual cells (see also chapter 2.8). For sterilization, coverslips were rinsed in absolute ethanol and flamed. For cell culture, they were placed in sterile petri dishes or in case of 76x26mm coverslips in quadriPERMs (rectangular cell culture dishes split into four separate chambers).

Materials:

- | | |
|--|-------------------------------|
| • Absolute ethanol (type 642) | • Hydrofluoric acid (conc.) |
| • Forceps | • Material as listed in 2.1.1 |
| • Glass coverslips (20x20mm, 76x26mm etc.) | • Petri dishes or quadriPERMs |
| • H ₂ O bidest. | • plastic dishes |

Methods

Etching coverslips

- 76x26mm coverslips are fixed in a modified float for 1.5ml test tubes made of rubber foam, where fine cuts were made on one side using a scalpel.
- Hydrofluoric acid is poured into a plastic dish; the depth will define the height of the coverslip that will be etched (~2cm).
- Coverslips are placed with the small side into the acid for exactly 1min.
- Coverslips are washed intensely under pouring H₂O bidest.

- After drying coverslips are stored in absolute ethanol within a Coplin jar.

Preparing coverslips for cell culture

- Coverslips are rinsed in absolute ethanol and flamed. Handling is accomplished using a forceps, which has been sterilized in the same way.
- Coverslips are placed in an adequate plastic dish.
- Before transferring cells, the dishes can be pre-filled with medium such that the coverslips are completely covered

2.1.3 Isolation of peripheral lymphocytes

Mouse blood was kindly provided by M. Moor from the Department of Molecular Animal Breeding and Genetics in Munich. Exclusively male animals from a C3HeB/FeJ hybrid strain were used. Between 5 to 10ml were usually processed. Lymphocytes isolated from 1ml of blood were loaded on 1 to 2 coverslips, for an area of approx. 30x26mm (see below). Lymphocytes were isolated using Ficoll, which allows a separation from granulocytes and erythrocytes by density gradient centrifugation. Isolated lymphocytes¹ were “glued” to glass coverslips, usually 76x26mm, using the compound Poly-L-lysine with which the coverslip were pre-coated. This basic amino acid polymer increases the substrate surface charge and hence intensifies interactions with the cell membrane. An area of approximately 30x26mm was pre-treated with Poly-Lysine and loaded with isolated blood cells. After one hour, during which the cells attached, lymphocytes were fixed as described in 2.3.

Materials:

- | | |
|--|--|
| <ul style="list-style-type: none"> • Centrifuge • Coverslips (e.g. 76x26mm) • Ficoll-Paque PLUS • H₂O bidest. • Heparin (conc.) • Mouse blood, ~0.5-1ml/coverslip | <ul style="list-style-type: none"> • Poly-L-Lysine (10 mg/ml) • QuadriPERMs • RPMI 1640 complete medium (50%FCS) • Sterile test tubes (15ml) • Sterile Pasteur pipettes |
|--|--|

Methods

Pretreatment of coverslips with Poly-L-lysine

- Coverslips are prepared as described in 2.1.2.
- Poly-L-lysine (10 mg/ml) is diluted 1:7.5 with H₂O bidest..
- Approx. 300µl of poly-L-lysine working solution is pipetted on the end of a 76x26mm coverslip, covering an area of ~30x26mm. If one coverslip end is frosted (see above) the non-frosted end is used.
- Coverslips are briefly rinsed in H₂O bidest. and air dried.

Isolation of lymphocytes

- Blood is collected in 15 ml test tubes containing a drop of heparin to prevent coagulation.
- Blood is diluted 1:2 with RPMI 1640 complete medium.
- As much Ficoll solution (RT) as blood has to be processed is centrifuged at 3000rpm for 30’.
- Blood is poured gently on the Ficoll with a sterile Pasteur pipette.
- This mixture is centrifuged at 2000rpm for 15’.
- The “buffy coat”, a milky fraction between the plasma on top and the Ficoll-phase on bottom is transferred to a 15ml test tube using a Pasteur pipette. Contaminations from top and bottom fractions should be avoided.
- 10ml of fresh medium is added and mixed cautiously.

¹ More precisely the fraction represents a mixture of “peripheral blood mononuclear cells”, consisting of 60-70% T- and 5% B-lymphocytes, 5-15% monocytes and 5-15% natural killer cells (Celis 1994).

- To remove plasma, Ficoll and possible platelets residues the cell suspension is washed 3 times by centrifuging it for 10' at 1000rpm, removing the supernatant and resuspending it in 10 ml medium..
- After the final washing step, the cell pellet is resuspended in medium using 300µl medium per coverslip that has to be loaded with the lymphocyte suspension.
- 300µl of the cell suspension is applied on the Poly-L-lysine coated area.
- Cells are incubated for at least 1h in a humidified incubator at 37°C, 5% CO₂, until they are firmly attached.
- Attachment of cells is monitored by phase contrast microscopy.

2.1.4 Differentiation

Two different mouse *in vitro* differentiation systems were studied. As one system I employed mouse myoblasts that can be easily differentiated into syncitial, polynucleated myotubes (see figure 2.1). As a second system, I used embryonic stem cells that could be induced to differentiate along the hematopoietic lineage to form macrophages. The latter cell cultures were kindly provided by R. Mayer and S. Dietzel, from the group of T. Cremer.

The myoblast/myotube system

Except for the *in vivo* experiments, a mouse myoblast cell line designated Pmi28 was used, originally established and first described by Irintchev et al. (Irintchev et al. 1997). A big advantage of this cell line compared to C2C12 myoblasts, was that the karyotype was almost normal (karyotypes on supplementary CD, see chapter 5.3). Though this culture was prepared from male BALB/c mice, a karyotype analysis showed that the Y chromosome had been stably lost. All analyzed metaphase spreads (n=8) showed a 39, X0 karyotype. Karyotyping was done by I. Jentsch from the group of M. Speicher from the Institute of Anthropology and Human Genetics, University of Munch using *Multiplex FISH* (Jentsch et al. 2001).

For *in vivo* studies I used the well characterized mouse myoblast cell line C2C12. One reason was that transfection protocols were well established on this cell line, another that they had been already successfully used for living cell observation.

For both cell lines maintenance cultures were grown in appropriate medium (see table 5.1 in *Supplementary material*) containing 20% fetal calf serum (FCS). Differentiation was induced by using Dulbeccos modified Eagle Medium DMEM, containing 10% horse serum. Alternatively, myogenic differentiation could also be induced by using medium without serum (Lawson and Purslow 2000).

Myotubes were fixed 3 to 5 days after induction of differentiation, showing extensive myotube formation that was monitored by phase contrast microscopy. Too long differentiation times leading to an increased myotube size and to a higher number of nuclei within a syncitium were avoided, because the cell layer would then become mechanically instable and easily be wiped off the coverslip during fixation. Differentiation periods of 10 days led to cultures showing spontaneous contractions, which served as a marker for proper differentiation.

Materials:	
<ul style="list-style-type: none"> • 1xPBS (Mg⁺⁺-, Ca⁺⁺-free) 	<ul style="list-style-type: none"> • DMEM complete medium with 20% FCS (for C2C12)
<ul style="list-style-type: none"> • Basic cell culture material as described above 	<ul style="list-style-type: none"> • F10 complete medium with 20% FCS (for Pmi28)
<ul style="list-style-type: none"> • Differentiation Medium (DMEM with 10% horse serum) 	<ul style="list-style-type: none"> •

Methods*Myoblast maintenance*

- Cell passaging equivalent to description in 2.1.1.
- Cell culture on coverslips equivalent to description in 2.1.2.
- Pmi28 cells are split 1/4 every second day during log-phase.
- C2C12 1/8 are split every second day during log-phase.
- **Confluence of the culture has to be avoided to prevent spontaneous differentiation!**

Myoblast differentiation

- Cells are washed twice with 1xPBS prior to application of differentiation medium.
- Differentiation medium is changed every second day.

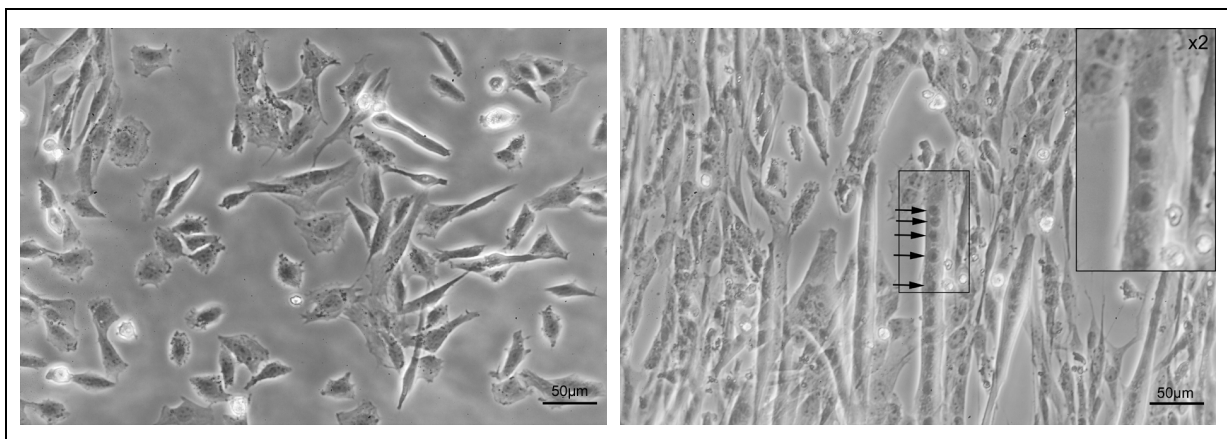


Figure 2.1: Differentiation of Pmi28 myoblasts. The left figure shows a Pmi28 myoblast culture at low cell density. In the right image several myotubes are visible. Arrows point at five nuclei within one syncytial myotube. Inset shows a two-fold magnification of the area within the square. Pictures were taken from specimen fixed in 3.7% formaldehyde using a digital reflex camera attached to an inverse phase contrast microscope. Scale bars: 50µm.

The ES cell/macrophage system

Undifferentiated ES cells as well differentiated macrophages were provided by R. Mayer and S. Dietzel, both from the group of T. Cremer, where the present thesis was accomplished. In the following only a brief presentation of the system is given, details can be found in the respective citations.

The ES cell line EB-5 (H2B-GFP) was established and kindly provided by Timm Schroeder from the GSF-National Research Center for Environment and Health, Institute for Clinical Molecular Biology and Tumor Genetics in Munich. It was derived from the ES cell line EB5 and harbored a stably transfected construct encoding the histone H2B fused to the green fluorescent protein (H2B-GFP) (Schroeder et al. 2003).

Cell passaging of EB5 (H2B-GFP) cells was accomplished by cultivation on gelatinized culture flasks. To prevent differentiation the culture medium was supplemented with the leukemia inhibitory factor (LIF) that was obtained from transgenic CHO 8/24 720 LIF-D cells, which secrete it into the culture medium. Before fixation, cells were harvested from culture flasks by trypsinization and plated on gelatinized coverslips.

Differentiation of ES cells to macrophages was accomplished by co-cultivation of ES cells on OP9 stroma cells (see (Nakano et al. 1994) for details). After 5 days, differentiating cells were plated on fresh OP9 cells. After another 8 days when developing hematopoietic stem cells started to detach from the substrate and grow in suspension they were transferred to cell culture flasks using medium containing the macrophage colony-stimulating factor (M-CSF) and interleukin 3 (IL-3). The cytokines were obtained by cultivation of L-cells and X63 AG-653 cells, transgenically expressing and secreting M-CSF and IL-3, respectively. After 12

days the culture was consisting mainly of adherently growing cells, most of them being macrophages and dendritic cells. Cells were transferred onto glass coverslips and fixed the following day. Terminally differentiated macrophages were identified by immunocytochemical detection of the surface antigen Cd11b (also known as Mac-1, see (Corbi et al. 1988; Kernohan et al. 1990)) and by being in G0. The latter was ascertained by a lack of BrdU incorporation, following a 24h BrdU labeling period (see 2.6).

2.2 Preparation of metaphase chromosomes (2D-fixation)

For karyotype analysis, as well to test FISH probes for quality and specificity, mitotic chromosomes of various cell types were prepared. A growing culture, if possible in log-phase, was treated with the spindle inhibitor colcemide that depolymerizes microtubules, inhibits their *de novo* formation and thus arrests cells in metaphase. Increasing the incubation time would augment the fraction of mitotic cells, but since chromosome condensation continues, it would also yield shorter chromosomes, which can be a drawback, if a high resolution is desirable. Cells were harvested by trypsinization. After a hypotonic treatment, which increases the internal cellular pressure and facilitates chromosome spreading, cells were fixed in a mixture of absolute methanol and glacial acetic acid at a ratio of 3:1. Extensive washings with fixative were crucial for improving the cleanliness of the preparations.

The dropping technique was a critical step for obtaining nicely spread metaphase preparations. Especially temperature and humidity are known to play an important role. Applying an optimized protocol by Deng et al. (Deng et al. 2003) gave the best and most reproducible results of this virtually “voodoo dependent” work step. This protocol standardizes temperature and moisture, by placing the slide in a metal box after dropping and the box then immediately in a closed water bath. Having a constant water temperature and water level, the conditions in which the dropped cell suspension on the slide dries up can thus be reproduced. The crucial parameter for the moisture conditions inside the closed water bath is the ratio R between the net area of water surface (total water surface minus surface covered by the metal box)

Materials:

- 0.01N HCl
- 1xPBS
- 50ml/15ml test tubes
- Centrifuge
- Colcemide (10µg/ml)
- Ethanol (type 642), 100%, 90%, 70%
- Fixative: Methanol/glacial acetic acid (3:1), ice cold
- Freezer (-20°C)
- Hypotonic solution: 0.56% KCl, 37°C
- Silicagel with moisture indicator
- Slide storage boxes
- staining jars (acc. to Coplin, Hellendahl or Schiefferdecker)
- Trypsin/EDTA (0.05%/0.02%)
- Waterbath at 37°C
- Waterbath at 50°C

and the volume of air between the water surface and the lid of the waterbath¹. Changing these two variables moreover allows an adjustment of the conditions.

In cases where the preparations would still show considerable cytoplasmic residues even after extensive washings, a few extra drops of ice-cold fixative were applied on the tilted slide after having dropped the cell suspension. It was important to apply these extra drops just when the fixative of the cell suspension drop was beginning to dry up.

To preserve a compact morphology of chromosomes that is affected by heat denaturation during FISH, the slides were artificially “aged” by incubation at 37°C ON or at 60°C for 2h. If necessary a final pepsinization was carried out, to further improve the quality.

¹ The ratio R giving the best results described in the paper was around 0.22, which was also applied in the present experiments.

Methods*Fixation*

- Cells are grown until 60%-70% confluence.
- 8µl colcemide per ml medium is added.
- Cells are placed back in the CO₂ incubator until many spherical (mitotic cells) cells appear. It should be kept in mind that longer incubation times result in shorter mitotic chromosomes. For fast growing culture 30'-60' can be enough, extremely slow growing cells might need a few hours or even an ON incubation
- Cells are trypsinized as described in 2.1.1. **“Old” medium is kept and added to the trypsinized culture, as it contains already many detached mitotic cells!**
- Trypsinization is stopped with “old” medium and cells are transferred to 50 ml test tubes
- Cells are centrifuged at 1000 rpm for 10'.
- Supernatant is removed and a few ml of a 37°C 0.56% KCl solution are applied. The suspension is mixed thoroughly with a pasteur pipette and filled up to 20ml with hypotonic solution.
- Cell suspension is incubated for 15'-20' at 37°C. (The duration of this hypotonic treatment is variable but crucial for an optimal spreading. It has to be optimized for individual cell types).
- Approx. 1ml ice-cold fixative is added and the suspension is thoroughly mixed. Agglutinations can be avoided by pouring the fixative slowly.
- Cells are centrifuged at 1000rpm for 10'.
- Supernatant is removed until 10-15ml are left and after resuspending the cells, they are transferred to 15ml test tubes.
- Cells are centrifuged at 1000rpm for 10'.
- Supernatant is removed until the taper of the tube.
- 1ml of ice-cold fixative is slowly added and cells are resuspended very gently.
- Further 14ml of fixative are added.
- Cell suspension is incubated 30' at -20°C
- For washing the following steps can be repeated up to 10 or more times:
 - Cells are centrifuged at 1000rpm for 10'.
 - Supernatant is removed.
 - 15 ml ice-cold fixative is applied and cells are thoroughly resuspended.

Dropping (according to Deng et al. (Deng et al. 2003) with modifications)

- Slides for dropping are incubated for ~30' in absolute ethanol, and cleaned using a dry lint cloth. Slides are stored at -20°C and should be completely cooled down before use.
- The water bath water level is adjusted in order to obtain a surface/volume ratio (R) of ~0.22¹
- Cell suspension (RT) is dropped (~10µl/drop) from a height of approx. 10cm on cold slides, while the slide is slightly tilted.
- The slide is put immediately into the metal box (RT) and into the water bath.
- After a few minutes, the slide is dried and can be checked for quality and cell concentration using a phase contrast microscope.
- If necessary, the concentration is adjusted by either adding fixative or by centrifuging and removing fixative.
- If the metaphases appear to have still residues of cytoplasm, they can be washed additional times with fresh fixative (see above).

¹ Since the net surface area of the used water bath was 30cm x 32cm (water bath) - 19.5cm x 10cm (metal box) = 765cm², the water level was adjusted to 3.6cm below the lid to obtain a surface/volume ratio (R) of 0.22.

- To increase cleanness the following can be applied instead of placing the slide in a water bath: After dropping, the slides are placed tilted with the narrow side on the bottom leaned against e.g. a test tube holder on a Kleenex. As soon as the fixative starts to evaporate from the slides periphery, a few drops of ice-cold fixative are poured over the slide. The timing when to apply these extra drops of fixative is crucial, as applying it too early will wipe chromosomes off, while applying it too late will have no effect at all.

Ageing of slides

- Slides are aged by incubation ON at 37°C or for 2h at 60°C

Pepsinization (optional)

- 0.01N HCl is warmed-up at 37°C.
- Slides are placed in staining jars.
- Pepsin (320-450u/μl) is diluted 1/2000 in 0.01N HCl (37°C) to a final concentration of 0.16-0.23u/μl.
- Slides are incubated in pepsin dilution for 10' at 37°C.
- Slides are washed 3 times for 5' with 1xPBS using a shaker.
- Preparations are dehydrated by successive incubation in 70% EtOH for 10', 90% EtOH for 1' and 100% EtOH for 1'.
- After complete drying, slides are placed in storage boxes together with silica gel pearls, to prevent rapid re-hydration (silica gel pearls are kept in perforated plastic bags and stored at 60°C to ensure maximum hygroscopy).
- Slides are stored at -20°C

2.3 3D-Fixation

The term 3D-fixation stresses the fact that the protocols used are designed to preserve the three dimensional morphology of the specimen as good as possible. The group wherein the present thesis was done has a lot of experience in the field of cell and tissue fixation and is constantly developing improved protocols for 3D-fixation approaches. The latest is described in detail in "FISH-A Practical approach" from "The Practical Approach Series" (Solovei et al. 2001). An article of Solovei et al. (Solovei et al. 2002) from the group of T. Cremer is worth to be mentioned in this respect. Herein the nuclear morphology after individual fixation steps was compared with the situation *in vivo*. By using cells expressing a histone H2B-GFP fusion protein and by labeling replicated DNA using fluorescently labeled nucleotides (Schermele et al. 2001), large scale topology of chromatin as well as chromatin domains at a 1Mb level could be visualized and mapped within the nucleus. At the light microscopic level as revealed by confocal-laser-scanning-microscopy, the fixation procedure did result in a good preservation of nuclear morphology, sufficient for studies at a 1Mb-domain level. Moreover, even after heat denaturation of cells during FISH no drastic changes were observable at this resolution. At the electron microscopic level however, a drastic change of the nuclear fine structure could be observed after heat denaturation.

In the following, the most important steps of the method are explained. Fixation was achieved by the crosslinking agent formaldehyde¹, usually at a concentration of 4% (w/v) in

¹ Sometimes it is also referred to as paraformaldehyde, which is actually not the correct term for the dissolved agent as it describes the polymerized form, e.g. the powder that is used to prepare a solution. The term paraformaldehyde is used to denote a freshly dissolved formaldehyde solution prepared from the solid substance, in contrast to a solution generated from a commercially available higher concentrated solution, usually 37%. The latter contains a significant amount of methanol for stabilizing purposes, which might have negative effects on the fixation quality. It should be kept in mind that if a 4% paraformaldehyde solution is mentioned a freshly dissolved formaldehyde solution is meant.

1xPBS. The crosslinking of cellular components like proteins, nucleic acids, and other compounds is chemically accomplished by the formation of methylene bridges between reactive groups of the cellular molecules with the formaldehyde-molecules. The major advantage of fixation protocols using cross-linkers instead of denaturing compounds like methanol, ethanol or acetone is that the morphology of the fixed material resembles much more the *in vivo* situation. Especially shrinkage of the specimens caused by the latter agents can be avoided using formaldehyde. To permeabilize cells and nuclei for antibody and probe penetration, incubation with the non-ionic detergent TritonX100 was performed. At this point fixation was stopped and cell preparations were stored in 1xPBS if immunofluorescence had to be applied. For FISH specimens were additionally permeabilized by a repeated freezing and thawing step using a glycerol solution and liquid nitrogen. To render chromatin more accessible to DNA-probes an additional treatment with 0.1N HCl was carried out. For specific cell types (see description in the *Methods*-table below), a supplementary pepsin treatment was performed to further permeabilize cells. Especially experiments with myotubes, which have a dense cytoplasm benefited from this treatment. Another positive effect of pepsinization was an increased signal/noise ratio by elimination of cross-reactive targets in the cytoplasm. Fixed cells were stored in 50% formamide/2xSSC, for at least one day. Prolonged storage correlated with better hybridization results, possibly by an increased destabilization of the DNA double-strand, caused by formamide.

Depending on the cell type, the fixation protocol was modified in order to preserve *in vivo* morphology as good as possible. Cell types like lymphocytes or ES cells for example were pre-treated and fixed under hypotonic conditions in order to prevent flattening of nuclei. In experiments, not intended for distribution and localization analyses, fixation was accomplished with 3.7% formaldehyde diluted from a 37% commercial solution containing 10-15% methanol.

Cave: At any step, drying of the cells has to be avoided. For those reasons buffers that were used after fixation contained small amounts of detergent. This would decrease surface tension and keep specimens covered with fluidity for a prolonged time, which was especially important during buffer changes.

Materials:	
<i>Immunofluorescence</i>	<i>FISH</i>
<ul style="list-style-type: none"> • 0.5% Triton X-100 in 1xPBS • 2xSSC • Formaldehyde (37%) • heatable magnetic stirrer • Paraformaldehyde (extra pure) • PBS, depending on the cell type: 1x, 0.5x, 0.3x, 0,75x (0.04% Na Azide) • Waterbath 37°C • Weighing machine 	<ul style="list-style-type: none"> • Material as in <i>Immunofluorescence</i> • 0.1N HCl • 20% glycerol (v/v) in 1xPBS • 50%FA/2xSSC pH 7.0 • fridge • Liquid nitrogen • Pepsin (10% in H₂O bidest. = 320-450u/μl) • Phase contrast microscope

A detailed description of the method for the various cell types is shown in *Supplementary material* (table 5.2).

2.4 Immunofluorescence

For immunofluorescence, cells were fixed as described in 2.3. Sufficient permeabilization was accomplished using the detergent Triton X-100 for intra-cellular and intra-nuclear antigens, but was not needed for the surface antigen Cd11b that was detected for macrophage identification. Detection schemes usually consisted of two layers, with a primary antigen-

specific antibody as a first layer and a secondary antibody, which was specific for immunoglobulins from the species the first antibody was generated in as the second layer. The latter was conjugated with a fluorophore allowing visualization by epifluorescence or confocal microscopy. Nuclei were counterstained with DAPI (4',6-Diamidino-2-phenylindole) and additionally with the DNA binding dye TO-PRO®-3 iodide, since the utilized confocal microscopes were not equipped with an appropriate UV-laser. The latter can be excited by a 633nm laser line and emits light in the infrared spectrum.

Materials:

- 1xPBT (1xPBS/0.02% Tween 20)
- Antifade (Vectashield®)
- Blocking solution (4%BSA/1xPBT)
- Bovine serum albumin fraction V (BSA)
- DNA staining dyes:
 - 4',6-Diamidino-2-phenylindole (DAPI) (5µg/ml)
 - TO-PRO®-3 iodide (1mM)
- forceps
- Incubator at 37°C
- Nail Polish
- Parafilm
- Primary/secondary antibodies (see *Methods*)
- Shaker
- Slides

Methods*Detection*

- Coverslips with cells are incubated in blocking solution for 10-15' at 37°C
- Antibodies are diluted in blocking solution as follows:

Primary antibodies			
CREST serum (human)	1:2	Rabbit-α MeCP2	1:25
Goat-α lamin B	1:100	Rat-α M31(HP1)	undiluted
Mouse-α B23	1:500	Rat-α Cd11b	1:500
Mouse- αOct3	1:50		
Secondary antibodies			
Donkey-α goat-Alexa488	1:400	Goat-α rabbit-FITC	1:100
Donkey-α goat-Cy3	1:500	Goat-α rat-Cy3	1:500
Goat-α mouse-Alexa488	1:400	Goat-α rat-FITC	1:500
Goat-α mouse-Cy5	1:100	Rabbit-α goat-FITC	1:200
Goat-α rabbit-Cy3	1:500	Rabbit-α human-Cy3	1:100
Goat-α rabbit-Cy5	1:200	Sheep-α mouse-Cy3	1:500

- Approx. 200µl of antibody solution are applied on a coverslip for an area of ~60x26mm.
- The coverslip is covered with parafilm to prevent drying and incubated for 30' at 37°C
- Between the changes of layers, coverslips are washed in 1xPBT at least 3x 3' at 37° by shaking.
- Specimens are counterstained using DAPI and TO-PRO®-3 diluted 1:100 and 1:2000 dilutions, respectively in 1xPBT. Coverslips are incubated between 3' to 5' at RT (flatter cells like fibroblasts were incubated 2', ES cells or lymphocytes 4'), briefly rinsed in 1xPBT and mounted.

Mounting

- A drop of Vectashield® is put on a thoroughly cleaned 76x26mm slide.
- Coverslips are put face down on the prepared slide trying to avoid the formation of air bubbles.
- Coverslips are dried carefully using a Kleenex and sealed by a thin film of nail polish at the coverslips' edge.

2.5 Fluorescence in situ hybridization (FISH)

As other techniques based upon hybridization, like southern or northern blotting, fluorescence in situ hybridization (FISH), makes use of the DNA's property to denature and renature in a sequence specific manner. Specific DNA sequences can be visualized *in situ*, i.e. in metaphase chromosomes or in interphase nuclei by hybridizing nucleic acids or derivatives¹ containing nucleotides carrying a tag. Such tags can consist of haptens like digoxigenin, biotin, estradiol or a dinitrophenyl residue (DNP), or of fluorophores. In the former case a detection of the tag via fluorescently labeled antibodies or other specifically binding reporter molecules like Avidin/Streptavidin binding to Biotin, are necessary, which is dispensable in the latter case. By using multiple detection layers, signal intensities can be amplified, increasing the resolution of sequences that can be detected. The smallest detectable DNA stretches are in the range of 1kb on single chromatin fibers (fiber-FISH), while on the other hand complex probe mixes permit the visualization of complete chromosomes. Numerous and diverse applications of FISH can be found in the book "FISH a practical approach" (Beatty et al. 2001).

2.5.1 Probe generation/amplification

The first important step was to generate sufficient amounts of the specific probes that were going to be used in the FISH experiments. To visualize pericentromeric heterochromatin, a probe specific for the mouse major satellite was generated by PCR using a specific primer pair and mouse genomic DNA as template.

For the studies on the distribution of chromosomes in interphase nuclei, chromosome paint probes for the whole mouse chromosome complement were available, which were kindly donated by Nigel Carter, from the Sanger Institute in Cambridge. To generate satisfactory amounts, these painting probes were amplified using a special PCR technique called DOP-PCR (see 2.5.1.2).

Mouse major satellite specific probe

The first step to generate a probe that would specifically label pericentromeric heterochromatin was to determine a primer pair that would amplify a large stretch of the 234bp long major satellite that makes up this region by tandem repetition. The primer pair was designed using published sequence information (Horz and Altenburger 1981) and the software MacVector (Accelrys). Software handling was done by M. Ulbrecht from the group of E. Weiss, from Institute for Anthropology and Human Genetics, LMU Munich. The resulting primer pair consisted of a 20nt and a 19nt long nucleotide, amplifying a 170bp sequence fully contained in the 234bp major satellite repeat. The specificity of the product was confirmed by hybridization of the labeled sequence to mitotic chromosomes, which resulted in the characteristic centromeric labeling pattern. The same pattern was also observed using an oligonucleotide probe, kindly provided by Harry Scherthan, for which a pericentric specificity had already been described (Scherthan et al. 1996). As template for the PCR, reaction genomic DNA isolated from mouse embryonic fibroblasts was used.

¹ PNA probes for example have a peptide backbone instead of a sugar phosphate one and are used for quantitative fluorescence measurements. An example for such commercially available probes can be found at http://dakousa.com/cat/cat_pdfs/MOLPATH.pdf.

Materials:*Isolation of genomic DNA*

- | | |
|------------------------------------|---|
| • 15ml test tubes | • Saturated NaCl solution (6M) |
| • Centrifuge | • SDS (10%) |
| • Ethanol (type 510) 100% and 70% | • SE-buffer (75mM NaCl, 25mM Na ₂ -EDTA, pH 8.0) |
| • H2O bidest. (sterile) | • Small glass hook |
| • Material for cell trypsinization | • Vortexer |
| • Photometer | • Water bath 55°C |
| • Proteinase K (15mg/ml) | |

PCR

- | | |
|--|--|
| • dNTPs (5mM) | • Primer for mouse major satellite (c=25pmol/μl): |
| • genomic DNA (10ng/μl) | forward: 5'-GCG AGA AAA CTG AAA ATC AC-3' ¹ |
| • H2O bidest. | backward: 5'-TCA AGT CGT CAA GTG GAT G-3' ² |
| • MgCl ₂ (25mM) | |
| • PCR buffer (10x) (100mM Tris-HCl, 500mM KCl, pH 8.3) | • Taq Polymerase (5000u/ml) |
| | • Thermocycler |

Methods*Isolation of genomic DNA (for 3 confluent 75cm² flasks of adherently growing cells)*

- Cells are trypsinized as described in 2.1.1.
- Trypsinization is stopped by adding 3ml medium/flask and cells are transferred to a 15ml test tube.
- Cells are centrifuged at 1500rpm for 10'.
- Supernatant is removed and 10ml 1xPBS are added for washing.
- Previous two steps are repeated.
- Cells are resuspended in 5ml SE-buffer containing 50mg/ml Proteinase K and 1% SDS.
- Cells are incubated 5h at 55°C. (Cell lysis)
- 3ml of a saturated NaCl solution are added and the solution is mixed thoroughly by vortexing for 20". (Protein precipitation)
- Lysate is centrifuged at 3000rpm for 15'.
- Clear fraction is transferred to a fresh test tube, avoiding co-transferring the foam.
- Twice the volume of absolute ethanol is added to the transferred fraction and incubated at RT for a few minutes. (DNA extraction)
- The DNA can be fished using a glass hook and is transferred to a fresh 1.5ml or 2ml test tube.
- DNA is washed once with a small volume of 70%EtOH (merely covered).
- After EtOH has completely vaporized DNA is resuspended in H2O (~500μl for 3 confluent flasks of adherently growing cells)
- The concentration can be measured using a photometer by determining the optical density (OD) at a wavelength of 260nm (OD₂₆₀).

¹ binds at positions 15 to 34 of the 234bp repeat

² binds at position 184 to 166 of the 234bp repeat

PCR

- The template DNA (genomic DNA isolated from mouse embryonic fibroblasts) is diluted to a final concentration of 10ng/μl
- For a 100μl reaction following ingredients are combined:

PCR buffer (10x):	10μl
MgCl ₂ :	8μl
Forward primer:	4μl
Backward primer:	4μl
dNTPs:	4μl
genomic DNA:	10μl
H ₂ O:	59μl
Taq-Polymerase:	1μl
- The following PCR program is used:

Primary denaturation:	94°C → 3'
Amplification: (x35)	
Denaturation	94°C → 1'
Annealing	56°C → 1'
Extension	72°C → 2'
Final extension	72°C → 5'
- The amplification success is checked by gel electrophoresis on a 1% agarose gel using standard protocols.

Mouse chromosome paint probes

Painting probes for the whole mouse chromosome complement were provided from Nigel Carter from the Sanger Center in Cambridge. Mitotic mouse chromosomes had been sorted by FACS (fluorescence activated chromosome sorting) as described in (Rabbitts et al. 1995). In brief flow sorting was accomplished by staining chromosomes with Hoechst 33258 and Chromomycin A3, which are fluorescent DNA binding dyes that have different AT/GC binding affinity. Thus, almost each chromosome could be individualized by its unique fluorescence properties depending from its size and GC content. Some very similar chromosomes were sorted from cell lines having homozygous translocations in one of the respective chromosomes

Those mitotic chromosomes served as templates for a special PCR method called DOP-PCR, which allows the amplification of complex templates. **D**egenerate **o**ligonucleotide-**p**rimed-PCR (DOP-PCR) (Telenius et al. 1992; Telenius et al. 1992) employs a mixture of primers, which consist of a defined 5' and 3' end and a variable sequence in-between (e.g. 6MW, 6A1). By using low stringency conditions during a first amplification steps, templates of high complexity like complete chromosomes can be amplified, with the products still representing the high sequence diversity. A second amplification step, using high stringency conditions, can then create a high amount of the product. This PCR approach is used in the so-called *primary* amplification of the "primordial" probe, i.e. of the sorted chromosome or the micro-dissected probe etc.. These primary PCR products can subsequently be further amplified by a so-called secondary PCR, which lacks the low stringency step. Since already secondary PCR products of the flow-sorted chromosomes were available, I just used additional secondary (actually tertiaries) PCRs to amplify the probes.

For the sake of completeness it should be noted that repeatedly performed PCRs on secondary, tertiary etc., products are said to lead to a loss of the probe complexity, resulting in a heterogeneous labeling of the region. This was not observed for the probes used in these experiments.

Materials:

- 6 MW primer (17 μ M):
- MgCl₂ (25mM)
- 5'-CCG ACT CGA GNN NNN NAT GTG-3'
- PCR buffer (10x) (100mM Tris-HCl, 500mM KCl, pH 8.3)
- dNTPs (5mM)
- Taq Polymerase (5000u/ml)
- Template DNA (secondary DOP product)
- Thermocycler
- H₂O bidest.

Methods

- For a 50 μ l reaction mix following components are combined:

PCR buffer (10x):	5 μ l
MgCl ₂ :	4 μ l
6 MW primer:	5 μ l
dNTPs:	2 μ l
H ₂ O:	32 μ l
Primary/secondary PCR product:	1 μ l
Taq-Polymerase:	0.5 μ l
- The following PCR program is used:

Primary denaturation:	94°C → 3'
Amplification: (x35)	
Denaturation	94°C → 1'
Annealing	56°C → 1'
Extension	72°C → 2'
Final extension	72°C → 5'
- The amplification success is checked by gel electrophoresis on a 1% agarose gel using standard protocols.
- Probe length and amount are estimated from the gel by comparing the PCR product with λ HindIII DNA molecular weight marker and by commercial C₀t1-DNA of known concentration.

2.5.2 Probe labeling

There are different possibilities to label the DNA probes, once generated as described above. Besides adding labeled nucleotides at the end of a probe (end labeling), nucleotides carrying a hapten or a fluorophore can be incorporated within a probe. The so-called Label-DOP-PCR is derived from the DOP-PCR method mentioned above, but features a partial substitution of one nucleotide type by a labeled analogue and uses a slightly modified amplification program. Besides this PCR based technique that has the great advantage to increase the probe amount while labeling, the so-called nick translation method incorporates tagged nucleotides by introducing nicks into the probe via DNase I, which serve as starting points for DNA Polymerase I (Kornberg polymerase). This enzyme elongates the generated 3'-OH ends and removes the old strand by its 5'-3' exonuclease activity. During strand elongation, labeled nucleotides are incorporated.

For the whole chromosome painting (WCP) probes, I used the Label-DOP-PCR approach because high amounts of probe were necessary to yield high-quality hybridization signals. To produce these would have been much more laborious using nick translation. Besides that a few more amplification rounds would have been necessary to prepare the probe amounts necessary for nick translation, which might had reduced the probe's complexity and thus the signal quality. Since in 3D-fixed cells directly labeled painting probes usually show insufficient signal intensities the probes were labeled using digoxigenin, biotin or DNP as tag. For visualization of pericentric regions, nick translational labeling with fluorochrome-tagged nucleotides (TAMRA-dUTP or Cy3-dUTP) turned out to give the best results. Employing dig-

oxigenin or biotin labeled probes resulted in signals showing an inhomogeneous appearance (see also 3.1). This might have been caused by an inadequate accessibility for the antibodies or avidin to bind the antigens within the dense heterochromatic clusters. Nick translation was used instead of Label-DOP-PCR because of its general higher incorporation efficiency of labeled nucleotides, which is especially important if no signal amplification by multi layer detection is used.

Label-DOP-PCR [chromosome painting probes]

As already mentioned the Label-DOP-PCR protocol is based on the DOP-PCR protocol. However instead of all nucleotides having the same concentrations one's is reduced and a labeled analogue is added. In the present case biotin, digoxigenin or DNP labeled dUTPs were used at a final concentration of 20nM while its unlabelled counterpart dTTP was present at a concentration of 80nM. The other three nucleotides were used at 100nM. Moreover, the amplification program differs from secondary DOP PCR in that the number of cycles is reduced to 20 compared to 35, and that the elongation time is decreased to 30 seconds compared to 2 minutes. For FISH on 3D fixed cells, it is important that the probe length does not exceed 800bp in order to maximize probe penetration on the one hand and reduce unspecific background signals on the other hand. To accomplish this, the products can be shortened by an digestion with DNase I. Alternatively increasing the primer concentration up to 5fold can also decrease the probe length drastically, so that a laborious digestion with DNase I that always holds the risk of a complete loss of the probe can be avoided. If the probes are very short like is the case using synthetic oligonucleotides, washing-stringency should not be too high, to prevent a complete removal of the probe from the target. Since in the present experiments using the described protocol generated probes in the optimal range, no post digestions or modifications of primer concentrations were required (see also 3.1).

Materials:

- | | |
|---|---|
| • 6 MW primer (17µM):
5'-CCG ACT CGA GNN NNN NAT GTG-3' | • MgCl ₂ (25mM) |
| • AGC-mix (dATP, dGTP and dCTP each
2mM) | • PCR buffer (10x) (100mM Tris-HCl, 500mM
KCl, pH 8.3) |
| • dTTP (1mM) | • Probe-DNA (from secondary, tertiary etc. PCR) |
| • H ₂ O bidest. | • Taq Polymerase (5000u/ml) |
| • Label dUTP (1mM):
Biotin-16-dUTP
Digoxigenin-11-dUTP
DNP-11-dUTP | • Thermocycler |

Methods

- For a 50µl reaction following components are combined:
- | | |
|---------------------------------|--------|
| PCR buffer (10x): | 5µl |
| MgCl ₂ : | 4µl |
| 6 MW primer: | 5µl |
| AGC-mix: | 2.5µl |
| dTTP | 4µl |
| Label-dUTP | 0.5µl |
| H ₂ O: | 27.5µl |
| Secondary/tertiary PCR product: | 1µl |
| Taq-Polymerase: | 0.5µl |

- The following PCR program is used:

Primary denaturation: 94°C → 3'

Amplification: 20 cycles
 Denaturation 94°C → 1'
 Annealing 56°C → 1'
 Extension 72°C → 30''

Final extension 72°C → 5'

- The amplification success is checked by gel electrophoresis on a 1% agarose gel using standard protocols.
- Probe length and amount is estimated from the gel by comparing the PCR product with λ HindIII DNA molecular weight marker and by commercial C₀t1-DNA of known concentration.
- *Optional:* If the fragments show a length significantly bigger than 800bp, a few μ l of a 1:500 - 1:1000 DNase I dilution are added and the tubes incubated between 5' to 15' at 15°C, depending on the length of the probe.

Nick translation (NT) [major satellite probe]

In contrast to Label-DOP-PCR, nick translational labeling does not augment the probe amount, so that already high amounts of unlabelled probe must be available. As recommended in standard protocols, 1 μ g of DNA was used for a 50 μ l reaction. Like already mentioned for the PCR labeling approach, the labeled product should consist of fragments not bigger than 800bp. DNase I concentration and incubation time are the relevant variables for generating an optimal probe length. After an incubation time of maximum 90' at 15°C, the products should be checked on a 1% agarose gel and if necessary post-digested, to further shorten the labeled fragments. Because using the described protocol generated sufficiently short fragment, an additional digestion was not necessary.

Materials:

- DNase I (>2000u/ml)
- dNTP-mix (dATP, dCTP and dGTP each 5mM, dTTP 2mM)
- EDTA (0.5M)
- H₂O bidest.
- Kornberg-Polymerase (5u/ μ l)
- Label dUTP (1mM):
 Cy3-dUTP
 TAMRA-dUTP
 Biotin-16-dUTP
 Digoxigenin-11-dUTP
- β -Mercaptoethanol (0.1M)
- Nick translation buffer (10x: 0.5M Tris-HCl pH 7.5; 50mM MgCl₂; 0.05% BSA)
- polystyrene box filled with water at 15°C (temperature constantly measured and adjusted with crushed ice)
- Unlabelled probe (~ 1 μ g)

Methods

- For one 50 μ l reaction mix following components are combined:

NT buffer (10x):	5 μ l	
β -Mercaptoethanol:	5 μ l	
dNTP-mix:	5 μ l	
Label-dUTP: (TAMRA- or Cy3-dUTP)	1 μ l	
Probe DNA	3 μ l	(the major satellite amplification product was estimated to have a concentration of ~400 μ g/ μ l)
H ₂ O:	17.5 μ l	
DNase I (diluted 1:250)	2.5 μ l	
DNA polymerase I	1 μ l	

- After adding the enzymes, the test tubes are incubated at 15°C using a water filled styrofoam box for 75'.
- The reaction is temporarily stopped by putting the test tubes on ice.
- The fragment length is checked by gel electrophoresis on a 1% agarose gel using standard protocols.
- Reaction is stopped by adding 0.5µl of EDTA (0.5M).¹

2.5.3 FISH setup

According to standard protocols for chromosome painting probes a DNA concentration of 40-60ng/µl, for repetitive sequences like the mouse major satellite 1ng/µl is recommended (Solovei et al. 2001). Nevertheless, it is advisable to try different concentrations if a probe is used for the first time. Furthermore, cell type specific adjustments of probe concentration might be necessary.

Probe precipitation:

To obtain the desired concentrations the probes first had to be precipitated and resuspended in an appropriate volume of hybridization mixture (50% formamide/10% dextranulphate/2xSSC solution). For an area of 18x18mm the probes were dissolved in a volume of 4-5µl.

Painting probes: The necessary volume of the respective chromosome painting probe(s) was precipitated with an approx. 50fold excess of mouse C₀t1-DNA and 50µg of salmon sperm (SS) DNA. The latter was important as carrier DNA to increase precipitation efficiency. The former was crucial as suppressor against unspecific cross hybridization of the probe. The more complex a probe is the higher is the probability to contain repetitive elements that bind unspecifically throughout the genome (LINES, SINES centromeric, telomeric repeats etc.). Such elements within the labeled probe are hybridized quickly by the excess of suppressor DNA and are thus prevented from binding their target in the specimen. C₀t 1 DNA is a fraction of the genome highly enriched for such repetitive elements and bears its name from studies on reassociation kinetics². Instead of C₀t 1 DNA, also genomic DNA can be used as suppressor.

DNA was precipitated by adding a 2.5fold volume of ethanol, incubating at -20°C for 30', followed by a centrifugation at 13000rpm for at least 30'. After complete drying of the pellet, employing vacuum centrifugation, the DNA was resuspended according to the desired concentration. Dissolving was done in a 50% formamide/10% dextranulphate/2xSSC solution (hybridization mixture). Formamide is used to destabilize interactions of the DNA double strand and thus to decrease denaturation-temperature, while the effect of dextranulphate is to increase the local probe concentration by DNA dehydration.

Major satellite probe: The adequate amount of major satellite probe was extracted by water evaporation using vacuum centrifugation. Thus, no salmon sperm DNA was necessary. Since the probe consisted of a repetitive element *per se*, no suppression was used either. This technique was favored as it gave brighter hybridization signals compared to ethanol precipitation (which was not the case for painting probes).

¹If the fragments are still too long a few µl of DNase I (1:250) are added and the tubes are incubated for further 10-15 minutes at 15°C depending on the length. For the present experiment using the described protocol, a post-digestion was not necessary.

² The name stresses the fact that it is DNA that re-associates very quickly, namely with the product of c₀ (starting concentration of single stranded DNA) and the time t equalling 1 (c₀t=1) (see (Knippers 2001) pp.15-17).

Materials:	
<i>Chromosome painting probes</i>	<i>Major satellite probe</i>
<ul style="list-style-type: none"> • Centrifuge (-13000rpm) • Ethanol (type 510) • Freezer • Labeled DNA ~40-60ng/μl hybridization mixture • Mouse C₀t 1 DNA (1μg/μl) • Salmon sperm (SS) DNA (10μg/μl) <ul style="list-style-type: none"> • Hybridization mixture (50% formamide/10% dextranulphate/2xSSC solution) 	<ul style="list-style-type: none"> • Labeled DNA ~1ng/μl hybridization mixture
	<ul style="list-style-type: none"> • test tube shaker (~40°C) • Vacuum centrifuge

Methods
<p><i>Chromosome painting probes</i></p> <ul style="list-style-type: none"> ➤ The appropriate volume of labeled DNA is mixed with an approx. 50 fold excess of mouse C₀t 1 DNA¹ and with 50μg (=5μl) of SS DNA. ➤ Ethanol is added using the 2.5-fold volume of the total DNA volume (including C₀t1 and SS DNA). The solution is thoroughly mixed by vortexing and incubated at -20°C for at least 30'. ➤ The test tube is centrifuged at 13 000rpm for at least 30'. ➤ A small pellet should be visible. The supernatant is carefully removed. ➤ Ethanol residues are evaporated by vacuum centrifugation (or alternatively by air-drying). ➤ The proper volume of hybridization mixture is applied and the DNA is resuspended by shaking at 40°C for at least 30-45'. Complete dissolving is checked visually. <p><i>Major satellite probe</i></p> <ul style="list-style-type: none"> ➤ The appropriate volume of DNA is extracted by vacuum centrifugation. For 10-20μl usually 30'-45' of centrifugation are applied. Complete evaporation is checked visually and by careful flipping of the tube. ➤ Dissolving is accomplished as described above.

Hybridization

Before hybridization was set up, "regions of interest" on the specimens were defined. On metaphase chromosome preparations areas with a high density and good quality of spreads were determined by phase contrast microscopy and marked underneath the slide using a glass marker diamond. For 3D-fixed cells the region with the mostly suited cell density was chosen and cut from the rest using also a glass marker diamond; coverslips smaller than 76x26mm were used as a whole.

There are generally two possibilities how the target DNA can be denatured. The specimens are either denatured before the probe DNA is applied, or afterwards. Since the former is more time consuming and requires handling with hot noxious formamide, the latter method was used exclusively. The probe DNA was denatured separately in a water bath at 80°C and applied onto the specimen. The area was covered with a coverslip in case of chromosome preparations or for cells growing on 76x26mm coverslips. In the case of 3D-fixed cells on smaller coverslips, the probe was put onto a slide and the cell-coverslip was placed face down on top of it. In any case coverslips and slides were sealed using rubber cement. Hybridization was performed in a metal box within a water bath at 37°C. Because of their high complexity, chromosome-painting probes were hybridized for 3 days, while for the repetitive major satellite an incubation of one or two days was sufficient.

¹ Since the probe concentration was ~80-100ng/μl, a 4-fold volume of C₀t 1 (1μg/μl) was used, in order to obtain a ~40-50-fold excess of C₀t 1.

Materials:

- Coverslips (9x18mm, 18x18mm etc. depending on the metaphase area to be hybridized)
- Forceps
- Hot plate (75°C)
- Metal box
- Rubber cement (Fixogum)
- Slides 76x26mm
- Water bath 37°C
- Water bath 80°C

Methods

- Probe DNA is denatured in a water bath at 80°C for 5' and immediately put on ice.

2D-fixed chromosomes and cells grown on 76x26mm coverslips:

- 4-5µl of the denatured probe is put onto the slide.
- A 18x18mm coverslip is put on the probe, trying to avoid the formation of air bubbles.

Cells grown on small coverslips (e.g. 18x18mm, or 23x23mm photoetched coverslips etc.)

- 4-5µl of the denatured probe is put in the middle of a cleaned 76x26mm slide (for an 18x18mm area).
- The cells-coverslip is put face down on the probe trying to avoid air bubble formation.
- The slide/coverslip or coverslip/coverslip transition is sealed by applying a small film of rubber cement at the edge.
- After rubber cement is completely dry, the specimens are denatured on a hot plate at 75°C for 2.5'.
- Slides/coverslips are incubated in a metal box in a 37°C water bath ON or for two days, using the major satellite probe or for three days using the painting probes.

2.5.4 Detection

After hybridization, rubber cement was removed carefully using a fine forceps. For 2D-fixed chromosome preparations, coverslips were simply lift off, while for 3D-fixed cells they were gently wiped off by shaking the slides/coverslips in a PBS containing Coplin-jar. If directly labeled probes had been used the specimens were washed a few times in 4xSSCT (4xSSC/0.02% Tween 20) and then counterstained and mounted as described in 2.4. For chromosome painting probes, the preparations were first washed using 2xSSC at 37°, i.e. at a low stringency, followed by a high stringency step using 0.1SSC at 60°C. High temperature and low salt concentrations both destabilize the DNA double strand, so that interactions at a lower degree of complementary are lost, thus decreasing unspecific signals. The detection of the haptens incorporated within the probe was essentially as described for *Immunofluorescence*, but with following variations:

1. 4xSSCT (4xSSC/0.2% Tween 20) was used instead of PBT as buffer.
2. RNase A was included in the antibody dilutions to further decrease background.
3. Besides immunoglobulins, avidin was used as a reporter molecule to detect biotin.

If BrdU detection was combined with FISH, specimens were first "FISH-detected", afterwards equilibrated in PBT and finally "BrdU-detected" using PBS buffered solutions and skipping the second blocking step (see also 2.6). Counterstaining and mounting was performed as described in the *Immunofluorescence* chapter.

Materials:

- 4xSSCT (4xSSC/0.2%Tween 20)
- Antifade (Vectashield®)
- Blocking solution (4%BSA/4xSSCT)
- Bovine serum albumin fraction V (BSA)
- DNA counterstain:
 - 4',6-Diamidino-2-phenylindole (DAPI) (5µg/ml)
 - TO-PRO®-3 iodide (1mM)
- forceps
- Incubator at 37°C
- Nail polish
- Parafilm
- Primary/secondary/tertiary antibodies and avidin conjugates (see *Methods*)
- RNase A (1%(w/v), >300U/ml)

Methods			
<i>Detection</i>			
➤ Coverslips/slides are incubated in blocking solution for 10-15' at 37°C			
➤ Antibodies are diluted in blocking solution as follows			
Primary antibodies and avidin		Secondary antibodies	
rabbit- α digoxigenin	1:500	g- α rabbit-Cy3	1:500
Avidin-Alexa 488	1:200	g- α avidin-FITC	1:200
rabbit- α DNP	1:200		
➤ RNAse A is added to the antibody solutions (at a dilution of 1/50).			
➤ Approx. 200 μ l of antibody solution are applied on a coverslips for an area of ~60x26mm.			
➤ The coverslip is covered with parafilm to prevent drying and incubated for 30' at 37°C			
➤ Between the changes of layers, coverslips are washed with 4xSSCT at least 3x 3' at 37° by shaking.			
➤ Specimens are counterstained as described in 2.4.			
<i>Counterstaining and mounting</i>			
➤ As described in 2.4			

2.6 BrdU-labeling

The principle behind BrdU labeling of DNA is that cells take up modified nucleosides that are added to the medium and incorporate them during S-phase. Using immunocytochemical techniques the replicated DNA having incorporated these thymidine analogs can be visualized. Besides bromine as hapten, other halogens like chlorine or iodine can be used as tags as well as fluorophores like Cy3 and FITC.

The purpose of applying a BrdU-incorporation for the present experiments was a) to distinguish between S-phase and non S-phase cells and b) to discriminate between cycling and non cycling cells. The latter needed a BrdU incorporation period that equaled approx. the cell cycle duration, in order to make sure that all cycling cells would have gone through S-phase during the label period. For the former task a pulse of 30-45' was sufficient.

Since the hapten is not readily accessible for the specific antibodies, the DNA has to be denatured. As BrdU labeling was only applied in combination with FISH, which includes a heat denaturation step, no extra steps had to be used. Alternative protocols to heat denaturation utilize DNase I, HCl or NaOH but were not employed in the present experiments.

After FISH detection, the specimens had to be equilibrated in 1xPBT, as BrdU antibodies do not bind their targets using SSC buffers that are usually used for hapten detection in FISH.

Materials:	
<ul style="list-style-type: none"> • Antibodies against halogenated nucleosides: <ul style="list-style-type: none"> ○ Mouse-αBrdU (Roche) ○ Mouse-αIdU (Becton Dickinson, detects also BrdU) ○ Rat-αCldU (detects also BrdU) • BrdU (10mM or 50mM), alternatively IdU or CldU in the same concentrations can be used 	<ul style="list-style-type: none"> • Material as used for <i>Immunofluorescence</i> • Secondary antibodies (examples): <ul style="list-style-type: none"> ○ Goat-α mouse-Alexa488 ○ Sheep-α mouse-Cy3 ○ Goat-α rat-FITC ○ Goat-α rat-Cy3

Methods
<i>Labeling</i>
➤ BrdU (IdU or CldU) is added to the cell culture, diluted to a final concentration of 10 μ M-50 μ M. For longer incubations (e.g. 24h), lower concentrations are used to minimize potential toxic effects.
➤ After the desired length of the pulse, the specimens are fixed as described in 2.3.

<i>Detection</i>			
➤ The detection procedure is identical to that described in 2.4 using appropriate antibodies and dilutions.			
➤ Antibody dilutions (in 4%BSA/1xPBT):			
Primary antibodies			
Mouse- α BrdU (Roche)	1:200	Rat- α BrdU	1:100
Mouse- α BrdU (Becton Dickinson)	1:100		
Secondary antibodies			
Goat- α mouse-Alexa488	1:400	Goat- α ratCy3	1:500
Goat- α mouse-Alexa350	1:100	Sheep- α mouse-Cy3	1:500
<i>Counterstaining and mounting</i>			
➤ As described in 2.4			

2.7 Transfection of cells

Transfection experiments were performed during a 3-week stay in the laboratory of M.C. Cardoso at the Max-Delbrück-Center in Berlin-Buch. Her group disposes of a large set of transfection constructs and has great experience in the transfection and living cell observation of mammalian cells.

Mouse myoblasts C2C12 and Pmi28 were used for transfection experiments applying two different constructs. One expression vector contained the sequence for MeCP2, a protein which binds methylated cytosines in the DNA in a CpG context and which is able to confer transcriptional silencing. C-terminally of the protein's open reading frame (ORF) the sequence of the yellow fluorescent protein YFP was fused. To determine cell cycle stages in *in vivo* experiments, cells were double-transfected with an additional construct coding for the DNA ligase I, an S-phase specific enzyme, N-terminally tagged with the red fluorescent protein DsRed.

Plasmid constructions were performed by H. Easwaran and A. Seifert from the group of M.C. Cardoso. Details are described in (Easwaran 2003).

In brief, as basic constructs commercially available expression plasmids (Clontech) were used, encoding the respective fluorescent protein. DsRed 1 sequence was fused to the N-terminus of the human DNA ligase I cDNA while the enhanced yellow fluorescent protein (eYFP) was cloned C-terminally of the rat MeCP2 ORF. Transcription was driven by the cytomegalovirus immediate-early enhanced-promoter (CMV). Plasmid constructs were generated according to standard cloning techniques and transformation of *Escherichia coli* (Sambrook and Russel 2001).

Two different transfection methods were applied. For *in vivo* observations of C2C12 myoblasts the $\text{Ca}_3(\text{PO}_4)_2$ co-precipitation method (Graham and van der Eb 1973) was used, while for fixed specimens a method using the transfection reagent PolyFect® (QIAGEN) was employed. Compared to the latter $\text{Ca}_3(\text{PO}_4)_2$ -transfection usually showed a somewhat lower transfection efficiency, but in contrast did not create any autofluorescence within transfected cells, which was important for an optimal signal/noise ratio during observation. Since in fixed specimens the autofluorescence generated by employing the PolyFect® method could be completely abolished simply by washing, this method was preferred for the correlation and differentiation studies.

Approximately 12h after transfection cells were checked for expression of the fusion proteins by an inverted epifluorescence microscope. *In vivo* observations were usually started ~20h after transfection. Fixation of cells was performed at different time points after transfection, ranging from 16h to 4 days.

2.7.1 Ca₃(PO₄)₂-method¹

The transfection of DNA by Ca₃(PO₄)₂ works by creating a fine Ca₃(PO₄)₂-precipitate in the cell culture medium that delivers the transfection constructs onto the cell surface, where they can be taken up endocytotically. This is enhanced by a glycerol-“shock”, which temporarily permeabilizes the cells’ membranes.

Materials:

- | | |
|--|--|
| <ul style="list-style-type: none"> • 2xHEBS (280mM NaCl, 50mM HEPES, 1.5mM Na₂HPO₄) • CaCl₂-solution (2M CaCl₂, 161.3mM Tris-HCl pH 7.5) • Complete medium • FACS tube or 15ml test tube | <ul style="list-style-type: none"> • Glycerol solution (1xHEBS, 15% Glycerol) • Glass Pasteur pipette • Growth medium w/o serum/antibiotics • Plasmid DNA: <ul style="list-style-type: none"> pc644 (1.4µg/µl): MeCP2-YFP pc822 (1.6µg/µl):DsRed-Ligase I |
|--|--|

Methods

For adherently growing cells in a Ø100mm Petri dish containing 10ml DMEM medium

- Cells in a Ø100mm Petri dish are grown until ~50% confluence. The dish should contain 10ml of medium. Otherwise, concentration of the used compounds should be properly adjusted.
- “DNA-solution” is prepared by using 15µg² plasmid DNA (10.7µl of pc644, 9.4µl of pc822) plus 31µl CaCl₂-solution and 449µl of H₂O bidest..
- 500µl of 2xHEBS are put into a FACS tube or a 15ml test tube.
- “DNA solution” is added to the 2xHEBS solution by intensely blowing it into the tube such that air bubbles are formed.
- The tube is incubated for 10’ at RT. The solution should become slightly milky.
- The solution is mixed by pipetting in and out once and then applied to the culture. This is done drop by drop over the whole area.
- The Petri dish is swayed gently and put back in the CO₂ incubator for 6h.
- Formation of the precipitate is checked by phase contrast microscopy.
- Old medium is removed from the Petri dish and cells are washed once using 5ml of medium or PBS (37°C).
- Medium or PBS is removed accurately by tilting the dish.
- 1ml glycerol solution (37°C) is added and cells are incubated at RT for 1’. **Too long incubations can detach cells!**
- 10ml medium is added gently and the Petri dish swayed to dilute glycerol.
- Medium is removed completely.
- 10ml complete medium is added and cells are put back in the CO₂ incubator.
- Transfection success can be checked after ~12h using an inverted fluorescent microscope equipped with suitable fluorescence filter sets.

2.7.2 PolyFect®-method (QIAGEN)

Transfection is achieved by simply adding the reagent together with the DNA constructs to the medium. According to the manufacturer³, the PolyFect® reagent is an activated-dendrimer (i.e. a branched polymer). It has a spherical shape with branches having positively charged amino groups at their ends, presumably able to interact with the negative phos-

¹ If other media than DMEM are used it might be necessary to modify the protocol, as Ca₃(PO₄)₂ precipitation is highly pH sensitive.

² Depending on the plasmid this value can vary from 10-30µg

³ See also:

http://www1.qiagen.com/literature/handbooks/PDF/Transfection/TF_PolyFect/1015222HBPolyFect_0900WW.pdf

phates of the DNA backbone. By building compact structures with DNA and interacting with the cells negatively charged receptors via its net positive charge it is supposed to promote endocytotic DNA uptake. Moreover, it changes the lysosomal pH, thus inactivating cellular nucleases and increasing the intracellular stability of the transfected DNA.

Materials:

- | | |
|---------------------------------------|---------------------------------|
| • Complete medium | • Plasmid DNA: |
| • Growth medium w/o serum/antibiotics | pc644 (1.4µg/µl): MeCP2-YFP |
| • PolyFect® reagent (QIAGEN) | pc822 (1.6µg/µl):DsRed-Ligase I |

Methods

For adherently growing cells in a Ø100mm Petri dish containing 10ml DMEM medium

- Cells in a Ø100mm Petri dish are grown until ~50% confluence. The dish should contain 10ml of medium. Otherwise, concentration of the used compounds should be properly adjusted.
- "DNA-solution" is prepared by mixing 6µg plasmid DNA (4.3µl of pc644) with 300µl medium (w/o serum/antibiotics) and 50µl PolyFect® reagent.
- "DNA-solution" is mixed thoroughly by vortexing for 10" and incubated for 5-10' at RT to allow complex formation of the polymers with DNA.
- Cell culture medium is removed and cells are washed once using 8ml 1xPBS.
- 8ml of fresh complete medium is added to the cells.
- 1ml of complete medium is added to the "DNA-solution", mixed by pipetting and applied onto the cell culture.
- The dish is gently swayed and put back in the CO₂ incubator.
- Transfection success can be checked after ~12h using an inverted fluorescent microscope equipped with suitable fluorescence filter sets.

2.8 Combination of FISH with transfected cells and immunofluorescence

The combination of FISH with the visualization of proteins by immunofluorescence or of proteins tagged with fluorescent proteins like GFP or DsRed usually causes problems due to the destruction of antigenic or fluorescent epitopes by heat denaturation applied during FISH. To circumvent this problem a pre-recording procedure was utilized that uses the possibility to relocate individual cells cultured on photoetched coverslips. One application where this approach was used was the identification of macrophages. After detecting the specific surface antigen Cd11b and recording images by epifluorescent microscopy, cells were post-fixed for FISH, and hybridized with a pericentromeric or chromosome specific probe. Such cells being positive for the macrophage-identifying marker were imaged by confocal laser scanning microscopy. In a similar way transfected cells expressing variable amounts of the fusion protein MeCP2-YFP were recorded by confocal microscopy to quantify the fluorescent label, post-fixed for FISH, hybridized with the major satellite probe and scored again by confocal microscopy, to determine the number of pericentromeric clusters. In any case, the key step was to collect an image that would define a cell's position within one of the 500 photoetched alphanumerical squares (see figure 2). This was accomplished by a phase contrast or transmitted light image at a low magnification.

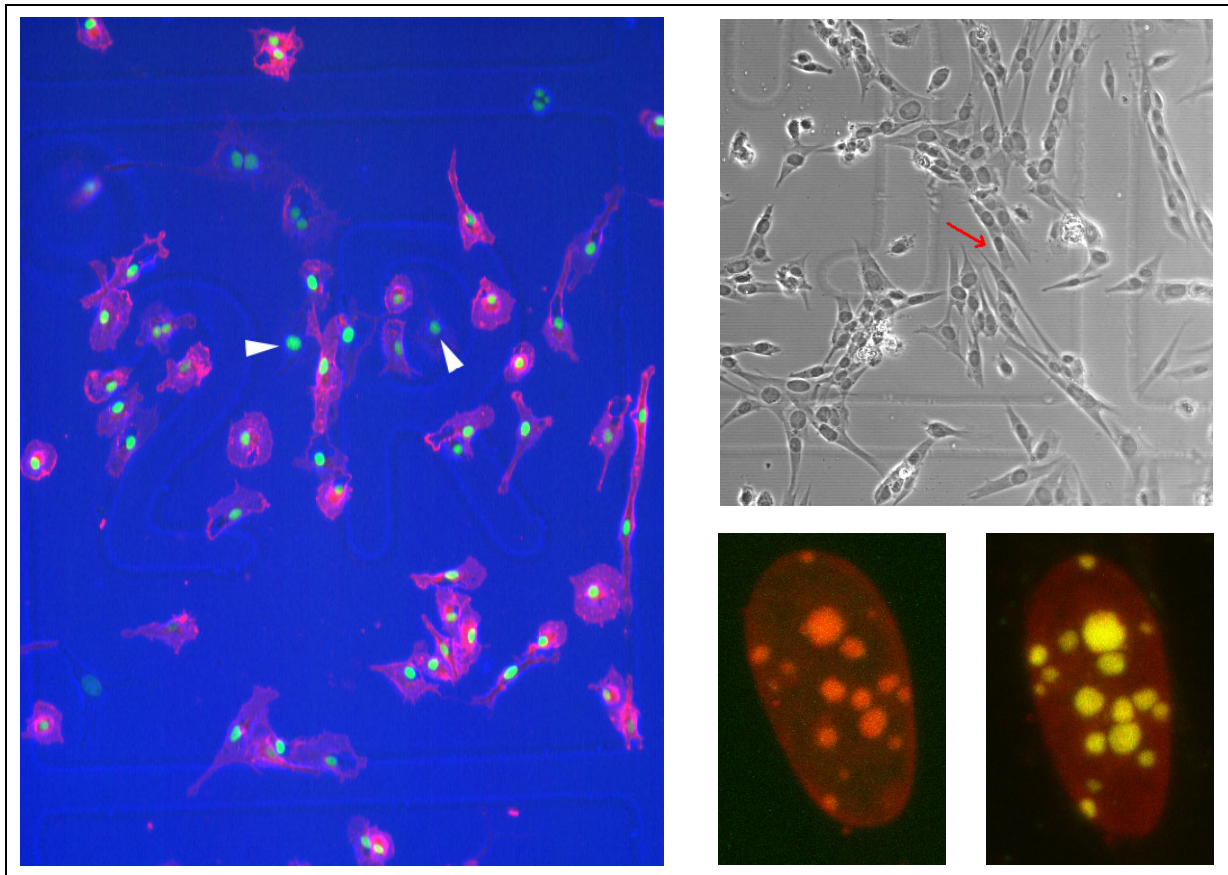


Figure 2.2: Relocation of cells with photoetched coverslips. Two examples using photoetched coverslips for cell relocation. Left: The picture shows macrophages derived from transgenic ES cells expressing H2B-GFP (green). Red staining corresponds to immunocytochemically labeled Cd11b. Arrow heads point at two negative cells, which would not have been included in the analysis of macrophages. Right: Three images of Pmi28 myoblasts transfected with MeCP2-YFP. Top: Phase contrast overview. Bottom: Maximum intensity projections of the nucleus highlighted with the red arrow in the top picture. Bottom left: Nucleus stained with TOPRO-3 (red), expressing hardly visible amounts of MeCP2-YFP (green). Bottom right: The same nucleus as on the left side after FISH with a major satellite specific probe (green). TOPRO-3 is shown in red. Note that the nucleus must have been slightly tilted during post-fixation steps and/or FISH since the relative chromocenter-distribution is not 100% identical.

Materials:

- Epifluorescent microscope or CLSM equipped with transmission light or phase contrast optics and low magnification lenses.
- Imaging software (e.g. Zeiss image browser, Irfan view etc.)
- Photoetched coverslips

Methods

- An overview picture is collected at a low magnification using transmission light or phase contrast optics. If the coordinates are not visible on the picture, they are noted separately. If an individual cell has to be relocated, it is marked on the overview picture by an arrow or a circle using appropriate software tools, which are already implemented in the Zeiss 510 CLSM software. An extra note describing landmarks to find a certain cell is written if necessary.
- To relocate cells the view of pre-recorded images has to be adjusted using the appropriate imaging software tools in order to match the new orientation of the coverslip after having performed FISH.

2.9 Microscopy

2.9.1 Epifluorescent microscopy

Epifluorescent microscopy was used for the following tasks:

- Checking the success and quality of FISH.
- Checking the success and quality of transfection.
- Prerecording and identification of macrophages immunocytochemically stained for Cd11b.
- Identification of endogenous MeCP2 expression in Pmi28 myoblasts and myotubes.

Except for the transfection experiments a Zeiss Axiophot 2 microscope was used, equipped with a Coolview CCD camera with a spectral response of 400-900nm and a CCD chip resolution of 753x576 pixels. In the course of the transfection experiments a Zeiss Axiovert 100TV inverted microscope was used, which had the advantage that living cells could be observed. In the following, utilized filter sets for the various fluorochromes and objective lenses for the different tasks are listed.

Filter sets			
Fluorochrome	Excitation filter	Beam splitter	Emission filter
<i>Axiophot 2</i>			
DAPI/Alexa 350	BP 365	FT 395	LP397
Alexa 488/FITC	BP 450-490	FT 510	LP 515-565
Cy3/TAMRA	BP 546	FT 580	LP 590
TOPRO3	BP 575-625	FT 645	BP 660-710
<i>Axiovert 100TV</i>			
YFP	500/20	515 LP	535/30
DsRed/Cy3/TAMRA	HQ 565/30	Q 585 LP	HQ 620/60
TOPRO3	BP 575-625	FT 645	BP 660-710

Objective lenses				
	FISH control	Transfection control	Macrophage prerecording	MeCP2 expression
Zeiss 10x/0.25 Achromat Ph1	-	x	-	-
Zeiss Plan-Neofluar 16x/0,5 Imm, Ph2	-	-	x	-
Zeiss Fluor 40x/1,3 Oil, Ph 3	x	-	-	-
Zeiss Plan- Neofluar 40x/1,3 Oil	x	-	-	X
Zeiss Plan- Aplanachromat 63x/1,4 Oil	x	-	-	X
Zeiss Plan-Neofluar 100x/1,3 Oil	x	-	-	X

2.9.2 Confocal-laser-scanning-microscopy

Compared to conventional epifluorescence microscopy confocal microscopy shows a much better axial resolution¹. The reason is that instead of using wide field illumination, focused laser beams scan the specimen exciting only small areas at a time. In combination with using a pin-hole in front of the detection device this step by step illumination excites and detects much less fluorescent entities that are not within the focus plane, resulting in highly decreased out of focus blur (for details on confocal microscopy and applications see (Pawley 1995)).

In the present work, confocal-laser-scanning-microscopy was used for image recording concerning all quantitative and semi-quantitative evaluations, including:

- radial distribution of chromosome territories (CTs) and pericentromeric heterochromatin,
- side-by-side distribution of CTs
- chromocenter clustering and intra-nuclear localization and
- correlation between MeCP2-YFP expression and number of chromocenters

Moreover confocal microscopy was used for documentation purposes in order to produce high-resolution images, as for example for the analysis of endogenous MeCP2 expression in Pmi28 cells. In the following, the microscopic set ups and parameters are listed that were used for picture acquisition of fixed as well as of living cells.

Fixed specimens

3D-fixed cells were imaged on three different confocal setups using following laser/filter combinations for the various fluorochromes:

	Laser	Beam splitter	Emission filter
Leica TCS SP			
Alexa 488/FITC	488nm	TD 488/568/647	AOTF (acousto optical tunable filter): allows an interactive definition of the detected spectrum
Cy3/TAMRA	514nm	RSP 525	
Cy5/TOPRO-3	633nm	RSP 650	
Zeiss LSM 410			
Alexa 488/FITC	488nm	FT 488/543	BP 502-542
Cy3/TAMRA	543nm		BP575-640
TOPRO-3	633nm		LP 650
Zeiss LSM 510			
YFP	488nm	HFT UV/488/543/633	BP 500-530
DsRed/Cy3/TAMRA	543nm		BP 565-615 IR
TOPRO-3	633nm		LP 650

Depending on the experiment and cell type, different settings were used as summarized in the table below:

¹ These values range from 900 to 600nm depending on the numerical aperture of the objective lens, the wavelength of the used laser beam, as well as the refractive index of the object medium (see (Pawley 1995), p. 3, equation (3)). The effective axial resolution of an individual microscopic set up depends in addition also on the correct alignment of the various optical components.

	FISH major satellite	FISH chromosome painting	Studies on MeCP2-YFP transfected cells
Image size (pixel)	256x256	256x256	512x512
Voxel size x*y*z (nm)¹			
Myoblasts	0.0992*0.0992*0.2	0.103*0.103*0.284	MeCP2-YFP:0.05*0.05*0.5 FISH: 0.05*0.05*0.25
Myotubes	0.065*0.065*0.284 or 0.049*0.049*0.203	0.099*0.099*0.25	MeCP2-YFP:0.05*0.05*0.5
ES cells	0.079*0.079*0.25	0.099*0.099*0.25	-
Lymphocytes	0.078*0.078*.0284	0.066*0.066*0.25	-
Macrophages	0.0793*0.0793*0.25	0.0793*0.0793*0.25	-
Fibroblasts	0.132*0.132*0.2	-	-
Averaging²	2-8	2-8	2

In vivo observation

For the living cell observation of C2C12 myoblasts that had been transfected with MeCP2-YFP and DsRed-Ligase I a Biopetechs “live-cell micro-observation chamber” was used. The chamber consists of a metal lower half and a plastic upper half. In between a microaqueduct slide and a special round coverslip on which the cells are grown are assembled using gaskets to seal the system (see also figure 2.3). Though perfusion of the chamber is generally possible, all observations were made using a closed system. Perfusion was regarded not necessary since the observation time did not exceed 14h using a limited time resolution of 1h. Moreover, cells kept dividing during the whole observation period. In addition, the pH remained constant as judged by the color of phenol red in the medium. During observation, the chamber was kept at 37°C using a temperature-controlling device.

Experimental setup

As already mentioned, cells had to be grown and transfected on special round Ø40mm coverslip to be assembled in the chamber. The chamber was sterilized by extensive washings in absolute ethanol and assembled under sterile conditions inside a laminar flow cabinet. As the cells were supposed to divide, care

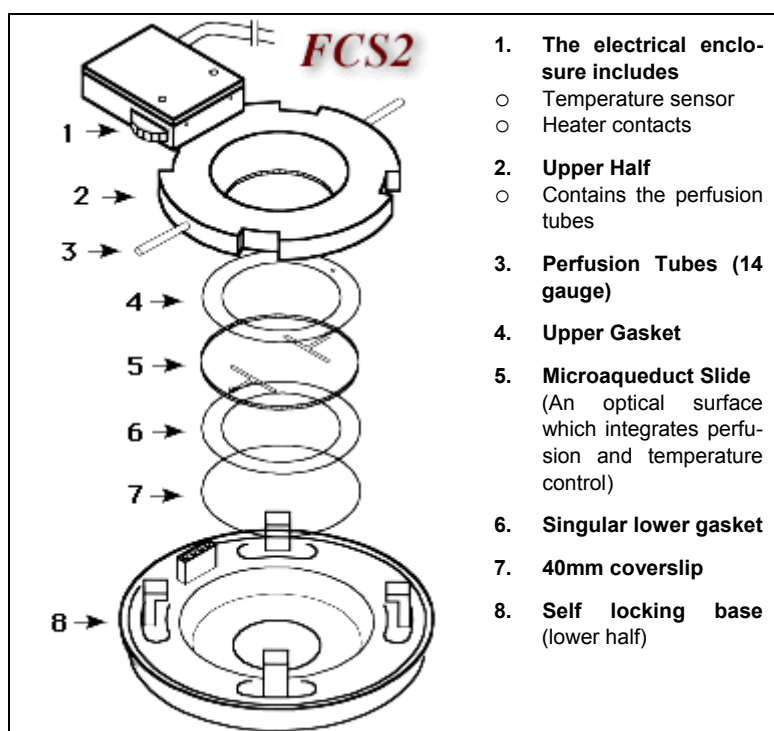


Figure 2.3: Biopetechs living cell chamber FCS2. Constituents of the living cell chamber (adapted from <http://www.biopetechs.com/Products/FCS2/fcs2.html#U%20h20%20duct>)

¹ These values are assigned by the microscope software. It should not be assumed that they are accurate at a 1nm level.

² The number of scans that were applied to create an averaged section image depended on the signal intensity and its sensitivity to bleaching.

was taken that the cell culture was not too dense when the observation was started. Preconditioned medium, i.e. complete medium that was incubated ON in a CO₂ incubator was used for the assembled chamber.

Materials:

- Cells growing on Ø40mm round coverslips
- Conditioned medium (~10ml DMEM complete medium incubated ON in a CO₂ incubator
- Ethanol (absolute)
- forceps
- Living cell chamber (Biopetechs FCS2):
 - metal frame
 - plastic frame
 - 2 gaskets, one with two small holes for the perfusion tubes.
 - Microaqueduct slide
 - Electrical enclosure
- Medium (DMEM, 37°C)
- Pasteur pipettes with a narrow tip
- Petri dish Ø100mm
- Silicon tubing for perfusion
- Vacuum pump with glass pasteur pipette attached

Methods

Note that the chamber is assembled inside a laminar flow cabinet.

- Two pipettes are cleaned thoroughly (inside and outside) with ethanol.
- All parts of the chamber are washed with ethanol inside a Ø100mm Petri dish using the pre-cleaned Pasteur pipettes. Washings should be very accurately including perfusion cavities.
- Drying is helped by using a cell culture vacuum pump attached to a sterile glass Pasteur pipette.
- The plastic frame is placed on two fragments of a 5ml cell culture pipette (to keep it even).
- The first gasket (with two holes) is put in the designated mold ensuring a perfect fit.
- The microaqueduct slide is put on top of the gasket with the cavities on top and the electrodes on bottom. In order to achieve a hermetical sealing of the chamber later it is important that it sits absolutely even and does not move.
- The second gasket is put on top of the slide. Attention should be paid to a perfect alignment with the slide.
- One silicon tube end is attached to one perfusion tube of the chamber.
- A few ml medium are pumped inside the chamber with a Pasteur pipette and removed again.
- The perfusion tubing is fixed at the other chamber side and another few ml medium are pumped from the other end and removed.
- A few ml of conditioned medium are pumped inside the chamber and removed again.
- The free tubing end is also fixed at the chamber. Air bubbles within the tubing should be avoided.
- A small amount conditioned medium is put directly on the microaqueduct slide, so that the whole area is covered and a convex meniscus is created.
- The cell containing coverslip is put face down on the slide. Coverslip should be flush with the rest.
- The metal frame should be opened up completely and the screwable part should be running smoothly.
- The metal frame is put on top of the already assembled parts. The hooks and temperature sensor plug are passed carefully through the notches.
- The hooks are moved clockwise and the chamber is closed tightly by screwing the top part also clockwise.
- If big air bubbles have formed inside the chamber the silicon tube is removed at one side and conditioned medium is pumped through the tubing until all air bubbles are removed.
- Small air bubbles are directed inside the silicon tubing and a clip, which seals the tubing is applied such that they are separated from the chamber.

- The chamber is cleaned with ethanol, especially the coverslip side and checked for leakage. In case of leakage it must be reassembled.
- The chamber is kept for at least an hour in a CO₂ incubator and is then ready to be mounted on the microscope.
- Before mounting the chamber on the stage, the electrical enclosure is screwed on, with a small drop of immersion oil applied on the temperature sensor.

Since the chamber assembly is very intricate, especially for beginners, it should be rehearsed before the first experiment! (see also <http://www.bioptechs.com/movies/FCS2.MPG> for a video demonstration)

Microscopy

Live cell microscopy was performed on a Zeiss LSM 510 Meta confocal-laser-scanning-microscope. The living cell chamber was attached using an appropriate stage adapter. The temperature was kept constant by using a temperature-controlling device, which was connected to the chamber via the electrical enclosure. Both the microaqueduct slide, as well as the metal frame was kept at a constant temperature of 37°C.

The microscope settings are summarized in the following table:

Voxel size x*y*z (μm)	0.050x0.050x0.75	Time interval¹	~60'
Image size (pixel)	512x512	Averaging	1

During one microscopic session between 9 and 15 individual nuclei could be observed simultaneously. This was possible due to an automated stage and a relocation software tool, which was able to save and recall individual xy stage-coordinates. This way many nuclei could be scanned at constant time intervals. For each time point and for each nucleus, the top and bottom boundaries were defined individually before starting image acquisition. In cases where the cell moved during observation the field of view had to be adjusted properly. Thus it should be stressed that the image stacks collected at single time points of one particular time series were often not aligned in xy and never in z.

It should be noted that some cells, which were monitored during S-phase seemed to become cell cycle arrested as was assumed from the changeless DsRed-Ligase I pattern. Reducing the DsRed image acquisition to one mid focal plane instead of a whole stack, as well as adding TroloxTM a powerful antioxidant to the cell culture medium could not eliminate this observation artifact (see also *discussion*).

2.10 Image processing

2.10.1 Documentation

For documentation purposes images were processed using Adobe Photoshop® version 7.0 or Image J version 3.29 and 3.30. Usually only slight grey levels adjustments and false color assignments were performed on the raw images.

2.10.2 Pixel shift correction

Since microscopic imaging of fluorescent objects is wavelength-dependent, microscopic images of multicolor specimens often suffer from chromatic aberrations. This optical artifact can be measured by imaging multi-fluorescent micro-spheres with known dimensions (figure 2.4). The determined pixel shift can then be used to correct the microscopic images of the speci-

¹ During mitosis, the time interval was reduced to a minimum of five minutes.

mens. For the present experiments, such pixel shift measurements were done regularly on the utilized microscopes using the relevant settings.

To measure the axial shift, image stacks of multi-fluorescent beads were collected using a very small z-step size ($\sim 50\text{nm}$). Then the particular z-step position of the frame showing the biggest diameter of an individual bead within the stack was determined for each fluorescence channel and compared. The difference in this z-step position was then multiplied by the step size to give the z-shift in nm. This was repeated for several individual beads and the mean was calculated.

To determine the lateral shift the frames showing the biggest bead diameter were combined into one rgb-image using Photoshop® software. Figure 2.5 shows how such an rgb image did look like if the combined fluorescence channels exhibited a significant lateral shift. Within this rgb image, one random pixel within the intersection was filled with black color to serve as a landmark. The complete frame of one channel was then moved until the bead images would be aligned. By moving only this one channel, the former black pixel would be split into two colored ones. Since the software could assign the image-coordinates of these two colored pixels (using a tool pointing at the respective pixels), the shift could be calculated from their xy difference on a pixel-based resolution. As for the axial shift, this procedure was repeated for several beads to calculate the mean.

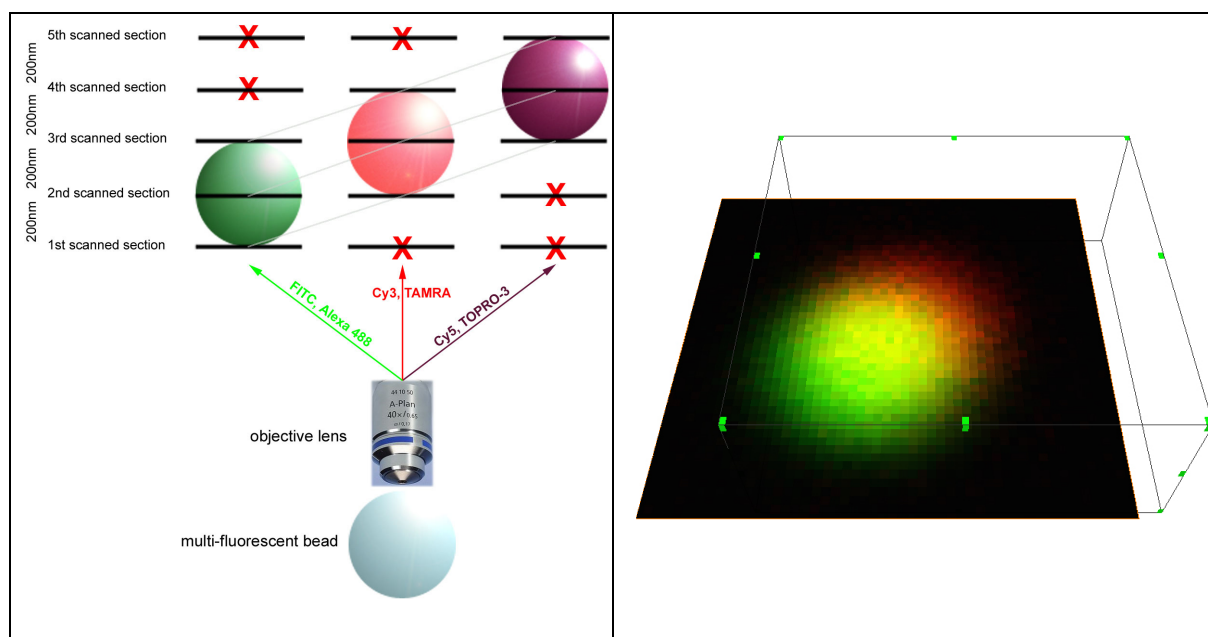


Figure 2.4: Axial chromatic shift. The sketch shows how a multi-fluorescent bead is imaged in different z-planes depending on the wavelength of the emitted light (arrows). Red crosses mark images that have to be deleted in the individual stacks in order to achieve a proper alignment (grey lines). This particular correction was applied on data collected on the Zeiss LSM 410.

Figure 2.5: Lateral chromatic shift. Lateral pixel shift between red and green fluorescence on a 500nm bead. The grey cuboid with the green landmarks shows how the image stack frame of the red channel must be moved in order to align the fluorescent signals.

The measured shift was usually higher axially than laterally. For a proper subsequent alignment of the individual fluorescent channels, the axial shift was used as z-step size. Axial shift correction could then simply be achieved by deleting the respective first and/or last picture(s) of the individual channel stack (figure 2.4). Lateral shift was mostly negligible. If a significant lateral shift was observed, it was corrected using the 3D-rendering software Amira™ that dis-

poses of a suitable implemented software tool to move the image stack frame¹ according to the measured shift (figure 2.5).

2.10.3 3D-reconstruction

3D reconstructions were generated using the software Amira™ (TGS) version 3.0, by surface rendering image stack data². The basic principle is that a surface is generated separating voxels beyond and above a certain subjectively set threshold. To improve the signal/noise ratio in order to facilitate threshold determination and to smooth signal boundaries, image stacks were modified using a 3D Gaussian filter, with a kernel size of 3. The threshold was chosen in a way that the generated surface would be aligned with the grey level images in the individual sections as close as possible, but without losing smaller, weaker signals.

2.11 Visual evaluations

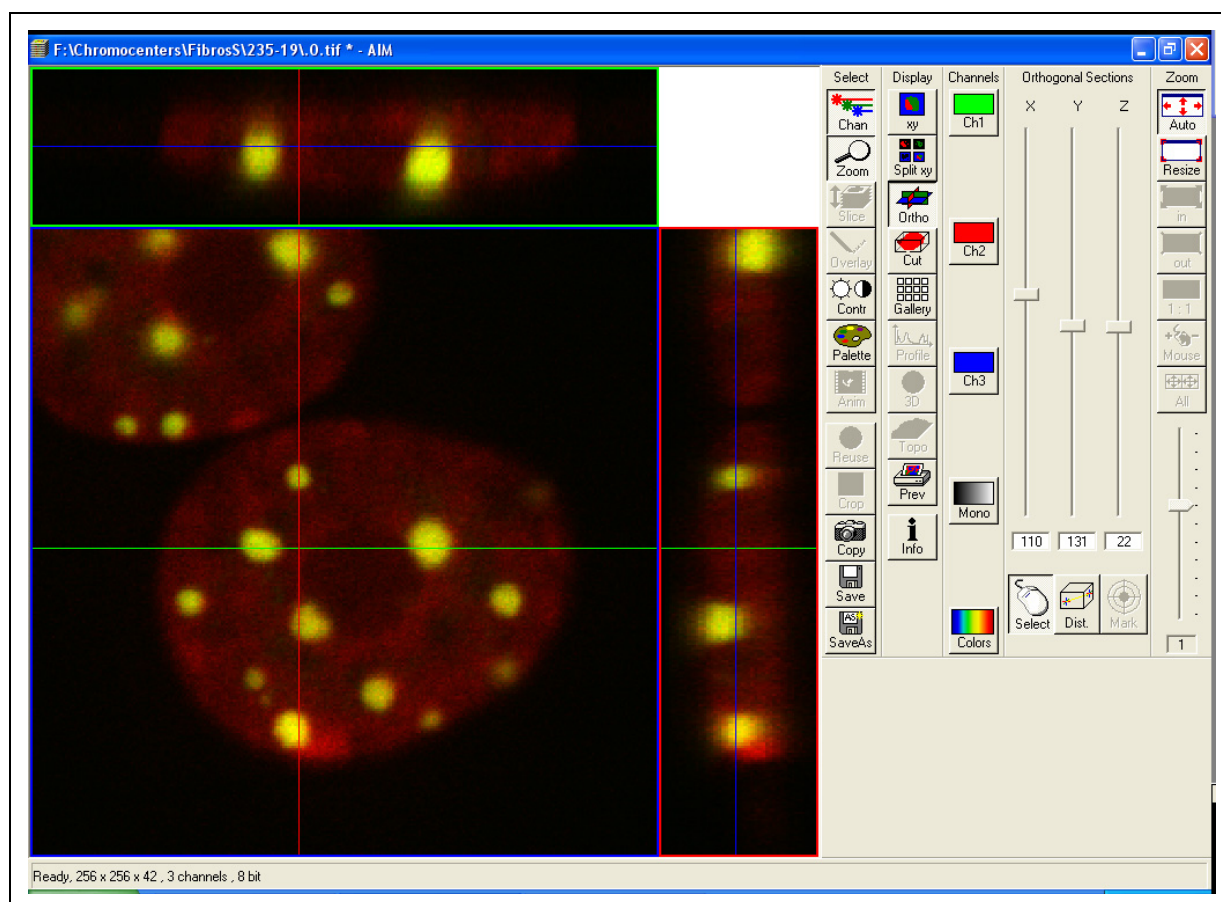


Figure 2.6: Zeiss image browser software. The image shows a screenshot of an active window of the Zeiss image browser software. The data set is displayed in the left part with the biggest window showing two nuclei in the xy plane. The red false color displays the DNA counterstaining with TO-PRO-3, while chromocenters are shown in green. The red and the green line in the xy-plane show the intersection with the yz (red) and the xz (green) plane, which are shown on the right and on top, respectively. In the right part various tools for changing the view of the data set can be seen, most important the sliders to change the visible plane position in x y and z.

The analysis of chromocenter-number and their intra-nuclear distribution was done visually, i.e. in a non-automated fashion. The number was determined by simply counting FISH sig-

¹ The software tool is actually designated “cropping“, but since a “negative” cropping, i.e. an extension of the frame at the opposite side of the real cropping is carried out in order to keep the image dimensions constant, it results in a frame shift.

² The actual rendering method applied isosurface generation.

nals. The position of chromocenters was assigned to one of three categories: a) peripheral, b) perinucleolar or c) internal¹. All evaluations were done on raw images of shift corrected stacks using the Zeiss image browser software. This program allows a neat overview over the 3D data set by an interactive display of xy, xz and yz image planes (figure 2.6). Counting was done by browsing mainly the xy plane. Additional inspection of the z-planes allowed discriminating between signals on top of each other. To facilitate counting especially of many chromocenters, the nucleus was subdivided into four parts using the intersection lines (green and red lines in figure 2.6). The positions of these lines are reproducible as they are displayed by image coordinates. The number of chromocenters within the individual quarters was scored separately and summed up later.

The individuality of chromocenters was usually clear-cut, yet some chromocenter signals were not easy to define as one or more objects. If such a very close proximity of signals comprised only small parts, and the signal intensity was very high, this “melting” of signals was ascribed to a limited resolution of fluorescent blurring (especially if it happened in z) and the signals were counted as more objects (figure 2.7).

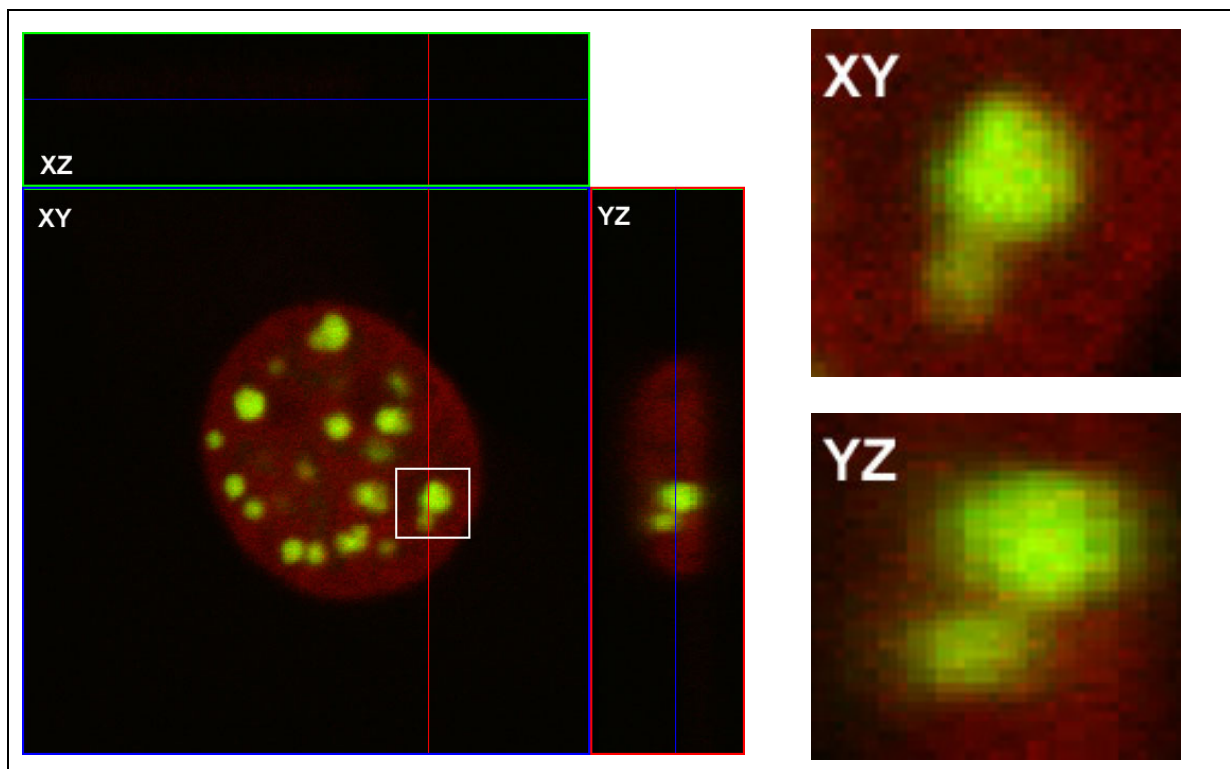


Figure 2.7: Discrimination of chromocenters in close proximity. The signal(s) within the white square represent a typical case, where the number of chromocenters within a signal cluster was ambiguous (magnified in the right top picture). From the yz point of view (magnified in the right bottom image), it becomes clear that the signals represent to separate objects with an only small intermingling part, most probably caused by fluorescent blurring.

The categorization concerning the intra-nuclear localization of chromocenter signals was done as follows (see also figure 2.8):

- a) Peripheral: The signal was tangent to the nuclear periphery, defined by TO-PRO-3 counterstaining.

¹ Intra-nuclear/radial distribution of pericentromeric heterochromatin as whole, i.e. not of chromocenters as individual entities was additionally assessed in a quantitative manner using the 3D-RRD software (see 2.12.1).

- b) Perinucleolar: The signal was tangent to a nucleolus. A nucleolus was identified as a region of a remarkable size showing very little DNA content as revealed by DNA counterstaining¹. Some signals showed both a perinucleolar and a peripheral localization, which were both considered in the scoring.
- c) Internal: Signals that touched neither the periphery nor a nucleolus.

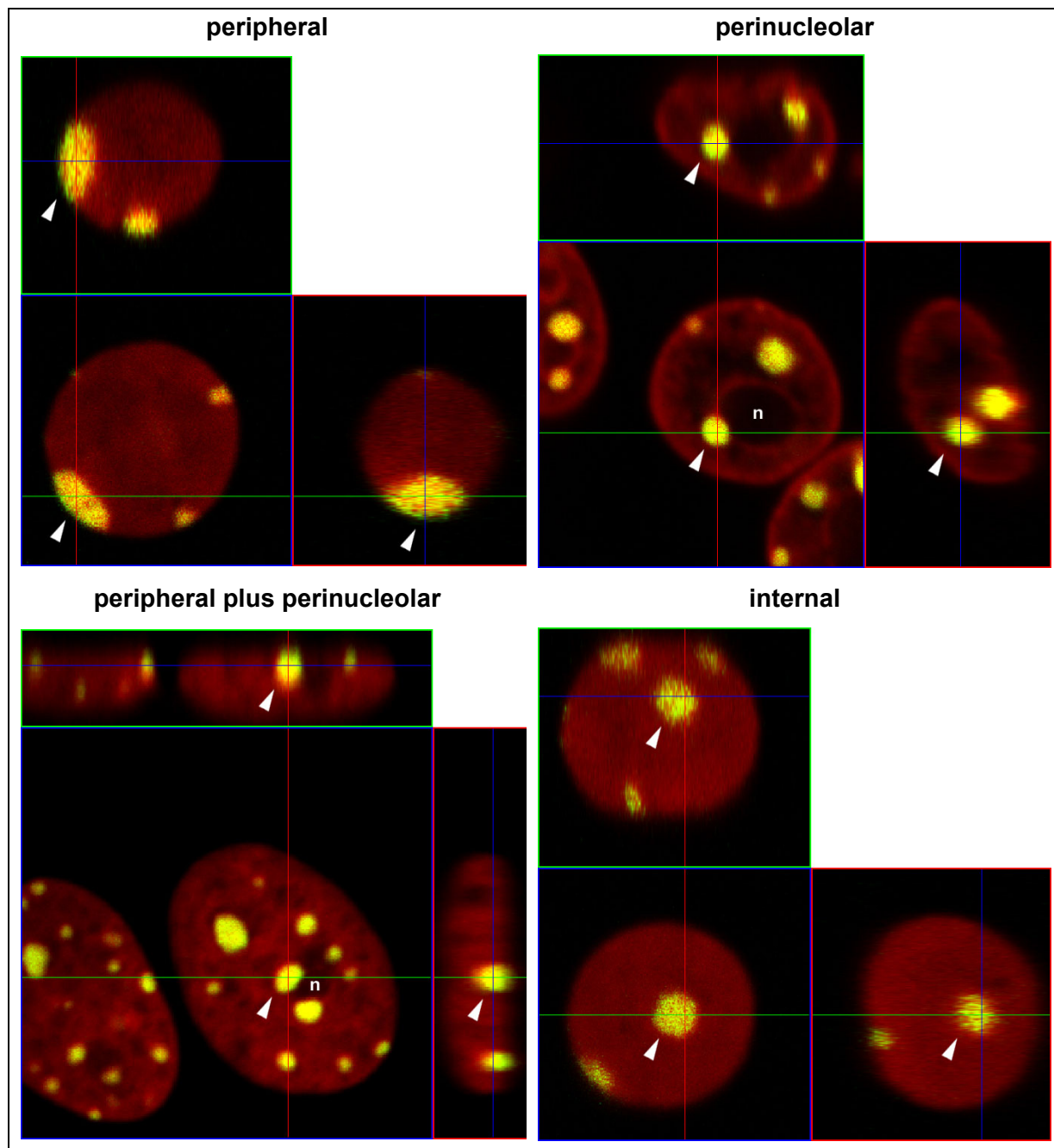


Figure 2.8: Classification of intra-nuclear location. An example is shown for each intra-nuclear distribution category. Chromocenters are shown in green, TOPRO-3 counterstaining in red. The view is equivalent to figure 7. The relevant signals (white arrowhead) are shown in all three planes. The cell types shown are lymphocyte for peripheral and internal signals, myotubes for perinucleolar and myoblasts for peripheral plus perinucleolar. n indicates a nucleolus.

¹ Immunofluorescent detection of nucleolar proteins approved this way of identifying nucleoli. Since smaller cavities devoid of DNA might also represent splicing compartments or other nuclear bodies they were not considered as nucleoli, such that nucleolar signals might be slightly underestimated (see *discussion*).

The data for chromocenter numbers was plotted using a binning of 5 chromocenters, i.e. the proportion of nuclei showing 1-5, 6-10, 11-15, 15-20, 21-25, 26-30, 31-35 and 36-40¹ chromocenters was plotted on the ordinate with the respective classes arranged along the abscissa (figure 9, left). Moreover, the data was also arranged as cumulative frequencies (figure 9, right), in order to test for significant differences between the observed chromocenter-number of the various cell types.

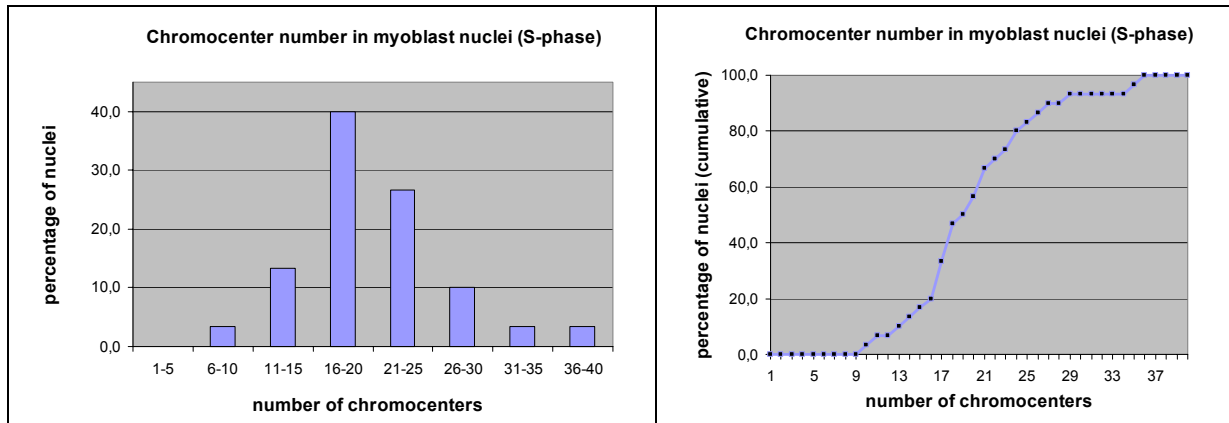
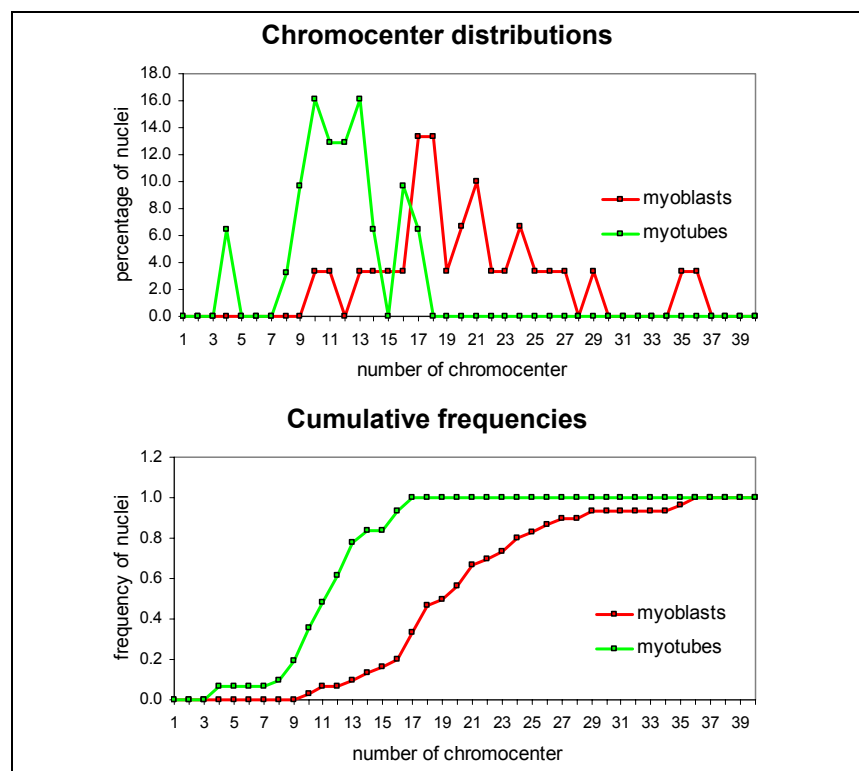


Figure 2.9: Two ways of plotting the chromocenter-number. Left: Histogram showing the proportion of nuclei in classes showing an increasing number of chromocenters. Right: The cumulative percentage of nuclei is plotted against the chromocenter number, i.e. values on the ordinate correspond to the percentage of nuclei having a given chromocenter amount or less.

Figure 2.10: Number of chromocenters in myoblast and myotubes. The upper plot illustrates the distribution of chromocenter numbers observed in myoblasts and myotubes, i.e. it shows the percentage of nuclei, which showed 1, 2, 3 etc signals. The lower plot illustrates the same data but as cumulative frequencies, i.e. the ordinate indicates the fraction of nuclei that had the number of signals plotted on the abscissa or less. The maximum distance between the cumulative curves is used in the KS test (see also *Calculation of relative radial distances*).



The number of chromocenters within a certain cell type was variable, but exhibited tendencies to either smaller values or larger values. In order to compare these distributions of

¹ 40 was the highest possible amount of chromocenters, equalling the chromosome number of an euploid mouse karyotype.

chromocenter numbers between different cell types, the data was arranged as cumulative frequencies and could then be compared using a two-sided Kolmogoroff Smirnov test. Figure 2.10 illustrates the proceeding.

2.12 Automated evaluations

2.12.1 Radial distribution analysis using the software 3D-RRD

The relative radial distribution of pericentromeric heterochromatin and chromosome territories was evaluated using the software 3D-RRD (3D relative radial distribution), which was developed by J. von Hase from the group of C. Cremer, Kirchhoff-Institute of Physics, University of Heidelberg in cooperation with the group of T. Cremer. As apparent from its name, the program measures relative 3D radial distances of pre-segmented objects from the nuclear center in a voxel dependent manner. The software was written in C++ and runs as an implement within the Khoros software on normal PCs with Linux as operating system. The user interface was adapted by S. Dietzel and J. von Hase, such that it was possible to run the program independently from the programmer. Details according to the mode of operation of this software are described in (Cremer et al. 2001), and (Cremer et al. 2003), as well as in the PhD thesis of J. von Hase (von Hase 2002). The most important steps are explained below:

Segmentation of the nucleus and the signal objects

In order to separate objects of interest from background signals a threshold has to be defined to subsequently set all voxels below this value to zero.

Threshold determination in the 3D-RRD software is achieved by an automated iterative method. The program starts with a preliminary threshold $T_{(1)}$ which is the mean voxel intensity of all voxels within the data set (figure 2.11). The mean signal intensities of all voxels below and above T are calculated and give the parameters $E1$ (below) and $E2$ (above). $E1$ is regarded as mean intensity of the background, while $E2$ as the mean intensity of the object to be segmented. Based on these two parameters a new preliminary threshold $T_{(2)}$ is calculated as the mean of $E1$ and $E2$. A second round subsequently determines a new $E1$ and $E2$, being the mean intensity values below and above this new threshold $T_{(2)}$. These calculations are repeated until the threshold T remains unchanged; i.e. it converges.

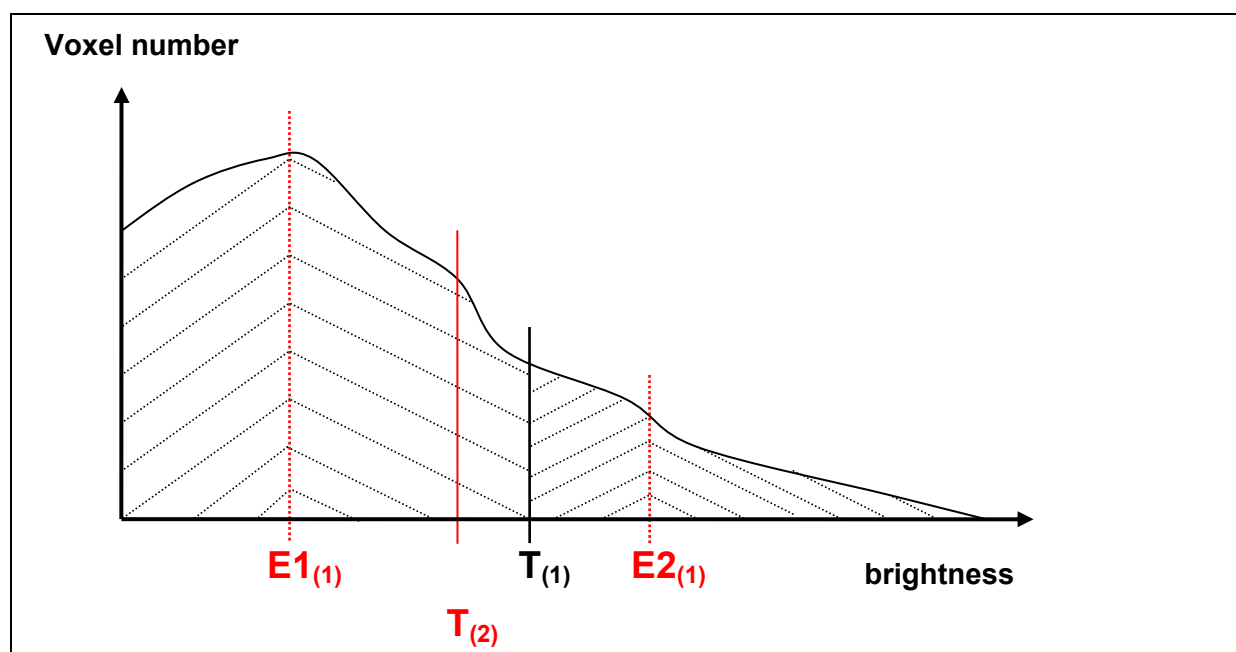


Figure 2.11: Threshold determination. The curve outlines a typical signal intensity distribution of a 3D-data set. Note that the majority of voxels shows a low intensity, belonging to the image background. Since no local maximum for the labeled object exists, it is difficult to define a threshold in order to separate the object(s) of interest from background. Therefore, an iterative method is applied in order to estimate the correct threshold. A first preliminary threshold $T_{(1)}$ is defined as the mean voxel intensity within the whole data set. $E1_{(1)}$ and $E2_{(1)}$ are the mean intensity values of all voxels below and above $T_{(1)}$. A new threshold $T_{(2)}$ is calculated as the mean of $E1_{(1)}$ and $E2_{(1)}$. The second round would calculate new $E1_{(2)}$ and $E2_{(2)}$ as the means of all voxel intensities below and above $T_{(2)}$. This procedure is repeated until $T_{(n)}$ converges. (Grey lines symbolize the mean intensity value of all voxels below or above $T_{(1)}$). Sketch was reproduced from (von Hase 2002).

This threshold T can interactively be changed by changing the weight (v) of $E2$ compared to $E1$ for the calculations of T .

$$T=(1-v)*E1+v*E2.$$

If $v=0.5$, i.e. $E1$ and $E2$ are weighted equally, then $T=(E1+E2)/2$ and thus the mean of $E1$ and $E2$. Increasing this v -value will result in a higher threshold, and thus the segmented objects will get smaller.

The most suited v -value is determined interactively, i.e. by comparing the results of the segmentation using different v -values with the raw data.

To smooth signal boundaries of the segmented objects, image stacks are filtered using 2D Gaussian filters. For nuclear counterstain a three step Gaussian-filtering is used by successively applying filters with following filtering masks: [1 4 6 4 1], [1 0 4 0 6 0 4 0 1] and [1 0 0 0 4 0 0 0 6 0 0 0 4 0 0 0 1]. Chromosome and pericentromeric signals are only filtered using the first filtering step.

In order to define the nuclear boundaries as precisely as possible, a further segmentation step is applied. First, the intensity gravity center of the nucleus is calculated, using the already thresholded counterstain channel data set. Now a straight line is drawn from each voxel in the data set to this point. Finally, all those voxels are set to zero, where this line crosses voxels, which had already been set to zero by the thresholding procedure. This nuclear segmentation moreover sets the boundaries also for the signal channels, such that only signals within this nuclear space are considered for the evaluation procedure.

Calculation of relative radial distances

All absolute distances of voxels to the nuclear center are expressed as relative distances. This is achieved by dividing the absolute nuclear distance of a voxel by the distance of the most peripheral nuclear voxel that is on a straight line through the nuclear center and the measured voxel (figure 10: r_1/r_0). That way, all values are between 0 (or 0%), for a voxel right in the center and 1 (or 100%), for one completely at the periphery of the nucleus. The center of the nucleus is determined as the gravity center of the segmented counterstain data set, i.e. the nuclear voxels are not weighted by their intensity. Next, the nuclear volume is subdivided into 25 equidistant shells. The relative distances of all measured voxels are finally assigned to one of these 25 shells. The relative DNA content, represented by the amount and the intensity of voxels divided by the amount and the intensity of the complete object is plotted against the relative nuclear distance. This means the proportion of a labeled object within one shell is plotted on the ordinate, while the various shells are arranged according to their distance on the abscissa (figure 2.12).

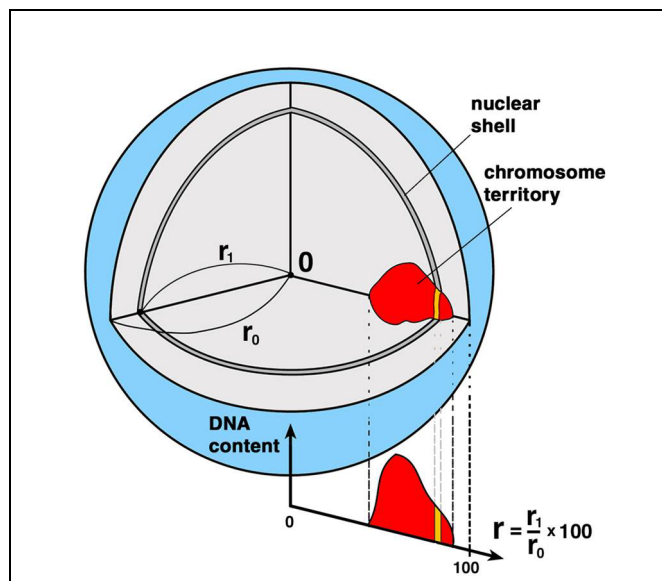


Figure 2.12: Functionality of the 3D-RRD software. The sketch illustrates how the relative distance of a segmented object (red) is measured and plotted by the 3D-RRD software. r =relative distance; r_1 =absolute distance of a voxel; r_0 =distance to the periphery through the measured voxel. "0" marks the nuclear center. The yellow label highlights voxels of the segmented object in a particular nuclear shell and how they are plotted (Illustration from (Tanabe et al. 2002), used with permission of I. Solovei).

The relative radial distribution for the whole set of analyzed nuclei is finally generated by plotting the averages of the relative DNA contents of all nuclei within the individual shells. Another parameter that is calculated by the program is the average relative radius (ARR) of the objects visualized in the respective channel, which represents the distance average of all voxels of the visualized objects over the whole sample. Using a separate module of the software allowed determining the ARR of a chromosome (or of any other segmented fluorescence object) within each individual nucleus. In order not to confound the ARR value of an individual nucleus with that for the complete data set, i.e. for all nuclei, the acronyms iARR for "individual Average Relative Radius" and gARR for "global Average Relative Radius" are used.

The radial distributions of #11 and #X CTs were tested for significant differences using two different approaches. The radial distributions of (1) **complete CTs** and of (2) **iARRs** were compared applying a two-sample Kolmogoroff Smirrnoff (KS) test on the normalized cumulative data set (figure 2.13). p -values for significantly different distributions were derived by comparing the $D(p)$ values corresponding to different levels of significance with empirical D -values. The empirical D value is the maximal difference between the compared distributions. $D(p)$ values were calculated as follows:

$$D(p) = K_p \cdot \sqrt{(n1 + n2)/(n1 \cdot n2)} \quad ((\text{Sachs 2002}) \text{ p. 380}),$$

whereas the constant K_p was derived from the table in (Sachs 2002) p. 380. $n1$ and $n2$ represent the number of analyzed CTs, either #11 CTs vs. #X CTs or CTs cell type 1 vs. CT cell type 2. The calculation of p -values was performed using the formula:

$$K_p = \sqrt{-0.5 \cdot \ln(p/2)} \quad ((\text{Sachs 2002}) \text{ p. 428}).$$

Radial distribution of iARRs of individual nuclei

Since CTs possess a considerable volume, with a radial extension that might substantially overlap between different chromosomes, even if their gravity centers are far apart, it is conceivable that subtle differences in the radial distributions of complete CT volumes might be overlooked, especially if the respective chromosomes are large. Accordingly, if a stringent statistical test is applied such differences might not be classified as significant. One possibility to still prove that subtle differences in radial distributions are reliable and significant would be to use a large sample size. Since for the present experimental setting, it was not possible to collect microscopic data in the necessary range, especially because no automated image acquisition was available, a less stringent approach was used in addition to compare the radial distributions of #11 and #X (and of pericentric heterochromatin between different cell types). Besides comparing radial distributions of complete CTs, which represented a more

stringent approach, I compared the radial distributions of individual average relative radii (iARRs) of CTs. Here the relative distance of a chromosome within one individual nucleus is represented by only one value, the iARR, and not by a distribution curve as in the more stringent approach. The iARR represents the mean relative distance of all voxels (weighted by their intensity) to the nuclear center. After determining the iARRs for the individual nuclei using an extra module of the 3D-RRD software the values were assigned to one of the 25 distance classes (=shells of the nucleus) resulting in the radial distribution of iARRs (figure 2.13 lower left plot). The distributions for #11 and #X were then compared as normalized cumulative data sets by using a two sample KS test (figure 2.13 lower right plot), just as the radial distributions of complete CTs (fig 2.13 upper right plot). Since the iARRs of the labeled objects exhibited a smaller variability in their radial position than the complete object, the resulting iARR distributions were narrower and had steeper slopes (figure 2.13 left plots). Accordingly, this resulted in a higher diversity between the cumulative curves (figure 2.13 right plots) and consequently the significance level was more readily reached. Consequences for the interpretation of the data are discussed in 4.1.1 *Evaluation methods*.

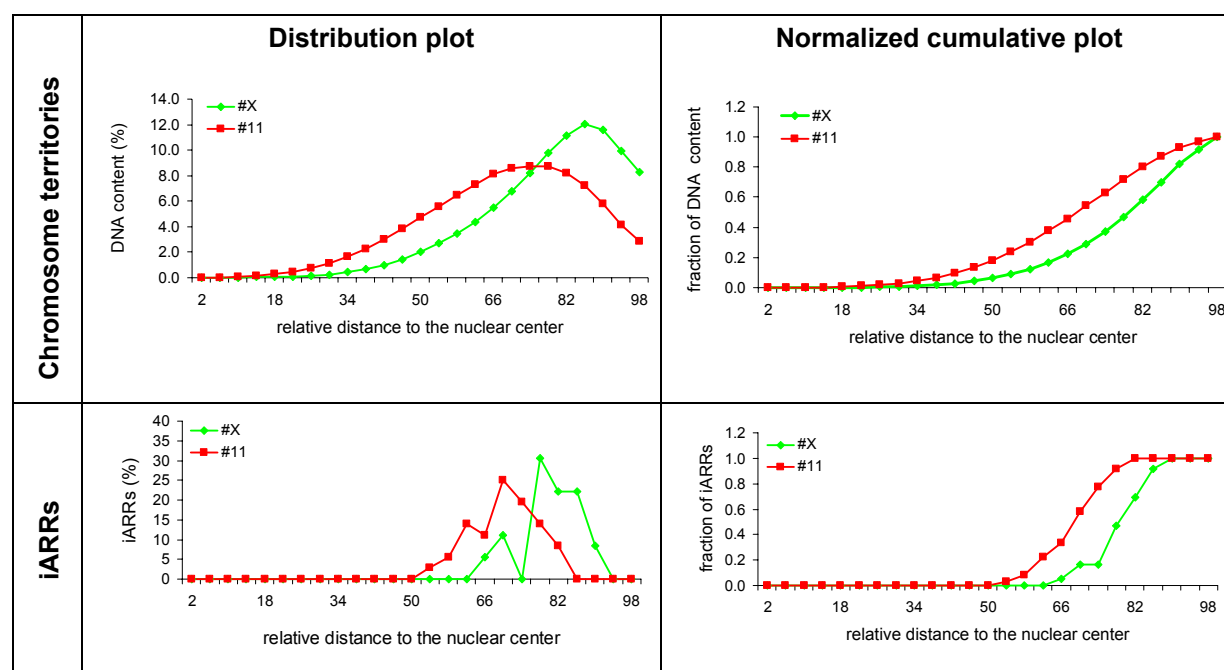


Figure 2.13: Distributions (left) and cumulative frequencies (right) of #11 (red) and X (green) complete territories (upper row) and iARRs (lower row). The panel top left shows the radial distribution of #11 and #X CTs in mouse ES cells as shown in figure 3.3. On the right, the same data is arranged in a normalized cumulative way. The lower left graph shows the radial distributions of the iARRs of #11 and #X. The graph on the right shows the same data set normalized and in a cumulative fashion. Note that the difference between the cumulative curves is bigger for the iARR distributions.

2.12.2 Angles and distances between intensity gravity centers using ImageJ

The determination of intensity gravity centers of CTs using the software ImageJ allowed the calculation of following topological parameters:

- angles included by the straight lines from intensity gravity centers of homologous/heterologous CTs with the nuclear center (NC)
- distances between intensity gravity centers of CTs and the NC
- distances between intensity gravity centers of homologous and heterologous chromosomes.

A specially developed software extension module (plugin) designated “Sync Measure 3D” was employed for this task, which had been elaborated by the former group member J. Walter. This module determines fluorescence intensity gravity centers (GCs) of 3D objects in

grey level image stacks. This has to be preceded by a threshold-based segmentation of the territories/nucleus. In order to determine the geometric center of the nucleus, the thresholded image stack must be converted into a binary one; i.e. all nuclear voxels must be set to the value 255, such that intensity differences are eliminated. To facilitate optimal thresholding and smooth signal boundaries, the image stacks were 2D gaussian filtered using a radius of 1¹.

By vector analytical and trigonometric calculations, the 3D coordinates of the GCs are used to calculate distances and angles:

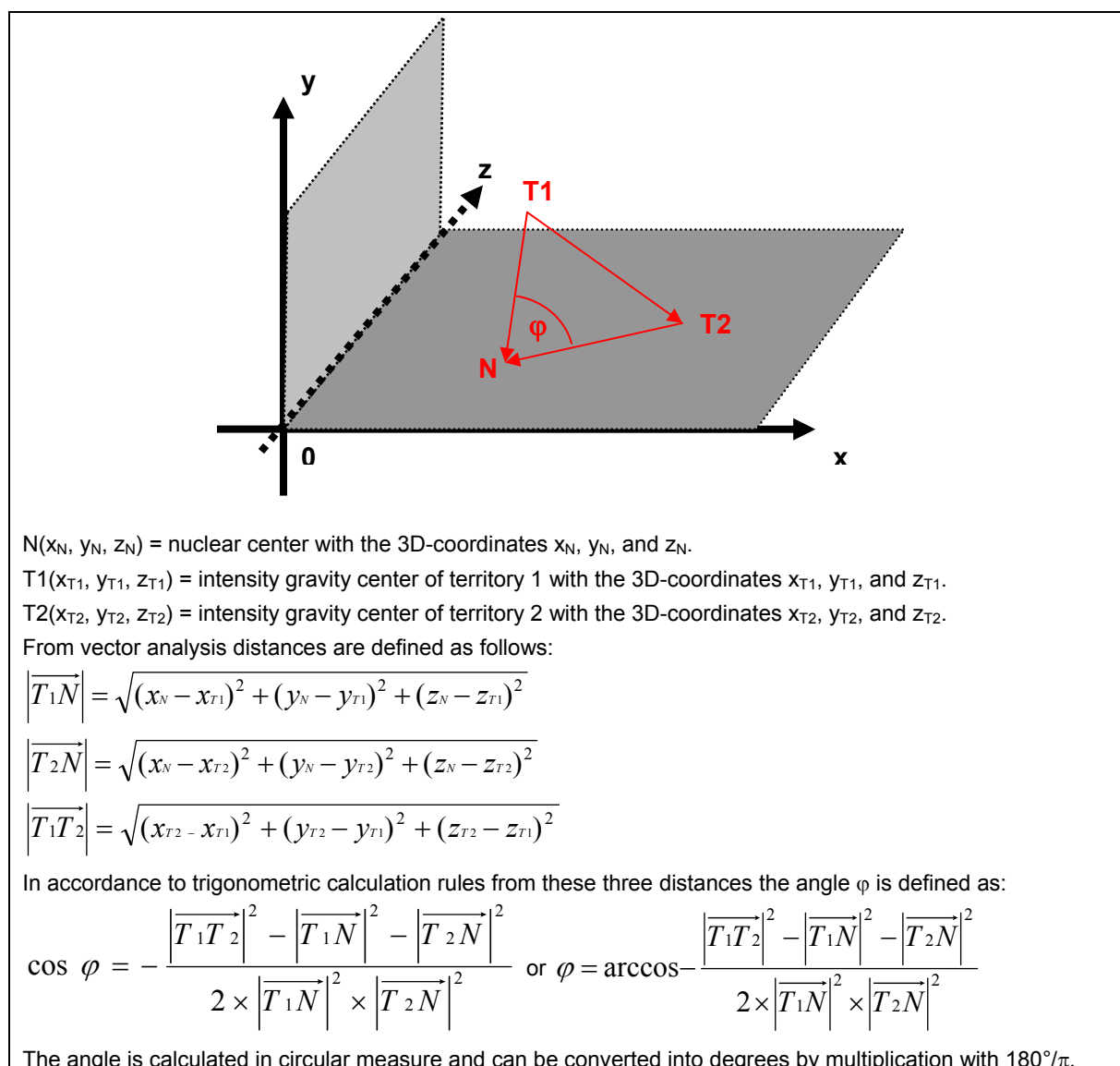


Figure 2.14: Calculation of distances and angles from 3D coordinates of fluorescence intensity gravity centers.

Distances were calculated directly with the “Sync Measure 3D” plugin in ImageJ, while angles were calculated from the distances using Microsoft Excel (XP) (figure 2.14). Absolute distances of GCs to the NC were normalized to the biggest nuclear radius. This maximum radius was calculated as the half of the long nuclear axis. The long axis was measured on projection images of the nuclear counterstain channel. These normalized distances were assigned to classes of relative distances to the NC.

¹ The kernel was [0.46 1 0.46].

The same subdivision of classes was used as in the 3D-RRD software, i.e. 2%, 6%, 10%...etc of the long nuclear radius. Relative distances were plotted as cumulative frequencies, i.e. the fraction of CT gravity centers having a distance to the NC within a certain distance class or smaller was plotted on the ordinate, the relative distance classes on the abscissa (fig 2.15). Differences between #11 and #X distributions were tested for significance using a two-sample KS test (Sachs 2002).

Absolute distances between GCs of homologous #11 CTs and between #11 and #X CTs were normalized to the long nuclear axis, which was measured using projections of the nuclear counterstain. Values of relative distances could thus be given as percentages of the long nuclear axis. Relative distances were assigned to one of ten distance classes with a class width of 10% (figure 2.16). This resulted in a frequency distribution plot with relative distance classes plotted on the abscissa and the fraction of #11-#X distances exhibiting a relative distance within one of the ten classes on the ordinate. Using cumulative frequencies allowed comparing the relative distributions between different cell types and with a normal distribution using a KS test. The normal distribution was reconstructed from measured values as described in detail in (Sachs 2002) pp. 424. To compare the distributions between two different cell types a two sample KS test (see (Sachs 2002) pp. 379) was used, while a KS test modified according to Lilliefors was used as test of goodness of fit to a normal distribution.

Distances between GCs of associated chromosome territories were approximated as follows:

- (1) The volume of the associated territories was determined. The number of voxels of the segmented object is provided by the 3D-RRD software, which can be converted into μm^3 by multiplication with the voxel size.
- (2) The volume was divided by two, yielding the volume of a single territory.
- (3) Assuming a perfect sphere as idealized shape of the territory, the radius r could be calculated using the volumetric formula for a sphere:
- (4) Association of two homologues was defined as both #11 spheres touching each other, with their centers representing their fluorescence intensity gravity centers having the distance $2r$.

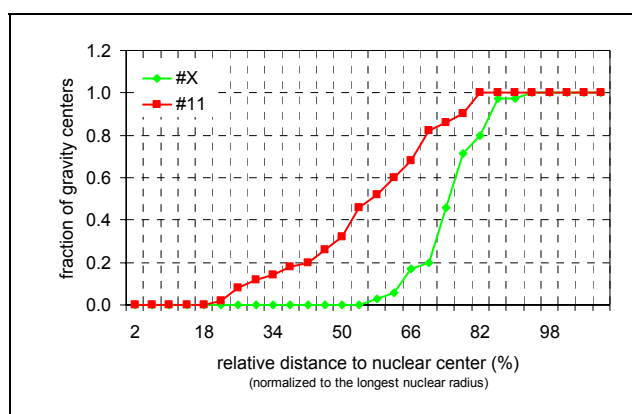


Figure 2.15: Cumulative frequencies of #11 and #X gravity centers (in lymphocytes). The fractions of CTs exhibiting a certain GC-NC distance or smaller are plotted against the classes of relative distances to the NC. #11 distances are shown in red, #X distances in green.

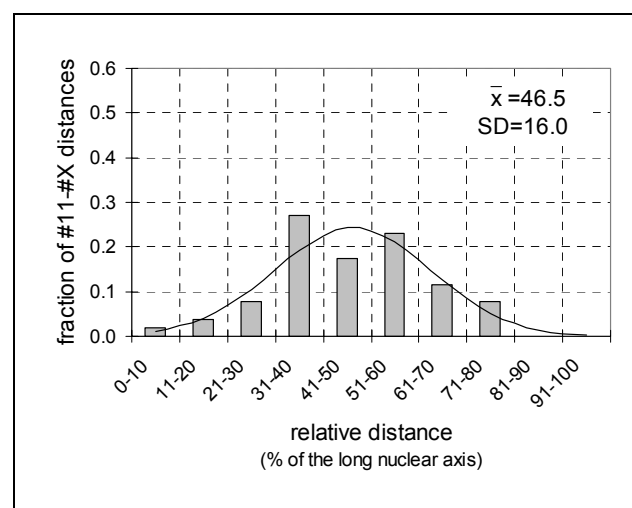


Figure 2.16: Relative distance distributions of #11-#X GC distances (in myoblasts). Columns represent the fraction of #11-#X pairs that had a relative distance within the respective class. The black line represents the normal distribution that was reconstructed from the measured data.

- (5) This distance was normalized according to the long nuclear axis and included in the distribution plots.

Although this approximation represents an only rough estimate, the approximated distance value were smaller or in the range of the smallest distances of separated CTs, which confirms the validity of this estimation.

Angles between GCs of homologous and heterologous chromosomes were assigned to classes with a class width of 20° comprising all possible angles up to 180° (figure 2.17). Similar to the relative distance distributions, the angle classes were plotted on the abscissa and the frequencies, i.e. the fraction of angles having a value within a certain class were plotted on the ordinate. Cumulative frequencies were then used to compare angle distributions between different cells types and to a normal distribution using a KS test (see above).

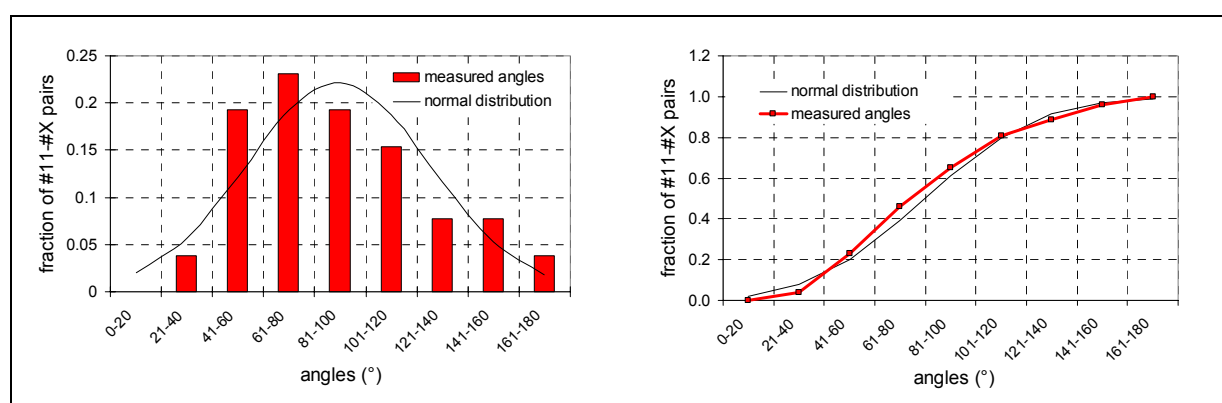


Figure 2.17: Distribution of angles between #11 GC and #X GC (in myoblasts). The left plot illustrates the frequencies of measured angles within the individual angle classes. The normal distribution is given as a black line. The left plot shows the same distributions as the right one, but as cumulative curve. Columns are converted to a line (red).

2.12.3 Correlation analysis of MeCP2 expression and chromocenter clustering

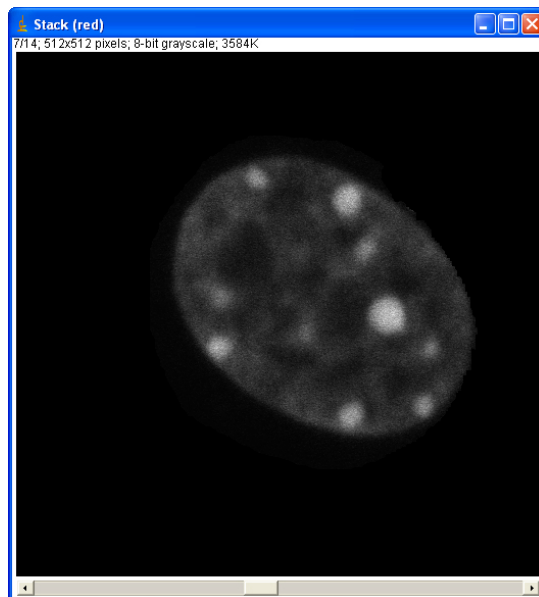
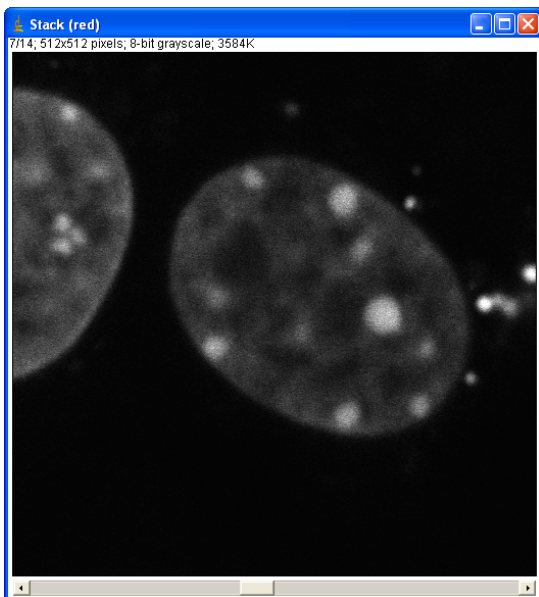
In order to correlate the number of chromocenters with the expression level of MeCP2-YFP its fluorescence intensity had to be quantified. First, image acquisition parameters had to be set in a way that differences in fluorescence would be resolved over the whole range of different expression levels. Setting all microscopic imaging variables (laser power, averaging, photomultiplier voltage etc.) in a manner that highly over-expressing cells would not show a saturation effect, i.e. being overexposed, led to a mean fluorescence intensity of lower expressing cells that was at the same level of background intensity. For that reason, I decided to accept the drawback of a non-linear intensity increase in nuclei with a high over-expression level, in favor of a better resolution of lower expressing cells. Nevertheless, nuclei with high but different over-expression levels did still show a clear-cut difference in their mean intensity level, despite some overexposed areas. The measurements of mean intensity levels were done using the imaging software ImageJ, employing the “Sync Measure 3D” plugin, that has already been described in 2.12.2. Besides having the functions already described, this plug-in also determines the total amount of voxels of a thresholded object as well as the total signal intensity. By simple division the mean fluorescence intensity can be derived.

In order to include only intra-nuclear MeCP2-YFP signals for the determination of the mean fluorescence intensity, a first step was to create a counterstain-derived mask for the MeCP2-YFP channel that would set all voxels outside the nucleus to zero. In the following the indi-

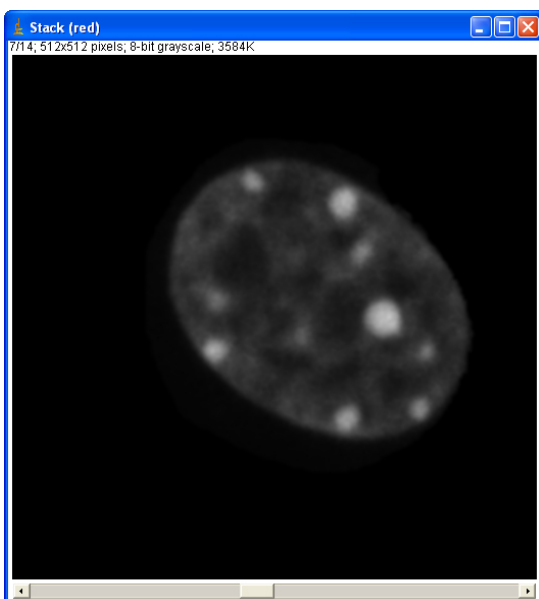
vidual working steps for the calculation of the mean fluorescence intensity are summarized including screen shots for a better understanding.

Creating a nuclear mask (on the counterstain data set)

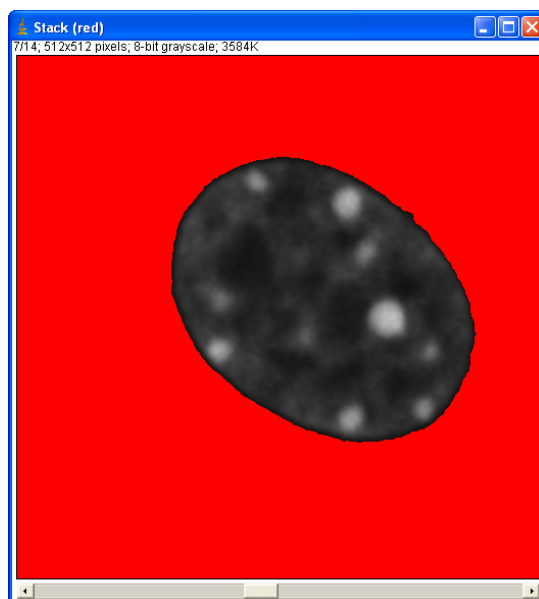
1. Background signals/additional nuclei are removed.



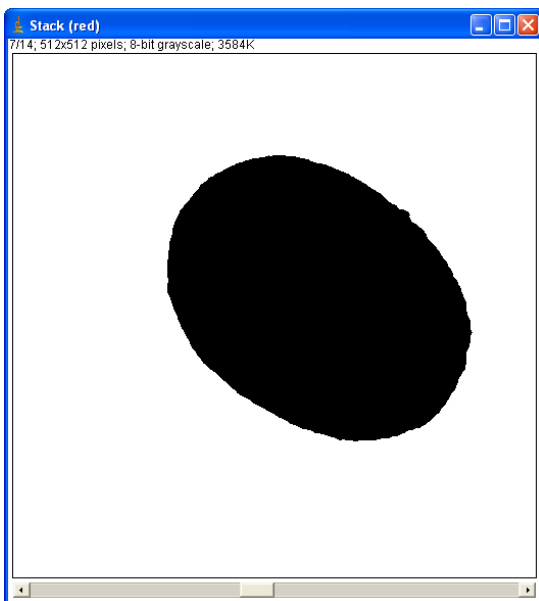
2. 2D Gaussian filtering.



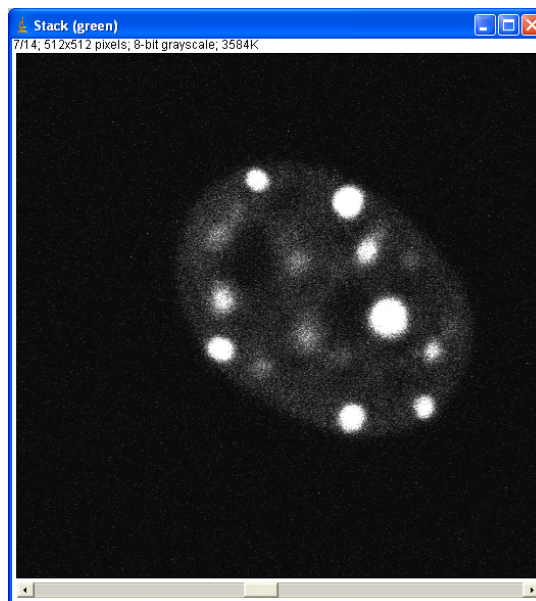
3. Thresholding of the image stack (red).



4. Binarization of the image stack (nuclear voxels are set to 0; extra-nuclear voxels are set to 255).

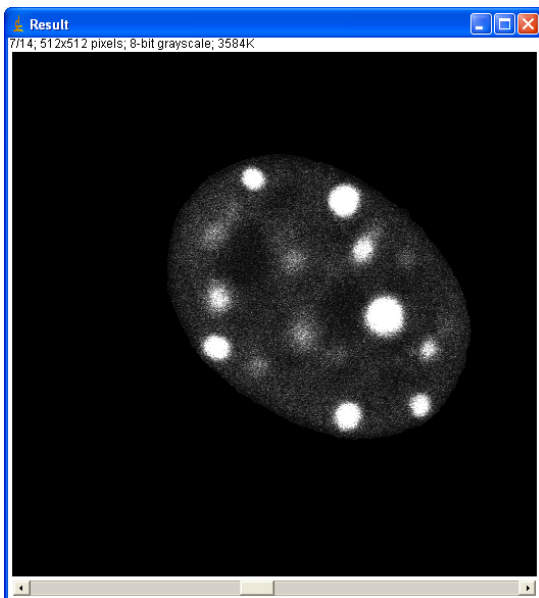


5. MeCP2-YFP stack is opened.

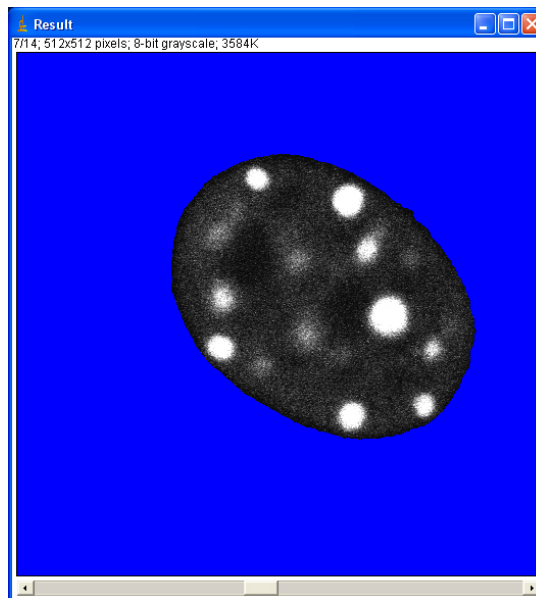


Calculation of the mean fluorescence intensity of MeCP2-YFP (on the MeCP2-YFP data)

6. Binary nuclear counterstain stack is subtracted from the MeCP2-YFP stack \Rightarrow all voxel intensity outside the mask is set to zero voxel intensity within the nucleus remains unchanged.



7. Threshold is set to 1. This way only voxels inside the mask and hence the nucleus are considered in the calculation of the total intensity and number of voxels.



8. The values for the total number of voxels and their intensity can now be used to calculate the mean intensity.

Result	X/pixels	Y/pixels	Z/pixels	Volume	Intensity	Threshold
1	286.677	242.646	8.099	1055971.000	18903206.000	1.000

All nuclei that were quantified for their MeCP2-YFP expression level were relocated after performing FISH with a satellite specific probe (2.8) and imaged by confocal-laser-scanning-microscopy in order to determine their chromocenter-number (2.11). A correlation analysis according to Pearson assuming linear regression was done using the statistical software SPSS 11.0 (SPSS Inc.).

3 Results

3.1 Distribution of gene dense and gene poor chromosomes in different mouse cell types and during differentiation

To date a differential radial distribution of gene dense and gene poor chromosomes has been described for human (Boyle et al. 2001; Cremer et al. 2001; Cremer et al. 2003), primate (Tanabe et al. 2002) and chicken (Habermann et al. 2001) cells. This distributional motif implies a generally more interior location of gene rich chromosomes versus a more peripheral distribution of gene poor chromosomes. One task of the present thesis was to test whether the conserved motif of a gene density dependent radial distribution of chromosome territories holds also true for mouse cells and whether differences would be observable depending on the cell type and differentiation status.

3.1.1 Choice of an appropriate chromosome pair

The first step was to decide which chromosome pair should be analyzed. The decision criteria were: (1) a gene density difference as big as possible; (2) a similar DNA content to rule out chromosome size-dependent distributional effects, as have been described for humans

(Sun et al. 2000; Cremer et al. 2001) and marsupials (Rens et al. 2003) (see also *Introduction*); and (3) the lack of a nucleolus organizing region (NOR) that might have tethered chromosomes to nucleoli and hence biased the radial distribution. Data base information concerning annotated genes were retrieved A) according to a publication coming from the RIKEN Mouse Gene Encyclopedia Project where 21076 mouse cDNAs were annotated according to radiation hybrid data sets of the Whitehead Institute and the Jackson Laboratory, (Kawai et al. 2001) B) from the NCBI data base (www.ncbi.nlm.nih.gov/genome/guide/mouse/) and C) from the ENSEMBL data base (www.ensembl.org/Mus)

Chromosome	Length (Mb)	Annotated genes		Gene Density (genes/Mb)	
		NCBI	ENSEMBL	NCBI	ENSEMBL
1	196	3080	1312	15.7	6.7
2	181	3388	1795	18.7	9.9
3	161	2587	1028	16.1	6.4
4	153	2615	1244	17.1	8.1
5	150	2560	1274	17.1	8.5
6	150	2492	1192	16.6	7.9
7	134	3004	1721	22.4	12.8
8	129	2322	1055	18.0	8.2
9	124	2330	1223	18.8	9.9
10	131	2051	1021	15.7	7.8
11	123	2636	1661	21.4	13.5
12 (NOR)	114	1861	770	16.3	6.8
13	116	2008	804	17.3	6.9
14	116	1796	792	15.5	6.8
15 (NOR)	104	1729	820	16.6	7.9
16 (NOR)	99	1509	689	15.2	7.0
17 (NOR)	94	1845	1052	19.6	11.2
18 (NOR)	91	1492	566	16.4	6.2
19 (NOR)	61	1225	725	20.1	11.9
X	150	1851	848	12.3	5.7
Y	NA	N.A.	NA	N.A.	NA
Σ	2577	44381	21592	17.2	8.4

Table 3.1: The table summarizes annotated genes according to the NCBI and ENSEMBL databases of August 2002. "NOR" denotes chromosome potentially bearing nucleolus organizing regions (Winking et al. 1980). The two most gene dense, NOR lacking chromosomes are highlighted in red, the most gene poor in green.

musculus/). Although all data base analyses yielded similar results, most attention was given to the NCBI and the ENSEMBL information as they had highest number of gene annotations. Additionally I considered homology data concerning big syntenic blocks to gene dense/poor human chromosomes (www.ensembl.org/Homo_sapiens/), as well the presence of so-called H2 isochores, which are genomic DNA fractions with a high GC-content, that can be isolated by density centrifugation and are thought to be gene rich (Saccone et al. 1997). Information concerning NORs was retrieved from (Winking et al. 1980). Since the NCBI and the ENSEMBL data base information on mapped genes were the main decision criteria, only this data is shown in table 3.1. A detailed table containing all information can be found in *Supplementary materials*. Considering all of the mentioned information on gene density chromosome X as a gene poor and chromosome 11 as a gene rich chromosome were finally chosen for the analysis. Chromosome 11 was preferred to chromosome 7 as it was assigned to be chromosome denser according to the RIKEN data. Since all cell types I wanted to analyze were derived from male mice I did not expect any distributional bias caused by X-inactivation and Barr body formation.

3.1.2 3D-FISH

Hybridizations with painting probes specific for chromosome 11 and X were performed and detected as described in *Material and Methods*. Figure 1 shows representative images of hybridizations on mitotic chromosomes and on a 3D preserved nucleus.

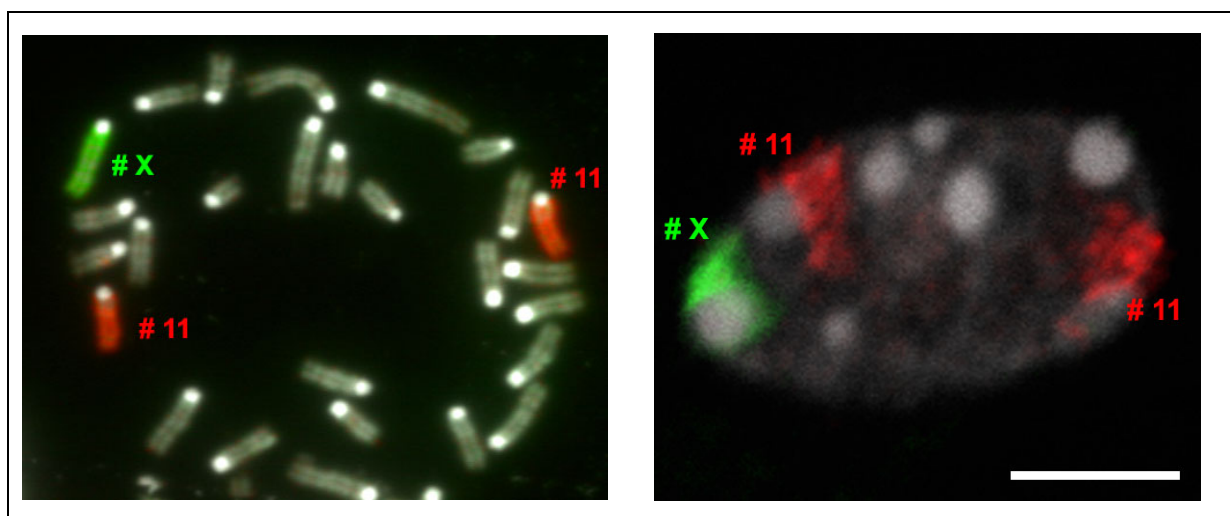
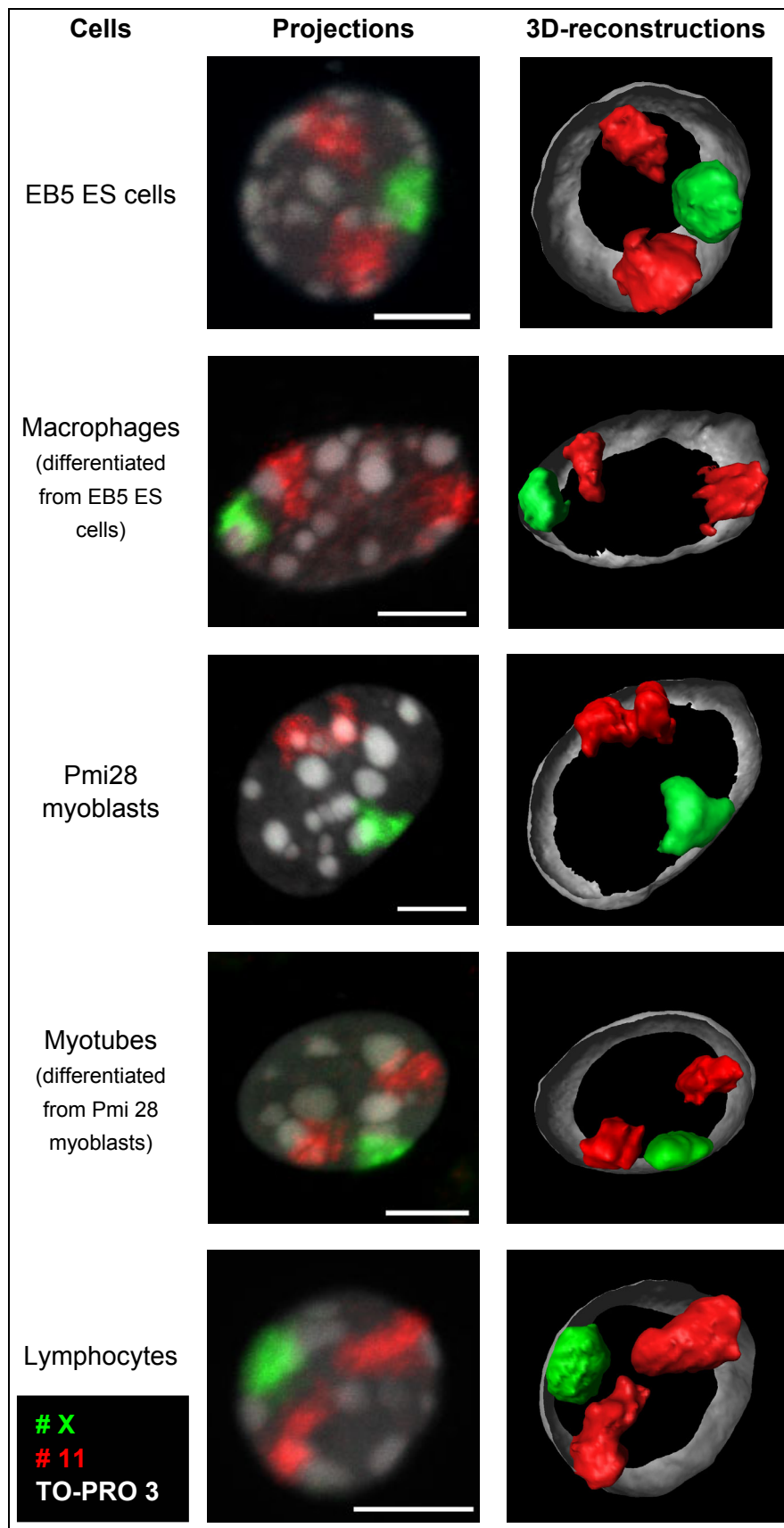


Figure 3.1: Hybridizations with #X and #11 specific paint probes. The left picture shows FISH signals on mitotic chromosomes of a Pmi28 metaphase spread (only a part is shown). The left image shows a confocal mid section of a mouse macrophage nucleus using the same probes as on the left. DAPI was used as counterstain on mitotic chromosomes (white), while the interphase nucleus was stained using TO-PRO 3 (white). Scale bar: 5µm.

The analysis of the radial distribution of chromosome X and 11 included EB5 embryonic stem cells, macrophages which had been derived from them, Pmi28 myoblasts and differentiated myotubes, as well as non stimulated lymphocytes from peripheral blood. All cells were originally derived from male animals. For cycling cells, i.e. ES cells, and myoblasts only S-phase cells were considered¹ for the evaluation, in order to exclude cell cycle dependent variations.

¹ S-phase cells were identified by BrdU incorporation (see 2.6).



Lymphocytes and myotubes were generally considered as G0 since they never showed BrdU incorporation even if incubation times >24h were used. Macrophages were differentiated from EB5 ES cells grown on photoetched coverslips identified by Cd11b specific antibodies, relocated after performing FISH and only included for quantitative evaluation, if they did not show BrdU incorporation, which had been applied for >24h.

The following figures show representative examples of each cell type. Besides a false colored projection of confocal image stacks, 3D-reconstructions of the corresponding nuclei are shown in which the nucleus was cut in an upper and lower plane to illustrate the intranuclear distribution of CTs.

As becomes clear in the examples shown in figure 3.2 both chromosomes show a tendency to abut the nuclear border. A quantification how often CTs would contact the nuclear periphery (defined by DNA counterstaining) revealed that

Figure 3.2: CTs #11 and #X in different mouse cell types. Representative examples of the analyzed cell types are shown. Images in the left column show maximum intensity projections of confocal image stacks. The right column shows 3D reconstructions of the nuclei shown on the left. Though both chromosomes are localized mainly peripheral, a general tendency of chromosome 11 to protrude more into the interior becomes visible, especially in the illustrated lymphocyte nucleus. Note also that homologous #11 CTs could be adjacent to each other, as shown here for a myoblasts nucleus.

in all cell types all chromosome 11 and X territories had contact with the nuclear periphery except for lymphocytes, where in 20% of the nuclei only one of the homologous chromosomes 11 touched the nuclear rim¹. Nevertheless, chromosome 11 showed a clear bias to protrude further into the nuclear interior, as can be seen in the exemplified lymphocyte nucleus.

To quantify the distribution of the chromosome territories within the nucleus, two different evaluation approaches were used. First of all a voxel based method was utilized using the software 3D-RRD, that was developed by J. von Hase, from the group of C. Cremer, University of Heidelberg. The software determines the relative radial distance of each voxel of a segmented fluorescence object from the nuclear center². The second method utilizes only the intensity gravity center of the respective chromosome territories to calculate distances from the nuclear center. This kind of evaluation was performed using Image J software and a specially developed plug-in written by J. Walter in the group of T. Cremer. The results from this latter analysis were a by-product of an angle measurement analysis (see below) and were rather used to verify results from the 3D-RRD analysis. It has the big disadvantage to measure only one spot within the CTs, while the former accounts for all voxels of a given object. Nevertheless investigations using intensity gravity centers have been used successfully to describe intranuclear distributions, proving its validity as evaluation method (Croft et al. 1999; Boyle et al. 2001; Bolzer 2002), in spite of some drawbacks compared to the voxel based approach, like reduced accuracy and less statistic impact, at least if the same number of nuclei are analyzed.

3.1.3 Radial distribution of #11 and #X CTs using the software 3D-RRD

Details on the mode of function of this software can be found in *Material and Methods* 2.12.1. In brief, first the nucleus and the objects to be measured such as chromosome territories are segmented in a threshold dependent manner. The nucleus is then divided into 25 equidistant shells and the position of each voxel of the segmented objects weighted by its intensity is assigned to one of those shells. Thus, a function is generated with 25 discrete measuring points, equaling the individual shells, to which the specific relative DNA content of the analyzed fluorescent object is assigned. The relative DNA content in an individual shell is defined as the proportion of all intensity weighted voxels in the respective shell relative to the complete segmented object.

Figure 3.3 summarizes the results of the analysis of the radial distributions of chromosome 11 and X territories. In all analyzed cell types, a distinct distribution between chromosomes 11 and X becomes evident, with an orientation of chromosome 11 towards smaller relative radial distances and of chromosome X towards the periphery. As already visible from the graphs the diversity between CT distributions showed cell type specific differences. Macrophages for example show an only small diversity between the radial distributions of #11 and #X.

¹ The characterization of CTs contacting the nuclear periphery was accomplished by visual inspection, using DNA counterstain as reference.

² For details, see *Material and Methods* 2.12.1.

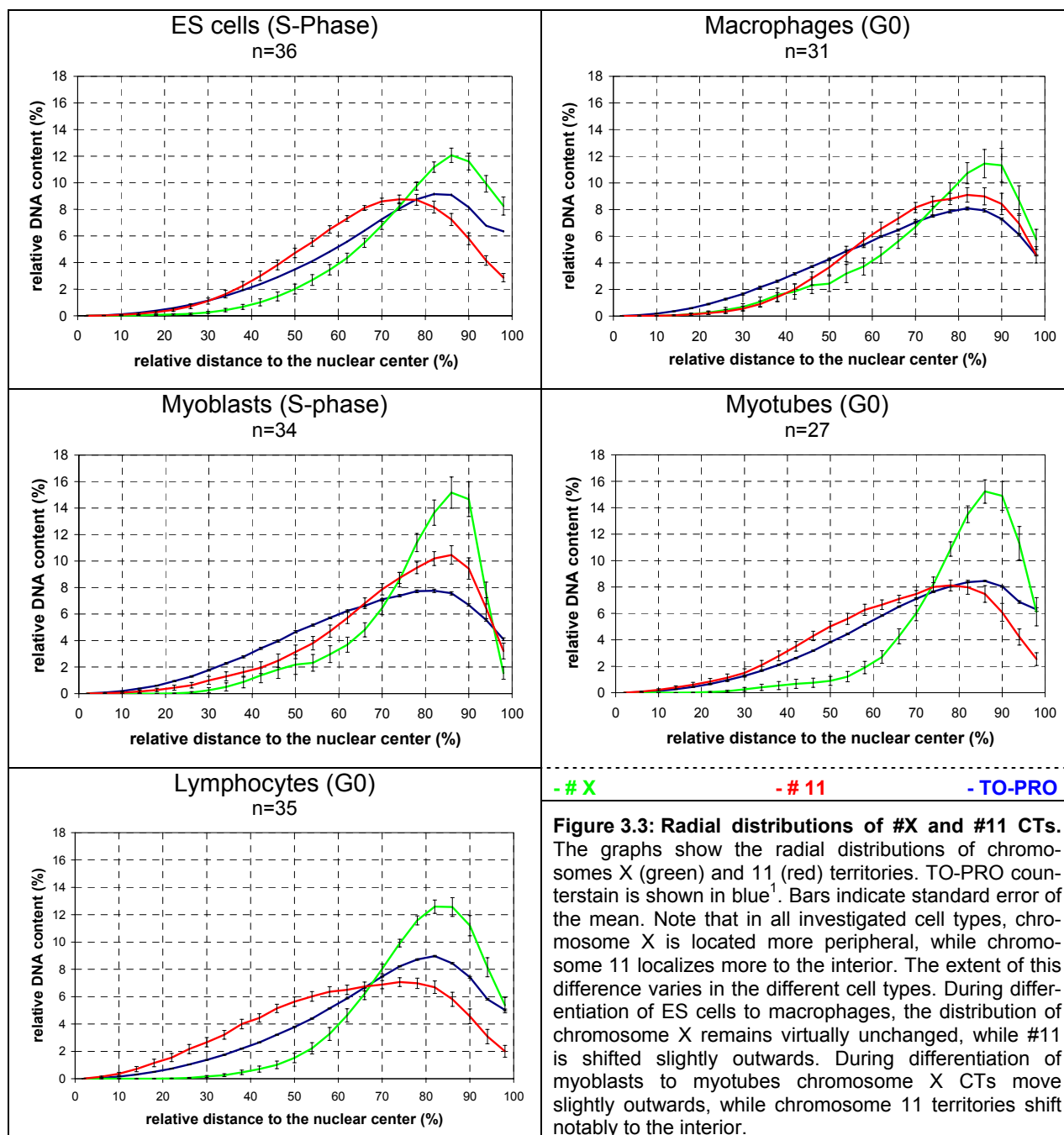
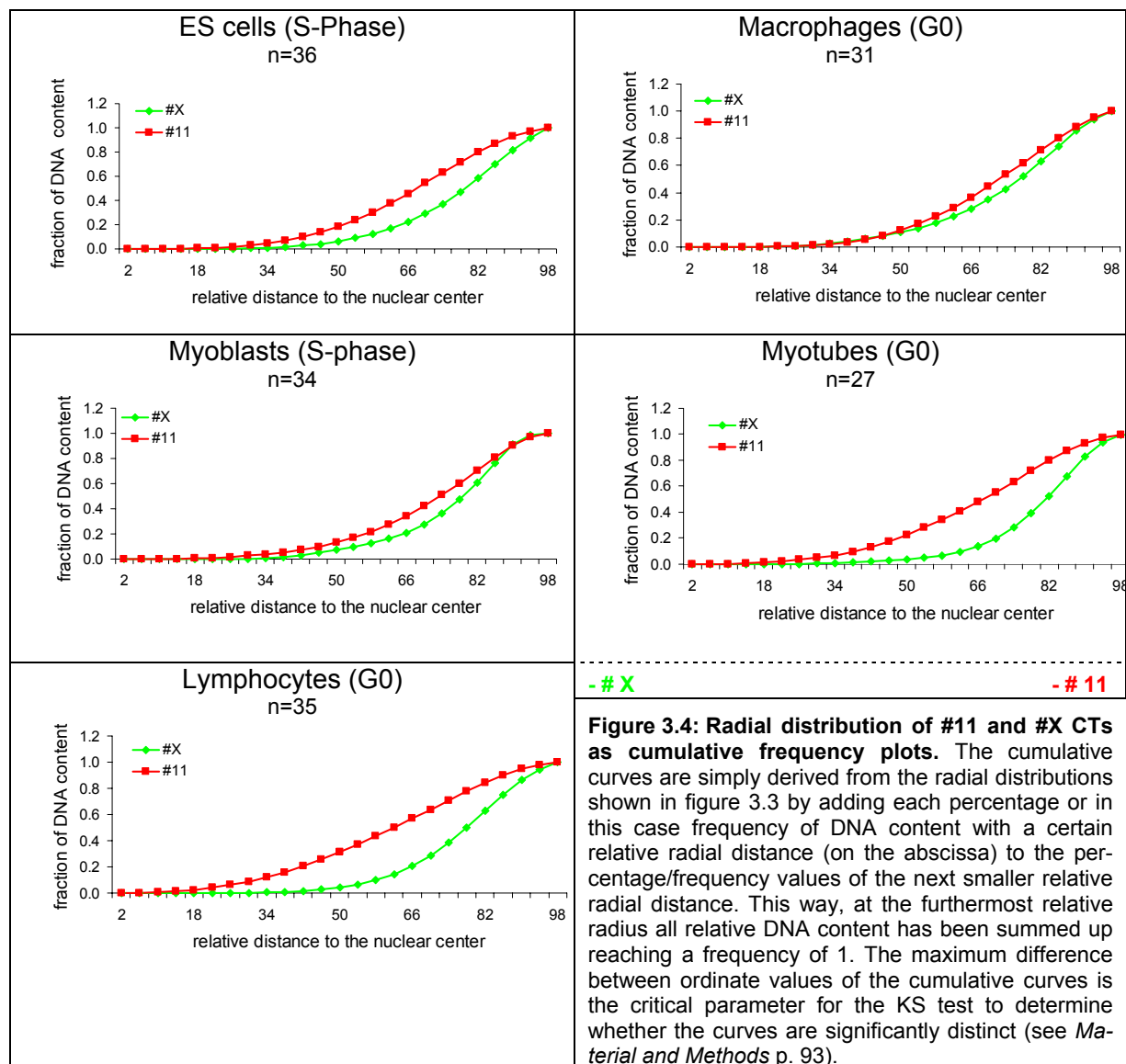


Figure 3.3: Radial distributions of #X and #11 CTs. The graphs show the radial distributions of chromosomes X (green) and 11 (red) territories. TO-PRO counterstain is shown in blue¹. Bars indicate standard error of the mean. Note that in all investigated cell types, chromosome X is located more peripheral, while chromosome 11 localizes more to the interior. The extent of this difference varies in the different cell types. During differentiation of ES cells to macrophages, the distribution of chromosome X remains virtually unchanged, while #11 is shifted slightly outwards. During differentiation of myoblasts to myotubes chromosome X CTs move slightly outwards, while chromosome 11 territories shift notably to the interior.

¹ Note that the DNA content as revealed by the TO-PRO 3 staining increases with increasing distance from the nuclear center, because the radial shells the nucleus is subdivided in, increase in volume. The counterstain curve is expected to rise until the nuclear edge, i.e. 100% of the relative distance to the nuclear center. This is apparently not the case, instead it reaches a peak usually between 80% and 90% and declines somewhat until 100% are reached. This anomaly could be an imaging artifact of the nuclear counterstain, caused by the point spread function (PSF) of the confocal optics. This PSF is known to result in a signal blurring, which might artificially increase the nuclear volume while the edges would gradually lose fluorescence intensity. In other words, the sharp edge of the nucleus, which is anticipated, cannot be resolved by the utilized microscopic setting. Alternatively, this decrease in DNA content at the very edge could also result from a fluorescence halo, representing chromatin that protrudes from the permeabilized nucleus, which could be a consequence either of fixation or of the FISH procedure. In conclusion, the "real" nuclear border is more probable at the peak of the counterstain curve than at 100% of the segmented nucleus.

Differences in the distributions of CTs within one cell type (table 3.2) but also between different cell types (tab 3.3) were tested for significance using two different approaches. (1) The radial distribution curves of CTs were arranged in a normalized cumulative fashion (see figure 3.4) and compared using a two sample Kolmogoroff Smirnoff (KS) test (see also (Cremer et al. 2003) and *Material and methods*).



Since this represented a very stringent test that might have left smaller differences undiscovered, especially since an only moderate sample size was used ($n \sim 30$), I decided to test additionally for a significant difference in the distributions of the iARRs (see *Material and Methods* 2.12.1 for details). Compared to the radial distribution of complete CTs, the iARR distribution appeared somewhat narrower with steeper slopes and the cumulative curves showed a higher diversity (see fig 2.13 for comparison). Figure 3.5 illustrates the radial distributions of iARRs in the various cell types including the cumulative plots.

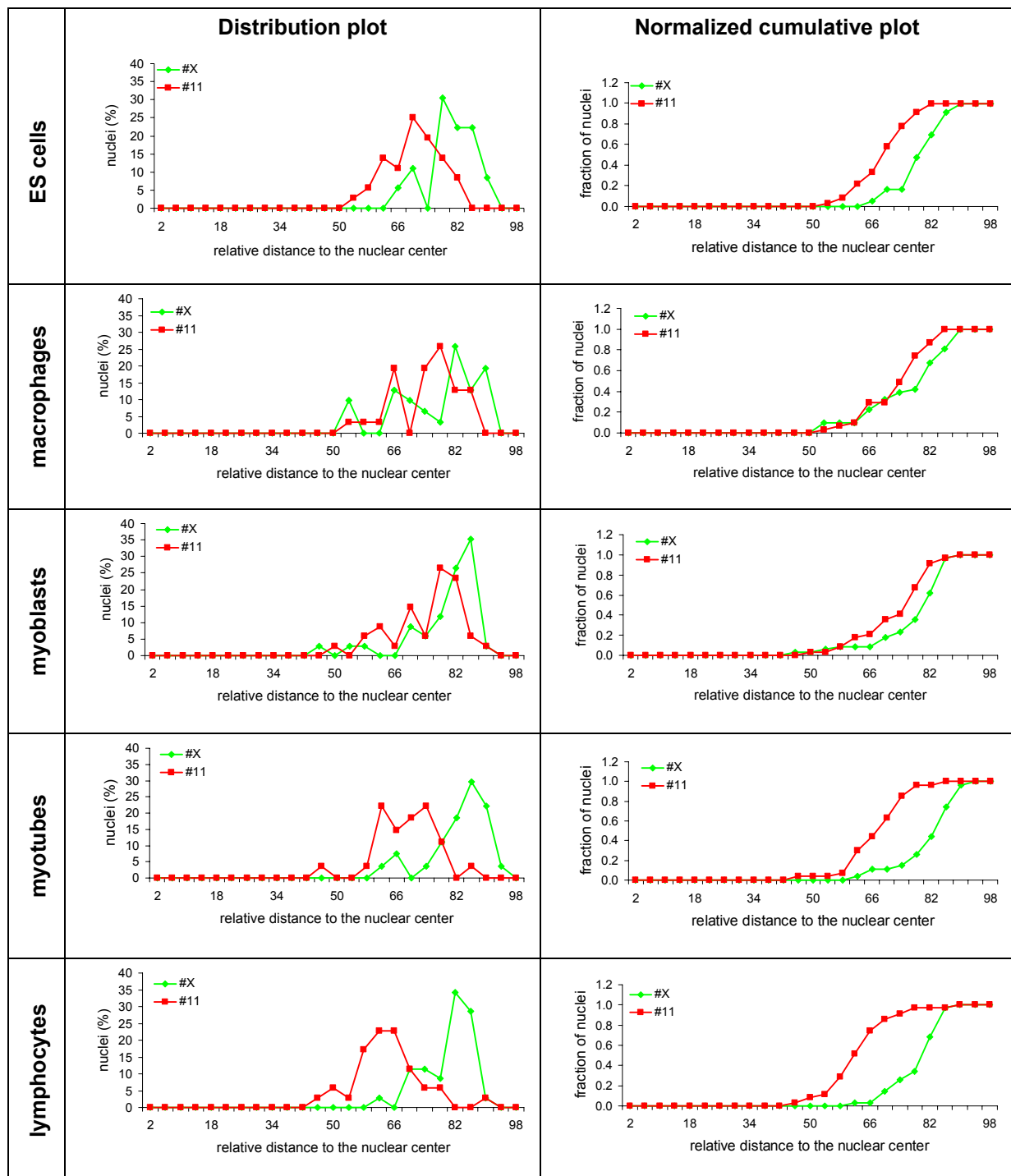


Figure 3.5: Radial distributions (left) and cumulative frequencies (right) of #11 (red) and #X (green) iARRs. The ordinates represent the percentage (left column) or cumulative fraction (right column) of nuclei with an iARR value according to the abscissa. Note the clear cut differences in the distributions of #11 and #X iARRs in ES cells, myotubes and lymphocytes in both plots. The curves in macrophages and myoblasts in contrast are very similar. Note also that the differences between #11 and #X cumulative curves representing the radial distribution of iARRs are much more pronounced than those for the radial distributions of complete CTs (figure 3.4).

(1) When the radial distributions of complete CTs were used for the statistical analysis, only in lymphocytes the difference between #11 and #X CTs turned out to be significant ($p < 0.05$). In myotubes a p -value of 0.06 was calculated, which exceeds the level of significance only slightly. The comparison of the radial distribution of CTs between different cell types revealed no significant differences.

(2) Differences between the radial distributions of #11 and #X CTs using iARRs instead of complete segmented territories were significant for all analyzed cell types, except for macrophages (table 3.2) and myoblasts. Since the calculated p-value for these cell types were 0.079 and 0.056 respectively and thus only slightly above the 0.05 level of significance a real difference between both radial distributions is still suggestive. The highest p-value for macrophages is reflected by the radial distribution curves, which show the highest similarity of all analyzed cell types (figure 3.3 and 3.4).

ES cells	macrophages	myoblasts	myotubes	lymphocytes
p<0.001	p=0.079	p=0.056	p<0.001	p<0.001

Table 3.2: Results of the KS-test comparing the radial distributions of #11 and #X iARRs in different cell types. The distributions are significantly different for ES cells myotubes and lymphocytes (yellow), but not for macrophages and myoblasts (red). Although #11 CTs are still located more internally than #X CTs (see figure 3.3 and 3.4), the difference especially in macrophages is not as clear cut as in the other cell types. Note that the p-values in macrophages and myoblasts are only slightly above the level of significance (0.05).

Comparing the iARR distributions of #11 and #X CTs, respectively between different cell types using the KS-test revealed no significant difference for the X chromosome, while chromosome 11 exhibited a differential distribution between some cell types (table 3.3). Namely, #11 CTs were significantly most internal in lymphocytes compared to all other cell types, besides myotubes (table 3.3). Myotube nuclei showed significantly more internal iARRs than myoblasts and macrophages, while in ES cells #11 iARRs were located more internally than in myoblasts. Thus, there seems to be a cell type specific radial distribution of #11 CTs with a most internal position in lymphocytes and myotubes followed by ES cells and most external in macrophages and myoblasts.

#X \ #11	ES cells	macrophages	myoblasts	myotubes	lymphocytes
ES cells	-	p=0.112	p<0.05	p>0.2	p<0.01
macrophages	p>0.2	-	p>0.2	p<0.05	p<0.001
myoblasts	p>0.2	p>0.2	-	p<0.01	p<0.001
myotubes	p>0.2	p>0.2	p>0.2	-	p=0.132
lymphocytes	p>0.2	p=0.2	p>0.2	p>0.2	-

Table 3.3: Results of the KS-test comparing the radial distributions of iARRs between different cell types. Red characters refer to the comparison of #11 distributions, green characters to the comparison of #X distributions. Differences between the radial distributions of iARRs were only significant for #11 CTs. In lymphocytes #11 iARRs were significantly more internal compared to all other cell types except for myotubes. Myotubes showed significantly more interior #11 iARRs than macrophages and myoblasts, while ES cells had more internal #11 iARRs than myoblasts. No significant differences were found between the radial distributions of #X iARRs. Yellow background: significant difference with p<0.05; red background: no significant difference with p>0.05.

This increase in the relative distances of # 11 iARRs from the nuclear center is demonstrated in figure 3.6, by presenting “global” average relative radii (gARRs) of #X and 11 CTs in the respective cell types (see also (Cremer et al. 2003)). gARRs are defined as the averages of iARRs within one cell type. This presentation of the data illustrates once more the general tendency of #11 CTs to localize more internally and #X more peripherally. The higher similarity #11 and #X radial distributions in macrophages and myoblasts is recapitulated by a smaller difference in their gARRs values. As already mentioned lymphocyte nuclei exhibited the most internal location of #11 CTs followed by myotubes and ES cells, which is reflected by increasing gARR values. Lymphocytes feature the biggest difference between gARR values of chromosome X and 11, which mirrors the highest significance in the radial distribu-

tions of iARRs and the fact that it was the only cell type where the differences in the radial distributions of the complete CTs met the stringent significance criteria.

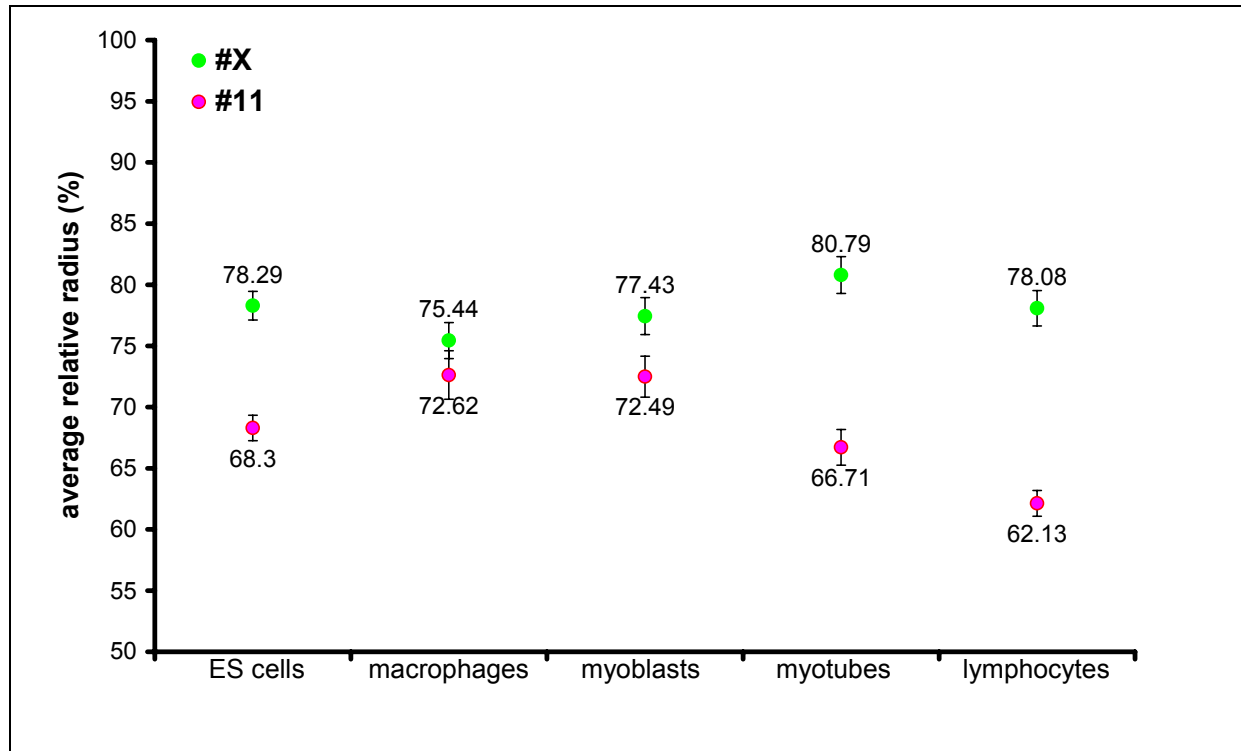


Figure 3.6: Global average relative radii (gARRs) of #11 and #X CTs in different cell types. gARRs represent the means of the iARR values within one cell type. Error bars correspond to the standard error of the mean. The differential radial arrangements of the gene dense # 11 and the gene poor #X are reflected by gARRs of #11 having smaller values, i.e. being more internal than those of #X. Moreover, differences concerning the degree of diversity of CT distributions are reflected by the distances between the respective gARRs (see also text). Note also the higher variability of #11 iARR values between different cell types compared to #X. gARR values are given above and below the respective spot.

Taken together these results militate in favor for a conservation of a gene-density-related radial distribution of CTs in mouse as it has been described for humans, higher primates and birds. Another important finding is that there seems to be a cell type specific difference in the radial distribution of #11 that appears to be independent of the cellular differentiation status: on the one hand a shift of #11 towards the periphery was monitored during ES cell differentiation to macrophages, on the other hand a shift towards the interior was observed during myogenesis. This cell type related changes appeared to correlate with the shape of the nuclei in the analyzed cell types. The flatter the nuclei the more peripheral #11 CTs were localized and consequently the less distinct was the radial distribution to #X CTs. In order to compare the nuclear shapes of different cell types I defined a roundness parameter (RP) that was characterized by the ratios of the nuclear axes in all three dimensions. RP was calculated as $z^2/x*y$, whereas z was the axial diameter, x the long and y the short axis of the nuclear ellipsoid. A perfect sphere thus would result in a RP of one, while a flat nucleus would accordingly yield RP value < 1. Using these values as parameter for nuclear roundness I found that the degree of difference between the radial distributions of #11 and #X CTs correlated with the degree of roundness of the nuclei in the respective cell types (see table 3.4); in other words: the flatter the nuclear shape the less different the radial distributions. These results are consistent with those concerning gene poor #18 vs. gene dense #19 in human cells (Cremer et al. 2001) where a high diversity in the radial distribution between both chromo-

somes could not be reproduced in flat-shaped fibroblast and amniotic fluid cell nuclei (see *Discussion*).

	ES cells	macrophages	myoblasts	myotubes	lymphocytes
p value	p<0.001	p=0.079	p=0.056	p<0.001	p<0.001
Nuclear dimensions (x,y,z in μm)	11.5x10.6x10.9	13.1x9.7x5.8	16.2x11.2x4.9	12.5x8.2x7.4	9.2x8.7x8.6
roundness ($z^2/x*y$)	0.97	0.26	0.13	0.53	0.92

Table 3.4: p values of the KS-test comparing the radial distributions of #11 and #X iARRs in different cell types in relation to an average nuclear roundness parameter. The roundness parameter (RP) is defined as $z^2/x*y$, with z being the nuclear diameter in the axial dimension, x representing the long axis and y the short axis of the ellipsoid. All three parameters were determined on xz yz and xy projections of confocal series sections of TO-PRO 3 stained nuclei. Note that a perfectly spherical nucleus would yield an RP of 1 while flatter nuclei have an RP <1. Note also that myotube nuclei exhibit a rather small RP compared to ES cells or lymphocytes, which is due to their cylindrical shape, i.e. they have an ellipsoid xy but a spherical z profile.

In this context, it must be added that ES cell nuclei were not always spherically shaped. Especially if present in larger cell aggregates the nuclei were often very irregularly shaped. Due to the limitation of the 3D-RRD software, that was not able to subdivide such irregularly shaped nuclei properly, only round shaped were included in the analysis, which might have potentially biased the results. On the other hand, non-floating cultured cells are generally prone not to represent the actual situation in the respective tissue as the third dimension is always lost by two-dimensional cultivation on an artificial substrate.

The fact that different approaches of analyzing the data yielded different outcomes concerning the statistical significance poses some general problems on choosing the correct methods for evaluating such data, and on defining a sufficient sample size in order to detect also small differences on a significant level (see *Discussion*).

3.1.4 Radial distribution of #11 and #X CTs using the software Image J

Besides using a voxel based evaluation method as described above, the data set was also evaluated via fluorescence intensity gravity center (GCs) of #11 and #X territories. Coordinates of GCs of individual CTs were determined using the software Image J. These were used to calculate distances to the nuclear center, as well as between homologous/heterologous CTs together with angles between homologous/heterologous CTs. Figure 3.7 shows the radial distributions of #11 and #X GCs plotted as cumulative frequencies (see also figure 3.4 and 3.5 for comparison). It should be added that the number of GCs for chromosome 11 does not equal the number of CTs, since in several nuclei both homologues were associated, i.e. the individual territories could not be separated. Therefore, some GCs represent the nuclear distance of both homologous CTs.

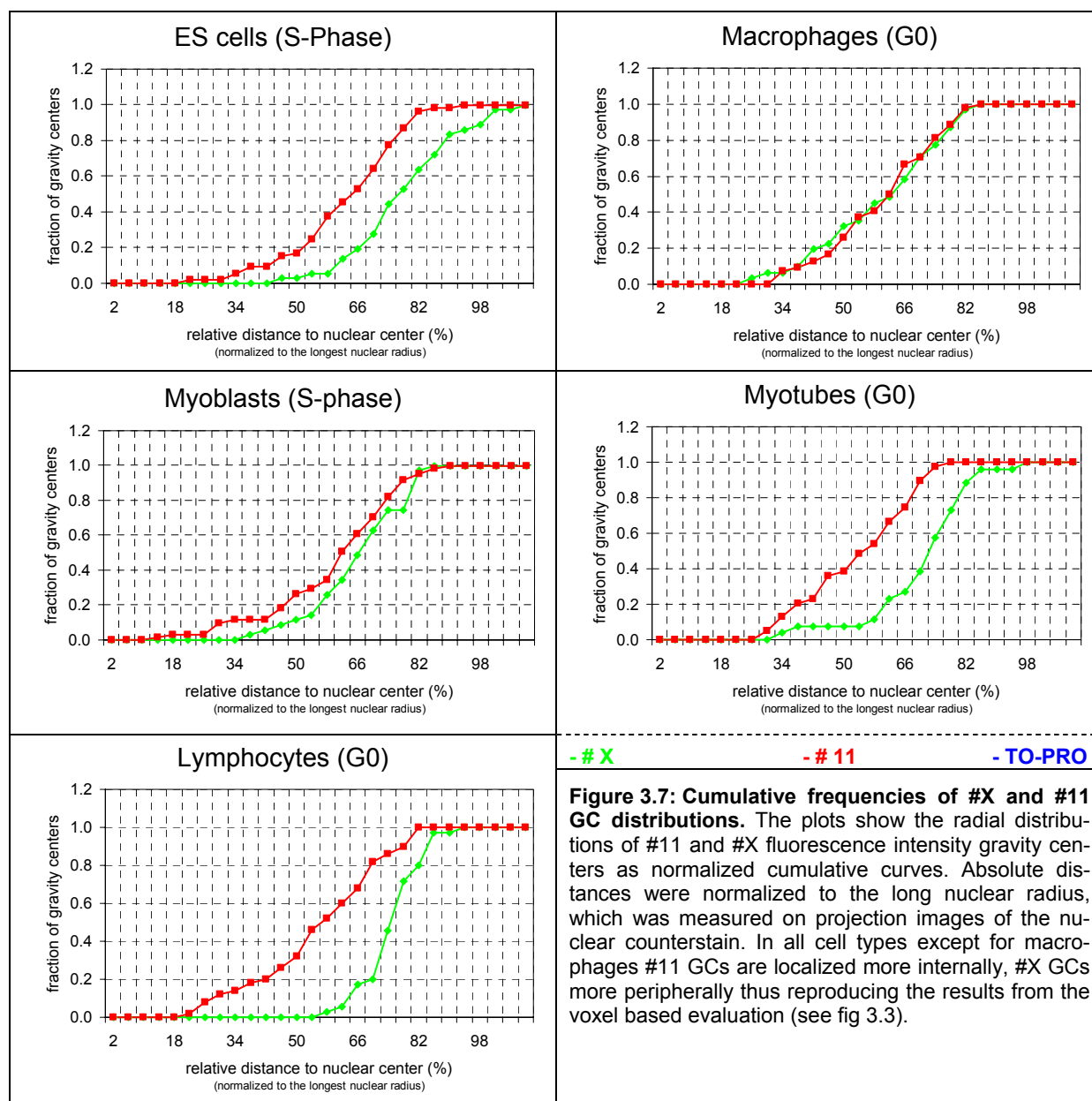


Figure 3.7: Cumulative frequencies of #X and #11 GC distributions. The plots show the radial distributions of #11 and #X fluorescence intensity gravity centers as normalized cumulative curves. Absolute distances were normalized to the long nuclear radius, which was measured on projection images of the nuclear counterstain. In all cell types except for macrophages #11 GCs are localized more internally, #X GCs more peripherally thus reproducing the results from the voxel based evaluation (see fig 3.3).

In all cell types with exception of macrophages, #11 CTs show a preference to localize more internally, #X CTs more peripherally. This result clearly reproduces the findings yielded by the evaluation of complete CTs using the 3D-RRD software. The statistical analysis using a two sample KS-test yielded almost the same results as the KS-test on the iARR radial distributions described in table 3.2, with the exception that in macrophages and myoblasts the p-values representing the “lack of diversity” were higher (table 3.5).

ES-cells	macrophages	myoblasts	myotubes	lymphocytes
p<0.01	p>0.2	p>0.2	p<0.001	p<0.001

Table 3.5: Results of the KS-test comparing the radial distributions of #11 and #X GCs in different cell types. Similar to the radial distribution of the iARRs (table 3.2) radial distributions of GCs are significantly different in ES cells, myotubes and lymphocytes. In myoblasts on the other hand, the distribution difference seen in the cumulative frequency plots was not significant.

Figure 3.8 illustrates mean values of GC distances to the nuclear center in the various cell types. Similar to the gARR shown in figure 3.6 average GC distances were higher for chro-

mosome X. Also analogous to figure 3.6 are the smaller differences between #11 and #X in macrophages and myoblasts, which reflect the similarity of their distribution curves (figure 3.7).

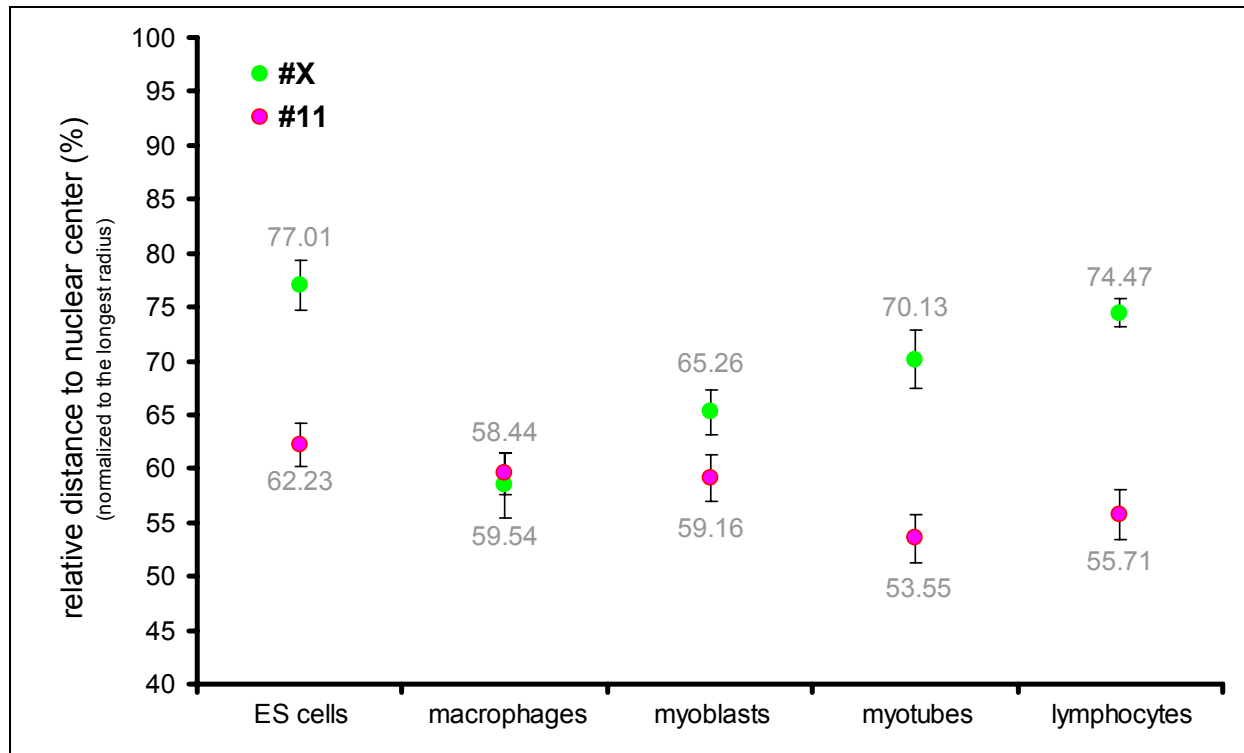


Figure 3.8: Average relative GC distances of #11 and #X CTs in different cell types. The plot shows the mean values of all relative distances between GCs of chromosome 11 and X, respectively and the nuclear center. Error bars correspond to the standard error of the mean. In all cell types except for macrophages, GCs of chromosome X are more peripheral than those of chromosome 11. Note that the differences.

Taken together the evaluation of the radial distribution of #11 and #X CTs, using fluorescence intensity gravity center reproduced the results from the evaluation using complete territories or iARRs derived by voxel information of the complete territories.

3.1.5 Side-by-side distribution of #X and #11

Besides a non-random radial distribution, it was also proposed that CTs might exhibit a non-random side-by-side distribution in the sense that their position would reflect a specific constellation in respect to each other (Nagele et al. 1999; Parada et al. 2002).

If such a fixed side-by-side organization of CTs would exist, one would expect to find characteristic distance values that would reflect the neighboring situation of CTs, either small for CTs near to each other or large for CTs that localize far away from each other. Moreover, the variability of these distances between individual nuclei should be very low. Accordingly, the angles between their gravity centers and the nuclear center should exhibit small variations and display characteristic and reproducible values. To test this hypothesis I analyzed homologous and heterologous distances and angles for #11 CTs and #X CTs¹.

¹ Note that the determination of angles and distances between homologous #X CTs was not applicable, since only cells derived from male animals were included,.

Homologous distances and angles for #11 CTs

In order to analyze whether #11 CTs show an association in interphase nuclei I first determined the fraction of nuclei in which there was only one coherent object, i.e. where the two homologues could not be distinguished. Those nuclei were defined as exhibiting a homologous association of #11 CTs. Figure 3.9 shows the percentage of nuclei showing such a homologous association in the different analyzed cell types.

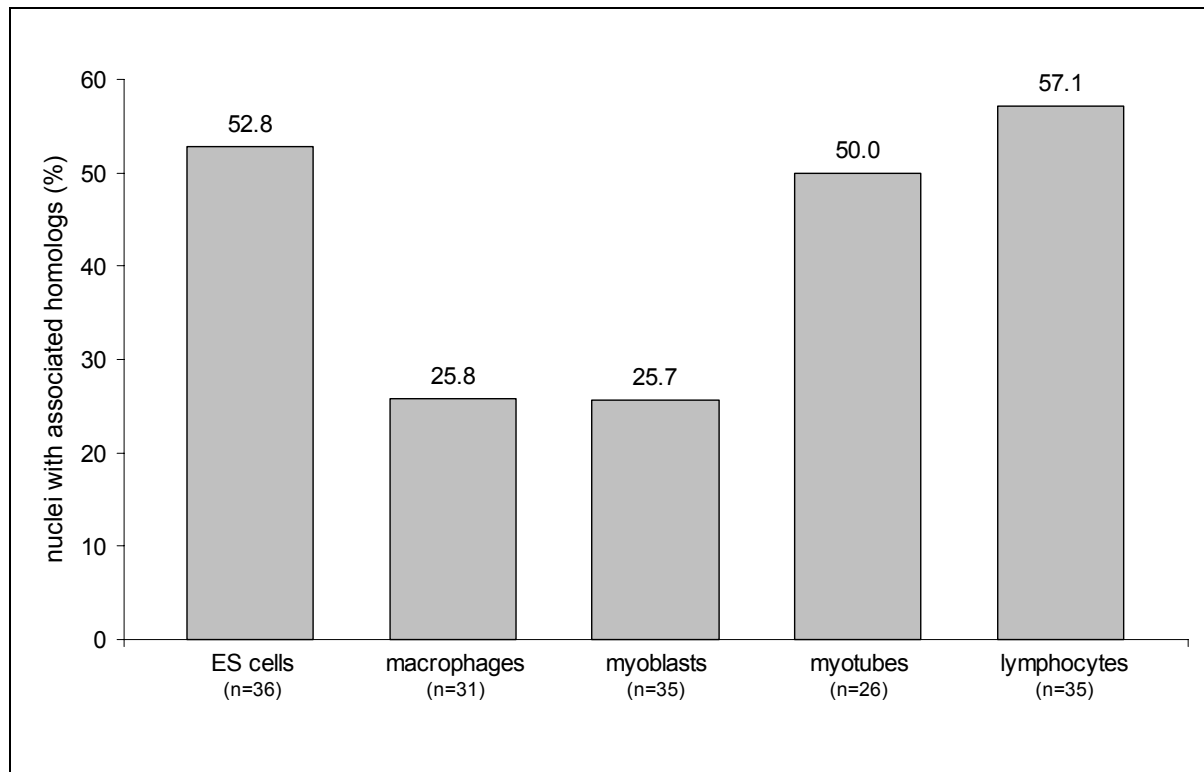


Figure 3.9: Percentages of nuclei showing association of #11 CTs. The columns represent the percentages of nuclei in which just one coherent territory could be segmented. In these cases, the territories of the individual chromosomes were defined to be associated. n= number of analyzed nuclei.

In macrophages and myoblasts approximately a quarter of all analyzed nuclei showed an association, while in ES cells, myotubes and lymphocytes 50% or more nuclei had undistinguishable #11 CTs. This high frequency of associated #11 CTs is indicative of a close proximity, but since at least 50% of nuclei show separated territories, a general association can be ruled out.

Figure 3.10 shows the distribution of relative distances of non-associated #11 CTs normalized to the long nuclear axis (see *Material and Methods*). Non-associated #11 CTs show a wide range of GC distances that can reach more than 80% of the long nuclear axis. Their distance distributions correspond to a normal distribution for all cell types, as determined by a one sample KS-test (modified according to Lilliefors; see (Sachs 2002), p. 429ff.). Moreover, the distance distributions do not differ significantly between different cell types (two-sample KS test).

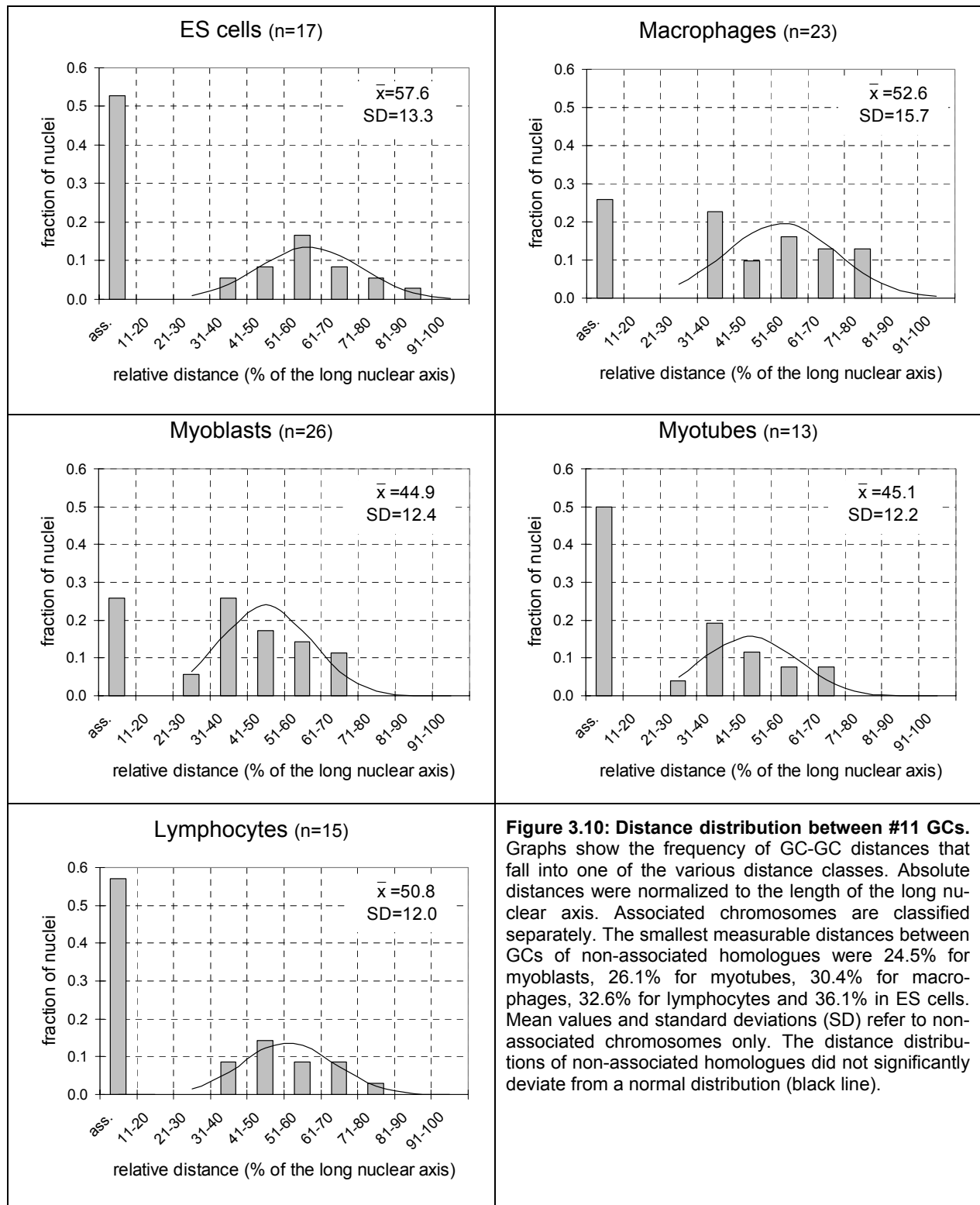
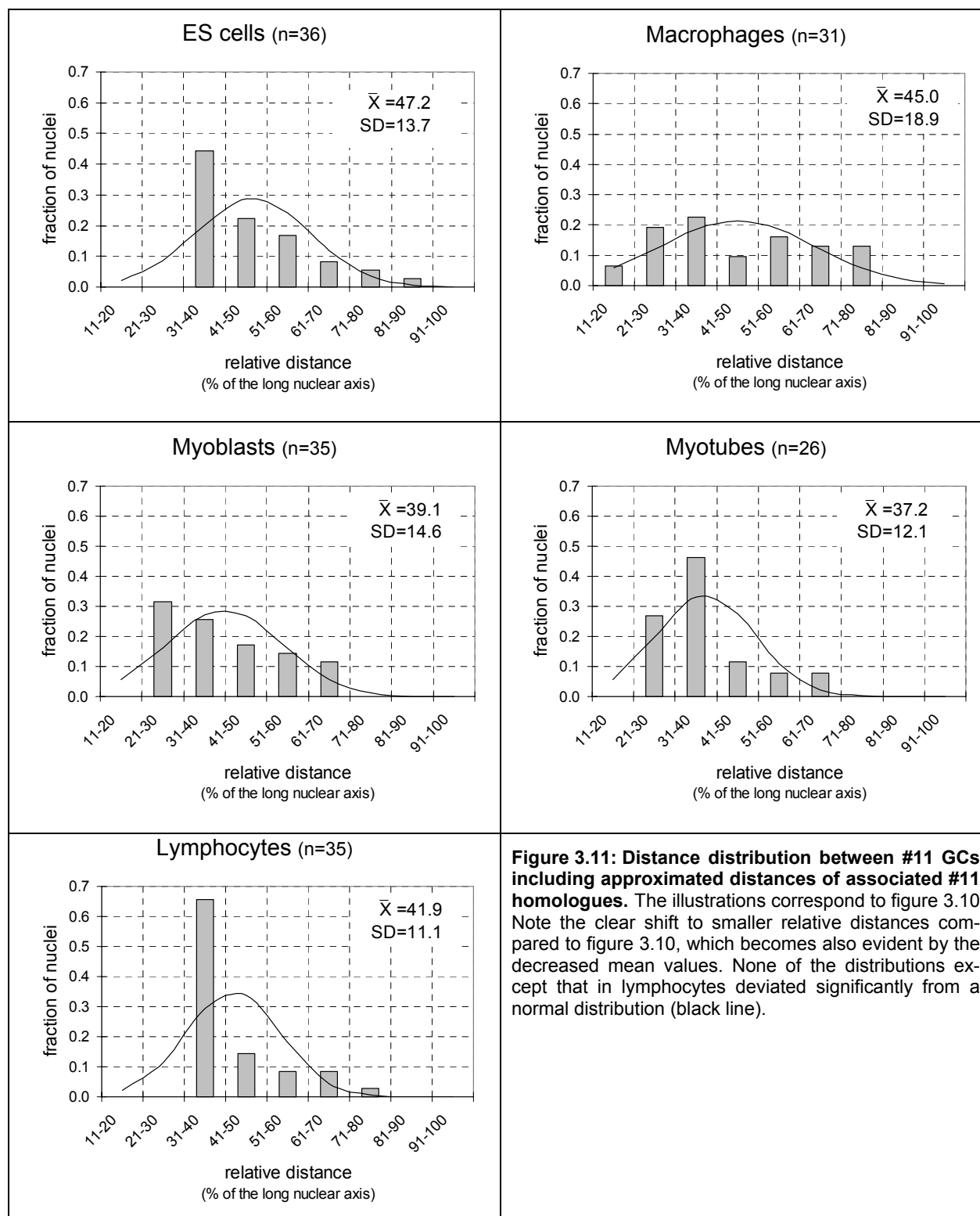


Figure 3.10: Distance distribution between #11 GCs. Graphs show the frequency of GC-GC distances that fall into one of the various distance classes. Absolute distances were normalized to the length of the long nuclear axis. Associated chromosomes are classified separately. The smallest measurable distances between GCs of non-associated homologues were 24.5% for myoblasts, 26.1% for myotubes, 30.4% for macrophages, 32.6% for lymphocytes and 36.1% in ES cells. Mean values and standard deviations (SD) refer to non-associated chromosomes only. The distance distributions of non-associated homologues did not significantly deviate from a normal distribution (black line).

In order to include nuclei showing only one coherent territory for the statistical analysis of #11 GC distances I estimated the distance between GCs of the “melted” territories by following approximation. The volume of the segmented object was divided by two, thus yielding the volume of a single territory. Assuming a perfect sphere for the territory’s shape allowed calculating the radius r of such a virtual reconstructed territory. The distance of two spheres abutting each other, i.e. being associated, can thus be described as $2r$ (see *Material and Methods* for details). The approximated relative distances of associated CTs were in the

range of the smallest distances of separated CTs or smaller. Figure 3.11 shows relative #11 GC-GC distances, similarly to figure 3.10, but this time including the approximated distances of associated #11 CTs.



If the distributions for the separated #11 CTs (figure 3.10) are compared with the corresponding ones including the approximated distances for associated #11 CTs (figure 3.11) a remarkable shift towards smaller values becomes evident, which is also reflected by a decreased mean relative distance (table 3.6). This reflects the physical proximity of the associated CTs and consequently their small values of the approximated distances. Comparing the relative distance distributions between the different cell types (two-sample KS test), revealed no significant differences, reproducing the results obtained for separated CTs. A test of goodness of fit to a normal distribution (KS test modified according to Lilliefors) revealed no significant deviations for all cell types, except for lymphocytes, which showed a clear bias toward smaller relative distances. This most probably reflects the pronounced internal location of #11CTs that was strongest in lymphocytes (see above). The broad range of measurable relative distances reflects a high variability of the relative positioning of homologous #11 CTs towards each other and argues against a fixed nuclear position of #11 CTs.

	ES cells	macrophages	myoblasts	myotubes	lymphocytes
w/o associated CTs	$\bar{x} = 57.6$ SD = 13.3	$\bar{x} = 52.6$ SD = 15.7	$\bar{x} = 44.9$ SD = 12.4	$\bar{x} = 45.1$ SD = 12.2	$\bar{x} = 50.8$ SD = 12.0
with associated CTs	$\bar{x} = 47.2$ SD = 13.7	$\bar{x} = 45.0$ SD = 18.9	$\bar{x} = 39.1$ SD = 14.6	$\bar{x} = 37.2$ SD = 12.1	$\bar{x} = 41.9$ SD = 11.1

Table 3.6: Mean relative distances and standard deviations between GCs of homologous #11 CTs. Mean values (\bar{x}) and standard deviations (SD) are given as percentages of the long nuclear axis. Note that if approximated distances of associated CTs are included the averages decrease remarkably, while the standard deviations remain almost unchanged.

Similar to distances, angles between fluorescence intensity gravity center of homologous chromosomes and the nuclear center are expected to be small with only a small variability between different nuclei if an association of homologues would be the rule. Other kinds of non-random side-by-side distributions would yield accordingly characteristic values with only small standard deviations within one population. Apart from the cases where both #11 CTs were associated (where an angle calculation was not possible), there was a great variability in measured angles. Table 3.7 summarizes the ranges of measured angles between separated #11 CTs in the various cell types.

	n	mean	range	sd
ES cells	17	118.9°	77.5° - 170.2°	27.7°
macrophages	23	129.2°	49.5° - 173.8°	40.0°
myoblasts	26	103.3°	40.0° - 172.3°	38.5°
myotubes	13	112.9°	57.3° - 147.4°	28.9°
lymphocytes	15	117.8°	74.8° - 161.0°	28.7°

Table 3.7: Angles between homologous #11 GCs.

A statistic analysis of the angle distribution (one sample KS test) revealed no significant differences to a normal distribution for all cell types and also between distributions of different cell types (two sample KS test) there were no differences of significant relevance ($p < 0.05$). These findings support the idea that there is no tendency for a specific angular position and hence for a non-random side-by-side orientation of #11 CTs.

Distances and angles between #11 and #X

Similar to homologous chromosomes the measurement of parameters like distances and angles between heterologous chromosomes can indicate deviations from a random distribution.

In case of a specific side-by-side orientation, one would expect characteristic, reproducible values and a small variability. To test this for chromosomes X and 11 I measured the relative distances between GCs of individual CTs and compared it with a normal distribution. To detect cell type specific differences the distance distributions were furthermore compared between the various investigated cell types. Accordingly, angles included by GCs of #11, #X and the nuclear centers were analyzed.

Figure 3.11 illustrates the distance distributions between #11 and #X GCs and the according normal distributions.

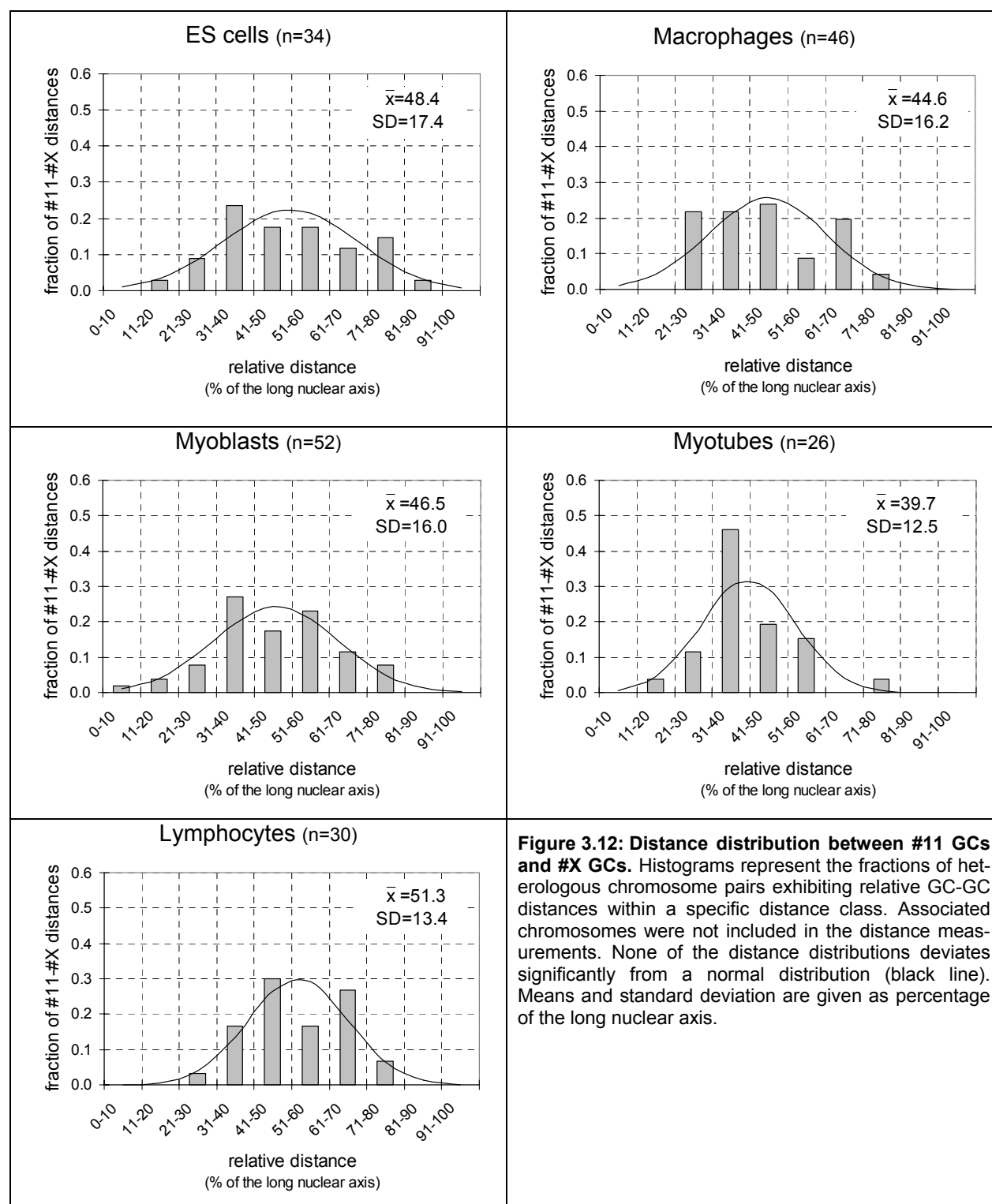


Figure 3.12: Distance distribution between #11 GCs and #X GCs. Histograms represent the fractions of heterologous chromosome pairs exhibiting relative GC-GC distances within a specific distance class. Associated chromosomes were not included in the distance measurements. None of the distance distributions deviates significantly from a normal distribution (black line). Means and standard deviation are given as percentage of the long nuclear axis.

None of the relative distance distribution showed a significant deviation from a normal distribution (KS test, modified according to Lilliefors) and the average distances were between 40% and 50% of the long nuclear axis. These findings argue clearly against a specific nuclear orientation of #X and #11 in relation to each other. Both CTs appear to localize rather randomly in respect to each other with relative distances that range from 10% to 80% of the long nuclear axis. Moreover, the relative distance distributions between #11 and #X GCs did not show any significant differences if the various cell types were compared among each other with one exception: in myotubes relative #11 - #X distances were significantly smaller than in lymphocytes.

Angles between GCs of #11, #X and the nuclear center showed a big variability with mean values around 88°-102° and high standard variations between 30° and 43° (table 3.8¹). A statistical analysis of the frequencies of angles revealed no significant deviations from a normal distribution for all analyzed cell types (KS test, modified according to Lilliefors). Moreover, the distributions did not differ significantly between different cell types (two sample KS test). Consequently #11 and #X CTs do not appear to be positioned following a specific side-by-side distribution in respect to each other.

	n	mean	range	sd
ES cells	34	91.0°	25.7° – 174.7°	39.6°
macrophages	46	101.5°	32.8° – 175.1°	41.9°
myoblasts	52	99.4°	13.5° – 176.8°	42.9°
myotubes	26	87.6°	38.7° – 161.9°	34.8°
lymphocytes	30	100.3°	37.8° – 163.0°	30.0°

Table 3.8: Angles between #11 GCs and #X GCs.

The results concerning distances and angles between #11 and #X are consistent with those between homologous chromosomes 11 and clearly support the idea of a random side-by-side orientation of CTs.

¹ Homologous chromosomes were not included in the evaluation.

3.1.6 Summary part 1:

Distribution of gene dense #11 and gene poor #X in nuclei of different mouse cell types and during differentiation

I could show that CTs of gene dense mouse #11 (15.3 genes/Mbp)¹ and gene poor mouse #X (7.4 genes/Mbp)² have a distinct radial position within the nuclei of 5 different cell types, with #11 always being localized more internally and #X more peripherally. These results are consistent with the findings in humans (Boyle et al. 2001; Cremer et al. 2001; Cremer et al. 2003), chicken (Habermann et al. 2001) and higher primates (Tanabe et al. 2002) and thus support the idea of a gene-density-related distribution of CTs as a general distributional motif of vertebrate CTs. The significance of this differential distribution in mouse showed cell type specific differences, but appeared to be independent from the cellular differentiation status.

#11 CTs showed a clear tendency to be in close proximity to each other resulting in a high proportion (25%-57%) of nuclei exhibiting associated CTs. Nevertheless, a general association of #11 CTs appears very unlikely, because in all analyzed cell types almost half or more nuclei did not show an association of homologues and exhibited distance and angle distributions that followed a normal distribution. The elevated frequency of nuclei with “fused” CTs is likely to be a consequence of the general tendency of #11 CTs to localize preferentially in the nuclear interior, where the probability that chromosomes get in contact is high due to the decreased volume.

The high variability of homologous and heterologous distances and angles do also not support the idea of a predetermined side-by-side distribution of #11 and #X CTs in the analyzed cell types, which included proliferating as well as postmitotic terminally differentiated cell types. The findings favor rather a model of random orientation of individual CTs in respect to each other.

¹ Gene density was calculated from the chromosome size and number of annotated genes from the *Ensembl* database (<http://www.ensembl.org>). Last update: July 2003. Note that the values from other databases (e.g. NCBI) can diverge. (see also *discussion*).

3.2 Organization of pericentric heterochromatin (chromocenters) in different mouse cell types and during terminal differentiation

Pericentric heterochromatin in mouse forms a very prominent nuclear compartment, which consists of a variable number of big heterochromatic blocks called chromocenters. These can be readily visualized using AT-selective fluorescent DNA staining dyes like DAPI, Hoechst 33258 or TO-PRO 3. Pericentric regions consist of large arrays of tandemly repeated 234bp long major satellite sequences that add up to ~10% of the mouse genome (Mitchell 1996). Centric or centromeric sites are strictly speaking sites where the actual centromere/kinetochore is thought to reside and are usually made up by the minor satellite sequence, which lies between the major satellite repeat and telomeric sequences. While major satellite sequences were estimated to span between 6-17Mb/chromosome, minor satellite repeats are usually thought to be between 250 and 500kb long (Garagna et al. 2002). In the following “centromeric” is used in a more general meaning including centromeric and pericentric regions, i.e. major and minor satellites. In the present thesis, I performed 3D FISH using a major satellite specific DNA probe to visualize pericentric heterochromatin in 6 different mouse cell types including fibroblasts, lymphocytes and two *in vitro* differentiation systems: ES cells/macrophages and myoblasts/myotubes (figure 3.13). In order to assess cell type specific and/or differentiation related arrangements of chromocenters the number of clusters as well as the intranuclear distribution was investigated.

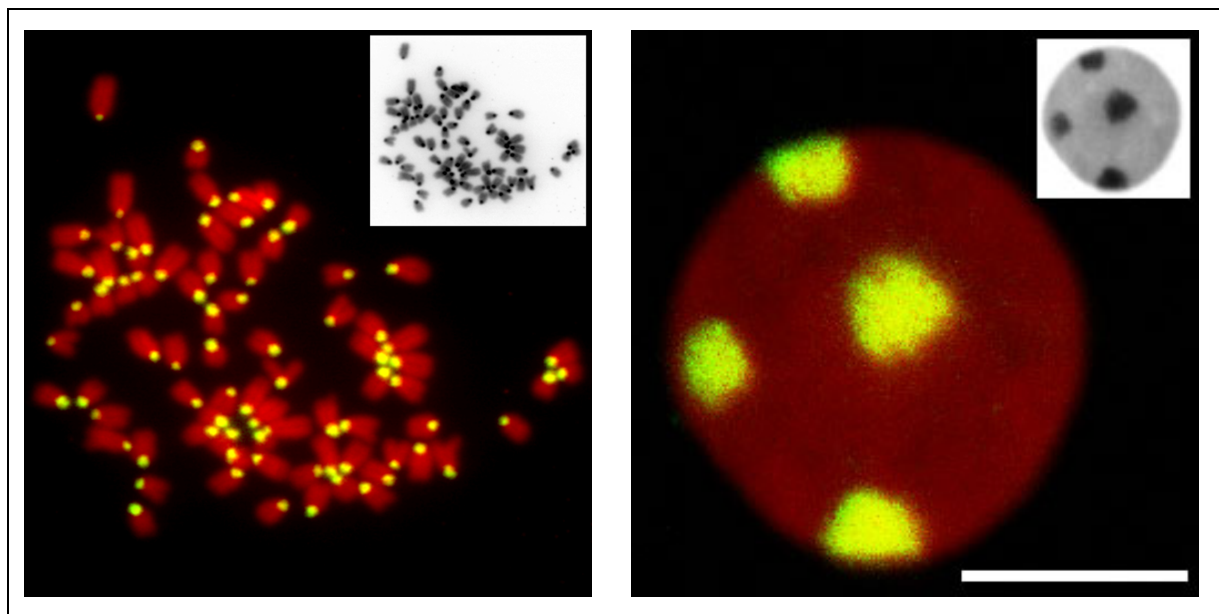
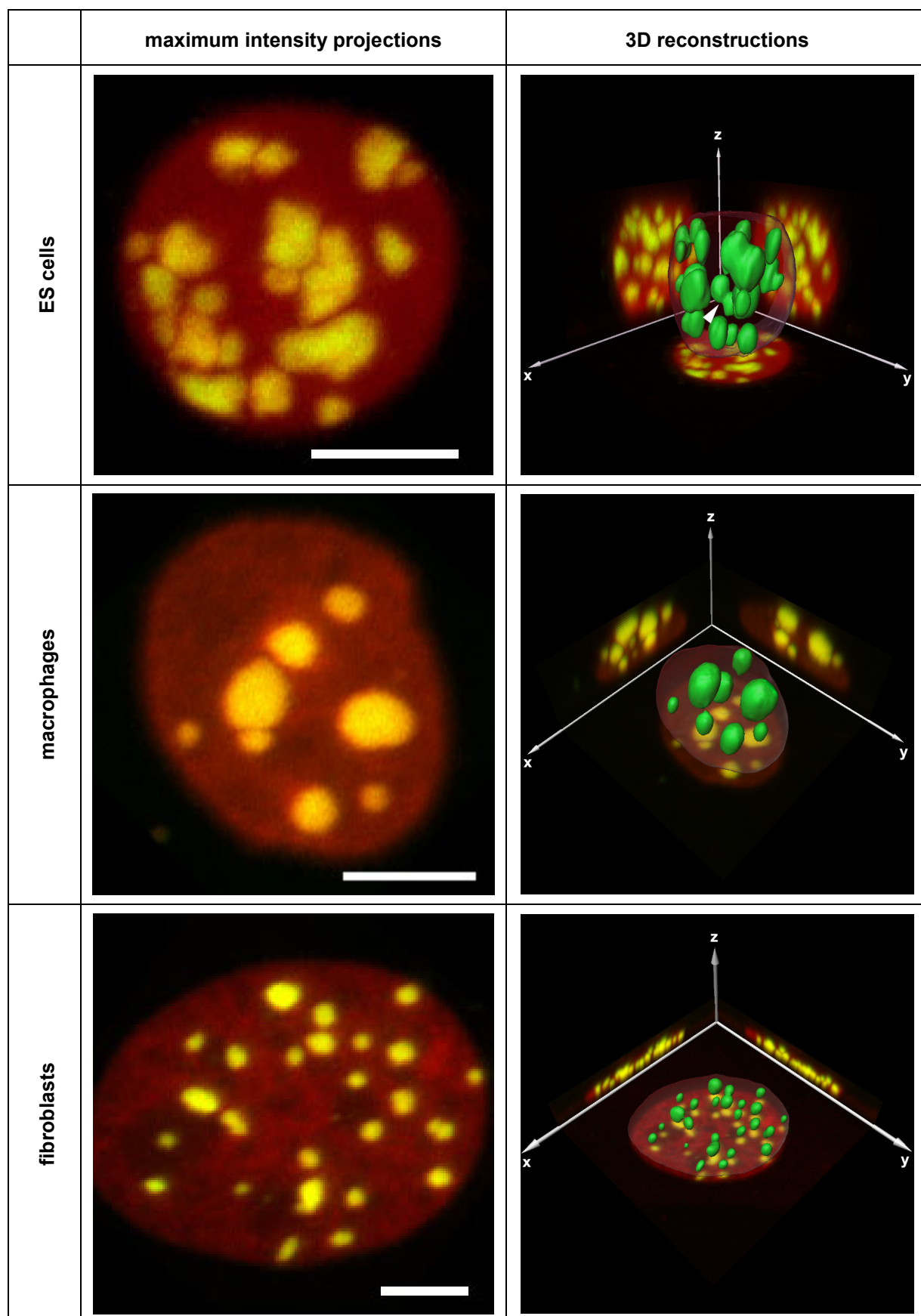


Figure 3.13: Major satellite in mouse mitotic chromosomes and in a lymphocyte nucleus. The DNA probe was labeled with Cy3-dUTP. The small inset shows the corresponding inverted DAPI (left) and TO-PRO 3 staining (right) respectively; note that pericentric heterochromatin appears as intensely stained regions. Note also that the mitotic chromosomes are all acro-/telocentric. The right panel shows a mid-confocal section of a lymphocyte nucleus. Pericentric heterochromatin is organized as big, mostly peripheral cluster. Scale bar: 5µm.

3.2.1 Number of chromocenters

The number of chromocenters was determined using unprocessed confocal image stacks, which could be analyzed in all three dimensions by the “Zeiss Image Browser” software” (for details see *Materials and methods*). Chromocenters were often spherical or ellipsoid and could be easily discriminated from one another, so that the counting procedure was straightforward. Sometimes pericentric heterochromatin was also arranged as irregular structures especially in ES cells. Such structures were often reminiscent of two or more chromocenters

just caught in the act of a fusion process. In figure 3.14, typical examples for each analyzed cell types are presented as maximum intensity projections and as 3D-reconstructions.



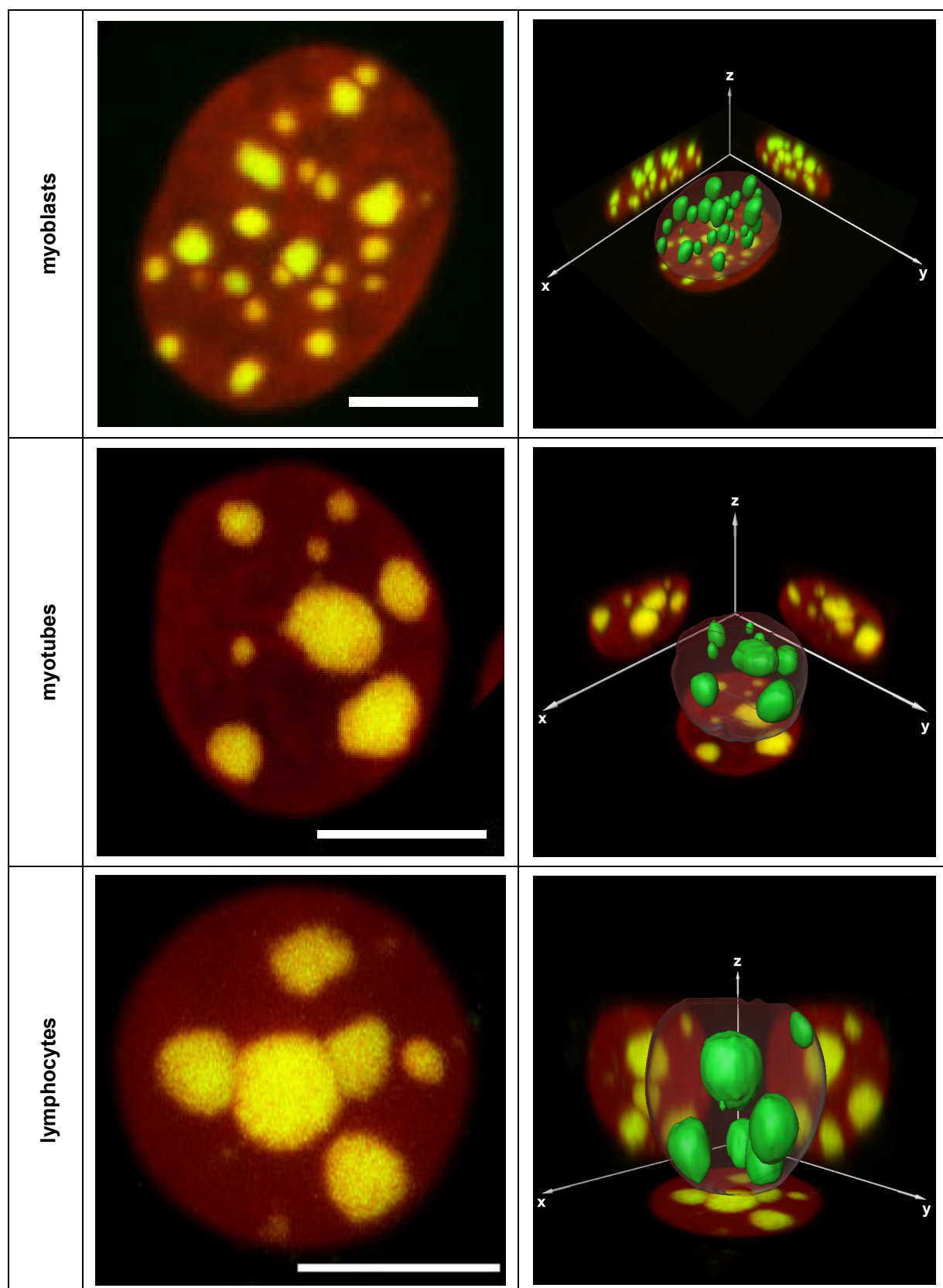


Figure 3.14: Maximum intensity projections and 3D-reconstructions illustrating typical examples of chromocenter arrangements in different mouse cell types. The left column illustrates false colored maximum intensity projections of confocal microscopic serial sections. Pericentric heterochromatin was visualized by 3D FISH using a major satellite specific probe. Major satellite FISH signals are shown in green, but appear yellowish since chromocenters are also intensely stained by the DNA counterstaining TO-PRO 3 shown in red, merging to a strong yellow color. Note the striking differences in number and size of chromocenters in different cell types, especially during differentiation of ES cells to macrophage and of myoblasts to myotubes. Scale bars represent 5 μ m. The right column shows a 3D overview of the nuclei presented in the left column, illustrating xy, xz and yz maximum intensity projections in the background and a 3D-reconstruction in front. Chromocenters are shown as solid green structures, while the nuclear counterstain is presented as a transparent shell. In ES cells chromocenters sometimes appeared to be interconnected as if two or more had just fused together (arrowhead) (see text); in some cases with many involved chromocenters network-like structures could be observed. Note that 3D-reconstructions of different cell types are not presented in the same scale.

The number of chromocenters in each nucleus was assigned to one of eight classes, which had a class width of 5 chromocenters (figure 3.15). Although in all analyzed cell types I found a high variability in the number of discernable chromocenters the distributions appeared to be cell type specific and differentiation related. If the histograms shown in figure 3.15 are compared between the different cell types, it appears that during differentiation of ES cell to macrophages and of myoblast to myotubes, the distribution shifts towards smaller values, while the variability of observed chromocenters decreases. This is also represented by the smaller averages. Moreover, if cycling fibroblasts are compared with non-cycling G0 lymphocytes a similar effect can be seen. In fact as the number of chromocenters between these cell types were compared statistically using a Kolmogoroff Smirnov test, they turned out to be highly significant (ES cells vs. macrophages: $p < 0.01$, myoblasts vs. myotubes: $p < 0.001$ and fibroblasts vs. lymphocytes: $p < 0.001$; for details concerning the evaluation see 2.11).

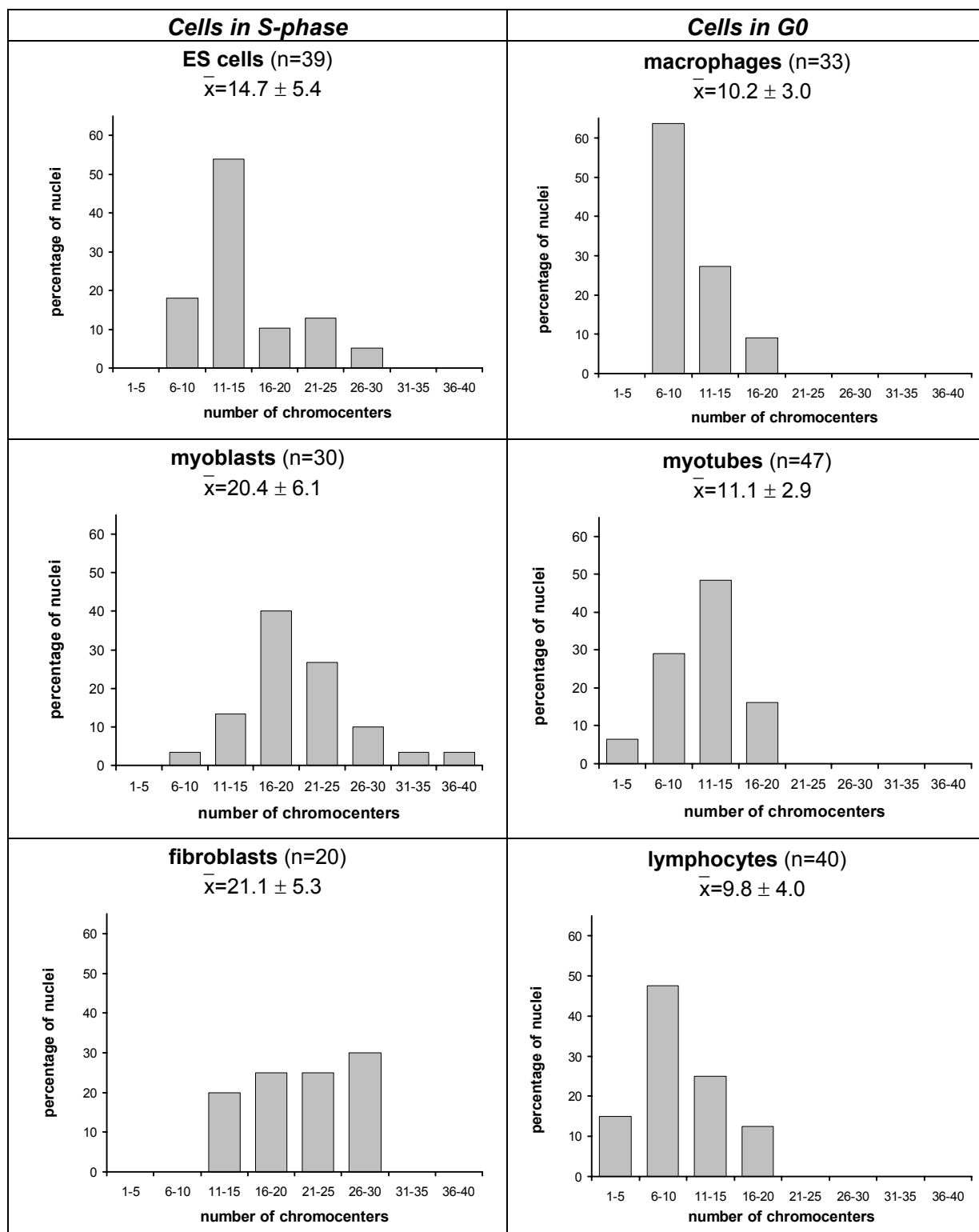


Figure 3.15: Chromocenter numbers in different cell types. Note that all cell types in the left row were cycling cells, more precisely S- phase cells, while cell types on the right were in G₀. n is the number of analyzed nuclei, while \bar{x} gives the average number of chromocenters \pm the standard deviation. It should be noticed that during differentiation of ES cells to macrophages and of myoblasts to myotubes the distributions shift to the left towards smaller values, while also the variability apparently decreases. If fibroblasts and lymphocytes are compared this trend appears to be generally applicable for S-phase cells vs. G₀ cells.

In order to test if the cell cycle exit was responsible for the observed increase in chromocenter clustering I compared the number of chromocenters between cycling (S-phase) fibroblasts and quiescent fibroblasts, which had been induced to exit the cell cycle by serum starvation. Figure 3.16 illustrates the chromocenter number distributions in S-phase fibroblasts versus non-cycling G0 cell. Although there was a decrease in the mean number of chromocenters as indicated by the increase of the class “16-20” and a decline of the class “26-30”, the difference was not significant ($p>0.2$)¹. This means that cell cycle exit occurring during terminal differentiation of ES cells and myoblasts does most probably not account for the observed extent of clustering during differentiation, although it might contribute to it.

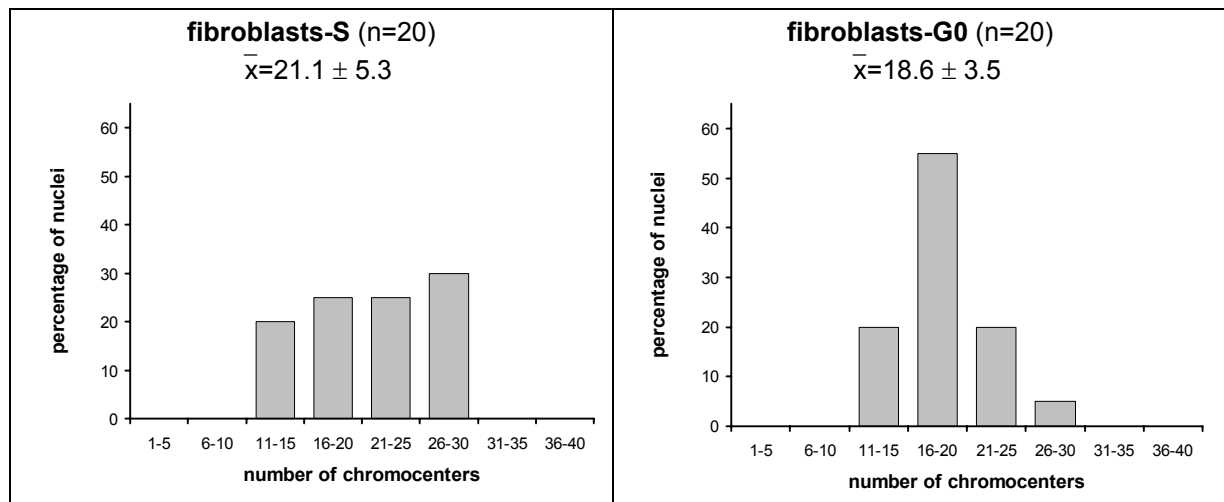


Figure 3.16: Chromocenter numbers in cycling vs. quiescent fibroblasts. Although there seems to be some decrease in the number of chromocenters, as illustrated by the percentage of nuclei in the class 16-20, which is almost doubled, the mean number of chromocenters is not changed substantially. In fact the statistical analysis did not reveal a significant difference between both cell cycle stages ($p>0.2$).

In order to elucidate at which point during differentiation the clustering of chromocenters takes place, I investigated cells at intermediate differentiation stages. In the cases of macrophage differentiation, I determined the chromocenter number of cells that were morphologically identical to G0 macrophages and were likewise positive for the macrophage marker Cd11b, but which had gone through S-phase in the 24h prior to fixation, as revealed by incorporation of BrdU that had been added to the medium accordingly. Such cells were assumed to be cycling or at least to have exit the cell cycle later than cells, which had not incorporated BrdU. Surprisingly such “immature” macrophages did not show a substantial decrease in the number of chromocenters compared to ES cells; in fact the average number was the same and the distribution showed only a slight trend towards smaller values (figure 3.17). The statistical analysis did accordingly not show a significant difference between these “immature” macrophages and ES cells ($p>0.2$), while the difference between both macrophage subsets was highly significant ($p<0.001$). This finding argues that the major part of chromocenter clustering that is observed during differentiation of ES cells to macrophages takes place in a post mitotic stage, whilst in cells in which the differentiation process is fairly advanced the number of chromocenters remains high.

¹ It should be kept in mind that the presentation of the data using classes can be misleading, as the actual number of signals can be on both extremes of the class width. Most reliable for the comparison of chromocenter numbers are the cumulative frequency curves, which were also used for the statistical evaluation as they are not based on classes, but instead consider the number of chromocenters of each nucleus individually (see 2.11).

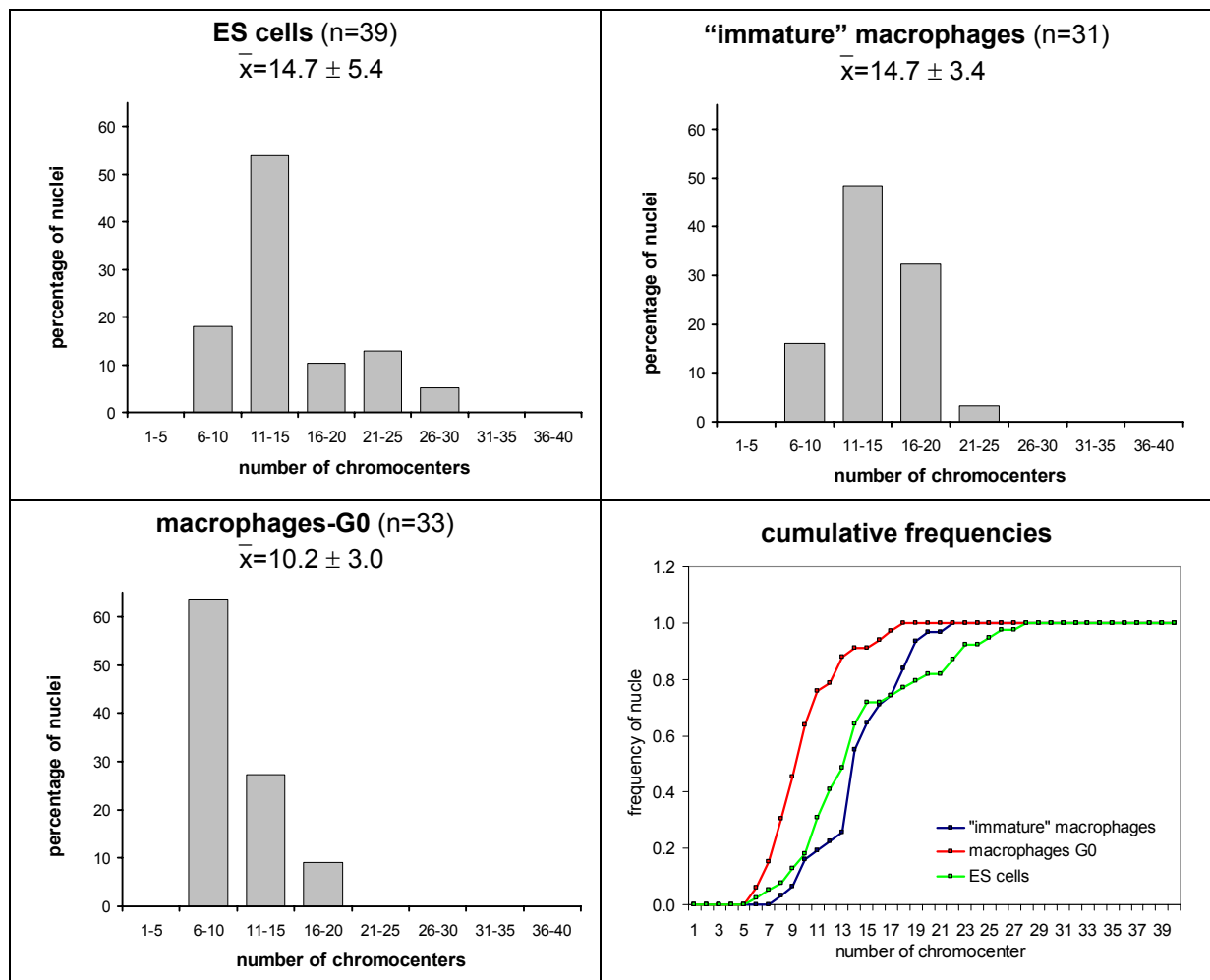
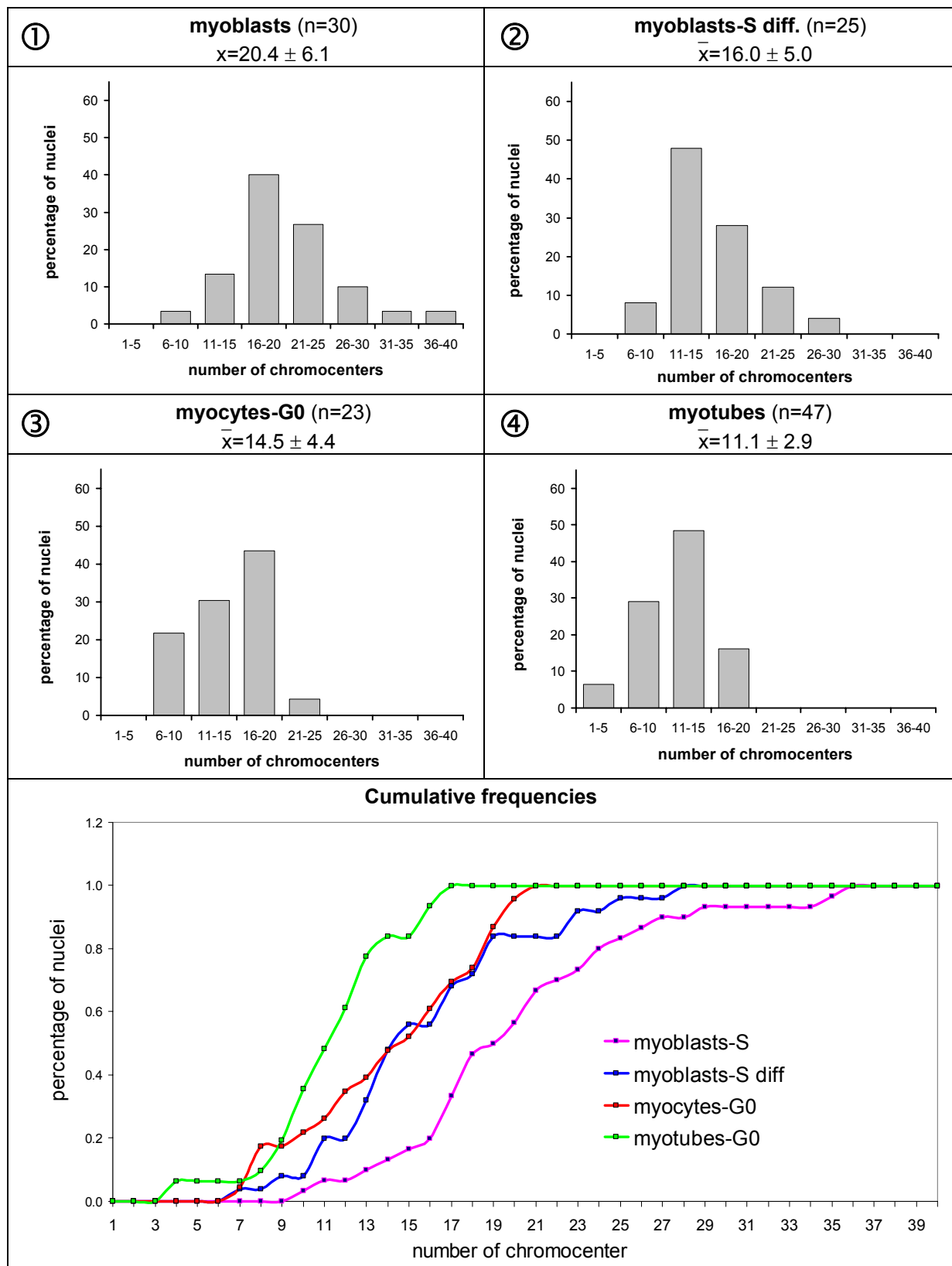


Figure 3.17: Chromocenter number during differentiation of ES cells to macrophages. The histograms indicate a slight decrease in the number of chromocenters between ES cells and "immature" macrophages, as the class 26-30 disappears completely and the class 21-15 decreases in favor of an increase in the class 16-20. However, from the cumulative frequencies it becomes evident that ES cells and "immature" macrophages are apparently not as different as both are from G0 macrophages.

In the course of myogenesis I determined additionally the number of chromocenters of postmitotic but non-fused myoblasts, which can be assumed to represent myocytes, i.e. cells which are committed to fuse and to build myotubes but haven't yet. Moreover, I looked at myoblast cells that were still cycling after being grown for 4 days in differentiation medium, in order to test whether such cells would already show an increased chromocenter clustering. Figure 3.18 summarizes the clustering behavior of pericentric heterochromatin during the presumed progression of myogenic differentiation.

Figure 3.18: Chromocenter number during myogenic differentiation. Encircled numbers indicate the assumed progression of myogenic differentiation. The histograms illustrate the stepwise decrease in the chromocenter number from myoblasts over differentiating but still cycling myoblasts to myocytes and finally myotubes. This gradual decline is mirrored in the average chromocenter number of the various cell types and in the according standard deviations indicating also a stepwise decrease in variability. The cumulative frequencies mirror this observation and illustrate comprehensibly the results of the statistical analysis, which showed a significant decrease in numbers of clusters from myoblasts to differentiating but still cycling myoblasts (myoblasts-S diff.; $p < 0.05$) as well as to myocytes ($p < 0.05$). Myoblasts-S diff. and myocytes were not significantly different, while the comparison between myoblasts-S diff. and myotubes showed a significant decrease ($p < 0.01$), just as the transition from myocytes to myotubes ($p < 0.05$).



As visible from the mean number of chromocenters as well as from the histograms, the increase in clustering of pericentric heterochromatin during myogenic differentiation appeared to take place stepwise. The statistical analysis of the data revealed a first significant decrease in the number of chromocenters between undifferentiated proliferating myoblasts and S-

phase myoblasts ($p < 0.05$), which had been growing 4 days in differentiation medium (myoblasts-S diff.). This means that clustering of chromocenters starts upon the differentiation cue placed by the medium change although the cells are still not postmitotic. In fact such differentiating but proliferating myoblasts were not significantly different from postmitotic G0 myocytes as far as their chromocenter number is concerned ($p > 0.2$). After myocytes had fused thereby forming polynucleated myotubes there was a second significant decrease in the number of pericentric heterochromatin clusters ($p < 0.05$), which finally led to the number of chromocenters that were initially observed in myotube nuclei.

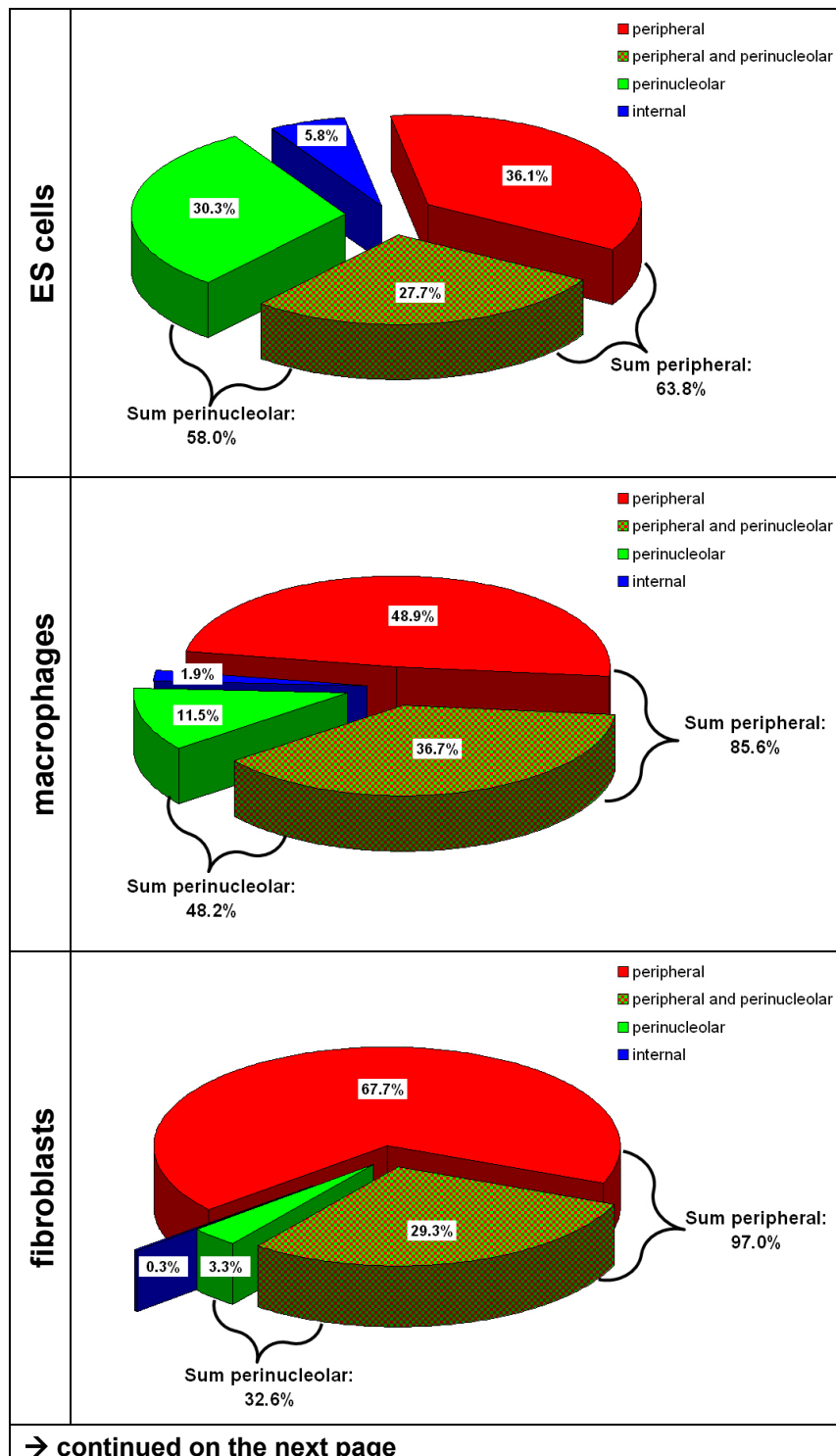
Taken together these results show that there is a cell type specific organization of pericentric heterochromatin in mouse regarding the number and as a consequence, the size of pericentric heterochromatin clusters (chromocenters). These chromocenters tended to cluster upon cellular differentiation, thereby reducing the number of clusters and simultaneously increasing their size. The timing of clustering appeared to be stepwise in the case of myogenic differentiation, with a first clustering “wave” upon induction of differentiation, while cells were still cycling. After cell cycle exit only a slight but not significant decline of chromocenter number was observable, while after fusion of postmitotic myocytes and formation of polynucleated myotubes a second “wave” of clustering led to a further significant reduction of chromocenters. At the end in myotube nuclei the initial number of clusters in myoblasts is reduced to almost half of it.

During differentiation of ES cells to macrophages the main clustering of chromocenters appears to happen after cell cycle exit and thus in the postmitotic cell. On the other hand it can not be ruled that macrophage progenitor cells might have an increased number of chromocenters compared to ES cells, so that a multi-step reduction similar as that during myogenesis might account for clustering in macrophages as well. Indeed such a differentiation dependent increase in the number of chromocenters is indirectly suggested by the present data, since the number of chromocenters in fibroblasts ($\bar{x} = 21.1$) and myoblasts ($\bar{x} = 20.4$) was significantly higher than that in stem cells ($\bar{x} = 14.7$) in spite having a more differentiated status (fibroblasts: $p < 0.001$; myoblasts: $p < 0.01$).

3.2.2 Intranuclear distribution

In addition to the number also the intranuclear distribution of chromocenters was investigated as a parameter to assess the nuclear architecture of pericentric heterochromatin during cellular differentiation. This task was addressed by two different approaches. In the first approach the intranuclear distribution of individual chromocenters was determined. For this purpose each chromocenter in each individual nucleus was categorized as either (a) peripheral, if it abutted the nuclear rim, (b) perinucleolar, if it abutted a nucleolus, (c) peripheral and perinucleolar, if a chromocenter had contact to both the nuclear periphery and a nucleolus or (d) internal, if it resided in the nuclear interior and hence neither (a), (b) or (c) were applicable. Thus, this first method takes into consideration each individual chromocenter and categorizes it according to nuclear landmarks, but does not answer the question how the bulk of heterochromatin is distributed within the nucleus. This task was achieved applying a second approach, where the radial distribution of pericentric heterochromatin was analyzed using the same evaluation software as described for the radial distribution analysis of chromosome territories (see 2.12.1). This latter method described the radial distribution of pericentric heterochromatin as one coherent nuclear compartment.

Intranuclear distribution of chromocenters



The categorization of individual chromocenters was performed by analyzing unmodified, i.e. raw confocal image stacks with the “Zeiss Image Browser” software, which allowed an overview of the data set by three dimensional sectioning. (see 2.11). Since nucleoli were only identified by DNA counterstaining it is possible that this class was underestimated since smaller nucleoli might not have been detected. Accordingly, the internal class might be overestimated by an “internal” classification of signals that were actually “perinucleolar”. In figure 3.19, the results of the classifications are presented as percentages of chromocenters in the respective category. Figure 3.20 recapitulates these results but considers additionally the average number of chromocenters in the respective cell type. One distributional motif all cell types had in common was that the majority of chromocenters was found abutting the nuclear periphery. The lowest percentage of peripherally localized chromocenters was found in ES cells equaling 63.8%, but accounted for 77.5% in myotubes, 85.6% in macrophages and was greater than 90% in lymphocytes (95.1%), myoblasts (95.9%) and fibroblasts (97%). This preferential localization of chromocenters at the nuclear periphery together with a generally high percentage of chromocenters found at nucleoli (15.9%-58%) is consistent with the well-accepted view of an increased concentration of heterochromatin at the nuclear edge and around nucleoli (see e.g. (Comings 1980)).

erally localized chromocenters was found in ES cells equaling 63.8%, but accounted for 77.5% in myotubes, 85.6% in macrophages and was greater than 90% in lymphocytes (95.1%), myoblasts (95.9%) and fibroblasts (97%). This preferential localization of chromocenters at the nuclear periphery together with a generally high percentage of chromocenters found at nucleoli (15.9%-58%) is consistent with the well-accepted view of an increased concentration of heterochromatin at the nuclear edge and around nucleoli (see e.g. (Comings 1980)).

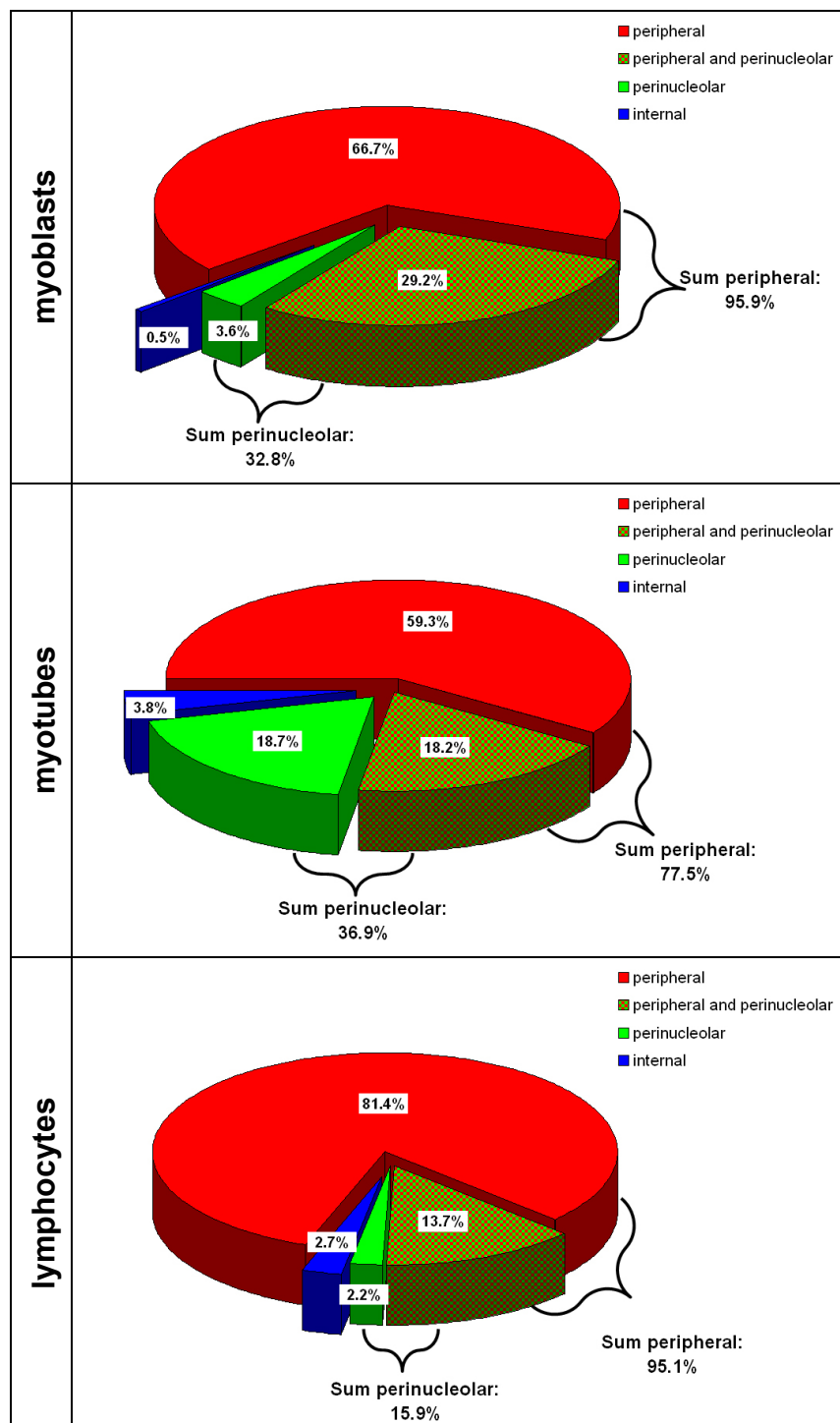


Figure 3.19: Intranuclear distribution of chromocenters. The disk segments represent the percentages of chromocenters in the respective intranuclear localization classes. Note that the “peripheral” class contains chromocenters that were exclusively at the periphery, while the “nucleolar” class contains only such found exclusively at a nucleolus. Consequently, these classes have to be joined with the “peripheral and perinucleolar” class, in order to address all “peripheral” or all “perinucleolar” chromocenters.

of chromocenters were found at nucleoli. This variability suggests a possible correlation to functional differences between the various cell types if e.g. translational activity is considered (see *discussion*).

In fact if “peripheral”, “perinucleolar” and “peripheral and perinucleolar” signals are summarized they make up between 94.2% and 99.7% of all signals.

Accordingly, only a small percentage of chromocenters were found internally, i.e. without apparent contacts to the nucleolus or the nuclear rim. The highest percentage was observed in ES cells, reaching 5.8%, while in myotubes only 3.8% and in lymphocytes only 2.7% were found in an interior nuclear compartment. The lowest levels of internal signals were found in macrophages (1.9%), myoblasts (0.5%) and fibroblasts (0.3%). The flat shape of these nuclei that increases the possibility of a chromocenter to abut the nuclear top or bottom (see table 3.4) could explain this.

The percentages of perinucleolar signals showed quite a high variability between different cell types. The maximum was observed in ES cells with 58% followed by macrophages (48.2%). Myotubes (36.9%), myoblasts (32.8%) and fibroblasts (32.6%) exhibited similar percentages while in lymphocytes only 15%

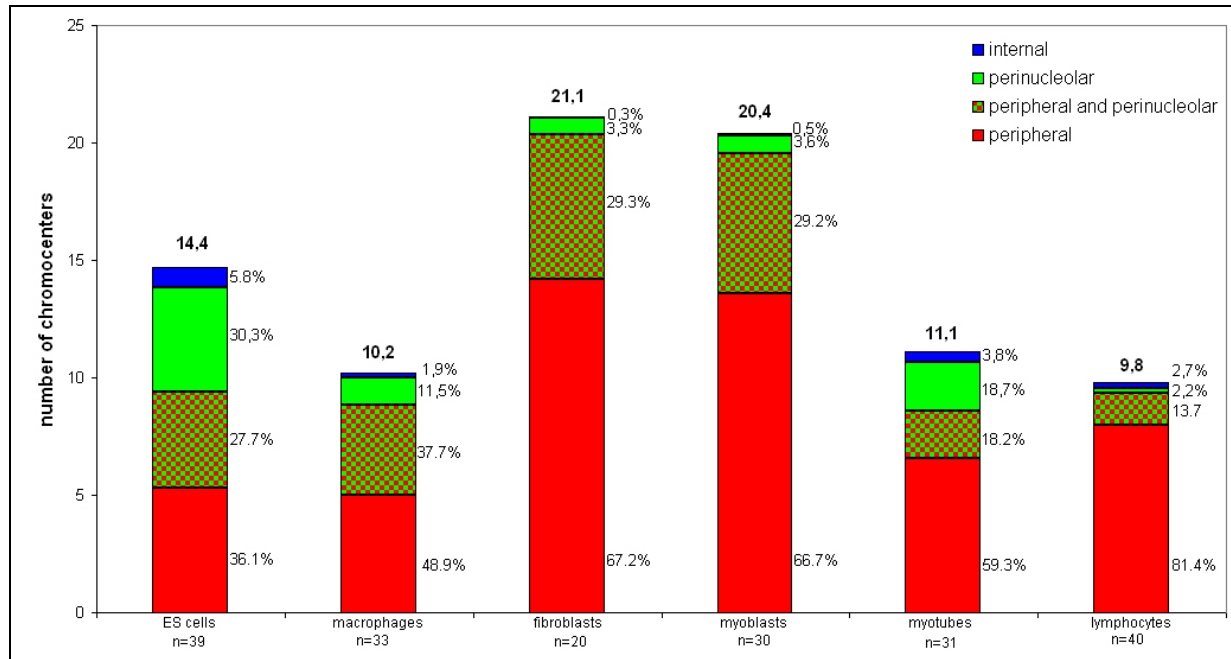


Figure 3.20: Average chromocenter number and intranuclear distribution of chromocenters. The height of the columns represents the average chromocenter number in the according cell type. The column segments representing the percentages of chromocenters in the respective categories are proportional to the chromocenter number and can therefore not be compared directly between cell types. Percentage values of chromocenters in the respective classes are given on the right of the column segments.

During differentiation of ES cells to macrophages, the total percentage of peripheral signals increased from 63.8% to 85.6%, while the total percentage of perinucleolar chromocenters decreased from 58% to 48.2%. Especially the fraction of exclusively perinucleolar signals decreased from 30.3% to 11.5%, while in contrast the fraction of “perinucleolar and peripheral” signals increased from 27.7% to 36.7%. This could be explained by a “relocation” of chromocenters, which in ES cell had been exclusively at a nucleolus to additionally touch the periphery in macrophages. Still this would not explain the net decrease of perinucleolar signals. Most probable an additional change of chromocenter positions from the nucleoli, but also from the interior compartment to the periphery must have taken place, which could explain the decrease of perinucleolar signals (58% to 48.2%) and internal signals (5.8% to 1.9%) as well as the increase of peripheral chromocenters (63.8% to 85.6%). How much of this reorganization is due to changes of the nuclear shape or to functional aspects remains to be elucidated. An argument for an implication of the nuclear shape is provided by the results during myogenic differentiation. Here the flat shaped nuclei in myoblasts were reshaped during formation of myotubes resulting in a cylindrical nucleus with a round cross section (table 3.4); hence the nuclear shape changes just in opposite to the ES cell differentiation, where a spherical nucleus was reshaped to an ellipsoid. As expected if the nuclear shape would drive the observed reorganization, the total percentage of peripheral chromocenters decreased from 95.9% in myoblasts to 77.5% in myotubes, just in opposite to the ES cell differentiation. Moreover, the total percentage of perinucleolar signals increased from 32.8% to 36.9%, which was mainly due to an increase of exclusively perinucleolar signals (3.6% to 18.7%). This also clearly mirrors the situation for the transition of ES cells to macrophages but again in the opposite direction. Similarly, the fraction of internal signals increased in myotubes compared to myoblasts (0.5% to 3.8%), while in macrophages it decreased compared to stem cells. Summing up these parallels (or rather anti-parallels) between both differentiation pathways argue against a differentiation related reorganization of chromocenter, and for the involvement of nuclear shape.

It should be considered that this particular approach to assess the intranuclear distribution of individual chromocenters did not take into account the variable size of chromocenters. This means that the localization of a big signal containing a large amount of chromatin had the same impact on the percentage distributions as a very tiny signal, which in an extreme case can contain pericentric heterochromatin of only one chromosome. Additionally the variable number and size of chromocenters found in different cell types or during differentiation might influence the geometrical constraints concerning the intranuclear distribution of chromocenters to an unknown extent. Therefore, these findings can only represent a coarse outline of the intranuclear distribution of pericentric heterochromatin. This in mind the relevant results of this approach can be summarized as follows.

The findings argue for a majority of chromocenters being positioned at the nuclear periphery, with only a very small percentage localizing in the nuclear interior without apparent associations with the nuclear edge or a nucleolus. Moreover, there was a high fraction of chromocenters associated with nucleoli, which was noticeably different between the various cell types. Since it was not known which of these perinucleolar cluster actually included NOR bearing chromosomes a correlation of this distributional variability with translational activity can only be speculative (see *discussion*).

In order to describe the radial distribution of pericentric heterochromatin as a consistent nuclear compartment instead of individual chromocenters the data set was additionally analyzed using the evaluation software that had been used to analyze the radial distribution of chromosome territories (see above).

Intranuclear distribution of pericentric heterochromatin

As already mentioned the data set used was the same as that for determining the number of chromocenters (3.2.1) and their intranuclear distribution (3.2.2.1). As delineated in detail in 2.12.1 the 3D-RRD software determines the relative radial distribution of segmented objects by describing the relative DNA content as a function of the relative distance from the nuclear center. In contrast to the first approach, which revealed the relative location of each individual chromocenter to specific nuclear landmarks such as the nuclear border or a nucleolus, using the 3D-RRD software allowed to measure the relative distance distribution of the complete pericentric heterochromatin compartment as visualized by the FISH signal using the major satellite specific probe. Figure 3.19 shows the relative radial distance plots for the various cell types.

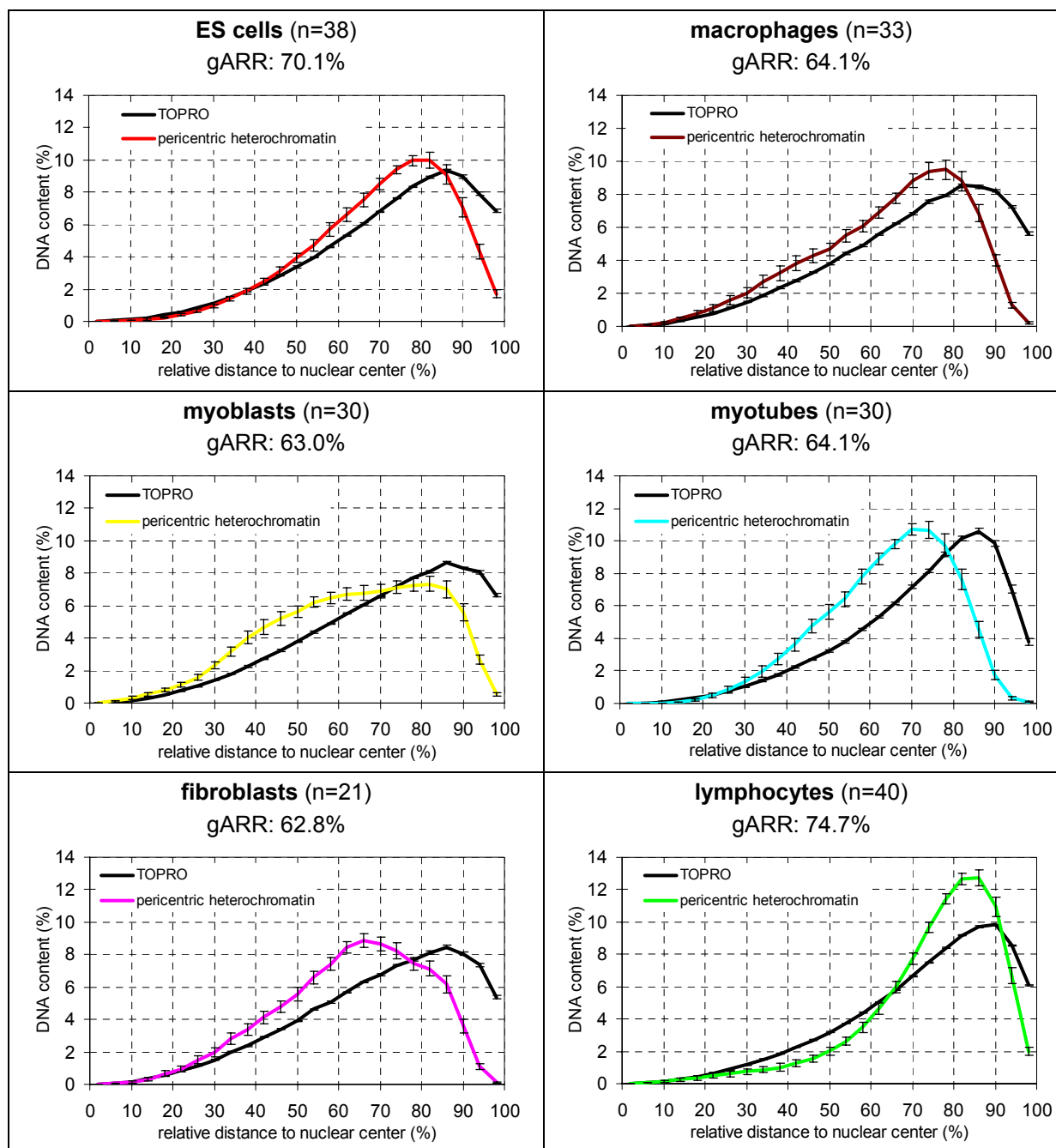


Figure 3.21: Radial distribution of pericentric heterochromatin in different mouse cell types. On the abscissa, the relative distance from the nuclear center is plotted, while the ordinate represents the relative DNA content. The black curve denotes the TO-PRO 3 counterstain (for an explanation concerning the decline of counterstained DNA at the very periphery see figure 3.3). Error bars correspond to the standard error of the mean. Note the increasing peripheral distribution of pericentric heterochromatin from fibroblasts < myoblasts < myotubes/macrophages < ES cells < lymphocytes, as also indicated by the increasing global average relative radius (gARR).

The distribution graphs disclose a noticeable difference between the radial organizations of pericentric heterochromatin in the various cell types. As exemplified by the global average relative radii (gARRs; see 2.12.1) the most peripheral orientation was found in lymphocytes (74.7%) followed by ES cells (70.1%), while in macrophages, myotubes, myoblasts and fibroblasts the gARRs were all around 63%-64% of the relative nuclear radius. This gradual decrease in peripheral localization becomes even clearer if the distribution data is plotted as cumulative curves as illustrated in figure 3.22.

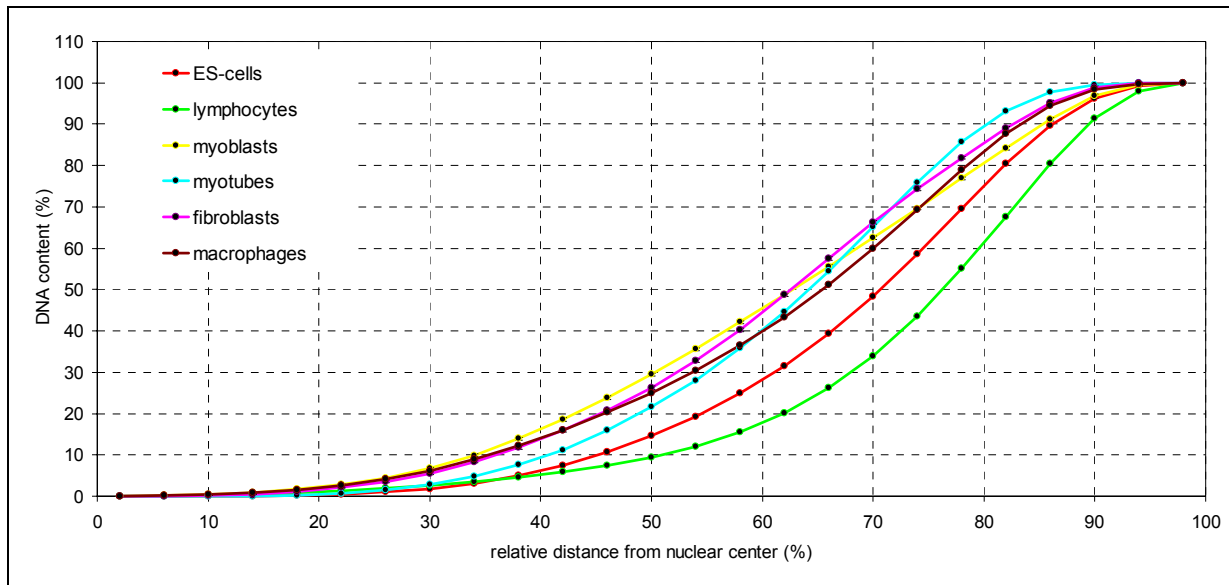


Figure 3.22: Radial distribution of pericentric heterochromatin as cumulative plots. The percentage DNA content at the 25 discrete distances from the nuclear centers, i.e. within each of the 25 shells is added with the DNA content of the more internal shells so that a cumulative plot is generated reaching 100% of the labeled DNA in the most distant shell. Note that lymphocytes and ES cells are shifted markedly to the right, which reflects a bigger percentage of signals in outer shells, while the curves for the other cell types appear to be similar.

When the radial distributions of the different cell types were compared among each other using a two sided Kolmogoroff Smirnov test, none of the comparisons resulted in a significant difference. Nevertheless the p-values (probability values that two compared distributions are falsely classified different although they are actually the same) for the comparisons including lymphocytes were apparently smaller and almost reached the significance level (table 3.9). This was not unexpected, since lymphocytes exhibited the most peripheral distribution of pericentric heterochromatin. Accordingly, the p-value for the comparison of lymphocytes with ES cells, which showed the second outermost distribution, was high again.

	macrophages	myoblasts	myotubes	fibroblasts	lymphocytes
ES cells	p>0.2	p>0.2	p>0.2	p>0.2	p>0.2
macrophages	-	p>0.2	p>0.2	p>0.2	p=0.17
myoblasts	-	-	p>0.2	p>0.2	p=0.1
myotubes	-	-	-	p>0.2	p=0.056
fibroblasts	-	-	-	-	p=0.11

Table 3.9:p-values comparing the radial distributions of pericentric heterochromatin. The p-values indicate no significant differences between the radial distributions of major satellite DNA between all different cell types. However, the somewhat reduced p-values for the comparisons highlighted in yellow suggest a bigger difference between those cell types. All these pairs included lymphocytes, which showed the most peripheral distribution of pericentric heterochromatin (as reflected in the cumulative plot, as well as by the highest gARR value).

As already noted above (see the chapter 3.1.3 on the radial distribution of CTs), the applied statistical approach is very stringent, especially if subtle differences are to be detected in combination with a moderate sample size. Therefore, I performed an additional, less strict approach, testing the radial distributions of iARRs of pericentric heterochromatin instead of the radial distribution of the complete stained subcompartment. As described in detail in 2.12.1, the iARR of the major satellite signal was calculated for each nucleus of the sample, and from these values a new radial distribution was created, whereas pericentric hetero-

chromatin of each individual nucleus is represented by only one value: the iARR. These iARR distributions were finally compared between different cell types using a two-sample KS test (the difficulty of choosing the appropriate statistical test approach is discussed in 4.1.1 *Evaluation methods*). This less stringent statistical comparison revealed significant differences between several of the compared cell types (table 3.9).

	macrophages	myoblasts	myotubes	fibroblasts	lymphocytes
ES cells	p<0.05*	p<0.05*	p=0.12	p<0.05*	p<0.01**
macrophages	-	p>0.2	p>0.2	p>0.1	p<0.001**
myoblasts	-	-	p>0.2	p>0.2	p<0.001**
myotubes	-	-	-	p>0.2	p<0.001**
fibroblasts	-	-	-	-	p<0.001**

Table 3.10: p-values comparing the radial distributions of pericentric heterochromatin iARRs. The p-values for the comparisons including lymphocytes, are among the most significant ones (except ES vs. lymphocytes), which recapitulates the smaller p-values found for these pairs using the stricter approach. Moreover, ES cells, which exhibited the second outermost distribution of pericentric heterochromatin, were significantly different to all other cell types but myotubes. * denotes significant, ** denotes highly significant deviations between compared radial distributions.

Interestingly this test method confirmed to some extent the outcome of the stricter approach, in that the distribution between lymphocytes and other cell types which by the stricter approach were suggested to be more different (because of the smaller p-values), were among the most significant ones using this less stringent approach. Apart from comparisons including lymphocytes, only such including ES cells leaped the significance level. Furthermore, by using this approach a significant difference was also detected between the radial distributions of lymphocytes and ES cells. All the results from this statistical analysis are properly reflected in the respective curve progressions shown in figure 3.20. The cumulative distribution graphs are clearly distinct between lymphocytes and ES cells, as well as between each of those and the other cell types, while the curves of macrophages, fibroblasts, myoblasts and myotubes are fairly intermingling, showing virtually no difference at all.

It is striking that cells with the most spherical nuclei like ES cells and lymphocytes exhibited the outermost distribution, while flat shaped nuclei (table 3.4) correlated rather with a more internal localization. However, myotube nuclei, which have a cylindrical shape and a round cross-section (table 3.4) seem to be exceptional, in the sense that they also exhibited a rather internal localization of major satellite DNA. Terminal differentiation did not appear to have a significant effect on the radial arrangement of pericentric heterochromatin during myogenesis but a difference was observable between ES cells and macrophages. However, since all cell types having a flatter shaped nucleus exhibited the tendency for a more internal localization of pericentric heterochromatin, (it this) did also account for the situation in macrophages.

It should be noticed from the distribution plots in figure 3.19 that at the very edge of the nucleus there seems to be nearly no pericentric heterochromatin. Even if it is assumed that the “real” nuclear border is at the peak of the counterstain graph (see figure 3.2 for a suggested explanation), the total concentration of major satellite sequence at the periphery is still relatively low. A possible reason therefor is that pericentric heterochromatin is mostly arranged as spherical or ellipsoid chromocenters, which as a matter of geometrical constraints can only contact the nuclear border in a tangent like fashion, so that the biggest part of such a peripherally located sphere/ellipsoid is actually located more towards the interior. Besides, it is known from replication labeling experiments that chromatin directly underneath the nuclear envelope comprises mainly mid replicating G dark chromatin, while later replicating constitu-

tive heterochromatin like centromeric regions are found in bigger cluster at the periphery but also around nucleoli and in interior compartments (Sadoni et al. 1999).

In conclusion, the radial distribution of pericentric heterochromatin appears to be arranged in a cell type specific fashion. The most central localization was found in macrophages, fibroblasts, myoblasts and myotubes, which all exhibited a similar distribution. A markedly more peripheral arrangement was found in ES cells, which was further exceeded in lymphocytes, in which it showed the outermost localization. The very edge of the nucleus appears to contain only moderate amounts of pericentric heterochromatin.

3.2.3 Summary part 2:

Organization of pericentric heterochromatin in different mouse cell types and during differentiation

The number of pericentric heterochromatin clusters (chromocenters) was found to be cell type specific. During terminal differentiation of ES cells to macrophages and of myoblasts to myotubes, the number of chromocenters decreased significantly, while the size of clusters increased accordingly. During myogenic differentiation this clustering process occurred stepwise, with a first round after the differentiation stimulus (differentiation medium) prior to cell cycle exit and a second round after fusion of postmitotic myocytes and formation of polynucleated myotubes. The majority of chromocenters was localized right at the nuclear edge (63%-97%). A variable percentage of chromocenters was either additionally (14%-37%) or exclusively (3%-30%) abutting a nucleolus. This perinucleolar fraction (16%-58%) differed between cell types. Only a minor part of chromocenters exhibited an interior position, i.e. was neither associated with the nuclear border nor with a nucleolus (0.5%-6%). During differentiation of ES cells and myoblasts, a spatial reorganization of chromocenters was observed, but since it was in opposite directions, I conclude that rather nuclear shape than differentiation accounted for the observed changes. The radial distribution of pericentric heterochromatin as one coherent entity showed cell type specific differences; the most peripheral localization was found in lymphocytes (gARR: 75%) followed by ES cells (70%), while macrophages, myotubes, myoblast and fibroblasts showed a similar substantially more internal localization (63%-64%). During myogenic differentiation no significant change in the radial distribution of pericentric heterochromatin was observable. During differentiation of ES cells to macrophages a shift to the interior was registered, which is most probably due to the flat shaped nucleus, since a more central location of pericentric heterochromatin was found reproducibly in all cell types with flat nuclei.

3.3 The role of MeCP2 in the reorganization of pericentric heterochromatin

In order to detect factors involved in the increase of chromocenter clustering during differentiation I focused on the methylated DNA binding protein MeCP2 (methyl-CpG-binding protein 2) for several reasons. First of all MeCP2, which has been shown to act as a transcriptional repressor (Nan et al. 1997) localizes mainly in pericentric heterochromatin foci of mouse nuclei (Lewis et al. 1992). Moreover mutations in the MeCP2 gene cause RETT syndrome in humans (Amir et al. 1999), a neurodevelopmental disorder, where MeCP2 is thought to be involved in the pathophysiology by affecting neuronal maturation and differentiation (reviewed in (Shahbazian and Zoghbi 2002; Ausio et al. 2003; Jellinger 2003; Kriaucionis and Bird 2003)). A further indication for an involvement of MeCP2 in differentiation processes comes from the finding that non differentiating mouse ES cells lacking functional MeCP2 do not show any proliferation deficiencies, while chimerical embryos consisting of a high propor-

tion of such mutant ES cells show severe developmental defects (Tate et al. 1996). Furthermore several recent studies have shown that MeCP2 expression increases during neuronal differentiation in humans (LaSalle et al. 2001), rats (Jung et al. 2003) and mice (Cohen et al. 2003). All the findings, which strongly suggest an implication of MeCP2 in cellular differentiation plus the fact that it is mainly located at pericentric sites made it an optimal candidate to test its potential involvement in the phenomenon of chromocenter clustering during terminal differentiation.

All the experiments concerning MeCP2 were performed in collaboration with the group of Cristina Cardoso from the Max-Delbrück-Center in Berlin.

First, I investigated whether MeCP2 levels would increase during mouse myogenic differentiation and thus be correlated with the observed aggregation of chromocenters. Therefore I compared endogenous MeCP2 levels in Pmi28 myoblasts with those in myotubes.

3.3.1 Expression of endogenous MeCP2 increases during myogenesis

The endogenous MeCP2 levels were assessed by immunofluorescence using specific antibodies. In order to exclude differences due to a variable detection efficiency in the different cell types I co-detected the ubiquitously expressed nucleolar protein B23 (nucleophosmin) as a positive control.

As visible from the fluorescence images in figure 3.22 A, MeCP2 expression was substantially different between myoblast and myotube cultures. Most of the myoblasts showed no detectable MeCP2 signals while the majority of myotube nuclei exhibited the characteristic intense staining at pericentric heterochromatin clusters (figure 3.23 D). A noticeable fraction of non-fused cells, presumably myocytes, also showed MeCP2 staining. To quantify this variability in MeCP2 expression I determined the percentages of myoblast, myocyte and myotube nuclei that stained positive for MeCP2. To avoid false negatives, only nuclei that showed staining for the nucleolar protein B23 were included. The results are summarized in the histogram shown in figure 3.23 C. In myoblast cultures only 10.9% of the analyzed cells exhibited the typical MeCP2 pattern, while in myotubes almost all nuclei (99.1%) showed MeCP2 staining (figure 3.23 A, C). In myocytes (non-fused cells in differentiated cultures) 75% showed detectable MeCP2 levels at chromocenters, suggesting that MeCP2 expression increases gradually during differentiation and starts already before myotube formation. A very faint fluorescence, homogeneously distributed throughout the nucleus was visible in cells, which were characterized as negative, but was also present at non-chromocentric sites in positive cells (figure 3.22 B). Therefore, it appears not very probable that the intense staining at pericentric sites in positive cells was a consequence of a relocation of dispersed MeCP2 molecules to chromocenters. Nevertheless, I cannot rule out the possibility that there is a pool of MeCP2 molecules that is not localized at chromocenters, both in undifferentiated myoblasts as well as in myotubes.

The increase of MeCP2 expression during myogenesis was corroborated by the group of Cristina Cardoso applying a western blot approach (Figure 2E). The net increase in protein concentration argues clearly against a mere relocation of the protein during myogenesis, but shows convincingly an increase in protein expression.

Since MeCP2 is known to bind selectively to methylated CpGs I investigated the methylation level in myoblasts and myotubes using antibodies against methylated cytosines. Intensive staining of pericentric heterochromatin was observed in an increasing percentage of nuclei from myoblasts (23.6%) over myocytes (54.5%) to myotubes (70.2%) (figure 2F), thus clearly paralleling MeCP2 expression levels. The somewhat lower percentages of nuclei exhibiting the chromocentric pattern for methylated cytosines, compared to MeCP2 could be due to a lower detection efficiency of the applied antibodies.

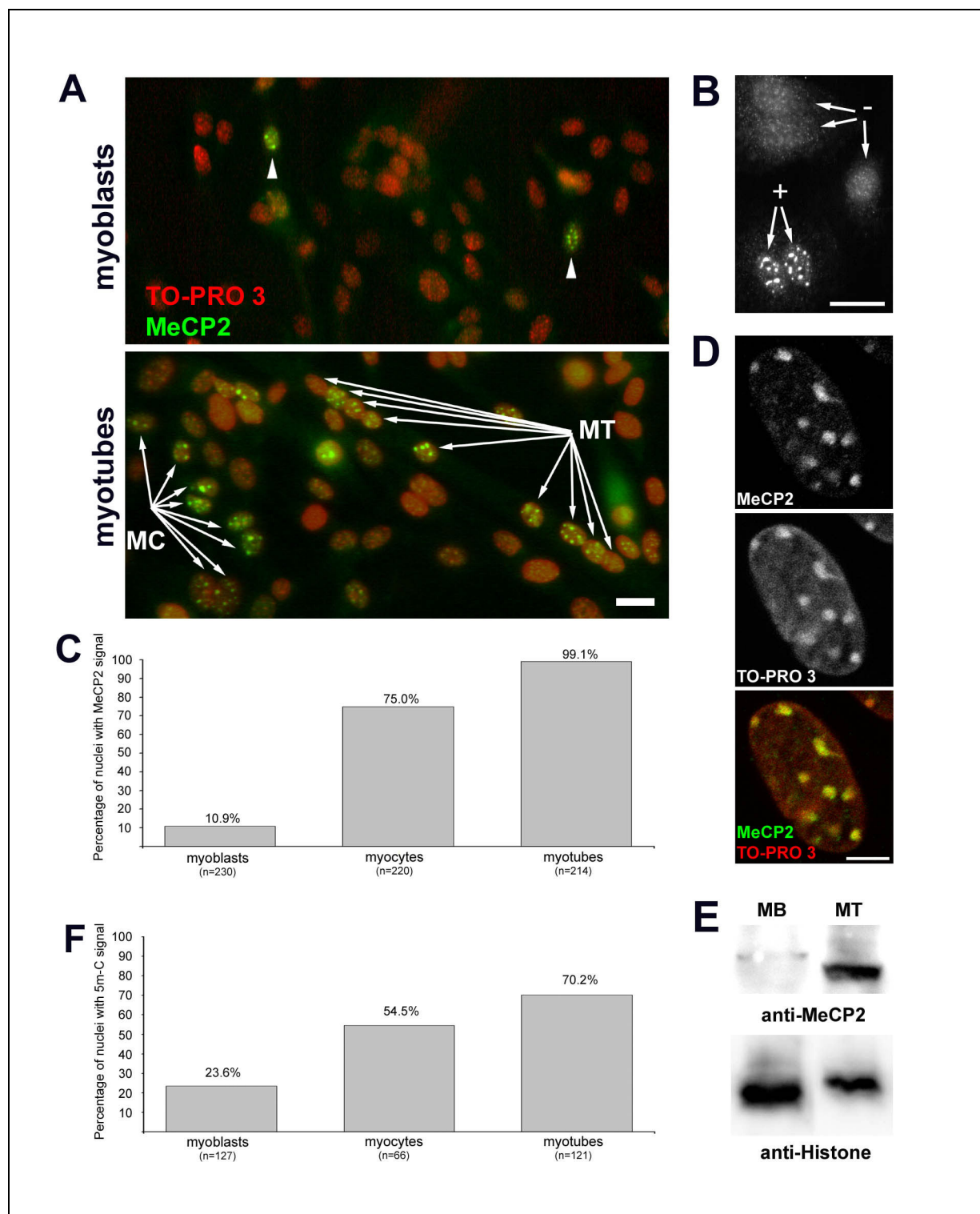


Figure 3.23: Expression of MeCP2 increases during terminal differentiation of myoblasts and is paralleled by an increased methylation of pericentric DNA. Undifferentiated and differentiated Pmi28 myoblast cultures were immunolabeled for MeCP2 (green) and counterstained with TO-PRO 3 (red). Panels in (A) show 2 equally sized areas of an undifferentiated myoblast culture (upper) and a culture, 3 days after induction of differentiation (lower). While in the myoblast culture, only two cells show MeCP2 staining (arrowheads), in the differentiated culture many myocyte (MC) and almost all myotube nuclei (MT) are stained (arrows). Scale bar: 20µm. For quantification, more than 200 myoblast, myocyte and myotube nuclei were scored for detectable MeCP2 signals. Scoring was performed by visual inspection of the fluorescent signal using epifluorescent microscopy. Figure B exemplifies scoring on five myocyte nuclei: three nuclei show only a faint homogenous staining (see text) but lack the chromocentric staining pattern (-), while two exhibit the typically bright staining of pericentric clusters (+) (see also D). Scale bar: 20µm. (C) The histogram summarizes the quantification results of detectable MeCP2 signals in myoblast, myocytes and myotubes. MeCP2 detection was lowest in myoblasts, with only 10.9% of all nuclei, while in myocytes already 75% revealed the characteristic MeCP2 pattern. The highest percentage of MeCP2 labeled nuclei was found in myotube nuclei, where it reached more than 99%. (D) The images recapitulate that MeCP2 (green) localizes mainly at pericentric heterochromatin clusters, which are demarcated by an in-tense TO-PRO 3 staining (red). The images display a myocyte nucleus. Scale bar: 5µm. (E) Western blot analysis comparing endogenous protein levels of MeCP2 in C2C12 myoblasts versus differentiated cells 3d after induction of differentiation with a high level of myotube formation. This result confirms the increase of MeCP2 expression during myogenic differentiation as suggested by the immunofluorescence analysis. Histone staining (H1-H4) was used for equal protein loading. (F) DNA methylation during myogenic differentiation was assessed using antibodies against 5-methyl-cytosine. Scoring was performed as for MeCP2. Similar to MeCP2, nuclei with intensely stained pericentric heterochromatin clusters were observed at a higher frequency in myotubes (70.2%), followed by myocytes (54.5%) and only in a minority in myoblasts (23.6%).

In conclusion, the observed clustering of chromocenters during myogenic differentiation clearly correlated with the expression levels of the methylated DNA binding protein MeCP2. The inevitable question following this finding was whether this correlation was causally connected to the phenomenon of chromocenter clustering or whether it was just a concomitant phenomenon.

3.3.2 Correlation of MeCP2 expression and increased heterochromatin clustering

In order to address this question I transiently transfected myoblasts with an expression vector coding for MeCP2 fused to the yellow fluorescent protein (YFP) and investigated whether levels of ectopically expressed MeCP2 correlated with the number of chromocenters. This approach should answer the question, whether a high expression level of MeCP2 would cause an increased clustering of chromocenters in myoblasts, even in the absence of differentiation. Using MeCP2 tagged with a fluorescent protein allowed to quantify expression levels by measuring relative fluorescence intensities, and permitted an observation of transfected cells *in vivo* by living cell microscopy.

Pmi28 myoblasts¹ were transfected with an MeCP2-YFP expression vector and fixed after expression of the fusion protein was detectable, usually 12-16 after transfection. 86 nuclei exhibiting different expression levels of MeCP2-YFP were imaged by confocal microscopy, keeping all imaging parameter constant in order to compare fluorescence intensities between different cells. After additional fixation pretreatments, 3D-FISH was performed with a major satellite specific probe to visualize chromocenters. Nuclei, which had been imaged for MeCP2-YFP expression, could be relocated since cultivation of myoblasts was run on etched coverslips with 500 alphanumeric squares. Figure 3.24 A, shows two examples of nuclei with either a very low expression level of MeCP2-YFP or with a very high expression. Visual

¹ Note that for transfection experiments the same cell strain was used as for the determination of chromocenter numbers during myogenic differentiation and for the analysis of endogenous MeCP2 levels (Pmi28 myoblasts), so that it was possible to compare the data from the diverse experiments.

inspection clearly showed an inverse correlation between the expression level of MeCP2-YFP and the number of chromocenters.

To quantify this correlation and to test it for significance, the number of chromocenters was plotted against the measured mean fluorescence intensity of MeCP2-YFP (see 2.12.3 for details) resulting in a function of chromocenter number against MeCP2-YFP fluorescence. Subsequently a Pearson correlation analysis was performed on the data set¹. Figure 3.24 B shows the respective plot with the mean fluorescence intensities arranged on the abscissa and the chromocenter numbers on the ordinate. The plot illustrates how the number of chromocenters decreases with increasing MeCP2-YFP expression. The correlation analysis revealed a significant ($p < 0.01$, two sided t-test) negative correlation with a correlation coefficient of -0.52 . The equation for the regression line was determined as $f(x) = -0.04 * x + 19.41$. As visible from the plot, the variability of the observable number of chromocenters decreased with increasing MeCP2-YFP expression.

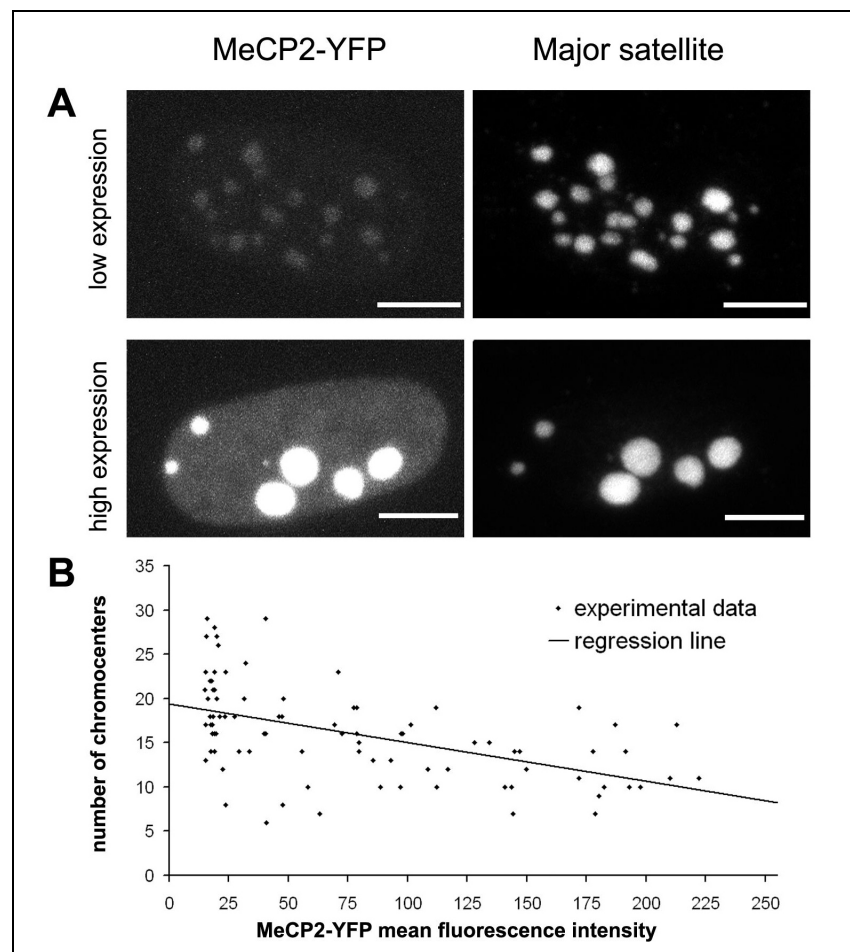


Figure 3.24: High MeCP2-YFP levels induce clustering of pericentric heterochromatin. (A) The images on the left represent maximum intensity projections from confocal image stacks of mouse Pmi28 myoblasts expressing different levels of MeCP2-YFP. Both nuclei were imaged using the same imaging settings. Images on the right show the same nuclei after staining of pericentric heterochromatin by 3D FISH. The cell expressing high amounts of the fusion protein exhibits fewer bigger chromocenters compared to that with a low expression of MeCP2-YFP. Scale bar: 5 μ m. (B) The graph illustrates the relation between mean MeCP2-YFP fluorescence and the number of chromocenters. According to a Pearson correlation analysis the parameters were negatively correlated with a correlation coefficient of -0.52 . Applying a two sided t test demonstrated that the correlation was significant with $p < 0.01$. The linear equation for the regression line was calculated as $f(x) = -0.04 * x + 19.41$.

The same was noticed during clustering of chromocenters at myogenic differentiation and during ES cell differentiation (figure 3.14). Control transfections with YFP alone had no effect on the clustering of chromocenters. High expression levels of MeCP2 fused to either GFP or DsRed instead of YFP resulted in the same clustering effect².

Taken together the result shows that increased clustering of pericentric heterochromatin can be artificially induced by ectopic expression of MeCP2 in the absence of differentiation. This

¹ A significant correlation ($p < 0.01$) was also found using the non parametric Spearman correlation analysis yielding a correlation coefficient of -0.57 .

² These control experiments were carried out by the group of Cristina Cardoso.

implies that the increased expression of endogenous MeCP2 during terminal differentiation (figure 3.22) must be directly involved in inducing the aggregation of chromocenters observed during myogenic differentiation (see 3.2.1).

In order to assess to what extent high levels of MeCP2-YFP expression had affected the physiological status of transfected cells, I tested if myoblasts expressing high levels of the fusion protein could still be induced to differentiate into myotubes. A positive outcome of this experiment would have also affirmed that the observed clustering of chromocenters by ectopic MeCP2 expression did not represent a completely artificial situation but was comparable to the genuine clustering observed during myogenic differentiation.

3.3.3 Effects of MeCP2 overexpression during myoblast differentiation

To test if the differentiation potential of myoblasts would be affected by high expression levels of MeCP2-YFP, I transfected Pmi28 myoblasts using the same approach as for the correlation analysis and induced differentiation after having verified that transfected cultures contained MeCP2-YFP expressing cells. After 3 days of differentiation, cells were fixed and screened for nuclei in myotubes expressing high levels of MeCP2-YFP. Figure 3.25 shows an example of a differentiated culture with a myotube including several nuclei with high levels of MeCP2-YFP located at pericentric regions.

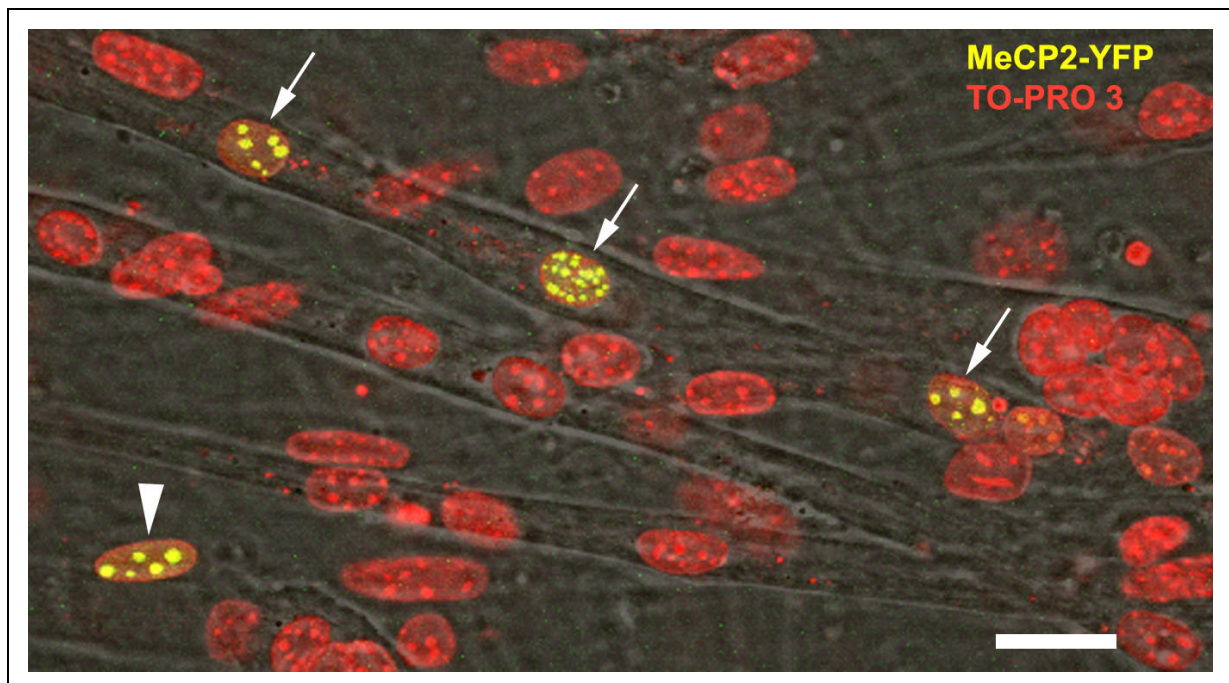
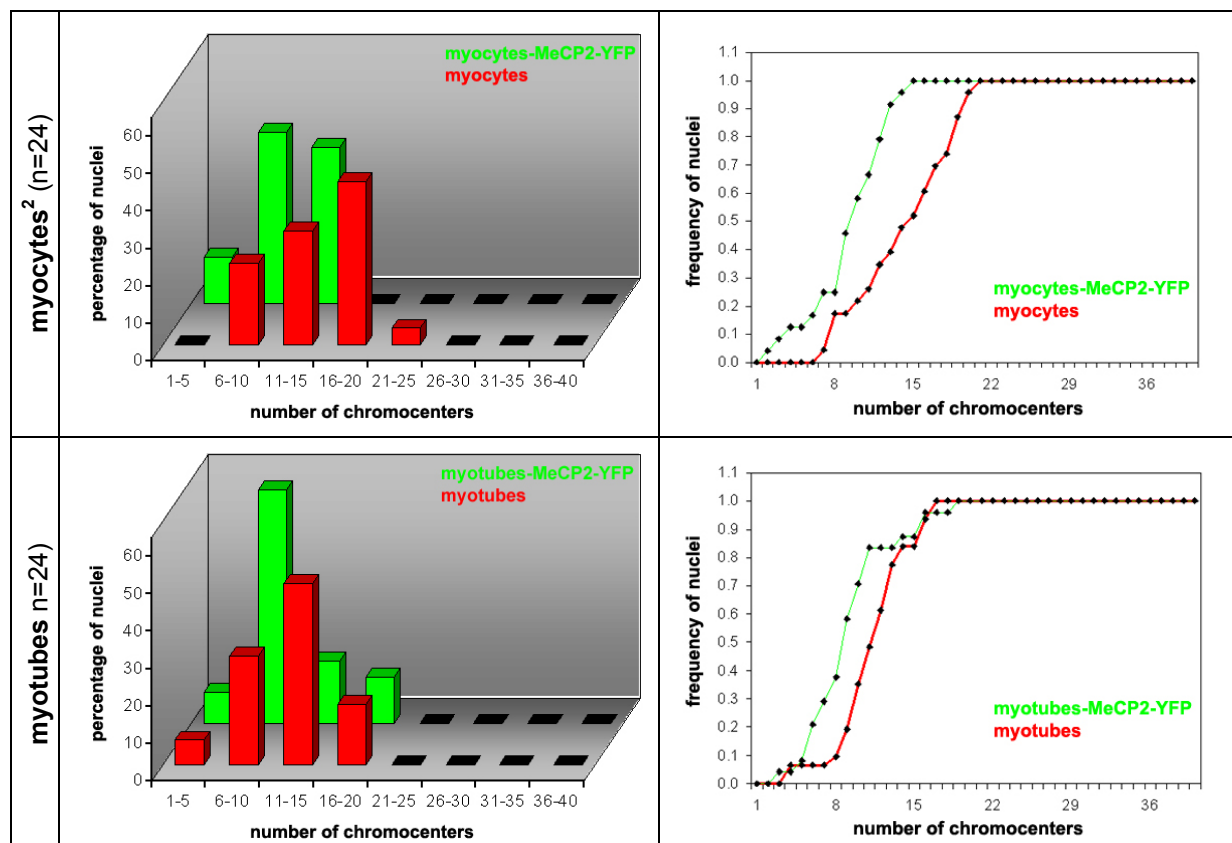


Figure 3.25: MeCP2-YFP transfected cells after induction of differentiation. Pmi 28 myoblasts were induced to differentiate approximately 14 hours after transfection with an MeCP2-YFP expression vector and fixed 3 days after induction of differentiation. Nuclei were counterstained using TO-PRO 3 (red). MeCP2-YFP is shown in green. Fluorescent signals represent maximum intensity projections of confocal image stacks, while the phase contrast image (dark gray) represents a single confocal plain outlining the progression of myotubes. Note that myotubes could contain several nuclei intensely stained by MeCP2-YFP (arrows) arguing that high MeCP2-YFP expression did not inhibit differentiation and myotube formation. Nuclei of non-fused cells, supposedly myocytes, with high concentrations of the fusion protein were also observed (arrowhead).

Since many myotube and myocyte nuclei were observed containing high levels of the fluorescent protein, it appears that a high level expression of MeCP2-YFP did not impede differentiation of myoblasts and fusion of myocytes. Although I cannot rule out that MeCP2-YFP expression in myoblasts started after some commitment steps as for example after they had

become postmitotic, expression must have taken place before fusion, otherwise all nuclei within a myotube should have contained the fusion protein, which was apparently not the case. Instead, within one myotube usually only a few or one nucleus was fluorescently labeled. The observation that MeCP2-YFP was already expressed before induction of differentiation also strongly argues that differentiated cells, be it myocytes or myotube before being committed to differentiate.

Since MeCP2-YFP expression did apparently allow myoblasts to undergo myogenic differentiation, I next asked whether clustering of chromocenters during differentiation of transfected cells was comparable to non transfected cells, or whether the increased concentration of MeCP2 by the additional, ectopic expression would lead to an enhancement of the clustering effect. For this purpose, I determined the number of chromocenters¹ in nuclei of transfected non fused cells in differentiated cultures, i.e. putative myocytes² and of transfected myotubes. Only nuclei with a high concentration of MeCP2-YFP were considered³ and compared to their non-transfected counterparts.



¹ Number of chromocenters could be determined directly through the MeCP2-YFP staining, which was possible since the staining of the analyzed cells was so bright that all chromocenters were visualized.

² It should be added that myocytes are strictly speaking committed cells, which are already postmitotic; since for transfected cells the cell cycle had not been determined they could contain a fraction of still cycling cells. However, when those transfected cells were compared to cycling cells within differentiated but non transfected cultures the difference was also significant ($p < 0.001$).

³ The choice of nuclei with a high expression of MeCP2-YFP was by visual inspection. Besides a high fluorescence intensity, non-aberrant nuclear morphology was an important criterion for the assortment in order to exclude cells exhibiting such high expression levels that they were probably about to die.

Figure 3.26: Chromocenter numbers in transfected vs. non transfected myocytes and myotubes. The histograms (left) already indicate a tendency of transfected myocyte and myotube nuclei for having a decreased amount of pericentric heterochromatin cluster. In case of myocytes, the classes including nuclei with 16-20 and 21-25 completely disappear in transfected cells, while those for a smaller number of chromocenters increase. Especially the class with very few chromocenters (1-5) contained 12.5% of nuclei in transfected cells while in non-transfected cells no nucleus was assigned to this category. For myotubes the shift towards smaller values can be seen mainly by a decrease in the class for 11-15 chromocenters and a concomitantly increase in the class 6-10. The cumulative frequencies validated this trend indicated by the histograms and accordingly a two sided KS test on the cumulative data set confirmed the observed differences as significant (myocytes: $p < 0.01$; myotubes: $p < 0.05$).

As discernible from the histograms and the cumulative frequencies in figure 3.26, the number of chromocenters in transfected cells with high concentrations of MeCP2-YFP was generally lower than that in non transfected cells. The average number of clusters in transfected myocytes was 9.6 compared 14.5 in non-transfected cells, while for myotubes it was somewhat less pronounced with 9.5 compared to 11.5. When the distributions of chromocenter numbers were compared between transfected and non transfected cells using cumulative frequencies (figure 3.26) and a two sided KS test (see 2.11 for evaluation details) the difference was confirmed to be significant (myocytes: $p < 0.01$, myotubes: $p < 0.05$). Interestingly when myocytes with high MeCP2-YFP concentrations were compared to myotube nuclei, which were also highly enriched for the fusion protein no significant difference in their chromocenter number was found. This is in contrast to the situation in non-transfected cells, where a significant decrease in the number of chromocenters was observed for the transition of myocytes to myotubes (figure 3.17). In this respect it should be noted that myotubes, which had been differentiated from transfected cells were only allowed to differentiate for 3 days while non-transfected ones had been differentiated for 4 days. Hence, it cannot be excluded that a further clustering might have taken place during a fourth day that may have resulted in a significant lower number as compared to myocytes. Another explanation could be that in transfected cultures a maximum clustering was already reached in myocytes, which in fact had a chromocenter number that was noticeably below that of non-transfected myotube nuclei (9.6 vs. 11.1).

Taken together, these results show that a high level of MeCP2-YFP does not impede terminal differentiation of myoblasts to myotubes but that it actually enhances clustering of chromocenters during myogenic differentiation. This further strengthens the hypothesis that MeCP2 is causally involved in inducing this major reorganization of pericentric heterochromatin during terminal differentiation.

3.3.4 Results of in vivo analysis of MeCP2-YFP transfected cells

After having shown, that during differentiation pericentric heterochromatin clusters merged, thereby reducing in number and increasing in size, and that this fusion could be induced by ectopic expression of MeCP2 I sought to find out at which cell cycle stage this congression would take place. The most straightforward approach was to perform an *in vivo* observation of cells expressing high levels of MeCP2-YFP. The cell cycle stage could be determined by co-transfecting cells with a fluorescently tagged version (DsRed) of the S-phase specific enzyme DNA Ligase I. S-phase cells could thus be recognized simply by the nuclear DsRed-Ligase I staining, which follows the characteristic DNA replication pattern (Nakayasu and Berezney 1989). Mitotic cells were identified by chromosome condensation and by cells rounding up, both of which could be visualized using a phase contrast mode. G1 cells were identified by a previous mitosis or by a subsequent S-phase. Accordingly, G2 cells were

characterized by a previous S-phase or a successive mitosis. Figure 3.27 shows a schematic overview for the *in vivo* cell cycle stage determination.

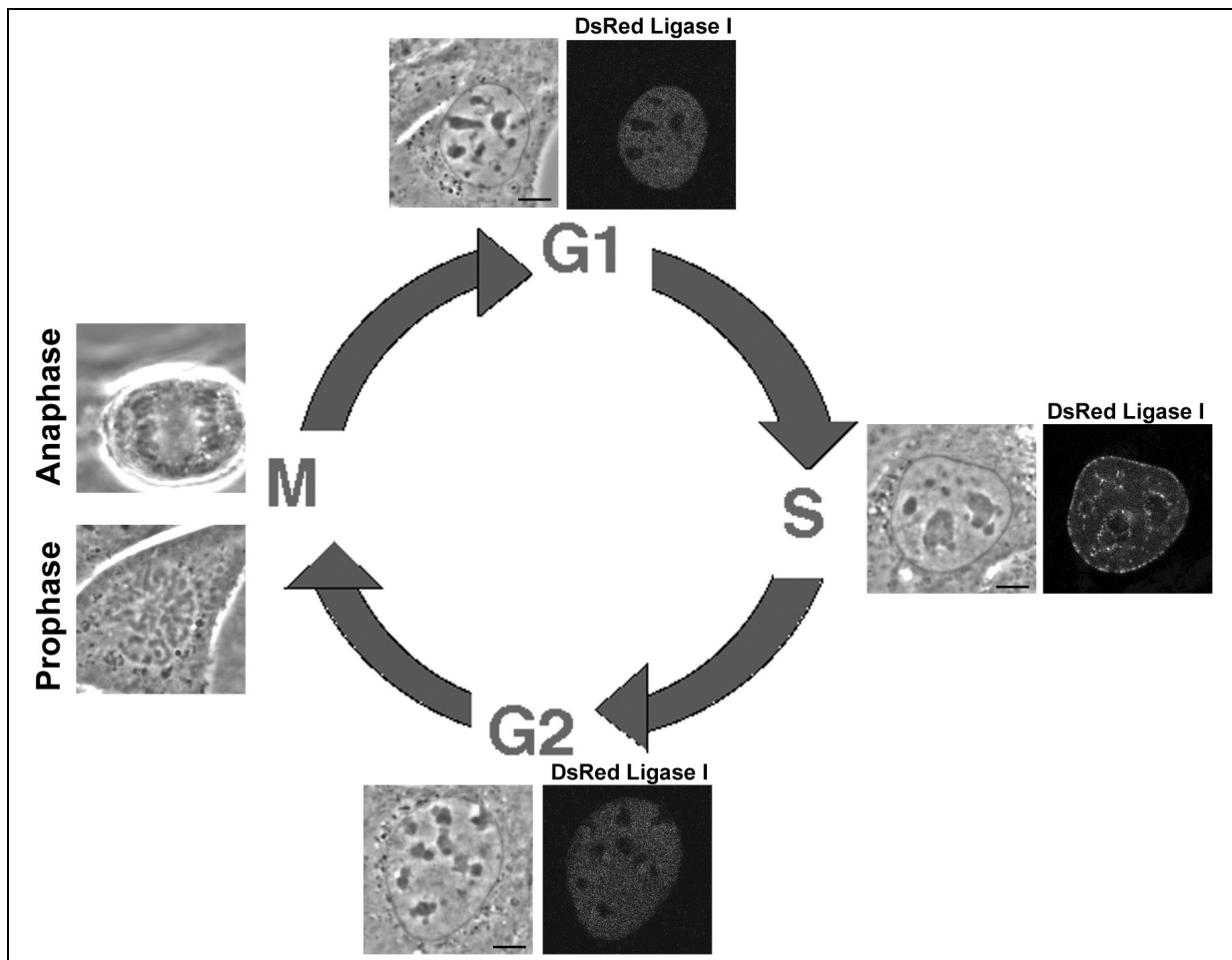


Figure 3.27: Determination of the cell cycle stage of *in vivo* observed cells. The sketch illustrates how the cell cycle stage of a cell under investigation could be recognized. S-phase cells could be identified directly by expression of DsRed Ligase I, which is spatially arranged according to classifiable DNA replication pattern corresponding to early, mid or late S-phase. The example shown here highlights a typical mid replication pattern. Mitotic cells could also be recognized directly by phase contrast imaging, which revealed condensing chromatin; sometimes even specific mitotic stages could be recognized as shown here. G1 and G2 cells were identified by previous or subsequent mitosis or S-phases. Note that in G1 and G2 nuclei, DNA Ligase I shows a faint homogeneous fluorescence pattern. Scale bar: 5 μ m.

For living cell experiments, I used C2C12 mouse myoblasts instead of Pmi28 myoblasts because transfection protocols as well as living cell microscopy were well established for this cell line in the laboratory of Cristina Cardoso where these experiments were conducted. Although this cell line shows an aberrant polyploid karyotype (see *Supplementary Materials* for details), increased clustering of chromocenters during myogenic differentiation, as well as inducible clustering by ectopic MeCP2 expression (figure 3.28) occurred in the same way as in Pmi28 myoblasts.

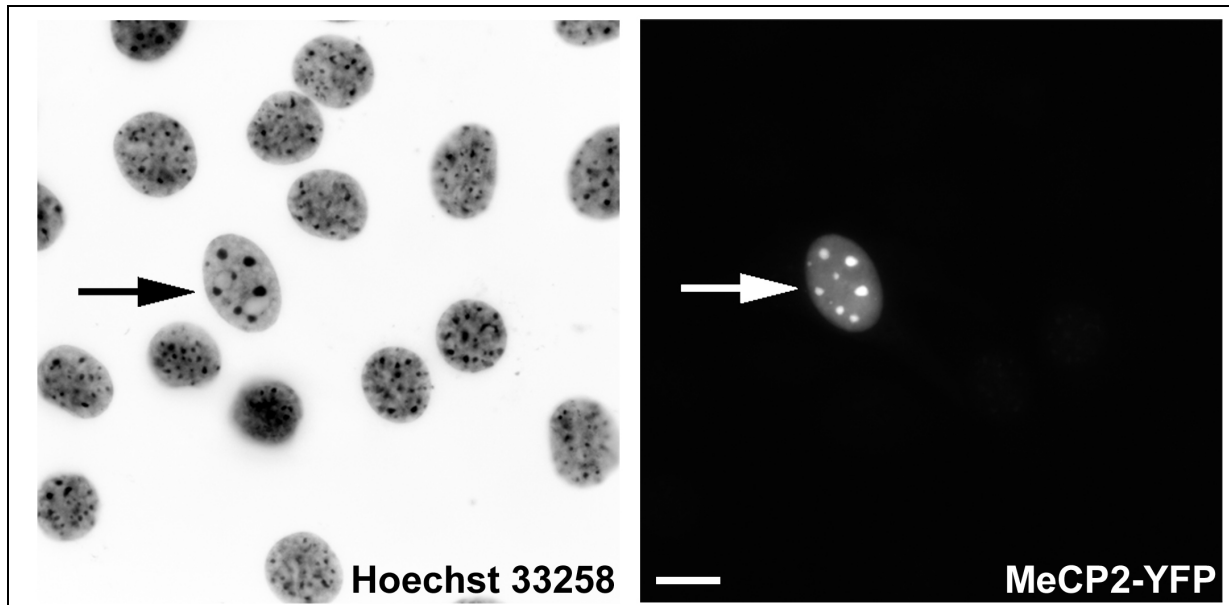
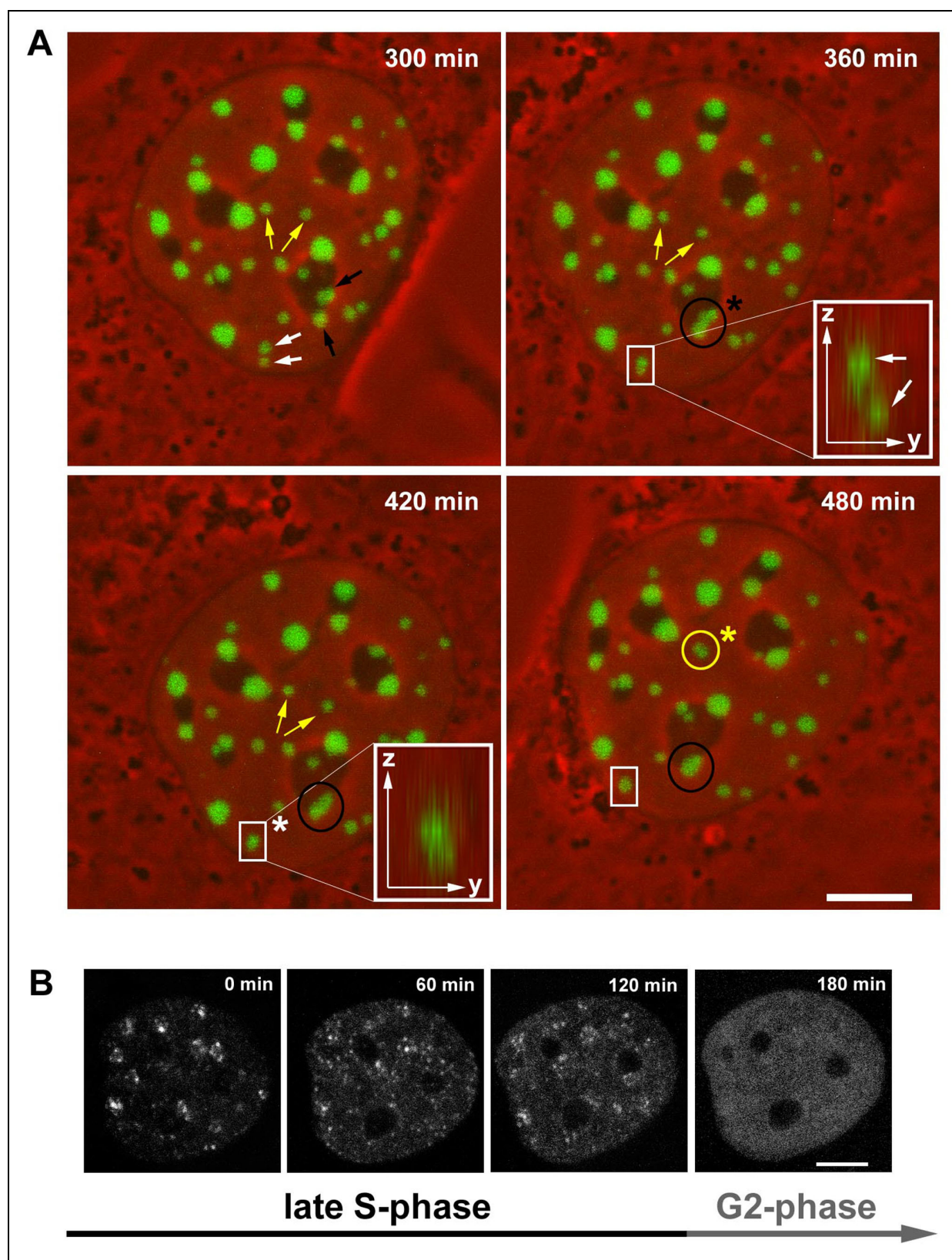


Figure 3.28: High levels of MeCP2-YFP induce chromocenter clustering in C2C12 myoblasts. Shown are epifluorescent images of C2C12 cells that had been transfected with MeCP2-YFP. Nuclei in the left image were stained with Hoechst 33258, which highlights chromocenters due to its AT selective binding, similar to DAPI or TO-PRO 3. The image was inverted to improve contrast. Note that the nucleus expressing high levels of MeCP2-YFP (arrow) shows a substantial lower amount of chromocenters compared to nuclei not expressing the fusion protein. Note also that the general number of chromocenters in C2C12 cells appears to be higher than in Pmi28 myoblasts, which is due to the polyploid karyotype of C2C12 cells (see *Supplementary Materials*). Scale bar: 5 μ m.

Observation periods lasted between 8h and 13h. The nuclei of 25 cells were imaged using confocal laser scanning microscopy. Light optical serial sections were recorded at time intervals of approximately one hour. For 14 of these cells the cell cycle stage could be unambiguously defined. In order to detect chromocenter fusion events, first maximum intensity projections were analyzed. By progressing backwards in time chromocenters especially larger ones were tested whether they originated from two or more smaller ones. Projections were used as they gave a clearer overview over all chromocenters in a nucleus irrespective of its axial position. A putative fusion event was finally verified by analyzing 3D stacks of the relevant time points in order to discriminate real chromocenter congression from axial overlapping. Figure 3.29, exemplifies the fusion of three chromocenters in a period of 4 hours. As shown by the DNA Ligase I staining for this particular cell the illustrated fusion events took place during G2 phase.

Figure 3.29: Fusion of chromocenters in a G2 cell. (A) Maximum intensity projections generated from confocal image stacks of four time points (tp) of a MeCP2-YFP transfected C2C12 myoblast are shown. MeCP2-YFP is shown in green, phase contrast images are shown in red. As apparent from the staining pattern of the co-transfected S-phase marker (B), this particular cell was in late S-phase when the observation was started and moved into G2 after approximately 3 hours, when DsRed-Ligase I became homogenously distributed. In (A) the last 180 minutes from the 480 minutes lasting time series are shown; hence, the illustrated time points in (A) the cell was in G2 phase. Three fusion events are highlighted in different colors (yellow, white and black). The time points where the actual fusion takes place are labeled by an asterisk. In order not to mistake an axial overlapping of signals for a real fusion event, confocal image stacks were analyzed in all three dimensions, as shown here for the signals highlighted by the white square. Note that as shown in the yz sections (insets) fusion did not occur until tp 420 min, though the two signals were indistinguishable in the projection view already at tp 360 min. Most observed fusions included very close chromocenters, but as in the case highlighted in yellow it could also affect chromocenters located more than 2.5 μ m apart. Scale bar: 5 μ m.



In 9 out of 14 nuclei, fusion of chromocenters could be undoubtedly demonstrated. 30 fusions could be traced, with a majority of 15 occurring in G2, while 10 were observed in G1 and five in S-phase (table 3.11).

Number of cells showing fusion (total)	Total number of fusions	Fusions in G1	Fusions in S	Fusions in G2
9 (14)	30	10	5	15

Table 3.11: Observed chromocenter fusions during interphase.

These results clearly show that MeCP2-YFP induced chromocenter fusion can occur during all interphase stages. Whether the difference in the occurrence of chromocenter fusions at different cell cycle stages is meaningful or rather a result of the small sample size remains unresolved.

In order to determine whether mitosis could also cause a diminution of chromocenters I compared the numbers of clusters in daughter nuclei with the number in the corresponding mother nucleus of five cells that went through mitosis during the observation.

Nucleus #	# of chromocenter in mother nucleus	# of chromocenters in daughter nuclei 1/2
1	36	42/30
2	22	31/21
3	22	29/26
4	18	36/24
5	39	40/38

Table 3.12: Number of chromocenters in daughter vs. mother nuclei. All analyzed nuclei went through mitosis during live cell observation. Chromocenters were counted as visualized by the intense MeCP2-YFP staining. In this respect it should be added that due to fluorescence bleaching, daughter nuclei usually showed a reduced signal intensity of MeCP2-YFP, so that as a consequence the number of chromocenters in daughter nuclei might have been underestimated.

As shown in table 3.11 the numbers of chromocenters in daughter nuclei was similar to that in the mother nucleus or often higher, so that extensive fusions set off by mitosis appear unlikely. This was somewhat surprising, as before the *in vivo* experiments were performed, it appeared conceivable that the observed fusions during differentiation and upon ectopic MeCP2-YFP expression could be mechanistically explained by a congression of centromeric regions during mitosis¹ followed by a lack of or a reduced separation of these regions in the subsequent G1 phase.

Besides fusion events I could also observe splitting of heterochromatin cluster, which occurred almost exclusively in G2. Only 2 chromocenters were observed to divide in G1. Three cells were followed for an extended period in G2 and all of them exhibited extensive splitting of chromocenters before they proceeded to mitosis. Hence, it is conceivable that disintegration of pericentric heterochromatin clusters is an important prerequisite to perform a proper mitosis. Figure 3.30 depicts the breaking up of large clusters in a cell, which is preparing to divide.

¹ Such a congression of centromeric regions can be seen in the prometaphase rosette (figure 4.3) or also in the anaphase figure where all centromeres are arranged at one pole during division of the chromatids.

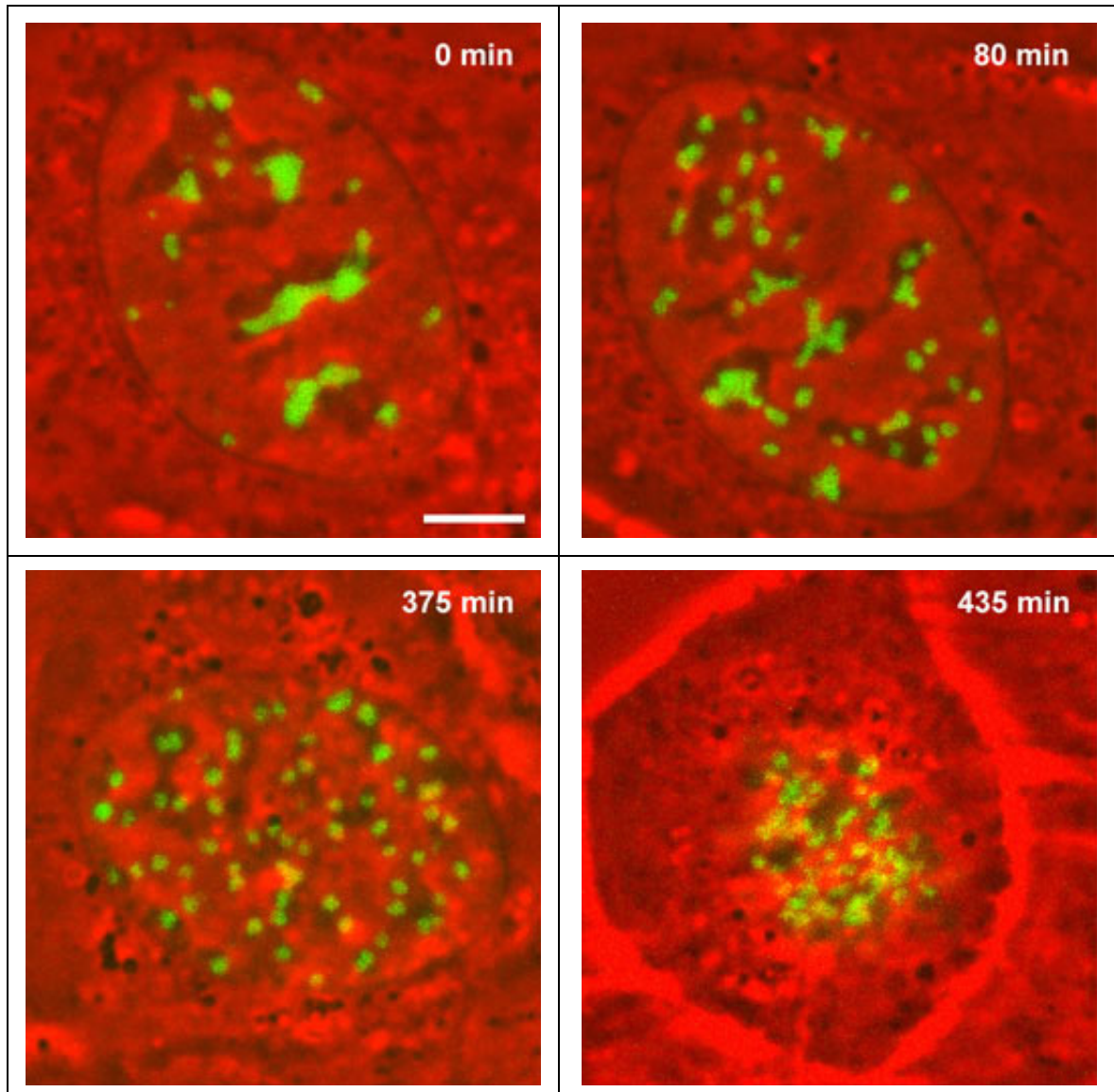


Figure 3.30: Splitting of chromocenters in a G2 cell. The images show a C2C12 mouse myoblasts expressing MeCP2-YFP at non-continuous observation time points. Maximum intensity projections of optical serial sections visualizing MeCP2-YFP (green) are combined with a mid optical section (red) outlining the nuclear profile. The upper and lower rows show two successive time points. Note that within 80 minutes many small chromocenters have already split from the larger “mother”-clusters. By 60 minutes prior to mitosis all signals are small and similar sized, suggesting a separating of each chromosome’s pericentric heterochromatin. Scale bar: 5 μ m.

To get a better 3D impression of chromocenter fusion and splitting an example showing both is presented as a 4D movie on the supplementary CD (“C2C12_MeCP1.avi” or “C2C12_MeCP1.mov”, see also 5.3 for a legend).

Summing up, the *in vivo* analysis revealed that fusion of chromocenters, which is induced by ectopic high-level expression of MeCP2-YFP, happens during all stages of interphase. Before mitosis however, frequent disintegrations of heterochromatic clusters were observed indicating that separating might be essential prior to the onset of mitosis.

3.3.5 Summary part 3:

The role of MeCP2 in the reorganization of pericentric heterochromatin

The implication of the methyl-CpG-binding protein 2 (MeCP2) in the phenomenon of chromocenter clustering during terminal differentiation was investigated for several reasons: (i) MeCP2 is highly enriched at pericentric sites (Lewis et al. 1992); (ii) several lines of evidence strongly suggest an involvement in neuronal differentiation/maturation, where its expression level was shown to increase in a differentiation dependent manner (Shahbazian et al. 2002; Balmer et al. 2003; Cohen et al. 2003; Mullaney et al. 2004). Using immunofluorescence, I was able to demonstrate an increasing expression of MeCP2 during myogenic differentiation, which was later confirmed by a western blot analysis. To elucidate whether these two findings were merely correlative or in fact causally connected, I tested whether ectopic expression of MeCP2 fused to YFP, as a fluorescent marker was able to induce clustering of chromocenters in the absence of differentiation. A highly significant correlation of the MeCP2-YFP expression level with the number of pericentric heterochromatin cluster supported the idea of a causal relationship. The fact that cells exhibiting high levels of MeCP2-YFP were still able to differentiate into myotubes thereby showing clustering that was even more pronounced than in differentiating non-transfected cells further strengthened the perception that MeCP2 is directly involved in the congression of pericentric heterochromatin during terminal differentiation in mouse. *In vivo* studies with MeCP2-YFP labeled chromocenters finally revealed that fusion could take place at any interphase stage; the observation of disintegrations of large clusters, especially before mitosis, indicates a certain incompatibility of such large pericentric aggregates with the onset of mitosis and proposes a highly dynamic organization of pericentric heterochromatin at least in cycling cells.

4 Discussion

The central question of the present thesis was to which extent large scale changes on a transcriptional level during differentiation are paralleled by changes of nuclear topology, or whether there are topological motifs that remain unchanged despite the gross modifications of the expression repertoire that alter cell function.

4.1 Distribution of gene dense and gene poor chromosomes in different mouse cell types and during terminal differentiation

The goal of this first part of the doctoral thesis can be subdivided into three components:

- 1.) The gene-density-related distribution of chromosome territories (CTs) as described for humans, chicken and higher primates was supposed to be tested in mice. Showing that this distributional motif is evolutionary conserved in mouse cells would strengthen the idea that there are selective forces favoring a gene-density-related distribution of CTs, may they be of a functional or a mechanistic kind.
- 2.) The second major point of this investigation was to assess the question whether besides a non-random radial distribution there would also be a predetermined side-by-side distribution of chromosome territories. Proposed non-random side-by-side distributions range from (a) an association of homologous chromosomes as described e.g. for diptera (reviewed in (Leitch 2000)) over (b) a preferential relative nuclear positioning of CTs (Nagele et al. 1999; Parada et al. 2002) to a complete spatial separation of parental genomes within the nucleus (Nagele et al. 1995; Nagele et al. 1998).
- 3.) Finally, I was interested in the question whether cell type specific differences would be observable in the organization of CTs, with the focus on cell types exhibiting a diverse differentiation status. Two *in vitro* differentiation cell systems were used including (a) mouse ES cells differentiating into macrophages and (b) myoblasts differentiating into myotubes. ES cells vs. macrophages and myoblasts vs. myotubes were used exemplarily for cells converting from a less specialized (in ES cells even pluripotent) status to a terminally differentiated one thereby assuming a drastic change in their expressed set of genes.

4.1.1 Radial distribution of #11 and #X CTs

Using 3D FISH with chromosome specific paint probes I could show in five different mouse cell types that gene dense #11 CTs and gene poor #X CTs exhibit a differential radial distribution. In myoblasts/myotubes, in ES cells/macrophages as well as in non-stimulated peripheral mouse lymphocytes #11 CTs were always distributed more internally, #X CTs more peripherally. This difference though turned out to be significant for myotubes, ES cells and lymphocytes, but not for myoblasts and macrophages. This result concerning a gene-density-related radial distribution of mouse CTs is consistent with the data obtained in humans (Croft et al. 1999; Boyle et al. 2001), higher primates (Tanabe et al. 2002) and chicken (Habermann et al. 2001). In all these studies, a general tendency for gene rich chromosomes to be distributed more internally and gene poor chromosomes to be localized more towards the nuclear border was described. This organization was even found in cell types where the originally analyzed chromosomes had undergone various chromosomal rearrangements, as in tumor cells (Cremer et al. 2003) or in specific primate species (Tanabe et al. 2002). A crucial prerequisite for the present investigation was the choice of a suited chromosome pair that would exhibit maximal gene density diversity. According to the *Ensembl* database¹ and the *NCBI* data base¹, which had 21592 and 44381 mapped gene en-

¹ http://www.ensembl.org/Mus_musculus/ <http://www.ncbi.nih.gov/genome/guide/mouse/>

tries, respectively I have chosen #11 (13.5 genes/Mbp) and #X (5.7 genes/Mbp) because they showed the biggest difference in their gene density values at the time when the experiments were performed¹. Additionally I considered cDNA mapping from the RIKEN Mouse Gene Encyclopedia project (Kawai et al. 2001), homology data to gene dense/poor human chromosomes as well as the distribution of CpG rich isochores as marker for gene rich regions (Saccone et al. 1997) (see *Supplementary Material* for a detailed table). The candidate chromosomes ought to be similar in their DNA content to exclude distributional differences due to chromosomal size, which had been shown to be a relevant factor in human fibroblasts and amniotic fluid cells (Sun et al. 2000; Cremer et al. 2001), in chicken cells (Habermann et al. 2001) as well as in cells of the long-nosed kangaroo (Rens et al. 2003). Chromosomes potentially bearing NORs (i.e.:#12 and #16-#19 (Winking et al. 1980)) were excluded as potential candidates because a distributional bias caused by the association of such chromosomes with nucleoli was very probable. The first studies that proposed a gene-density-related radial distribution of CTs were conducted in human cells analyzing #18 (4.4 genes/Mbp)² and #19 (22.3 genes/Mbp)³, which exhibit an extreme difference in their gene density corresponding to a factor of 5.1. The gene density between mouse #11 and #X differs only by a factor of 2.1. This means that if distributional differences of CTs correlate with their gene content a somewhat smaller diversity in the radial distributions between the chosen mouse CTs and human #18/19 CTs had to be expected. Indeed, the distributions between mouse #11 and #X were more similar than between human #18 and #19 even in lymphocytes, which showed the most significant difference. Figure 4.1 illustrates the respective distributions for mouse and human lymphocytes, both of which exhibited the most significant differences of all analyzed cell types. While #X in mouse and #18 in human distribute almost identically, #11 appears to be oriented more towards the nuclear border compared to human #19. It should be added that mouse #11 and #X are rather large chromosomes, while human #18 and #19 belong to the smallest of the chromosome complement. Hence the more peripheral location of #11 in mouse could also be due to its size, since for humans (Sun et al. 2000; Cremer et al. 2001), chicken (Habermann et al. 2001) and potoroo (Rens et al. 2003) it has been shown that larger chromosomes tend to lie more at the periphery, smaller ones more in the nuclear interior. In fact, although #11 chromatin tended to localize more towards the interior, almost all #11 CTs in all analyzed cell types were abutting the nuclear rim. Apart from 7 lymphocyte nuclei, where one #11 homolog was not touching the nuclear border, all other #11 and #X CTs were adjoining the nuclear edge. Hence, the more interior location of #11-chromatin must result from an expansion or protrusion of the territory into the interior nuclear compartment.

Though in all cell types, #11 CTs were generally located more internally than #X, in myoblasts and macrophages I observed a clear shift towards the periphery. In fact in both cell types the radial distributions between #11 and #X were not significantly different, if the radial iARR distribution was tested using a two sample Kolmogoroff Smirnov test, although the determined p-values were only slightly above the significance level (see also 4.1.1 *Evaluation Methods*). Using this significance test resulted in p-values for myoblasts and macrophages of 0.079 and 0.056 respectively, which were only slightly exceeding the significance level of $p=0.05$.

¹ Gene densities were calculated from the values of the *Ensembl* database in August 2002. Most recent values (July 2003) are #11: 15.3 genes/Mbp and #X: 7.4 genes/Mbp

² Calculated from the values of the *Ensembl* database in January 2004.

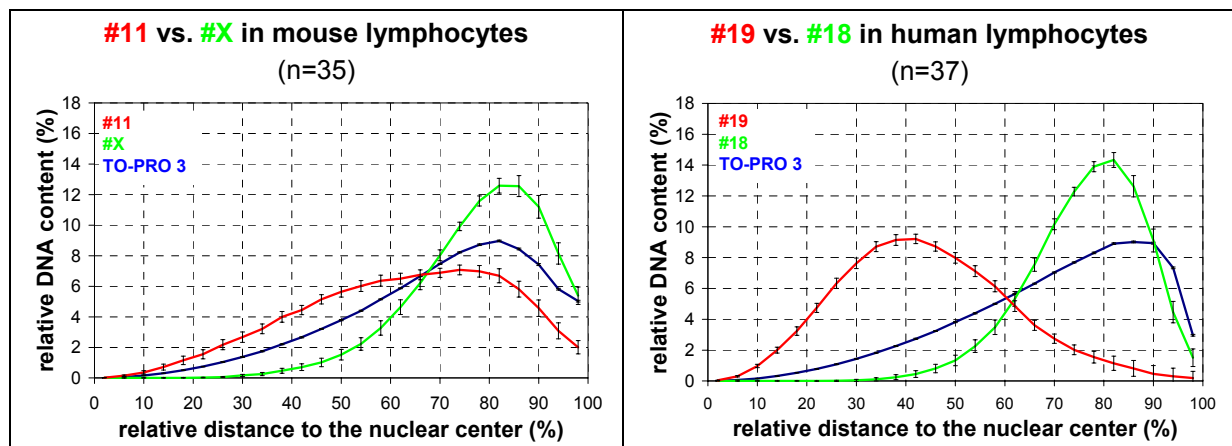


Figure 4.1: Radial distribution of gene dense vs. gene poor chromosomes in mouse and human lymphocytes. In both species non-stimulated, i.e. G0 lymphocytes were used. Note that the curves in mouse cells are less distinct compared to human cells, and that while mouse #X and human #18 show a very similar distribution mouse #11 is clearly oriented more towards the nuclear periphery compared to human #19. Data for human lymphocytes was taken from (Cremer et al. 2001).

The reason for the more peripheral radial distribution of #11 CTs in these cell types appears not to be connected to some general feature of terminal differentiation as the observed distribution changes during differentiation were in the opposite directions. After terminal differentiation of ES cells to macrophages #11 CTs were located more peripheral, while during myogenesis the distribution shifted towards the interior. A possible explanation comes from studies on human cells. As already mentioned above we had previously shown that the position of gene poor #18 CTs at the nuclear periphery and of gene rich #19 CTs in the nuclear interior was not maintained in fibroblast and amniotic cell nuclei (Cremer et al. 2001). Rather both chromosomes were located internal, nevertheless contacting the nuclear envelope (NE) on top and/or on bottom of the flat shaped nuclei. We argued that besides gene density, also chromosome size would play a role in the radial distribution of CTs with small chromosomes being located more internally and large chromosomes more at the periphery. The idea is that such a size or DNA content related organization of CTs is set during mitosis¹ and only later modified according to gene density, by specific interactions of the nuclear envelope with gene poor chromatin. In case of flat shaped nuclei this interactions could be established without disrupting the mitotically set organization. In contrast in spherical nuclei which expands in all directions during reconstitution of the nucleus this original distribution would be destroyed by the NE dragging gene poor chromosomes out of the center to the periphery (for a detailed description of a hypothetical mechanism, see 4.1.1). The present results concerning the more peripheral distribution of mouse #11 CTs in myoblasts and macrophages is consistent with this hypothesis of a size-related distribution in flat nuclei. In both flat shaped nuclei, #11 (123Mbp) and #X (150Mbp) show a similar radial distribution with a slight tendency of #X CTs to be more peripheral, just as expected from their relative DNA content. The average height in myoblasts and macrophages was 5 μ m and 6 μ m, respectively compared to 11 μ m in ES cells, 8 μ m in myotubes and 9 μ m in lymphocytes (table 3.4).

Recent results by R. Mayer a PhD student in the group of T. Cremer further support the idea that a gene-density-related distribution of CTs is not present in flat shaped nuclei. He extended the experiments of the present thesis using mouse fibroblasts, where he could demonstrate that #11 and #X CTs are distributed equally, similar as shown for #19 and #18 in

¹ The idea that a size-related distribution of CTs might result from mechanistic aspects during mitosis is discussed in (Sun et al. 2000) as the “mitotic preset model”.

human fibroblasts (figure 4.2). The plots in figure 4.2 moreover suggest that human #18 and #19 are located more internally, than mouse #11 and #X. This observation additionally supports the hypothesis that in flat shaped nuclei the radial distribution of CTs resembles the radial organization in prometaphase rosettes, where human #18/19 were shown to be more internal (Bolzer et al. submitted), while mouse #11/X extend more to the periphery of the rosette structure (figure 4.3)

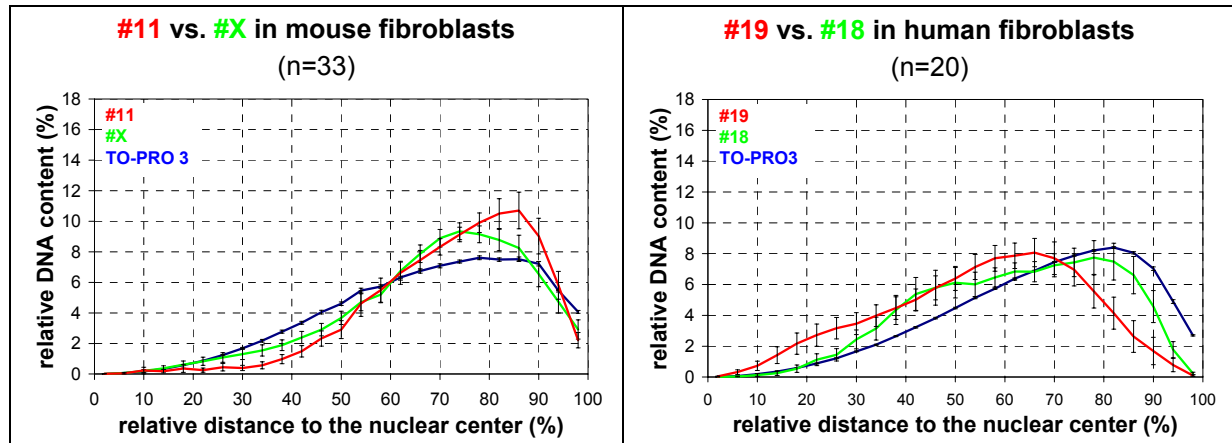


Figure 4.2: Radial distribution of gene dense vs. gene poor chromosomes in mouse and human fibroblasts. Data on the radial distribution of mouse #11 and #X was provided by R. Mayer, data on human #18 and #19 is from (Bolzer et al. submitted). Note that in both cases the radial distributions of gene poor vs. gene dense chromosomes were shown to be **not** significantly different. The average height of mouse and human fibroblasts was determined as $\sim 4\mu\text{m}$.

The present finding that the gene density-related radial distribution of CTs in mouse appears to be independent of cellular differentiation, has been described previously by Habermann et al. for chicken cells (Habermann et al. 2001). He could show that in cycling fibroblasts as well as in terminally differentiated neurons gene dense microchromosomes were generally more internal than gene poor macrochromosome that were located more at the periphery. It should be kept in mind that the preservation of this distributional motif during differentiation, which represents a very broad organizational level does not at all rule out the possibility that topological mechanisms influence transcriptional regulation during cellular differentiation on a more subtle level. During myogenesis Moen et al. for example described a dynamic reorganization of muscle specific genes to the periphery of so-called SC-35 domains, which are known to be enriched in pre-mRNA processing factors and are believed to be involved in mRNA metabolism (Moen et al. 2004). Other examples demonstrating an implication of nuclear topology in differentiation dependent transcriptional changes include the recruitment of heritably silenced genes to heterochromatic regions during T-lymphocyte and thymocyte differentiation (reviewed in (Fisher and Merckenschlager 2002)).

Hypothetical mechanisms

An important unsolved question concerning the gene-density-related distribution of CTs is how mechanistically such an order is established/maintained and connected to this question how and to what extent also chromosome size plays a role in determining the radial position of CTs. It should be stressed that deviations from a gene density correlated radial distribution of CTs featuring a chromosome size dependent distribution have only been described for nuclei with a flat shape. In fibroblasts and in amniotic fluid cells for example we could demonstrate a clear cut deviation from an exclusively gene content related distribution for #18 and #Y, which tend to lie internally though they are extremely gene poor (Cremer et al. 2001). A proposed explanation for the apparent antagonism between chromosomal gene content and

DNA content is proposed by the Cremer group in (Habermann et al. 2001), (Cremer et al. 2003) and (Schermelleh 2003) and shall be discussed here in detail:

Two different forces are postulated that can exert an organizational potential to a different extent, depending whether the nucleus has a flattened or a spherical shape. One force attracts chromatin to the nuclear periphery. This chromatin is presumed to be poor in gene containing sequences and rich in transcriptionally inert sequences. Such chromatin could be defined by modifications like increased DNA methylation, histone modifications including the utilization of histone variants or any other kind of "label" that is suitable to discriminate chromatin on a functional level. Such modifications are known to categorize the genome into transcriptionally competent/euchromatic regions and transcriptionally non-permissive/heterochromatic regions. DNA methylation for example is known to be compartmentalized over the mammalian genome with hypermethylated regions that are usually gene poor but rich in tandem repeats and in "parasitic DNA", like transposable elements, while gene rich regions containing so-called CpG islands in gene promoter regions are generally hypomethylated (reviewed in (Robertson 2002)). How chromatin subtypes can be defined by histone variants was recently described by Rangasamy et al. (Rangasamy et al. 2003) and by McKittrick et al. (McKittrick et al. 2004). The former could show that the histone variant H2A.Z was present in constitutive, but not in facultative heterochromatin during early mammalian development, suggesting a role in discriminating these chromatin subtypes. The fact that H2A.Z is essential for early development underscores the importance of such variant chromatin constituents for a proper execution of developmental programs. In *Drosophila* McKittrick et al. could demonstrate that the histone variant H3.3 was enriched for histone modifications correlating with transcriptional activity, while histone H3 showed modifications involved in transcriptional silencing (McKittrick et al. 2004). The authors proposed an epigenetic regulation potential through differential assembly mechanisms of the histone variants, as H3 is deposited in a replication dependent fashion, while H3.3 exhibits a replication independent assembly. Histone tail modifications can define chromatin by a number of different covalently bound molecules, including small chemical groups like methyl-, acetyl-, phosphate-, or ADP-ribosyl-residues or even small peptides as ubiquitin or SUMO (for reviews see (Jenuwein and Allis 2001; Geiman and Robertson 2002; Imhof 2003; Sims et al. 2003; van Driel et al. 2003)). This variable tag repertoire combined with multiple modification sites within histone tails and a variable number of added groups (e.g. mono-, di-, tri-methylation) creates a "histone code" with many possibilities to fine-tune chromatin labeling. As recent studies have shown an important modification for discriminating euchromatin, facultative and constitutive heterochromatin is a differential mono-, di- and tri-methylation of lysine residues at different positions on histone H3 (Peters et al. 2003; Rice et al. 2003). Hypermethylation of histone H3 at lysine 9 has been shown to be distributed in a G-band like pattern in mouse metaphase chromosomes and thus concentrated in gene poor chromosomes and chromosome stretches (Cowell et al. 2002). Adaptor molecules recognizing specifically such heterochromatic gene-poor regions and simultaneously interacting with components of the NE either directly or indirectly would have the ability to concentrate these regions at the nuclear periphery. Heterochromatin protein 1 (HP1) could act as such an adaptor molecule as it has been shown to interact *in vitro* indirectly with the lamin B receptor at the NE via a tetrameric complex with histones H3/H4 (Polioudaki et al. 2001). Since methylation of histone H3 is known to create a HP1 binding site (Lachner et al. 2001) it is conceivable that gene poor chromosome regions, which are enriched in hypermethylated histones H3 might be tethered to the nuclear periphery in an HP1 dependent manner. Targeting of the respective chromosomal segments could be established by HP1 interactions already during early stages of NE reassembly at mitosis. Involvement of HP1 during early NE reassembly steps is suggested by its presence in cap like structures at the polar ends of anaphase configurations (Kourmouli et al. 2000). More-

over, HP1 was shown to be important for the recruitment of NE components (LAP2 β and B-type lamins) to the surface of chromosomes, during early stages of NE reassembly (Kourmouli et al. 2000). Thus once the nuclear membrane has been completely rebuilt and the nucleus expands again to take its final shape (see (Burke and Ellenberg 2002) for a review on NE dynamics during mitosis), gene poor chromatin with a high frequency of HP1-NE interactions could be dragged to the nuclear periphery while gene dense chromatin with less associations to the NE would remain more internally located. Such a mechanism would explain how gene rich/poor chromosomes could be radially organized by a variable intrinsic potential to interact with the nuclear envelope¹. Another example demonstrating the intimate relationship between the NE and gene poor chromatin is provided by the autosomal dominant Pelger-Huët anomaly, in which affected individuals have mutations in the lamin B receptor gene. Apart from several developmental delays, affected individuals have neutrophils with hypolobulated nuclei and an abnormal “chromatin organization” (Hoffmann et al. 2002). Mice with mutations at the same locus show a similar phenotype including distribution anomalies of heterochromatin (Shultz et al. 2003).

This proposed NE driven distribution of CTs cannot explain the size-related distribution as described for humans (Sun et al. 2000; Cremer et al. 2001), and for marsupials (Rens et al. 2003). Here is where the second organization principle comes into play. The basis for the proposed mechanism is the arrangement of chromosomes during mitosis. In the prometaphase stage, condensing chromosomes form a wheel-like structure called prometaphase rosette (Chaly and Brown 1988). Within such a rosette chromosomes are arranged almost planar, with their centromeric regions building the hub of the wheel, from which the chromosome arms protrude outwards analogous to the spokes of the wheel (figure. 4.3). As outlined in figure 4.4 the gravity centers of smaller chromosomes are nearer to the center of the rosette than those from larger chromosomes. Consequently, the organization of prometaphase-chromosomes is size-related. Using 3D FISH with a combinatorial probe set visualizing all human chromosomes simultaneously Bolzer et al. could convincingly show that the size-related distribution present in prometaphase rosettes is maintained in interphase nuclei of human fibroblasts (Bolzer et al. submitted). Studies on so-called squash-preparations of proliferating tissues (see (White 1961) and citations therein), in which snap-shots of mitotic cells can be prepared were in-

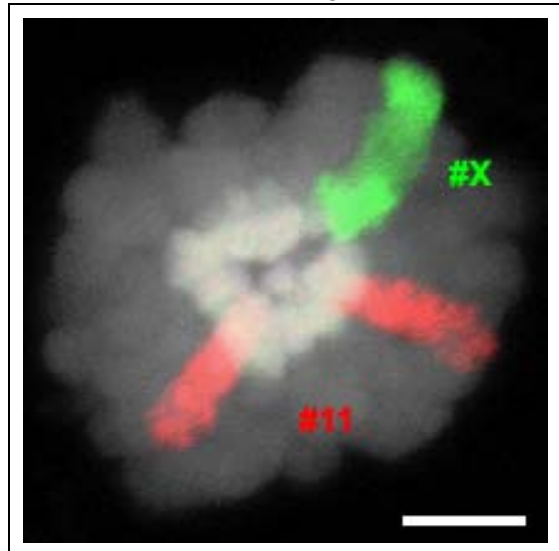


Figure 4.3: Mouse prometaphase rosette. Chromosome 11 and X are labeled by 3D FISH. TO-PRO 3 counterstaining highlights centromeric regions building an internal ring-like structure. Note that the rosette is not completely planar; otherwise the centromeric regions would be arranged as an open ring. Scale bar: 5 μ m.

¹ This hypothetical mechanism would also result in a gene-density-related chromatin/chromosome distribution if nuclear assembly would be accomplished via the fusion of so-called karyomeres, which represent small single chromosomes containing vesicles, and which have been observed in *in vivo* studies in *Xenopus*, *Drosophila* and sea urchin (see (Burke and Ellenberg 2002) and citations therein). During fusion of these “mini-nuclei”, gene rich regions lacking extensive membrane associations are prone to be pushed into the nuclear interior, while gene poor chromatin/chromosomes would remain attached at the inner nuclear membrane while the complete nuclear envelope is reconstituted. Additional extension of the nuclear envelope in the course of further chromatin decondensation would additionally separate gene poor and gene dense chromatin/chromosomes.

dicative that a size-related distribution is maintained also during metaphase. Similar observations were done in studies on metaphase spreads where chromosomes of fixed mitotic cells are spread on a glass surface (Hens et al. 1982; Wollenberg et al. 1982; Wollenberg et al. 1982). As described by Allison and Nestor (Allison and Nestor 1999) the prometaphase organization of chromosomes is probably maintained during anaphase, where they observed similar ring-like structures as during the prometaphase stage. In fact, in the model of the Cremer group they posit that the anaphase conformation declines and is oriented parallel to the substratum (figure 4.4) similar to the anaphase/telophase described by Allison and Nestor. During the subsequent decondensation, the arms of larger chromosomes would then push smaller chromosomes into the nuclear interior.

The main difference in the organization of small chromosomes between spherically shaped nuclei and flat nuclei is that in spherical nuclei the radial order set by the prometaphase organization is partially destroyed during the shaping of the nucleus, when gene poor small chromosomes are dragged to the periphery in all different directions. Gene dense small chromosomes on the other hand lacking extensive associations with the NE are left in the interior. In flat nuclei, the prometaphase organization is maintained because extensive contacts between the NE and small gene poor chromosomes can be accomplished on the top and bottom surface of the reconstituting NE. Indeed in fibroblast nuclei we could show that #18 CTs though being internal have extensive contacts with the NE on top and/or on the bottom of the nucleus (Cremer et al. 2001), which is predicted by the proposed mechanism. Such a mechanism would also implicate that in flat nuclei large gene dense chromosomes would be more peripheral reflecting the situation in the prometaphase rosette, while in spherical nuclei the lack of extensive NE associations would increase the probability to remain in the interior. This could indeed be observed for mouse #11 where in myoblasts and macrophages with a flat nucleus the global average relative radius (gARR) was 72.5% and 72.6%, respectively compared to 68.3% in ES cells, 66.7% in myotubes and 62.1% in lymphocytes, which had either a spherical or cylindrical nucleus (figure 3.6; see table 3.4 for nuclear dimensions).

The observation mentioned above, that almost all #11 CTs were abutting the nuclear border just like #X CTs, but protruding further into the nuclear interior than #X, does also fit in this model. If a peripheral #11 and #X localization is assumed in the prometaphase configuration due to their intermediate to large size, during early G1, gene dense #11 chromatin could expand into a more internal position, thereby still keeping to a certain degree a peripheral contact. In contrast, #X having a higher amount of gene poor chromatin and thus more NE associations would be tethered more stringently to the nuclear periphery.

Another mechanistic aspect that should be considered is a potential influence of a nuclear matrix that could concentrate gene dense chromatin in an internal nuclear compartment via specific associations, similar to those proposed for gene poor chromatin at the NE. Supportive data for such an assumption comes from a study by Cremer et al. concerning the radial distribution of #18 and #17 in the tumor cell line SW 620. This cell line carries a #17/#18 translocation chromosome enclosing the centromeric region of #18 plus two normal copies of #17 and one of #18 (Cremer et al. 2003). #17 has a high gene density (15.7 genes/Mbp) and was previously shown to localize internally (Boyle et al. 2001). Interestingly #17 material of the derivative chromosome was distributed identically as the complete #17 material in the cell line, while #18 material of the rearranged CT was positioned more internally than the normal copy. This means that #17 material was influencing the distribution of #18 and not vice versa which argues against a mere passive mechanism responsible for the internal location of gene dense chromatin. This finding has an impact on yet another proposed mechanism concerning the spatial arrangement of CTs. Gerlich et al. proposed a mechanism in which the amount of pericentric heterochromatin has an influence on the timing of sister

chromatid separation and therefore determines the relative position of chromosomes within the nucleus in a heritable fashion from mother to daughter nuclei (Gerlich et al. 2003). If this would be indeed the case the der(18)t(17;18) in the cell line mentioned above should behave as a “normal” #18 and thus localize at the periphery since it possesses the centromeric region of #18. As already described this was not the case, instead the derivative chromosome behaved rather like #17, “dragging” #18 material more towards the interior.

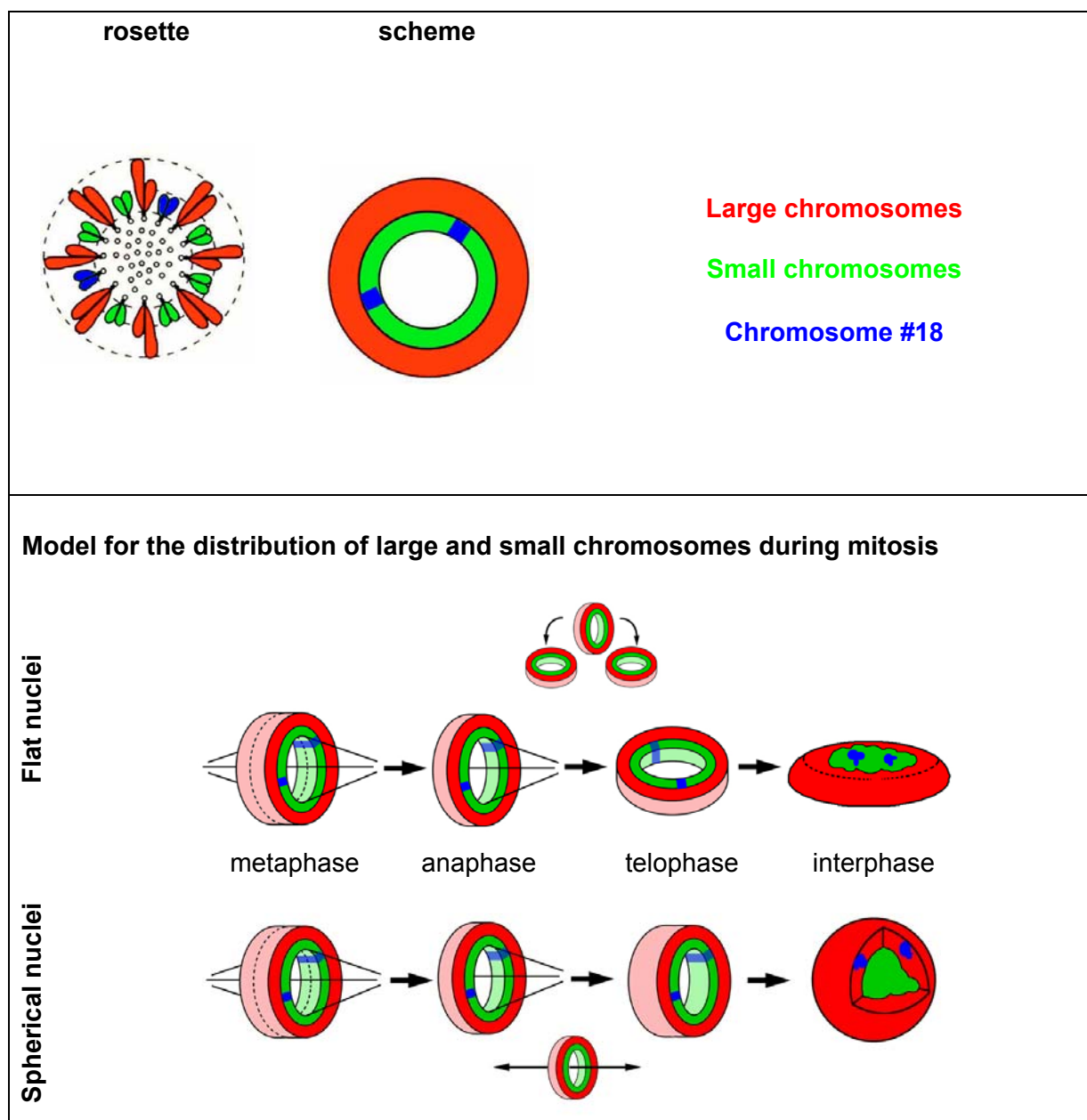


Figure 4.4: Schematic illustration of a possible mechanism for the differential radial distribution CTs in flat and spherical nuclei. Top: The distribution of large (red) and small chromosomes (green), including #18 (blue) in human metaphase rosettes is shown schematically. Note that the gravity centers of small chromosomes are nearer to the center of the rosette. Bottom: For flat nuclei, the small inset illustrates the possibility that the anaphase configuration declines to one side or the other. In any case, it results in a conformation of chromosomes parallel to the substratum. For spherical nuclei of non-adherently growing cells, the anaphase configuration is not supposed to be oriented in a specific manner. During expansion and reshaping of spherical nuclei extensive contacts with the NE are responsible that #18 CTs are dragged to the NE, of the nuclear interior, while in flat nuclei the contacts are accomplished with the top and bottom surface of the reconstituting NE, thereby maintaining the prometaphase configuration. The scheme was published in (Habermann et al. 2001) and was adapted to illustrate the distribution of #18 CTs.

Functional aspects

The currently available data clearly supports the hypothesis of an evolutionary conserved gene-density-related distribution of chromosome territories. Actually, this distribution motif was previously shown to be valid on a subchromosomal level. Replication labeling experiments had convincingly revealed that there was a differential distribution of gene dense, early replicating chromatin located in the nuclear interior and gene poor mid to late replicating chromatin concentrated at the nuclear periphery and around nucleoli (O'Keefe et al. 1992). This nuclear organization was not only demonstrated for mammalian cells (Sadoni et al. 1999) but turned out to be applicable in an increasing number of other species including birds (Habermann et al. 2001) or even such distantly related species as the simple polyp Hydra (Alexandrova et al. 2003). This far-reaching evolutionary conservation of nuclear architecture suggests some kind of functional relevance that to date is still a matter of speculation. One possibility is that compartmentalization of the nucleus in domains facilitates the performance of nuclear functions as transcription, RNA processing etc. The nucleolus is a well-known example for such a functional/topological correlation, where a territorial sub-compartmentalization follows a functional reason, i.e. rDNA transcription rRNA maturation, assembly of ribosomal subunits etc. Similarly, the concentration of transcriptional competent euchromatin in an internal nuclear compartment and transcriptionally non-permissive chromatin at the periphery and around nucleoli could facilitate transcription and transcriptional repression, respectively by concentrating relevant factors and their corresponding sequence targets. Yeast nuclei for example are known to harbor a heterochromatic, transcriptional repressive compartment at the nuclear periphery (Cockell and Gasser 1999), that was shown to induce silencing of a transgene, which had been artificially tethered to the NE (Andrulis et al. 1998).

The positioning of gene poor chromosomes/chromatin at the nuclear periphery might also be a consequence of the fact that specific sequences or chromatin modifications that function as an interface during NE reassembly after mitosis might interfere with a proper transcriptional regulation if present in chromosome regions that are gene dense. As discussed above HP1 appears to be involved in NE reassembly (Kourmouli et al. 2000) possibly via an interaction with the lamin B receptor (Polioudaki et al. 2001). At the same time HP1 is known to interact preferentially with hypermethylated histones H3 at lysine 9 (Lachner et al. 2001), which represents a histone modification that is usually absent in euchromatin as it is thought to confer a transcriptionally inactive status. Thus the necessity of such a specific chromatin modification for a proper chromatin-NE contact during reassembly of the nucleus after mitosis would clearly interfere with the chromatin conformation necessary in regions with many potentially transcribed genes.

An explanation for a selective advantage of a gene-density-related radial distribution of chromatin is the so-called "bodyguard hypothesis". It was originally described by T.C. Hsu (Hsu 1975) in the light of a peripheral localization of constitutive heterochromatin and recently discussed by Tanabe et al. (Tanabe et al. 2002) and previously by Hens et al. (Hens et al. 1982) in the context of a peripheral distribution of gene poor chromosomes (see also 1.1.1). The underlying rationale is that gene less/poor chromatin could act as a protection shield at the nuclear periphery protecting gene dense chromatin from potential mutagens and other DNA damaging agents. However, there are several aspects arguing against this hypothesis. First of all chromatin at the nuclear periphery is not exclusively composed of constitutive heterochromatin as originally described by Hsu, but as replication labeling has shown it consists to a high degree of mid replicating chromatin. This has been shown to correspond to G dark bands of mitotic chromosomes (Ferreira et al. 1997), which are known to contain tissue specific and with that most probably essential genes. We showed in human fibroblasts and amniotic fluid cells that #19 CTs were partially abutting the NE similar to #18, most

probably as a consequence of the flat shape of the nucleus, while in lymphocytes, #19 was “protected” in the interior (Cremer et al. 2001). It appears very unlikely that the evolution of such a defense mechanism would act cell type specifically. Finally, if the function of peripheral chromatin would really be a protection of internal gene dense chromatin by “sacrificing” peripheral DNA to damaging agents one would expect a higher DNA damage frequency in such regions. Apparently this is not the case as studies on double strand breaks and endonuclease- and radiation-induced chromosome aberrations have shown that such DNA lesions occur rather in R-bands and thus in gene rich regions (see (Tanabe et al. 2002) and citations therein) than in G-bands.

Evaluation methods

The statistical interpretation of experimental data is crucial in order to detect differences or similarities between the properties (i.e. radial distributions) and samples (i.e. cell types) under investigation. The radial distribution of CTs in the present thesis was assessed using three different approaches, yielding partially different results. Basically three different parameters describing the radial distributions of #11 and #X were utilized and compared within one and between different cell types: (1) The radial distributions of the complete territorial volume were used. (2) The radial distributions of the chromosome iARRs were used. (3) The radial distributions of the fluorescence intensity gravity centers of CTs were used.

(1) The distribution of the complete territories, as for example shown in the graphs in figure 3.3 or 3.4 is determined by averaging the relative DNA content within each individual shell of each individual nucleus over all nuclei within the given sample. Applying a Kolmogoroff Smirnov test using the distributions of the complete territories or more precisely the cumulative frequency distributions of the complete territories (see *Material and methods*) turned out to be the most stringent approach to compare the radial arrangements of #11 and #X CTs. The high stringency of this approach was already exemplified in a study by Cremer et al. (Cremer et al. 2003) where the radial distribution of human #18 vs. #19 was analyzed in several cell types. Besides a KS test applied on the distribution of complete territories, they used also a median quartile test applied on the CT iARRs distributions; in several cell types where the former approach failed to prove significance the latter confirmed a significant difference. When this stringent approach was used for the present mouse data, none of the differences between the radial distributions of #11 and #X CTs appeared to be significant except for lymphocytes, which showed also the clearest difference in the distribution curves (figure 3.3). Table 4.1 summarizes the obtained p-values for the various cell types using this approach. In myoblasts and macrophages, the p-values are much higher than in the other cell types, while in myotubes, having a p-value of 0.06 the significance level of 0.05 is almost reached. Although only for lymphocytes the distributions between #11 and #X were significantly different the variability in the p-values suggests an increasing difference between the radial arrangements of #11 and #X with macrophages < myoblasts < ES cells < myotubes < lymphocytes; this corresponds well to the according curve progressions as shown in figure 3.3/3.4.

ES cells	macrophages	myoblasts	myotubes	lymphocytes
0.18	$p \gg 0.2$	> 0.2	0.06	0.02

Table 4.1:p-values using complete territories: The calculated p-values represent the probability of error that the radial distributions of #11 and #X are different. The test of significance was a two sample Kolmogoroff Smirnov test.

Generally, it should be kept in mind that the more stringent the statistical test is and the smaller the difference, the bigger the sample size has to be in order to prove the significance

of the difference. In ES cells for example, where 36 nuclei were analyzed the difference between the radial distributions were determined to be not significantly different with a p-value of 0.18, which clearly exceeded the significance level of 0.05. The same difference in the radial distributions would have been significant if it would have been measured for 56 nuclei, instead of 36, as the p-value would then have dropped to 0.047¹.

(2) In the second approach, the radial distributions of the iARRs of #11 and #X CTs instead of the radial distributions of complete territories were used. The iARR was calculated for each nucleus, for each channel corresponding either to #11 or #X and represents the average distance of the chromatin visualized in the respective channel. This means that the radial distribution of the complete territory/territories within each nucleus was reduced to one value, which then represented the relative distance of the complete chromosome/chromosomes within this nucleus. The iARRs of all nuclei were then assigned to one of the 25 shells of the nucleus representing the relative radial distance from the nuclear center. Thereby a new distribution was created describing the iARR distances for the complete data set. Since the iARR values showed usually a small variability, with #11 iARRs concentrated around smaller relative distance values, while those of #X were concentrated around larger values the resulting curves showed more distinct peaks with steeper slopes than the corresponding distributions of the complete territories (figure 4.5). Accordingly the differences in the cumulative frequencies, which were finally used for determining the significance via the KS test increased markedly (figure 4.5)..

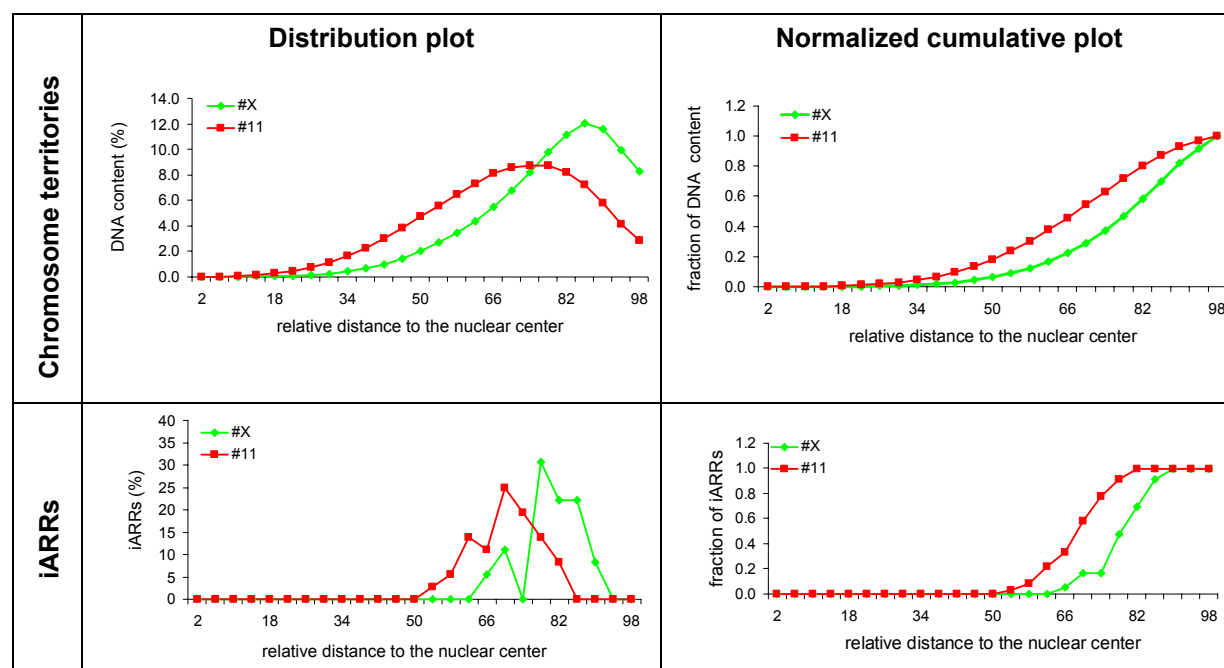


Figure 4.5: Distributions (left) and cumulative frequencies (right) of #11 (red) and X (green) complete territories (upper row) and iARRs (lower row). The panel top left shows the radial distribution of #11 and X CTs in mouse ES cells as shown in figure 3.3. On the right, the same data is arranged in a normalized cumulative way. The lower left graph shows the radial distributions of the iARRs of #11 and #X. The graph on the right shows the same data set normalized and in a cumulative fashion. Note that the difference between the cumulative curves is bigger for the iARR distributions.

¹ The required number of nuclei n was determined by calculating the p-value for the observed distributions for a successively increasing n , until it became smaller than 0.05.

Using this approach the differences between the radial distributions of #11 and #X turned out to be significant for lymphocytes, ES and for myotubes, but remained insignificant for myoblasts and macrophages although the p-values were only slightly above the significance level (table 4.2). In this respect it should be added that the iARR distribution could also have been evaluated using a median quartile test, which has been shown to be less stringent than the KS test (Cremer et al. 2003) (M. Neusser, personal communication). Accordingly, I anticipate that using this test on the present data would have resulted in a significance difference in myoblasts and macrophages as well.

The calculated p-values increased from lymphocytes over myotubes, ES cells to myoblasts and macrophages just as for the KS test on complete territories (table 4.1), but in contrast more cell types leaped the significance level.

ES cells	macrophages	myoblasts	myotubes	lymphocytes
2.9×10^{-6}	0.08	0.06	3.1×10^{-6}	3.5×10^{-8}

Table 4.2:p-values using CT iARRs: The calculated p-values represent the probability of error that the radial distributions of #11 and #X are different. The test of significance was a two sample Kolmogoroff Smirnov test.

(3) This last approach was in principle equivalent to that comparing the iARR distributions but instead of using iARRs, fluorescence intensity gravity centers (GC) of the respective territory/territories were used. 3D coordinates of GCs and absolute distances were determined using the software *Image J* via a threshold dependent segmentation approach (see *Materials and methods*).

An important difference between relative GC and iARR distances was the normalization. While all distance values that were used to calculate the iARR (i.e. the relative distances of all voxels belonging to #11 or #X) were normalized to the “individual” nuclear radius, i.e. the radius through the point to be measured, GCs were normalized to the long nuclear radius (see *Materials and methods*). This was done because the software could not determine the “individual” radius. Thus, an unknown proportion of all measured relative distances were underestimated, so that the distributions of iARRs and GCs cannot be directly compared. This underestimation results in smaller values of average GC distances in comparison to the corresponding iARR distances (compare figure 3.5 vs. 3.7). The relative GC distances were assigned to one of 25 distance classes, just as in the two other approaches thus generating a radial distribution of GCs (figure 3.6). Applying a two-sample KS test on the relative distribution data of GCs yielded the same qualitative results as that for the iARRs, with a corresponding increment of p-values from lymphocytes to macrophages (table 4.3).

ES cells	macrophages	myoblasts	myotubes	lymphocytes
0.01	$p \gg 0.2$	$p > 0.2$	5.5×10^{-4}	2.7×10^{-7}

Table 4.3:p-values using CT gravity centers: The calculated p-values represent the probability of error that the radial distributions of #11 and #X are different. The test of significance was a two sample Kolmogoroff Smirnov test.

Taken together both approaches using either iARRs or GCs prove a differential radial distribution of #11 and #X in ES cells, myotubes and lymphocytes. Additionally the iARR distribution indicates a differential distribution also in myoblasts and macrophages although at a lower significance level ($p < 0.1$), whereas the GC distribution does not. The most stringent approach using the distributions of complete territories detected only in lymphocytes a significant difference ($p < 0.05$) and on a lower level in myotubes ($p < 0.1$) and ES cells ($p < 0.2$), but clearly failed to detect a significant deviation between both distributions in myoblasts and macrophages.

The question, which approach is finally the most adequate and reasonable to interpret the data, is difficult, if not impossible to answer. I personally believe that it is a valuable tactic to use different approaches and statistic evaluation tests covering different stringency levels to analyze data in order to detect also more subtle deviations, which might be left undetected if too stringent approaches are used, especially in combination with moderate sample sizes, as was the case also in the present work. The described differences between the radial distribution of #11 and #X are believed to be reliable and meaningful for lymphocytes, myotubes and ES cells for following reasons. First of all, a differential intranuclear arrangement was noticeable already by visual inspection. Secondly, the relative radial distribution curves of #11 and #X CTs (figure 3.3) show a clearly distinct progression. Most importantly, the statistic analysis using iARRs and GCs yielded the same significant differences for these three cell types, and a similar trend concerning the cell type specific extent of the differences was also observed applying the most stringent comparison using the complete territories for testing. In macrophages and myoblasts the radial distributions of #11 and #X do not appear to be different or at least only marginally since all three approaches could not detect significance.

Conclusions and outlook

Similar to the results obtained in humans, chicken and higher primates the presented results argue for a gene-density-related distribution of CTs in mice, thereby supporting the idea that it represents an evolutionary conserved motif. A unifying model explaining the data obtained so far has to consider the influence of chromosome size and of the nuclear shape as influencing parameters additionally to gene density. This is achieved if mechanistic constraints set by the organization of prometaphase chromosomes in the rosette structure are posited as basis of the radial distribution in interphase nuclei. Additional organizational motifs, like gene density are conceivable to act on top of this basic mitotic organization. A combination of this mitotically set order plus an additional affinity of gene poor chromatin to associate with the NE could explain the observations concerning CT distributions in all analyzed cell types so far including the apparent anomalies between flat and spherical nuclei. Additional investigations of the radial CT distribution in different cell types of different species will help to increase the understanding of the concepts behind the nuclear organization of chromosome territories. Especially a variable composition of the karyotypes in the analyzed organisms as far as differences in chromosome size and gene density are concerned will facilitate to dissect the respective influence of these parameters. Living cell experiments using labeled chromosomal landmarks, such as centromeric, telomeric, euchromatic or heterochromatic regions will further increase our understanding concerning the mechanistic basis underlying the organization of chromosomes during early stages of NE reassembly and will consequently help estimating the influence of mitosis on the distribution of chromatin in the interphase nucleus.

4.1.2 Side-by-side distribution of #11 and #X CTs

In the presented experiments I assessed the side-by-side distribution of #11 and #X in five different mouse cell types by measuring distances and angles between homologous CTs as well as between heterologous CTs. All measurements were done using the 3D coordinates of fluorescence intensity gravity centers of the respective CTs. The results support the concept of a random relative positioning of chromosome territories in respect to each other.

A high percentage of nuclei exhibited an association of homologous #11 CTs. In myoblasts and macrophages ~26%, in myotubes 50%, in ES cells 53% and in lymphocytes even 57% of all analyzed nuclei showed only one coherent volume. A legitimate reason to argue anyway against the association of #11 homologues as a general phenomenon is the still high frequency (ca.43%-74%) of nuclei which did not exhibit an association; in some cases ho-

mologous #11 CTs resided even at opposite poles of the nucleus. Besides, some of the associated chromosomes were reminiscent of two CTs merely touching each other with only a limited surface contact, suggesting that the observable associations in the various nuclei were not qualitatively the same, but rather represented variable degrees of contacts. Most probably, the elevated percentages of nuclei with associated #11 homologues are due to the more internal localization of #11 CTs, which increases the probability that both touch each other due to a smaller volume in the nuclear interior. A similar result concerning an increased association was found for human #19 CTs in human lymphocytes where they had been shown to localize internally due to their high gene density (see above and (Cremer et al. 2001)). In order to test whether the radial distribution indeed determines the frequency of chromosome associations and not homology, similar experiments as the presented ones could be performed including an additional chromosome with a similar radial distribution as #11¹. If homology does not play a role homologous associations should be as frequent as heterologous ones. Accordingly, chromosomes with a peripheral location should exhibit a lower frequency of association despite their homology². Another supporting reason that the internal radial distribution of #11 could account for the high incidence of observed homologous associations is that the frequency of observed homologous associations apparently correlates with the extent of internal location, i.e. cell types where #11CTs are localized more internal show also a higher frequency of associated chromosomes. Myoblasts and macrophages which show the most peripheral gARR (~73%) of all analyzed cell types exhibit homologous association in only 26% of the nuclei, which is the lowest number of associations, while lymphocytes having the smallest gARR (62%) show the highest number of associations (57%).

Earlier studies had shown a homologous association of centromeric regions of human #1 and #17 in cerebellar neurons (Arnoldus et al. 1989; Arnoldus et al. 1991) and more recently of human chromosomes 3, 7, 8, 13, 17, and 21 in human Sertoli cells (Chandley et al. 1996). Since both cell types represent terminally differentiated cells, Leitch et al. proposed the idea that association of homologues might correlate with the frequency of mitosis and thus with cellular differentiation (Leitch et al. 1994). In the present work terminal differentiation does not seem to affect the frequency of mouse #11 CT associations in any specific direction. Both an increase could be observed during myogenic differentiation as well as a decrease during terminal differentiation of ES cells to macrophages. The observed changes correlate rather with the nuclear shape, in such a way that the more spherical a nucleus is the higher is also the frequency of associations (see table 3.4 for nuclear dimensions). A similar influence of the nuclear shape was proposed above for the differences observed in the radial distribution of #11 CTs, with spherical nuclei correlating with a more internal position. If the mutual effects of these three parameters (a) nuclear shape, (b) radial distribution and (c) frequency of homologous association are considered simultaneously, the following interdependence can be described: the more spherical a nucleus is, the more internal is the distribution of #11 CTs (see 4.1.1) and the higher is the frequency of associated #11 CTs. However, it should be added that in the present experiments only one chromosome was analyzed, which cannot rule out that other chromosomes might indeed show an increased association

¹ Mouse chromosome 7 would be an appropriate candidate for such an experiment, as it is similar-sized as #11 and shows a similar gene density.

² Mouse #3 or #14 would be suitable candidates as they are similar sized as #11 but show a low gene density.

^{1, 2} The radial distribution of the respective CTs should however be determined before these experiments, to confirm the presumed internal (#7) or peripheral (#3/14) localization.

upon differentiation. Furthermore, the utilized *in vitro* differentiation systems might also not reflect the situation in the living organism.

The presented results moreover argue clearly against an organization of chromosomes as proposed by Nagele et al. (Nagele et al. 1995). Analyzing the angular arrangement of chromosomes 1, 7, 8, 9, 16 and X they found homologous chromosomes to be separated by an angle of 144° to 166°, from which they concluded that rosettes would consist of two haploid sets, possibly arranged according to their parental origin. Since they found a juxtaposition of #X and #16 and in a subsequent study of #8 and #11 (Nagele et al. 1999) in both prometaphase rosettes and interphase nuclei, they proposed that relative positions of chromosomes in mitotic stages would be maintained in the following interphase. Consequently, they proposed that homologues of all chromosomes should have an angular position that is larger than 90° in prometaphase rosettes as well as in interphase nuclei. This concept was further supported by a study of Koss (Koss 1998), who showed that the angular separation of #1, #X and #7 in interphase nuclei of human bronchial cells was almost identical to that described by Nagele et al. (Nagele et al. 1995) in prometaphase rosettes of fibroblasts.

In the present work, I analyzed the angular separation between homologous #11 CTs in 5 different mouse cell types. The angle distribution between non-associated #11 CTs showed a wide range of angles between 40° and 170°, which argues against the “dogma” of Nagele et al. claiming that the angles between homologous chromosomes should be larger than 90°. The study of Koss (Koss 1998) basically supports Nagele’s model as mentioned above, although one third of the analyzed nuclei showed an average angle between 70°-90°, which is smaller than expected by the Nagele model. Koss assigned this to a nuclear rotation, which, since the angles were measured in a 2D approach, would lead to the difference in the measured values; tracing this rotation back would again yield angles around 150°. The reason for such a rotation of the nucleus, that has to be quite precise, in order to yield predominantly angles around 70°-90° without completely randomizing the angle values, remained unclear. The presented data for mouse #11 homologues as well as the data on human chromosomes by Bolzer et al. (Bolzer et al. submitted) clearly contradict this possibility, since all angle measurements were done in 3D, i.e. the 3D coordinates of the CT fluorescence intensity gravity centers and of the nucleus were used for the angle calculation. This means that if the angular separation in prometaphase rosettes is between 150° and 160° and maintained until interphase, it should be detected by a 3D approach, no matter how the complete nucleus might rotate. The concept proposed by Nagele et al. is furthermore inconsistent with the high frequency of observed homologous association, since homologous chromosomes are not supposed to be juxtaposed in the prometaphase rosette¹.

The overall high variability of measured inter-homolog and –heterolog distances and angles argues against any kind of non-random side-by-side distribution for the analyzed chromosome territories. The results also argue against a general association of homologous #11 CTs. However, since in the present study only 2 out of 20 chromosomes were analyzed, it would be presumptuous to completely rule out the possibility of such a general association for other chromosomes, although all available data for mammalian cells argue against such a possibility. Moreover, a specific association or spatial proximity of specific heterologous chromosomes can only be ruled out for combinations including #11 and #X. The neighboring position of #12, #14 and #15 in several mouse cell types as described by Parada et al.

¹ As described above some #11 associations involved only small parts of the chromosomes, which could still be explained by the Nagele model since they allow other chromosomes to lie in between. However, several nuclei showed an intimate “fusion” of both CTs, resulting in one big territory, which is clearly incompatible with the “Nagele” concept.

(Parada et al. 2002) can thus be neither confirmed nor rejected. An elegant approach to uncover the relative relationships of all chromosomes in respect to each other would be a multi-color FISH study as performed by Bolzer et al. in human cells (Bolzer et al. submitted), although the technical realization is complicated and laborious. Additional studies using conventional FISH approaches will nevertheless be helpful help to extend our knowledge until a comprehensive view for the complete mouse chromosome complement is obtained.

4.2 The nuclear organization of pericentric heterochromatin in different cell types and during terminal differentiation

From the results concerning the nuclear organization of pericentric heterochromatin in mouse cells, three main conclusions can be summarized:

- 1.) There is a cell type specific intranuclear arrangement of pericentric heterochromatin cluster in terms of number and size that changes upon differentiation. During differentiation, the clustering of chromocenters increases, thereby reducing in number and increasing in size.
- 2.) There is a cell type specific intranuclear arrangement of pericentric heterochromatin in terms of intranuclear localization that appears to be independent from differentiation, but to correlate with nuclear shape.
- 3.) The methyl-CpG-binding protein 2 (MeCP2) plays a major role in the aggregation of pericentric heterochromatin.

Aspects 1 and 3 will be discussed together as the present results strongly suggest that chromocenter clustering is causally linked to MeCP2.

4.2.1 Intranuclear distribution

Pericentric heterochromatin, which is composed of large arrays of tandemly repeated “major satellite” sequences, was visualized by a fluorescent in situ hybridization (FISH) approach using a fluorescently labeled probe that was specific for the satellite repeat. The intranuclear localization of pericentric heterochromatin was assessed by two different approaches. In the first approach, I determined the localization of individual chromocenters in respect to a) the nuclear border and b) to a nucleolus. Doing this a distribution of chromocenters could be described, in which the frequencies of chromocenters was assigned to one of four distribution classes. These classes included (1) peripheral, for clusters abutting the nuclear boundary, (2) perinucleolar, for those abutting a nucleolus, (3) peripheral and perinucleolar for chromocenters associated with both the nuclear border and a nucleolus or (4) interior, for clusters contacting neither the nuclear rim nor a nucleolus. Utilizing a second approach, I evaluated the global radial distribution of pericentric heterochromatin as one coherent domain, utilizing the “3D-RRD” software that was already used to evaluate the radial distributions of #11 and #X CTs (see 2.12.1).

It should be kept in mind that the nuclear border was defined by a DNA counterstaining, i.e. the nuclear periphery was defined by the chromatin itself. If the lamina had been used to demarcate the nucleus, a non-equivalent characterization of “peripheral” and “internal” would have resulted, since it has been shown that the nuclear lamina forms invaginations protruding into the chromatin “interior” (Broers et al. 1999). Consequently, an “internal” signal as defined in the present experiments could actually have been “peripheral” in respect to the nuclear lamina.

The first method revealed that a majority of chromocenters was located at the nuclear periphery in all cell types, followed by a high fraction of clusters associated with nucleoli and only a minority being located in an interior nuclear compartment. This finding is consistent with the generally held view that constitutive heterochromatin is often found at the nuclear

periphery (Comings 1980; Spector 1993; Leitch 2000) or if located near active NORs also around nucleoli (Wachtler et al. 1986; Cerda et al. 1999).

Concerning the interpretation of the results obtained by this first approach, the following should be considered:

(1) The definition of a peripheral or a nucleolar signal was based on the observation that the respective chromocenter would contact the nuclear or nucleolar border¹. Since most of the pericentric heterochromatin clusters had a spherical shape, the association with the nuclear periphery was consequently tangential, such that the main portion of the cluster actually resided more within the nucleoplasm. Consequently, the frequency of chromocenters at the periphery or at a nucleolus was not indicative for the nuclear distribution of pericentric heterochromatin as a whole. This explains why ES cells, which showed the lowest percentage of peripheral chromocenters (63.8%), showed actually the second most peripheral distribution of pericentric heterochromatin, when they were analyzed with the second approach, which determined the radial distribution of pericentric heterochromatin as one coherent structure.

(2) This chromocenter-based approach did not consider the size of the signal, i.e. if a chromocenter consisted of larger or smaller amounts of pericentric heterochromatin. Consequently, this approach did not give clues concerning the intranuclear distribution of pericentric heterochromatin as a whole. Still it proved useful to describe general distribution patterns of chromocenters, which could be compared between different cell types in order to find characteristic similarities or differences.

One major point of interest was whether distributional patterns would change upon differentiation. In fact a substantial redistribution of chromocenters from a perinucleolar/internal location to the nuclear periphery was observed during differentiation of ES cells to macrophages. On the other hand, during myogenesis a redistribution just in the opposite direction was found. These reverse changes of intranuclear distribution patterns during terminal differentiation rule out that they represent a general feature of differentiation. Interestingly the nuclear shape changed also in a reverse fashion during both differentiation pathways, from a rather spherical shape in ES cells to a flatter ellipsoid in macrophages, and from a flat ellipsoid nucleus in myoblasts to a cylindrical in myotubes (table 3.4). Therefore, it is tempting to speculate that the observed changes could be consequences of the nuclear shape change. A prediction of such interdependence would be that the probability of chromocenters that are located at a nucleolus, to contact additionally the nuclear periphery should be higher the flatter the nucleus is. The experimental data does indeed fit this prediction, as the fraction of chromocenters abutting both a nucleolus and the periphery was higher in flat shaped nuclei² (see figure 3.18). In conclusion, the distribution of chromocenters during differentiation seems to correlate rather with the shape of the nucleus than with differentiation, although it cannot be completely excluded that distinct functional needs in the different differentiation pathway might have driven this apparently opposed reorganization of chromocenters.

The observed decrease in the percentage of peripheral chromocenters during differentiation of mouse myoblasts to myotubes (95.9% to 77.5%) appears at first glance in contrast to the results by Chaly and Munro, who showed that centromeres were relocated to the periphery during myogenic differentiation of *rat* L6E9 myoblasts (Chaly and Munro 1996). Using serum from CREST patients, they visualized centromeric regions in rat myoblast and myotube nu-

¹ It should be kept in mind that this characterization was done on raw images, i.e. with out applying any thresholding of the data.

² The total fraction of nucleolar signals, i.e. "perinucleolar" and "peripheral and perinucleolar" was both in macrophages and myoblasts somewhat smaller than in myotubes and ES cells, so that the fraction „peripheral and perinucleolar“ was higher in spite of a slight decrease in perinucleolar signals in general.

clei and categorized the intranuclear signal distribution according to visual evaluation of confocal image stacks. A nuclear pattern was regarded peripheral if most signals were in the uppermost or bottommost section or at the periphery of mid sections. Upon differentiation they describe a dramatic change of the observed centromere positions from a random distribution in myoblasts (>90% of analyzed nuclei) to a peripheral distribution in myotube nuclei (>90% of analyzed nuclei). This apparently contrary result compared to the presented findings in mouse becomes actually confirmative if one considers that in rat myotube nuclei are flatter than myoblast nuclei, unlike in mice where essentially the opposite is true. Hence the proposed correlation of a peripheral localization of centromeric regions with the flatness of the nucleus is only further strengthened by the data on rat myogenesis. Another relevant finding reported in the study of Chaly and Munro, using electron microscopy is that they describe a reorganization of condensed chromatin masses in terms of a decrease in number with a concomitant increase in size. This finding affirms the increased clustering of pericentric heterochromatin during mouse myogenic differentiation as described in the present thesis (see 3.2.1 and below).

A dynamic reorganization of pericentric heterochromatin was furthermore described by Manuelidis (Manuelidis 1985) and Solovei et al. (Solovei et al. 2004) for postmitotic mouse cerebellar Purkinje neurons during maturation. During postnatal development, chromocenters were shown to move from the nuclear periphery to the interior thereby abutting a central nucleolus. Martou and de Boni obtained similar results by staining kinetochores (Martou and De Boni 2000). Since the nuclear shape of Purkinje neurons does not change during maturation, the observed reorganization of centromeric regions might have some functional implications.

The biggest variability in the intranuclear distribution of chromocenters between different cell types was found for the perinucleolar fraction (including exclusively perinucleolar signals and those being additionally peripheral). This varied from 15.9% in lymphocytes to 58% in ES cells. In this case it is particularly persuasive to speculate that some functional implications might underlie these differences, as one can assume that a perinucleolar association involves potentially one or more active “nucleolus organizer regions” (NORs), which reside in close proximity to the major satellite region on the long arms of #12 and #15-#19¹ (Winking et al. 1980). The variable frequency of chromocenter associations with nucleoli could thus reflect differences in the number of active NORs and thus in translational activity of the cells. This would explain the most pronounced difference found between ES cells and lymphocytes. Since ES cells cycle very fast (doubling time 14-20h) it is conceivable that they need to have an increased translational rate in order to accomplish the production of all necessary proteins to share to their daughter cells in a limited time period, consequently recruiting more NOR bearing chromosomes to nucleoli. In contrast, non-stimulated lymphocytes are known to exhibit low transcriptional and translational activity (Lester and Cooper 1985) and should consequently have less NORs at nucleolar sites. Indeed Wachtler et al. demonstrated that in quiescent human lymphocytes only a few active NORs were located around nucleoli, while upon stimulation with phytohemagglutinin, which induces cell cycle reentry and differentiation, formerly inactive NORs were recruited to nucleoli (Wachtler et al. 1986). Another supporting argument for the assumption of a generally low translational activity in quiescent mouse lymphocytes is the observation that the size of nucleoli was usually very small.

Such a functional connection might appear tempting, however the results should be interpreted with caution since as already mentioned, the size of associated nucleolar signals is not considered in this approach. It could well be that the perinucleolar association of larger

¹ The presence of NORs on the mentioned chromosomes was shown to vary between different laboratory inbred strains (Dev et al. 1977).

chromocenters, containing several NORs could compensate for a lower frequency of perinucleolar association. Consequently, since the actual number of NOR bearing chromosomes participating in perinucleolar signals was not known (a limitation that is also valid for smaller chromocenters), the proposed correlation between the frequency of perinucleolar signals and translational activity must be considered as very speculative. A FISH approach visualizing NORs with an rDNA specific probe could help to elucidate whether the variable association of chromocenters at perinucleolar sites actually reflects the variability in number of active NORs and thus in the level of protein biosynthesis. Such an approach should moreover also employ a reliable staining of nucleolar antigens (e.g. B23/nucleophosmin), in order to detect also smaller nucleoli, which was not always possible in the present study, where nucleoli were solely identified by nuclear counterstain, which might have led to an underestimation of perinucleolar signals.

The analysis of the radial distribution of pericentric heterochromatin as a whole using a voxel based software based method detected the most peripheral distribution in lymphocytes, followed by ES cells, while all other cell types, namely myotubes, macrophages, myoblasts and fibroblasts showed a similar but characteristically more interior localization (figure 3.20 and 3.21). The finding that ES cells showed the second most peripheral distribution of pericentric heterochromatin did not fit the observation that they exhibited the lowest frequency of chromocenters assigned to be “peripheral”. This apparent antagonism reflects the limitation of the chromocenter based approach showing that the mere attachment of a chromocenter at the nuclear periphery does not allow extrapolating positional information for the complete chromatin mass, since neither the size nor the shape of the chromocenter is considered. Combining the results of both approaches consequently suggests that ES cells had a more peripheral distribution than other investigated cell types but with less attachment points at the nuclear periphery. An observation that might account for this effect is that in ES cells chromocenters were often irregularly shaped, building elongated, sometimes sheet-like or network-like structures immediately adjacent to the nuclear periphery. In contrast, all other cell types had predominantly spherical chromocenters. Thus, a limited number of chromocenters abutting the nuclear rim, but shaped in such a way that the bulk chromatin does not protrude far into the nuclear interior could account for both findings using the different approaches. Figure 4.6 illustrates an example where the irregular shape of chromocenters was fairly pronounced.

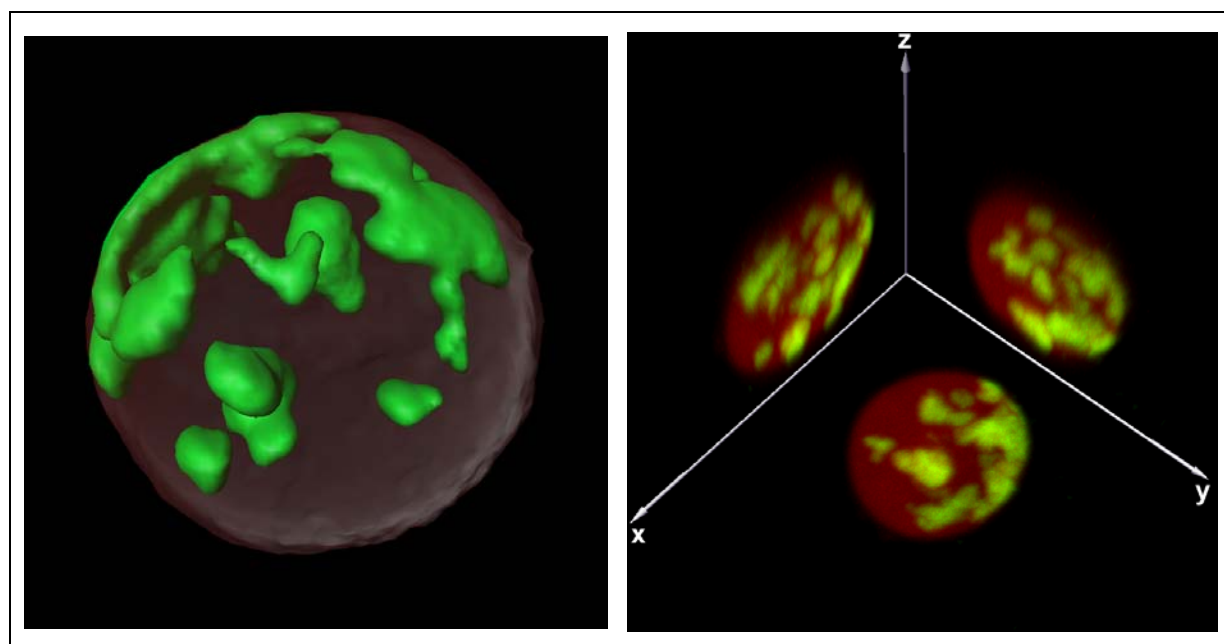


Figure 4.6: ES cell with irregularly shaped chromocenters. The left image shows a 3D reconstruction of an ES cell nucleus exhibiting very irregularly shaped chromocenters (green). Indeed pericentric heterochromatin is arranged almost like sheets underneath the nuclear rim. TO-PRO 3 counterstain is shown as a transparent reddish shell. The right illustration depicts the same nucleus (from a different angle) showing maximum intensity projections in all three planes. Note that this cell represented an extreme case. Usually just a few irregularly shaped chromocenters were present among mostly spherical shaped. Several nuclei exhibited also exclusively round chromocenters.

The reason for these irregularly shaped pericentric heterochromatin clusters that in such extreme variants were only observed in ES cells remains obscure. A possible explanation might come from the rapid cell cycle progression of this cell type, which had by far the shortest doubling time of all analyzed cell types. In living cell observations of C2C12 myoblasts, which usually have spherical chromocenters, early G1 and sometimes late G2 cells showed also irregular chromocenters. In early G1, these irregular chromocenters could have resembled an intermediate stage during formation of bigger cluster after pericentric regions of individual chromosomes had been separated during mitosis. In G2 cells, such “non-spherical” chromocenters might have represented intermediate stages during the splitting of larger clusters preceding mitosis, since during prophase centromeric regions were usually already found as individualized structures. Although all analyzed ES cells were in S-phase, as revealed by BrdU staining, the limited time period between two successive mitoses might not have been sufficient for pericentric heterochromatin, which was still “in the middle of” clustering, to round up and form spherical shaped chromocenters. If one posits that the default state of a chromocenter would be to adopt a spherical shape as long as there is enough time to do so, a round shape should correlate with the time interval between two mitotic events. An extreme case would be quiescent or postmitotic cells, which completely lack cell division; indeed non-stimulated, i.e. non-cycling lymphocytes and terminally differentiated myotubes both showed exclusively spherical shaped chromocenters.

Since ES cells were fixed under moderate hypotonic conditions using 0.5xPBS instead of 1xPBS, one might argue that the irregularity of chromocenters was artificially induced by swelling of ES cell nuclei. Since this effect was also seen in ES cells, which were fixed applying isotonic (1xPBS) or mildly hypotonic (0.75xPBS) conditions, it appears rather unlikely. Moreover, a fixation series of myotubes using strongly hypotonic conditions (0.3xPBS) resulted in still roundly shaped chromocenters and not in irregular cluster, which would be expected if hypotony would play a role.

The apparently more peripheral distribution of pericentric heterochromatin in lymphocytes and ES cells is at first difficult to explain as both cell types are functionally very distinct. While ES cells proliferate and are in a pluripotent state, lymphocytes are in an advanced stage of commitment and quiescent. A possible explanation for the markedly more peripheral location of pericentric heterochromatin in these two cell types comes from observations regarding the radial distribution of #18 CTs in humans (Cremer et al. 2001). Here the gene poor chromosome 18 is located peripheral in lymphocytes, but internal in fibroblasts. As a possible mechanism for this observation, it was suggested that gene poor #18-chromatin could be associated with the nuclear envelope thereby localizing most of the chromatin in the nuclear periphery, especially in such cell types which have a spherical nucleus. In flat shaped nuclei on the other hand the lack of extensive nuclear expansions after mitosis especially in an axial direction would result in #18 being left at its position in the prometaphase rosette, where it localizes fairly internal (Bolzer et al. submitted). Associations with the top and bottom part of the nuclear envelope could still be accomplished though but without dragging the chromosome outwards (see also pp. 150 for a detailed description of the model). Similarly, centric regions, which are found most centrally in the prometaphase rosette (figure 4.3), could be

dragged to the nuclear periphery by interacting with the nuclear envelope in lymphocytes and ES cells which have spherical nuclei, while in fibroblasts, myoblasts and macrophages such associations would not necessarily result in gross positional changes after mitosis. This mechanism on the other hand cannot explain the more internal position of pericentric heterochromatin in myotube nuclei which have also an axially expanded shape (table 3.4). It could well be that besides interactions with the nuclear periphery, additional positional constraints, as the number of active NORs participating at nucleoli, influence the overall distribution of pericentric regions.

Another consideration what might have caused the more peripheral localization of pericentric heterochromatin in ES cells and in lymphocytes is that it could have been artificially introduced by the hypotonic fixation procedure. Critical steps were the incubation in 0.5xPBS for ES cells and in 0.3xPBS in lymphocytes, for a period of one minute before fixation using 4% paraformaldehyde in 0.5xPBS or 0.3xPBS, respectively. Although at least for human lymphocytes this fixation protocol is known to rather conserve nuclear morphology than altering it¹, it cannot be excluded that in mouse lymphocytes and ES cells hypotonic treatments might have had a substantial effect on the nuclear topology of pericentric heterochromatin. To question this possibility I compared approximated mean nuclear volumes of ES cells fixed under hypotonic conditions (0.5xPBS) with such under isotonic (1xPBS) conditions, which did not reveal a substantial difference. The mean nuclear volume in hypotonically fixed ES cells was $705\mu\text{m}^3 \pm 59\mu\text{m}^3$ (n=31) compared to $620\mu\text{m}^3 \pm 90\mu\text{m}^3$ (n=9)² for cells fixed using isotonic PBS. Furthermore I compared the radial distribution of pericentric heterochromatin of ES cells fixed under hypo- and isotonic conditions. The radial distribution turned out to be not significantly different, no matter whether a stringent test approach was applied using averaged relative radial distributions of the complete labeled chromatin ($p>0.5$) or a less stringent one employing iARR distributions ($p>0.5$) (see also 4.1.1 *Evaluation Methods*). In conclusion, it appears unlikely that the markedly more peripheral localization of pericentric heterochromatin in ES cells and lymphocytes is the result of hypotonic fixation conditions.

During terminal differentiation of myoblasts to myotubes, no significant changes of the radial distribution of pericentric heterochromatin could be observed, no matter whether a stringent or a less stringent approach was used (see above). This lack of a clear difference between terminally differentiated cells and their proliferating precursors argues clearly against a radial redistribution of pericentric heterochromatin during myogenesis. This means that in spite of the observed reorganization of pericentric heterochromatin in terms of an increased aggregation during differentiation, the overall radial distribution remains unchanged. This constancy in radial nuclear patterning, in spite of gross changes on a transcriptional level, strengthens the idea of a radial compartmentalization of the nucleus as a stable framework on which dynamic mechanism can additionally act. A similar constancy in the radial organization was found for early and mid replicating chromatin during myogenic differentiation, which kept its intranuclear distribution during the transition from myoblast to myotube nuclei (Klier-Choroba 2002). During differentiation of ES cells to macrophages, however a shift of pericentric heterochromatin to the nuclear interior was detected that turned out to be significant if a less stringent statistic test was applied. Since all cell types where the nucleus was flatter than in ES cells exhibited a more interior localization of pericentric heterochromatin, the easiest ex-

¹ Staining of living lymphocytes with DNA dyes and comparing nuclear morphology and diameter with lymphocytes fixed under different conditions revealed an optimal conservation using the described fixation protocol (Marion Cremer personal communication and own observation)

² Nuclear volumes were approximated by calculating the spherical volume using the half nuclear diameter as radius, which was derived from maximum intensity projections of nuclear counterstain confocal image stacks.

planation for the observed shift is the reduction of height in macrophages. If differentiation would indeed be responsible for the observed distributional changes, it should also have been observed between ES cells and myotubes or between ES cells and lymphocytes, since both are eventually derived from ES cells. Since myotubes showed no difference in the distribution, while in lymphocytes pericentric heterochromatin was found even more peripheral than in ES cells, it appears very unlikely that cellular differentiation causes *per se* a specific change in the radial distribution of pericentric heterochromatin.

4.2.2 Clustering

Employing a FISH approach I visualized mouse pericentric heterochromatin by using a probe specific for the major satellite sequence, which is a 234bp sequence tandemly repeated at pericentric sites. In total, the major satellite accounts for ~10% of the mouse genome. Generally, centromeric regions¹ tend to cluster thereby building heterochromatic blocks, which are referred to as chromocenters and which contain centromeric regions of several individual chromosomes. The number of observable chromocenters was variable within cell populations, but showed significant differences between different cell types. Non-cycling cells as lymphocytes or myocytes as well as terminally differentiated cells like macrophages and myotubes showed a significantly reduced number of chromocenters and a concomitant increase in chromocenter-size compared to cycling cells as fibroblasts myoblasts or ES cells. Since quiescent fibroblasts showed only a small and non-significant decrease in the number of chromocenters compared to their proliferating counterparts, it appeared that rather differentiation than cell cycle exit was correlating with the reduction of pericentric heterochromatin cluster. In fact during both differentiation pathways, ES cells to macrophages and myoblasts to myotubes a significant decrease in the number of clusters could be demonstrated.

The decrease in chromocenter number during myogenesis appeared to be a stepwise process, in which a first “wave” of enhanced clustering was seen in myoblasts, which were still cycling but had been induced to differentiate 4 days prior to fixation. A second “wave” of clustering was observed after fusion of myocytes to myotubes. In case of ES cell differentiation to macrophages, a significant decrease in the number of observable chromocenters was only seen for CD11b positive cells that had not passed through S-phase 24 h before fixation. CD11b positive cells with a clearly macrophage-like morphology, but which still had incorporated BrdU 24h prior to fixation, i.e. were either still proliferative or at least had become postmitotic only shortly before fixation, exhibited a similar number of chromocenters as ES cells. Since ES cells certainly went through many intermediate differentiation stages before becoming postmitotic macrophages, it cannot be ruled out that the chromocenter number might have fluctuated in between, including stages where the number might also have increased. Actually, it is assumed that ES cells necessarily have to show an increase in chromocenter-number during differentiation, because fibroblasts and myoblasts exhibited a higher number of chromocenters (21.1 and 20.4) than ES cells (14.7), but are supposed to be derived from ES cells after all. In this respect it should be added that the analysis of two other ES cell lines R1 and CCE, revealed a similar mean number of chromocenters as in EB 5 cells (EB5: 14.7 (n=39), R1: 13.3 (n=21) and CCE: 16.5 (n=11)). In both cell lines, the number of chromocenters was smaller than in myoblasts and fibroblasts, arguing that the clustering behavior of pericentric heterochromatin correlates with the cell type and not with a specific cell line. However, even if there might be a transient increase in the chromocenter

¹ As already mentioned above „centromeric“ in the present text is used to describe the regions including both minor and major satellite sequences, although only minor satellite sequences are strictly speaking *centromeric* as only they are associated with the primary constriction/kinetochore (Mitchell 1996).

number during differentiation, terminally differentiated cells appear to represent an “end point” of clustering. In some extreme cases as in neuronal cells in the mouse retina (I. Solovei, personal communication) or in kidney cells (Cerdeira et al. 1999) the clustering actually reaches a maximum, where pericentric heterochromatin of all chromosomes is unified into one large structure.

This differentiation dependent reorganization of centromeric heterochromatin is consistent with results of Hsu et al. (Hsu et al. 1971), Chaly and Munro (Chaly and Munro 1996) and of Beil et al. (Beil et al. 2002). Hsu et al. showed already in 1971 by Giemsa staining of different mouse tissues that the number of pericentric heterochromatin clusters was cell type specific and proposed a “...tendency for more differentiated cell types to possess fewer heterochromatin blocks... than cells with a potential to proliferate. ...”. During *in vitro* myogenesis of rat myoblasts to myotubes Chaly and Munro reported also a noticeable aggregation of condensed chromatin visualized by electron microscopy. Using kinetochore staining with human CREST serum Beil and colleagues showed that clustering of centromeric regions increased during differentiation of the human promyelocytic leukemia cell line NB4 along the neutrophil pathway. In studies on differentiated, postmitotic Purkinje cells Manuelidis (Manuelidis 1985) and Solovei et al. (Solovei et al. 2004) describe also a strong clustering of pericentric heterochromatin, with chromocenters numbers varying between 2 and 10 in these cerebellar neurons. Moreover Solovei and co-workers using FISH with a major satellite specific probe confirmed a previous finding by Martou and de Boni (Martou and De Boni 2000), who had used kinetochore staining; both found that clustering of centromeric regions is dynamic during postnatal development of Purkinje neurons. After a transient increase in clustering 3 days after birth, centromeric regions split up again and finally remain constant in number until adulthood. Besides this reorganization in terms of cluster formation, all three studies demonstrated a spatial rearrangement of centromeric regions during postnatal development in which centromeric sites were redistributed from the nuclear periphery to the interior, surrounding one or two central nucleoli. Apart from these results obtained in rodents and humans there is recent still unpublished data on centromeric regions in the polyp hydra, which also confirms an increased clustering after differentiation of so-called interstitial cells (O. Alexandrova, personal communication; (Ebbing 2003)).

Therefore, one might speculate that aggregation of centromeric/pericentric heterochromatin represents an evolutionary conserved motif during terminal differentiation. It would be interesting to elucidate to what extent aggregation of heterochromatin during differentiation does also occur for non-centromeric regions, like interstitial constitutive heterochromatin, telomeres, transposable elements or heterochromatic regions on the Y chromosome. It would be also worth investigating how facultative heterochromatic regions like the inactive X-chromosome in female mammals behave, in order to enlighten the involvement of different types of heterochromatin in remodeling nuclear architecture during differentiation. The long term goal is to get a comprehensive view on the large scale reorganization of functionally different chromatin during differentiation. However, the oversimplified view of a dichotomous/tripartite chromatin classification with constitutive/facultative heterochromatin on the one hand and euchromatin on the other will have to be replaced by a more molecular defined subdivision, considering the individual composition of chromatin subtypes in respect to histone/DNA modifications, histone variants, and chromatin associated proteins.

The presented finding of a reproducible reorganization of pericentric heterochromatin during terminal differentiation is *per se* a fascinating phenomenon especially as there is indication for an evolutionary conservation. However, it remains enigmatic whether and to what extent this large-scale organizational rearrangement is functionally implicated in transcriptional regulation. Insights into the mechanisms underlying such major chromatin redistributions are

an important step towards assessing the question of a functional relevance, as they open the possibility to interfere with the proper action of a given system and in doing so, to test for relevant changes on a functional level. Consequently, the identification of MeCP2 as a central component involved in this machinery of centromeric heterochromatin clustering cannot be overestimated. The increase of endogenous MeCP2 levels during myogenesis¹ combined with its ability to induce clustering by high level ectopic expression argues for a strong involvement in the aggregation process of pericentric heterochromatin in differentiating cells. Although details on the actual mechanism can at this point only be speculative, some of the following considerations might help to focus on potential relevant factors.

An intuitive and comprehensible mechanism how increasing levels of MeCP2 could contribute to an aggregation of heterochromatin becomes evident if one posits an oligomerizing property of MeCP2. In an *in vitro* assay Georgel et al. (Georgel et al. 2003) tested the chromatin compaction ability of MeCP2 on nucleosomal arrays² and showed that it not only had a capacity to condense individual arrays, but that MeCP2 at higher concentrations had additionally the capability to interconnect individual arrays creating supra-structures consisting of several compacted oligonucleosome units. The authors proposed MeCP2-MeCP2 or DNA-MCP2-DNA bridges to explain the observed chromatin remodeling activities. Such interactions could also account for the observed clustering of pericentric heterochromatin during terminal differentiation. Elevated concentrations of MeCP2 at pericentric sites could simply increase the frequency of interconnections between individual chromocenters acting as heterochromatic “glue”. However, it should be added that in this *in vitro* assay by Georgel et al., MeCP2 was shown to interact with DNA independently of methylated cytosines. Still in the *in vivo* situation, a local increase in MeCP2 levels at methylated sites like in pericentric regions might be necessary to reach a certain threshold for an effective oligomerization or simply enhance this effect at these sites. This would also explain the concomitant increase in DNA methylation at pericentric sites in myotube nuclei compared to myoblasts as a “bait” to increase local MeCP2 concentrations. Further studies investigating the interaction capacities of MeCP2 will help to elucidate if such self-interactions between individual MeCP2 molecules or associations with other binding partners are responsible for the observed aggregation effect. A similar oligomerization based mechanism as the one just suggested for MeCP2 was described for chromatin compaction during avian blood cell development by the protein MENT (Myeloid and Erythroid Nuclear Termination stage-specific protein) (Grigoryev et al. 1992). This protein, which was assigned to the serpin protein family (Grigoryev et al. 1999) is highly expressed in terminally differentiated avian blood cells including erythrocytes, lymphocytes and granulocytes and was shown to be highly concentrated in heterochromatic regions (Grigoryev and Woodcock 1998). MENT was shown to bind DNA and nucleosomal arrays *in vitro* and to induce conformational changes leading to compaction as well as to oligomerization of oligonucleosomes (Grigoryev et al. 1999), just as described by Georgel et al. for MeCP2 (Georgel et al. 2003). This chromatin remodeling capacity of MENT was suggested to be caused by (1) a conformational transition, which had previously been shown to lead to polymerization in other serpins and (2) to the fact that MENT is a basic protein with high local concentrations of positive charges. Via these positively charged surface clusters MENT can undergo ionic interactions with DNA, similar to bivalent cations or linker histones which had been demonstrated previously to cause an increase in chromatin compaction (see citations in (Grigoryev and Woodcock 1998) and (Horn and Peterson 2002)). Since MeCP2 is also a highly basic protein (pI~9.9 (Kriaucionis and Bird 2004)), having a stretch of 7 (!) tandemly

¹ Kriaucionis and Bird showed in a very recent study that the concentration of MeCP2 mRNA increases also during neuronal differentiation of ES cells *in vitro* (Kriaucionis and Bird 2004).

² *In vitro* reconstituted oligonucleosomes.

arranged histidine residues at its C-terminal end, it could act in a similar way as proposed for MENT, linker histones or inorganic, bivalent cations by neutralizing negative charges on the DNA. This could enable or enhance interactions between major satellite DNA located on individual chromocenters.

However, this proposed “heterochromatic glue” hypothesis does not account for movements of individual heterochromatin cluster that are necessary to place individual chromocenters in physical proximity so that interactions can be established. Most of the available experimental *in vivo* studies argue against large-scale movements of chromatin during interphase but instead favor a concept of constrained diffusion (Shelby et al. 1996; Abney et al. 1997; Gerlich et al. 2003; Walter et al. 2003). Therefore a conceivable scenario for heterochromatin clustering could be that random spatial approximations of pericentric regions driven by diffusion could account for transient juxtapositions, which then could be stabilized by a high concentration of MeCP2, promoting inter-chromatic associations. In cell types with no or low levels of MeCP2 such juxtapositions of chromocenters would consequently be only temporary and less stable. However, an active or directed movement cannot be ruled out completely. In this respect, it would be interesting to test whether the observed aggregation of pericentric heterochromatin is energy dependent or temperature sensitive, which would argue for an active movement (Phair and Misteli 2000).

A further interesting aspect possibly involved in a mechanism aggregating pericentric heterochromatin is the finding that MeCP2 has been shown to recruit histone deacetylases (Nan et al. 1998) and histone methyltransferases (Fuks et al. 2003). Increased deacetylation or methylation of histones in pericentric regions prompted by MeCP2 could attract other chromatin remodeling complexes participating in the observed aggregation effect.

An expansion of the experiments, which I performed in the laboratory of Cristina Cardoso concerning the inducible clustering by ectopic expression of MeCP2 was recently carried out by Hariharan Easwaran from her group employing mouse embryonic fibroblasts lacking both histone H3 Lysine 9 (H3K9) methyltransferases, Suv39h1 and -h2. These enzymes are responsible for tri-methylation of histones H3 at lysine 9 at pericentric heterochromatin (Peters et al. 2003; Rice et al. 2003), which is a binding site for heterochromatin protein 1 (HP1) (Lachner et al. 2001). Double null fibroblasts consequently exhibit hypomethylated H3K9 at pericentric site¹ and a HP1 distribution that is homogenous and not concentrated at pericentric regions as in the wild type (Peters et al. 2001) (figure 4.7A). Double null fibroblasts transfected with MeCP2-YFP expressing high levels of the fusion protein were still exhibiting an increased clustering of chromocenters despite lacking di-/tri-methylated histones H3K9 and high levels of HP1 at pericentric sites (figure 4.7). This result clearly suggests that MeCP2 inducible aggregation of pericentric clusters is independent from the HP1/H3-K9 di-/tri-methylation pathway.

¹ Lachner et al. who generated these double null mice characterized Histone H3 K9 methylation with an antibody that retrospectively was shown to recognize di- as well as tri-methylated H3K9 epitopes (Perez-Burgos et al. 2004).

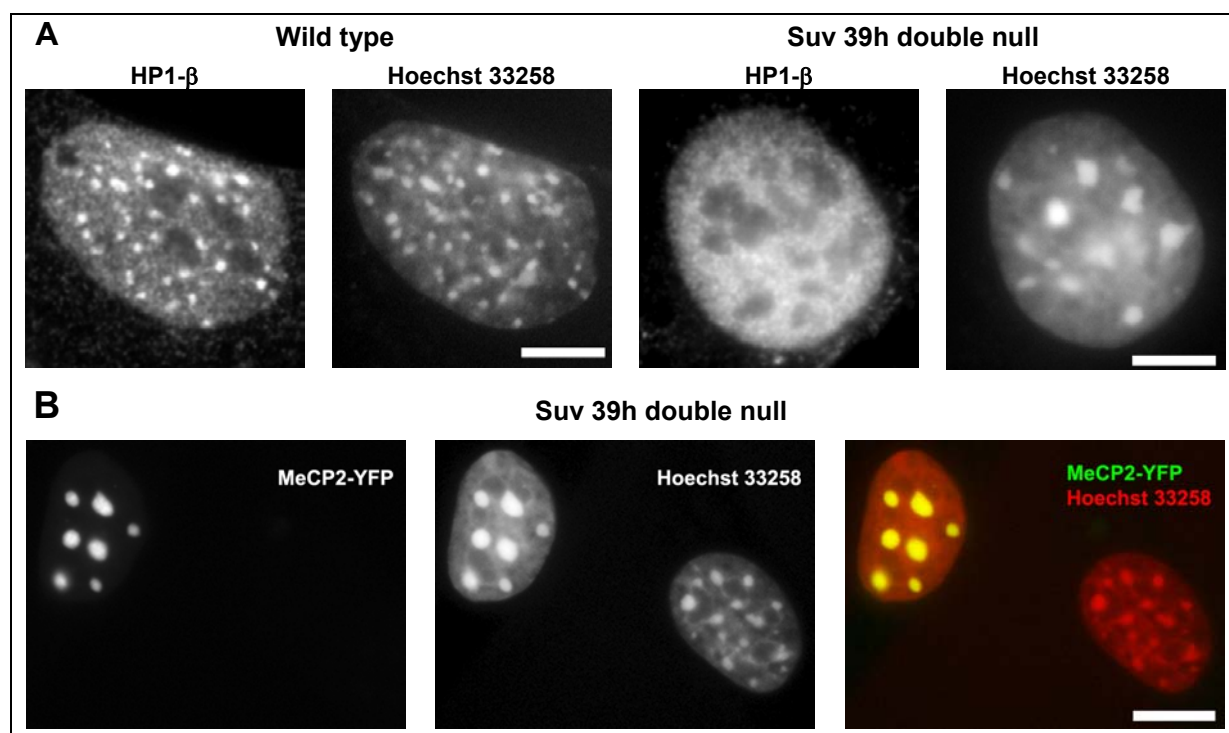


Figure 4.7: Suv 39h double null fibroblasts show clustering of chromocenters upon high level expression of MeCP2-YFP. (A) Epifluorescent images of wild type fetal fibroblasts and of fibroblasts derived from fetuses carrying a double knock out for histone methyltransferases Suv 39h1 and -h2. The lack of these enzymes results in a reduced methylation of histones H3 at lysine 9 at pericentric regions (not shown) and as a consequence in a loss of HP1 β binding at pericentric heterochromatin (pericentric regions are highlighted by intense Hoechst staining). Scale bar: 5 μ m (B) Panels show epifluorescent images of Suv39h double null fibroblasts transfected with MeCP2-YFP. Note that the nucleus with a high level of MeCP2-YFP has fewer chromocenters than the neighboring nucleus showing no expression at all. Aggregation of chromocenters by ectopic MeCP2-YFP expression consequently appears to be independent from tri-methylation of histone H3 at lysine 9 and from binding of HP1 β at pericentric sites. Scale bar: 10 μ m. (Images used with permission of Hariharan Easwaran)

What is behind the observed aggregation of centromeric regions during differentiation remains enigmatic but deserves some speculative deliberations.

(1) One possible reason was already proposed by Hsu et al., who to my knowledge was the first one describing a cell type specific arrangement of centromeric regions in mouse (Hsu et al. 1971). Using Giemsa staining on several different mouse cell types, he recognized the tendency of increased clustering in more differentiated cells (see above). His idea was that the organization of centromeric regions would reflect the organization of nucleoli since NORs reside proximal to mouse centromeric regions. Following his rationale, a reorganization of nucleoli during differentiation in the sense of a fusion of individual nucleoli and/or an additional recruitment of inactive NORs to perinucleolar regions could result in an increased accumulation of NOR bearing chromosomes at nucleolar sites. Due to the spatial proximity of rDNA and major satellite sequences on the respective chromosomes, such nucleolar reorganization would inevitably affect the distribution of the juxtaposed pericentric regions. Moreover the centromeric region of an NOR

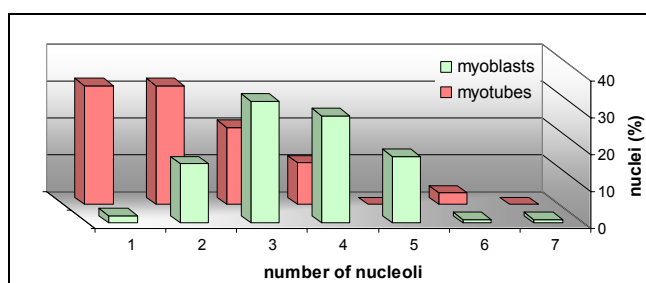


Figure 4.8: Number of nucleoli in myoblasts vs. myotubes. Note that upon myogenic differentiation the number of nucleoli is markedly reduced.

bearing chromosome could already be engaged with the centromeric region of a chromosome without an NOR constituting a common chromocenter, such that a redistribution of rDNA sequences would additionally affect the distribution of the “non-NOR” centromeric region. Chromosomes potentially carrying NORs are #12 and #15-#19 (Dev et al. 1977). In case that all of them would actually possess rDNA arrays the number of relevant chromosomes would sum up to almost a third of the mouse chromosome complement. In order to test for a reorganization of nucleoli during myogenesis I compared the number of nucleoli between myoblasts and myotubes and found a statistically significant decrease ($p < 0.001$) from 3.5 nucleoli per nucleus to 2.2 (figure 4.8)¹, which could account at least partially for the observed clustering of pericentric regions. Even if both phenomena appear to correlate, the question whether the reduced number of nucleoli is cause or consequence of the observed chromocenter aggregation remains unsolved. Concerning a possible recruitment of additional NORs as a potential reason causing congression of chromocenters, it should be noted that I did not observe that very large chromocenters consisting of centromeric regions from many chromosomes would effectively wrap around nucleoli, which would be indicative for an increased number of NORs participating in rRNA transcription. Big chromocenters were usually contacting nucleoli at a single spot. FISH experiments using rDNA specific probes would help to reveal whether clustering of chromocenters is correlated with the recruitment of additional NORs, enhancing the accumulation of centromeric heterochromatin at perinuclear sites.

(2) Another explanation for the observed clustering of chromocenters during differentiation could be an intrinsic affinity of pericentric heterochromatin to aggregate during interphase. In proliferating cells, this tendency would be counteracted by the dissociation and individualization of chromosomes during mitosis. In *in vivo* observations, I could actually follow such dissociations of chromocenters in G2 nuclei prior to mitosis (figure 3.30). Since terminally differentiated cells have exited the cell cycle and chromosomes are no longer subjected to mitotic events a “default” aggregation affinity would be untamed leading to very large clusters. Indeed such extreme cases with only one big chromocenter unifying all pericentric heterochromatin in one large cluster have been occasionally observed in mouse kidney cells (Cerdeira et al. 1999) and found in almost all photoreceptor cells in the mouse retina (personal communication I. Solovei). Following this reasoning, cells exiting the cell cycle should consequently show likewise a clustering effect even in the absence of differentiation. To test this I have compared the number of chromocenters of cycling mouse fibroblasts with that of G0 fibroblasts that had been serum starved for 3 days (figure 3.15). A slight decrease in the chromocenter number (21.1 ± 5.3 to 18.6 ± 3.5) was noticed, but which was not statistically significant ($p > 0.2$). It could well be that such a default aggregation mechanism might be dependent on additional factors that were not present in serum starved fibroblasts, since they were in a reversible state of cell cycle arrest, but which on the other hand might be present in terminally differentiated, irreversibly postmitotic cells. MeCP2, which was proposed to play a mechanistic role in clustering of centromeric regions (see above), could be such a factor. Therefore, it would be interesting to determine MeCP2 levels in cycling versus quiescent fibroblasts.

Both of the proposed scenarios describe the observed aggregation-phenomenon as a mere bystander effect without any functional relevance.

(3) A functional interpretation of the data would be that the reorganization of pericentric heterochromatin plays a role in establishing and/or maintaining a transcriptional program, which is specific for differentiated cells. The fact that heterochromatin, especially pericentric

¹ Nucleoli were visualized using anti-B23 (nucleophosmin) antibodies. Normalized cumulative frequencies of myoblasts (n=100) and myotubes (n=62) having 1 (minimum), 2, 3 etc. 7 (maximum) nucleoli were compared using a two sided Kolmogoroff Smirnov test.

is specific for differentiated cells. The fact that heterochromatin, especially pericentric heterochromatin conveys transcriptional silencing in many different settings, from position effect variegation (PEV) in drosophila (reviewed in (Weiler and Wakimoto 1995; Schotta et al. 2003)), over transgene silencing (Francastel et al. 1999) to endogenous gene silencing (reviewed in (Fisher and Merckenschlager 2002)) makes this idea very attractive. It is conceivable that the silencing effects depend on a threshold concentration of factors that are bound or attracted by pericentric heterochromatin or some of its constituents. Forming bigger cluster would thus lead to an increase of such a critical concentration leading to the formation of effective silencing domains. Our results showing that MeCP2, which is known to act as a transcriptional repressor, plays an important role in inducing aggregation of heterochromatin clusters favors this speculation. Moreover MeCP2 was shown to interact with the Sin3/histone deacetylase complex (Jones et al. 1998; Nan et al. 1998), as well as with a histone H3K9 methyltransferase (Fuks et al. 2003). Both enzymes introduce histone modifications that are involved in transcriptional repression (reviewed e.g. in (Jenuwein and Allis 2001; Czermin and Imhof 2003; Thiagalingam et al. 2003)). Increasing the local concentration of such regulatory chromatin modifiers at pericentric sites via MeCP2 could thus define a general nuclear silencing compartment. Experiments using tagged RNA precursors, like BrUTP, to visualize nascent RNA could show if transcription at/near chromocenters deviates substantially between terminally differentiated cells and their proliferating precursors.

The role of MeCP2 as a transcriptional repressor is to date still not completely clear. Because of its high binding affinity to methylated DNA, which is found genome wide at CpG dense regions of promoters, MeCP2 was initially thought to act as a global transcription repressor (Nan et al. 1997). Recent results however comparing transcription profiles of brain tissues of MeCP2 deficient mice with normal mice found only subtle changes (Tudor et al. 2002). Instead, three recent studies have demonstrated that two concrete target genes are regulated by MeCP2 binding at methylated promoter regions. Stancheva et al. showed that MeCP2 binding at a methylated site near the promoter region was involved in the transcriptional regulation of the *Hairy2a* gene in *Xenopus*, which codes for a protein involved in embryonic neurogenesis (Stancheva et al. 2003). Chen et al. (Chen et al. 2003) and Martinowich et al. (Martinowich et al. 2003) could show that KCl induced depolarization of rodent cortical neurons triggers transcriptional activation of the BDNF gene (brain-derived neurotrophic factor) involving MeCP2 release from the methylated promoter. The BDNF gene codes for a secreted protein essential for neural plasticity, learning and memory. Additionally Chen and colleagues found that upon induction of transcription MeCP2 was subjected to phosphorylation, while in the study by Martinowitch et al. a decrease in DNA methylation was observed. Both mechanisms were proposed to be involved in the loss of MeCP2 promoter binding during gene activation. An interesting finding concerning the regulation of BDNF was that in neurons lacking MeCP2, BDNF transcription levels in the uninduced state were only slightly elevated compared to neurons with functional MeCP2 (2% vs. 1% of the induced level), while transcription levels in the induced state were essentially the same. This argues that MeCP2 plays a role in repressing the basal transcription rate of its target genes. This might also explain why transcription-profiling approaches failed to detect such subtle changes that consequently might also affect transcription on a more global scale. A current idea is that MeCP2 might be involved in the reduction of transcriptional noise (Hendrich and Tweedie 2003). Actually, the function of MeCP2 could be bipartite. On the one hand, it could affect specific target genes in a dynamic way via reversible binding at methylated promoter regions as described for BDNF or *Hairy2a*. On the other hand, it could act globally by minimizing basal transcription rates of genes that are already inactive, but which have to be permanently and stringently silenced. In particular, the latter could be favored by a nuclear organization that provides a stringent suppression of leaky transcription by creating non-

permissive nuclear subcompartments. Noise minimization of gene expression has recently been shown to play a fundamental role for the cellular fitness in yeast (Fraser et al. 2004), and might also be relevant for multicellular organisms, especially in settings where a balanced concentration of many proteins acting in a precise concerted fashion is crucial, such as during development.

A possibility to test the hypothesis that heterochromatin aggregation is responsible for establishing/maintaining an adequate transcriptional program in terminally differentiated cells would be (1) to prohibit clustering in differentiating cells or (2) to disrupt clusters in already differentiated cells and to follow the effects on the differentiation status. Applying this to the myoblasts/myotube system might lead in case of a functional involvement (1) to a decrease in the differentiation potential of myoblasts or (2) to an impairment of myotube specific functions as contractility or even to re-differentiation events like re-entry into the cell cycle. In designing such experiments, one should be particularly cautious that while trying to affect clustering of pericentric heterochromatin by molecular means no additional global effects are induced that might also interfere with differentiation, which could lead to false positive results. A starting point for such experiments could be MeCP2 as it was shown by the presented results that it is capable to induce clustering. Using siRNA techniques against MeCP2 mRNA or depleting the protein using specific antibodies would be useful approaches to test if removal of the protein interferes with chromocenter clustering and myotube formation in differentiating myoblasts or if myotube nuclei would show increased splitting of chromocenters and signs of re-differentiation like DNA replication.

4.3 Concluding remarks and prospects

Admittedly, most yet not all of the results in the present thesis are descriptive. However, the impact of experiments designed to describe accurately changes or the invariability of a given system should not be underestimated. After all it were the descriptive findings of early cytologists at the turn of the century that, combined with the prime results of classical genetics presented by Gregor Mendel, culminated in the *chromosome theory of heredity*.

Choosing consciously a descriptive approach my main purpose was to investigate aspects of large-scale nuclear organization in different cell types and during terminal differentiation in order to look for stable motifs as well as for dynamic reorganization principles.

(1) One reason for describing stable organization patterns is to obtain a reference point through which anomalies can actually be defined. The correlation of such anomalies with functional impairments either on a cellular level or on the level of a complete organism, might serve as a first indication for a functional involvement. An example for such a correlation is the so-called Pelger Huët anomaly in human (Hoffmann et al. 2002) or the equivalent *ichthyosis* phenotype in mouse (Shultz et al. 2003). The genetic basis is a mutation of the lamin B receptor, which leads to hypo-lobulation of neutrophilic granulocytes and to an aberrant distribution of heterochromatin. Affected homozygous individuals show a developmental delay, epilepsy and skeletal abnormalities to a variable degree (Hoffmann et al. 2002), while homozygous mice exhibit alopecia, syndactyly and hydrocephalus, likewise to a variable extent (Shultz et al. 2003). Although neither the mechanisms responsible for the observed changes on the nuclear level nor the involvement of the lamin B receptor in the neurological, skeletal and developmental deficiencies are understood, it represents a striking example of the broad effects of mutations in a structural nuclear protein.

(2) The discovery of preserved organizational motifs among different species or even between clades indicates a strong selective force responsible for an evolutionary conservation, which does also suggest a functional implication. An example for such an evolutionary highly preserved organization is the intranuclear distribution of chromatin with a specific replication

timing (Nakayasu and Berezney 1989). Early replicating chromatin is distributed mainly within the nuclear interior, mid replicating DNA is concentrated at the nuclear periphery and around nucleoli, while late replicating chromatin is organized as bigger clusters at the nuclear periphery and in the interior. This distribution was shown to be present in many different species from man to hydra (Alexandrova et al. 2003) and even with some exceptions for late replicating chromatin in plants (Sparvoli et al. 1994; Mayr et al. 2003). Moreover, these replication patterns have been demonstrated to remain unchanged upon terminal differentiation of myoblasts to myotubes (Klier-Choroba 2002). Although the functional relevance of this spatial patterning of chromatin, which is equivalent to the G-(R) banding pattern of mitotic chromosomes (Ferreira et al. 1997; Sadoni et al. 1999) is not yet understood, it is speculated that spatial proximity of functionally equivalent chromatin might have evolved to facilitate interactions with other functional nuclear compartments, such as speckles that are enriched for splicing factors (Shopland et al. 2003).

(3) The detection of a reproducible, dynamic reorganization of nuclear architecture concomitant with functional alterations, as e.g. during cellular differentiation suggests a possible functional implication of the observed phenomenon. However, the mere description of such a correlation leaves the question unanswered, whether the observed reorganization is cause or consequence of the paralleling functional changes. An important step towards this answer is the assessment of the underlying mechanisms. The identification of involved constituents opens the possibility (a) to search for further contributing elements and (b) to interfere with the proper progression of a given mechanism and by doing so to test for functional significance.

In the present thesis, I investigated several cell culture systems of mouse and found both (1) a stable distributional pattern of chromosome territories that was apparently independent of cellular differentiation and (2) a reorganization of pericentric heterochromatin that changed markedly and reproducibly during terminal differentiation. Moreover, I was able to identify MeCP2 as a key player in the reorganization of chromocenters during terminal differentiation. The finding that in mouse gene dense #11 CTs localize more internally and gene poor #X CTs more peripheral, expands the present hypothesis of an evolutionary conserved radial distributional pattern that to date has been approved for humans, higher primates and chicken. Additional studies with other species and the employment of sub-chromosomal probes, which offer a better resolution than whole chromosome painting probes, will help to develop a more detailed distribution map of functionally distinct chromosome regions. It would be also interesting to describe the intranuclear distribution of *de facto* transcribed genes within a given cell type instead of gene rich regions *per se*, especially in relation to functionally relevant nuclear compartments involved in transcription or mRNA processing. Moreover, the characterization of sequences that have the ability to interact with structural components of the nuclear envelope or with nucleoli will help to enlighten additional organizational principles of nuclear order.

The finding of an increased clustering of centromeric regions during terminal differentiation represents an important starting point for further investigations on the influence of nuclear organization on broad transcriptional changes. Especially the discovery of MeCP2 as a major component of this differentiation dependent aggregation, with its ability to induce clustering can be considered a first step towards understanding the mechanism of this large-scale reorganization of nuclear topology. It will be important to investigate whether protein levels of endogenous MeCP2 increase also during other differentiation pathways that are correlated with increased chromocenter clustering like the differentiation of ES cells to macrophages, in order to test whether it is a general clustering mechanism. Functional assays trying to pinpoint the protein domains, which are essential for clustering, but also the search for interac-

tion partners of MeCP2 will help to further the understanding of the essential mechanism. Messing this mechanism or what is known of it should furthermore help to enlighten, whether changing a specific centromeric organization interferes with functional aspects of differentiation.

5 Appendix

5.1 Materials

5.1.1 Chemicals and enzymes

Chemicals	Company, distributor	URL
1M Tris-HCl pH 7.5	Sigma-Aldrich, Deisenhofen	www.sigmaaldrich.com
Agarose SEAKEM ME	FMC, Rockland ME, USA- Biozym Diagnostik GmbH, Oldendorf	www.biozym.com
BSA (fraction V) (PBS solutions)	Sigma-Aldrich, Deisenhofen	www.sigmaaldrich.com
BSA (fraction V) (SSC solutions)	ICN Biomedicals GmbH, Eschwege	www.icnbiomed.com
Calciumchloride	Merck, Darmstadt	www.merck.com
Colcemide (10 µg/ml)	Biochrom AG, Berlin	www.biochrom.de
Dextranulphate	Amersham Biosciences Europe GmbH, Freiburg	www4.amersham biosciences.com
Diethyl ether	Merck, Darmstadt	www.merck.com
Dimethylsulphoxide (DMSO)	Sigma-Aldrich, Deisenhofen	www.sigmaaldrich.com
Disodium hydrogen phosphate dihydrate	Merck, Darmstadt	www.merck.com
EDTA (Titriplex III)	Merck, Darmstadt	www.merck.com
Ethanol absolute (type 642, 510)	Bundesmonopolverwaltung für Branntwein, München	www.bfb-bund.de
Ethidium bromide	Sigma-Aldrich, Deisenhofen	www.sigmaaldrich.com
fetal calf serum (FCS)	Biochrom AG, Berlin	www.biochrom.de
Ficoll-Paque PLUS	Amersham Biosciences Europe GmbH, Freiburg	www4.amersham biosciences.com
Formaldehyde (37%)	Sigma-Aldrich, Deisenhofen	www.sigmaaldrich.com
Formamide	Merck, Darmstadt	www.merck.com
Gel-loading-buffer (6x)	Sigma-Aldrich, Deisenhofen	www.sigmaaldrich.com
Glacial acetic acid	Merck, Darmstadt	www.merck.com
Glycerin	Merck, Darmstadt	www.merck.com
HCl 1N	Merck, Darmstadt	www.merck.com
Heparin	Braun, Melsungen	www.bbraun.de
HEPES	Merck, Darmstadt	www.merck.com
hydrofluoric acid (conc.)	Copalit-GmbH, Hamburg	-
Isopropanol	Merck, Darmstadt	www.merck.com
Magnesiumchloride	Merck, Darmstadt	www.merck.com
Methanol	Merck, Darmstadt	www.merck.com
Nitrogen (liquid)	Messer Griesheim GmbH, Krefeld	www.messer.de
Paraformaldehyde	Merck, Darmstadt	www.merck.com
Penicillin/streptomycine	Biochrom AG, Berlin	www.biochrom.de
Phytohaemagglutinin (PHA-E)	Biochrom AG, Berlin	www.biochrom.de
Poly-L-Lysine	Sigma-Aldrich, Deisenhofen	www.sigmaaldrich.com
Polyfect Transfection Reagent	Qiagen, Hilden	www.qiagen.com
Potassium chloride	Merck, Darmstadt	www.merck.com
Potassium dihydrogen phosphate	Merck, Darmstadt	www.merck.com

Silica gel with moisture indicator	Merck, Darmstadt	www.merck.com
Sodium acetate	Merck, Darmstadt	www.merck.com
Sodium Azide	Merck, Darmstadt	www.merck.com
Sodium chloride	Merck, Darmstadt	www.merck.com
Sodium citrate dihydrate	Merck, Darmstadt	www.merck.com
Triton X-100	Merck, Darmstadt	www.merck.com
Trolox™	Fluka, Sigma-Aldrich, Deisenhofen	www.sigmaaldrich.com
Tween 20	Merck, Darmstadt	www.merck.com

Cell culture materials	Company, distributor	URL
Dulbeccos MEM	Biochrom AG, Berlin	www.biochrom.de
Fetal bovine serum (FBS)	Biochrom AG, Berlin	www.biochrom.de
Ham's F10	Biochrom AG, Berlin	www.biochrom.de
Horse serum	Gibco™/Invitrogen, Karlsruhe	www.invitrogen.com
Meliseptol	B.Braun Biotech International, Mellungen	www.bbraunbiotech.com
Penicillin/streptomycin	Biochrom AG, Berlin	www.biochrom.de
RPMI-1640 Medium	Biochrom AG, Berlin	www.biochrom.de
Trypsin/EDTA (10x)	Biochrom AG, Berlin	www.biochrom.de
enzymes & buffers	Company, distributor	URL
10xTrypsin/EDTA	Biochrom AG, Berlin	www.biochrom.de
DNA-Polymerase I (Kornberg-Polymerase)	Roche, Mannheim	www.roche.de
DNase I	Roche, Mannheim	www.roche.de
MgCl ₂ solution (25mM) for PCR	Perkin Elmer, Wellesley, USA	www.perkinelmer.com
PCR-Puffer (10x)	Perkin Elmer, Wellesley, USA	www.perkinelmer.com
Pepsin	Sigma-Aldrich, Deisenhofen	www.sigmaaldrich.com
Nick translation buffer (10x)	Roche, Mannheim	www.roche.de
Proteinase K	Roche, Mannheim	www.roche.de
Taq-polymerase	Amersham Biosciences Europe GmbH, Freiburg Invitrogen GmbH, Karlsruhe	www4.amershambiosciences.com www.invitrogen.com

Nucleotides & DNA	Company, distributor	URL
Biotin-16-dUTP	Roche, Mannheim	www.roche.de
dATP, dCTP, dGTP, dTTP	Amersham Biosciences Europe GmbH, Freiburg	www4.amershambiosciences.com
Digoxigenin-11-dUTP	Roche, Mannheim	www.roche.de
DNP-11-dUTP	NEN Life Science Products, Inc, Boston	www.nen.com
Lambda/Hind III marker	MBI Fermentas, St.Leon-Rot	www.fermentas.de
mouse C ₀ t-1 DNA	Invitrogen GmbH, Karlsruhe	www.invitrogen.com
Salmon sperm DNA	Invitrogen GmbH, Karlsruhe	www.invitrogen.com

Primer	Company ,distributor	URL
6MW	MWG-Biotech, Ebersberg	www.mwg-biotech.com
Major satellite primer 1(5'→3'): GCGAGAAAACCTGAAAATCAC Major satellite primer 2(5'→3'): TCAAGTCGTCAAGTGGATG	MWG-Biotech, Ebersberg	www.mwg-biotech.com
Telomere primer: Tel1: (TTAGGG) ₅ Tel2: (CCCTAA) ₅	Gene centre Munich, AG Arnold	www.lmb.uni-muenchen.de
Antibodies	Company, distributor	URL
Primary antibodies		
Avidin-Cy5	Sigma-Aldrich, Deisenhofen	www.sigmaaldrich.com
Avidin-FITC	Vector, Burlingame CA, USA	www.vectorlabs.com
CREST antiserum	Euroimmun, Lübeck	www.euroimmun.de
Goat- α lamin B	Santa Cruz Biotechnology,	www.scbt.com/
Mouse- α digoxigenin	Sigma-Aldrich, Deisenhofen	www.sigmaaldrich.com
Mouse- α digoxigenin-Cy3	Diananova, Hamburg	www.dianova.de
Mouse- α digoxigenin-Cy5	Diananova, Hamburg	www.dianova.de
Rabbit- α digoxigenin	Sigma-Aldrich, Deisenhofen	www.sigmaaldrich.com
Rabbit- α MeCP2	Upstate, Lake Placid NY, USA	www.upstate.com
Rat- α Cd11b	gift from Constanze Bonnifer (Leeds)	www.leeds.ac.uk
Rat- α M31 (human HP1)	Serotec GmbH, Düsseldorf	www.serotec.co.uk
Sheep- α digoxigenin-FITC	Diananova, Hamburg	www.dianova.de
Secondary antibodies		
Goat- α avidin-Biotin	Vector, Burlingame CA, USA	www.vectorlabs.com
Goat- α avidin-FITC	Sigma-Aldrich, Deisenhofen	www.sigmaaldrich.com
Goat- α mouse-AlexaFluor350	Molecular probes, Leiden	www.probes.com
Goat- α mouse-Cy5	Diananova, Hamburg	www.dianova.de
Goat- α rabbit-Cy3	Sigma-Aldrich, Deisenhofen	www.sigmaaldrich.com
Goat- α rabbit-Cy5	Amersham Biosciences Europe GmbH, Freiburg	www4.amersham-biosciences.com
Goat- α rabbit-FITC	Sigma-Aldrich, Deisenhofen	www.sigmaaldrich.com
Rabbit- α goat-FITC	Sigma-Aldrich, Deisenhofen	www.sigmaaldrich.com
Rabbit- α human-Cy3	Diananova, Hamburg	www.dianova.de
Sheep- α mouse-Cy3	Diananova, Hamburg	www.dianova.de
Sheep- α mouse-Cy3	Diananova, Hamburg	www.dianova.de
Sheep- α mouse-FITC	Sigma-Aldrich, Deisenhofen	www.sigmaaldrich.com
DNA stains, antifade-solutions		
4',6-Diamidino-2-phenylindole (DAPI)	Sigma-Aldrich, Deisenhofen	www.sigmaaldrich.com
Propidiumiodide (PI)	Sigma-Aldrich, Deisenhofen	www.sigmaaldrich.com
SYTO 16	Molecular probes, Leiden	www.probes.com
TO-PRO-3 iodide	Molecular probes, Leiden	www.probes.com
Vectashield® mounting medium	Vector, Burlingame CA, USA	www.vectorlabs.com

5.1.2 Media, buffers and solutions

Item	Constituents	Annotations
2M CaCl ₂ -161.3mM Tris pH 7.6	2M CaCl ₂ , 161.3mM Tris-HCl	2.22g CaCl ₂ + 1.61ml 1M Tris-HCl pH 7.5 + 0.65ml 1N NaOH → ad 10ml using H2O bidest. → adjust pH to 7.6 → use sterile filtered. Store at -20°C
4×SSC/Tween Agarose gel	0.2 % Tween 20 in 4×SSC 1% agarose in TAE-buffer	2 ml in 1000 ml 4×SSC 5 g in 500 ml, warm up in a microwave, sway every 3 to 4 minutes, until solution is clear, cool down to ~60°C before pouring
Blocking solution (SSCT) Blocking solution (PBT)	4 % BSA (ICN) in 4×SSC/Tween 4 % BSA (Sigma) in PBS/Tween	Diluted from 10% BSA in 4×SSC stored at 4°C Diluted from 10% BSA in PBS stored at 4°C
DAPI stock solution	0.2 mg/ml in H2O bidest	use sterile filtered
Differentiation medium	500ml Dulbeccos MEM + 50ml horse serum + 5ml penicillin/streptomycine	Preheat to 37°C when used in regular cell culture
DMEM complete medium for fibroblasts	500ml Dulbeccos MEM + 50ml FCS + 5ml penicillin/streptomycine	Preheat to 37°C when used in regular cell culture
DMEM complete medium for myoblasts (C2C12)	400ml Dulbeccos MEM + 100ml FCS + 5ml penicillin/streptomycine	Preheat to 37°C when used in regular cell culture
dNTP-Mix	5 mM dATP, dTTP, dGTP and dCTP	25 µl of dATP, dGTP, dCTP, dTTP (100 mM) each + 400 µl H2O bidest. (autoclaved)
Ethanol (30%, 50%, 70%, 90%)	ethanol (type 642 or 510)	30,50,70,90 ml EtOH → ad 100 ml using H2O bidest.
F10 complete medium	400ml Ham's F10 + 100ml FCS + 5ml penicillin/streptomycine	Preheat to 37°C when used in regular cell culture
Fixative (Carnoy's) freezing medium	Methanol/acetic acid 3:1 (v/v) 10 % DMSO in cell type specific working medium	Freshly made, stored at -20°C 45ml DMEM working medium + 5ml DMSO
Glycerol (20%) Glycerol shock solution	20% glycerol in 1xPBS 1xHEBS, 15% glycerol	100ml Glycerol + 400ml 1xPBS 5ml 2xHEBS + 1.5ml glycerol + 3.5ml H2O bidest. → use sterile filtered. Store at -20°C
HCl (0.1M)		50 ml HCl (1M) + 450 ml H2O bidest.
HEBS	2xHEBS: 280mM NaCl, 50mM HEPES, 1.5mM Na ₂ HPO ₄	20xHEBS: 8.16g NaCl + 5.95g HEPES + 0.106g Na ₂ HPO ₄ → ad 50ml using H2O bidest. → use sterile filtered. Store at -20°C 2xHEBS: 1ml 20xHEBS → ad 10ml using H2O bidest. → adjust pH to 7.1 with 1N NaOH → use sterile filtered. Store at -20°C
Hybridization mastermix	20% dextran sulphate in 2×SSC	Dissolve 8g in 40 ml 2×SSC, vortex, filter using 0.45µm filter and aliquot. Store at -20°C
KCl-solution 0.56%	0.075 M KCl in H2O bidest.	Dissolve 0.56g in 100 ml H2O bidest.
NaOH (1N)	1N NaOH in H2O	4g NaOH → ad 100ml using H2O bidest.

Item	Constituents	Annotations
Nick translation stop-Mix	0.1% Bromophenol Blue, 0.5% Dextran blue, 0.1M NaCl, 20mM EDTA, 20mM Tris-HCl pH 7.5	40mg Bromophenol Blue + 200mg Dextran blue + 800µl 5M NaCl + 1,6ml 0,5M EDTA + 800µl 1M Tris-HCl pH 7,5
Paraformaldehyde (4%)	4% paraformaldehyde in 1x, 0.5x or 0.3xPBS	4g paraformaldehyd → ad 100 ml mit 1xPBS (0.5x or 0.3x) → adjust pH to 7,4 → dissolve by heating and stirring. Avoid boiling. Always freshly made!
PBS-buffer (pH 7.4)	140 mM NaCl, 2,7 mM KCl, 6,5 mM Na ₂ HPO ₄ , 1,5 mM KH ₂ PO ₄	20xPBS: 160 g NaCl, 4 g KCl, 36 g Na ₂ HPO ₄ · 2 H ₂ O, 4,8 g KH ₂ PO ₄ → ad 1 l H ₂ O bidest. adjust pH to 7,4 with 1M HCl → dilute to 1xPBS Cell culture: Autoclave appropriate aliquots Laboratory use.: Add 4g Na-Azide to 10l Na-Azide (0,04%)
pepsinization solution	0.005% Pepsin in 0,01M HCl	50µl Pepsin (10%) + 10ml 0,1M HCl → ad 100ml using H ₂ O bidest. → warm up to 37°C
Propidiumiodide solution	10 µg/ml	
RPMI 1640 complete medium	480 ml RPMI 1640 + 80 ml FCS + 5 ml Penicillin/Streptomycin	Preheat to 37°C when used in regular cell culture
solution for denaturing slides	70% formamide in 2xSSC	50 ml 20xSSC + 350 ml formamide + 100 ml H ₂ O bidest. adjust to pH 7.0 with 1 M HCl, store at -20°C; solution can be reused 5 times
SSC-buffer (pH 7.0)	150mM NaCl, 15mM Na-Citrate	20 x SSC: 175,3 g NaCl + 88,2 g Na-Citrat → ad 1l using H ₂ O bidest., adjust pH to 7.0 with NaOH → dilute to 4x, 2x or 0,1xSSC Cell culture: Autoclave appropriate aliquots Laboratory use.: Add 4g Na-Azide to 10l Na-Azide (0,04%)
Storing solution for fixed cells	50% formamide in 1xSSC	250ml formamide + 250ml 2xSSC → adjust pH 7,4 with
TAE-Puffer (pH 8.0)	40mM Tris-Acetat, 1mM EDTA	50xTAE: 242 g Tris + 8,6 g EDTA + 57,1 ml glacial acetic acid → ad 1l using H ₂ O bidest. → adjust pH to 7.0 with glacial acetic acid → dilute to 1xTAE
TOPRO-3 iodide stock solution	1mM TOPRO in DMSO	
Triton X-100 permeabilisation solution	0.5% TritonX100	0.5 ml Triton X-100 → ad 100ml using 1xPBS → dissolve by stirring
Trolox	100mM	Dissolve 100µg in 430µl methanol → wait until crystals disappear → add 3,2 ml H ₂ O bidest. → add 330 µl 1N NaOH → pH should be between 9,0 and 9,5 or
	10mM	Dissolve 100µg in 430µl methanol → add 39ml H ₂ O bidest → add 330µl 1N NaOH pH should be between 6,0 and 6,5 ¹

¹ Protocol from the laboratory of M. C. Cardoso, Max-Delbrück-Center, Berlin.

5.2 Equipment and software

5.2.1 Glass, plastic ware and other implements

Items	Company ,distributor	URL
6 well plates	Greiner bio-one, Frickenhausen	www.greinerbioone.com
Cell culture flasks (75cm ² , 25cm ²)	Falcon/Becton Dickinson, S. Jose Greiner bio-one, Frickenhausen	www.bd.com www.greinerbioone.com
Coverslips 12×12mm	Hecht Assistant, Sondheim	www.hecht-assistent.de
Coverslips 15×15mm	Menzel-Gläser, Braunschweig	www.menzel.de
Coverslips 18×18mm	Marienfeld, Lauda-Königshofen	www.superior.de
Coverslips 20×20mm	Marienfeld, Lauda-Königshofen	www.superior.de
Coverslips 22×22mm	Hecht Assistant, Sondheim	www.hecht-assistent.de
Coverslips 24×24mm	Marienfeld, Lauda-Königshofen	www.superior.de
Coverslips 24×60mm	Menzel-Gläser, Braunschweig	www.menzel.de
Coverslips 26×76mm	Hecht Assistant, Sondheim	www.hecht-assistent.de
Coverslips, photoetched 23×23mm	Bellco Glass, Inc., Vineland	www.bellcoglass.com
Cryo vials 2ml	Greiner bio-one, Frickenhausen	www.greinerbioone.com
Forceps	Dumont, Montignez	www.dumonttools.com
Freezing box (filled with isopropanol)	Nalgene, Rochester	http://nalgene.com/nalgenunc.com/
Glass marker diamond	Kraus & Winter, Hamburg	www.kraus-und-winter.de
Gloves Nitril	Ansell, Richmond	www.ansell.com
Gloves Latex	Meditrade, Kiefersfelden	www.meditrade.de
Metal box with lid (for surgical instruments)	Schubert Medizinprodukte GmbH,	www.schubert24.de
Mikro-Pipette tips	Greiner bio-one, Frickenhausen	www.greinerbioone.com
Mikro-Pipettes (2µl, 10µl, 200µl, 1000µl)	Gilson, Inc., Middleton	www.gilson.com
Nail polish	Manhattan, Müller GmbH & Co. KG, Ulm-Jungingen	www.mueller.de
Parafilm-M®	Pechiney Plastic Packaging, Inc., Neenah	www.parafilm.com
Pasteur pipettes	Falcon/Becton Dickinson, S. Jose	www.bd.com
PCR test tubes 0.5 ml	Molecular Bioproducts, S. Diego	www.mbpinc.com
Plastic dishes, different sizes, round and square	Falcon/Becton Dickinson, S. Jose Greiner bio-one	www.bd.com www.greinerbioone.com
Quadriperms (4 well plates)	VivaScience AG, Hannover	www.vivascience.de
Rubber cement	Marabu, Tamm	www.marabu.de
Safety pipette filler	Deutsch & Neumann, Berlin	www.deutsch-neumann.com
Slide briefcases and boxes	Schubert Medizinprodukte GmbH,	www.schubert24.de
Slides 76×26 mm	R. Langenbrinck, Teningen	www.r-langenbrinck.de
Staining Jars acc. to Coplin Staining Jars acc. to Hellendahl	Hecht Assistant, Sondheim	www.hecht-assistent.de
Sterile plastic pipettes 25ml, 10ml, 5ml, 2ml, 1ml	Falcon/Becton Dickinson, S. Jose	www.bd.com
Sterile tubes 50ml/15ml	Falcon/Becton Dickinson, S. Jose	www.bd.com

Test tubes 1.5ml/2ml	Eppendorf, Hamburg	www.eppendorf.com
----------------------	--------------------	-------------------

5.2.2 Various technical equipment

Items/type	Company ,distributor	URL
Centrifuge/Biofuge pico	Kendro, Langenselbold	www.kendro.com
Centrifuge/Rotana / S	Hettich, Tuttlingen	www.hettichlab.com
CO2 incubator/BB6220 CU	Kendro, Langenselbold	www.kendro.com
CO2 incubator/Hera Cell	Kendro, Langenselbold	www.kendro.com
freezer (−80°C)/6485	GFL, Burgwedel	manuf.labworld-online.com/gfl
Freezers/various types (−20°C)	Privileg/Quelle, Fürth AEG, Frankfurt a. M.	www.privileg.de www.aeg.de
fridge (+4°C)	Bosch, Gerlingen-Schillerhöhe	www.bosch.de
Gel electrophoresis chamber & equipment, various sizes	Owl Scientific Inc., Portsmouth	www.owlsci.com
Gel imager	MWG-Biotech, Ebersberg	www.mwg-biotech.com
Heating block/DB 2-D	Techne, Cambridge	www.techne.com
Ice machine/AF-10	Scotsman, Bettolino di Pogliano	www.scotsman-ice.com
Incubator/Certomat HK	B.Braun Biotech International, Melsungen	www.bbraunbiotech.com
Laminar air flow cabinet	Biohit, Helsinki	www.biohit.com
Living cell chamber including temperature controller	Biopetechs, Beck Rd. Butler	www.biopetechs.com
Magnetic stirrer/IkaMag RH	Ika Labortechnik, Staufen	www.ika.de
Magnetic stirrer/RCT basic	Ika Labortechnik, Staufen	www.ika.de
Minicentrifuge	National Labnet, Woodbridge	www.labnetlink.com
pH-meter/pH538	WTW, Weilheim	www.wtw.com
Reflex camera/Ricoh XR/KR 10-M	Ricoh, Frankfurt, a.M.	www.ricoh.de
Test tube rotator/34528	Snijders, Tilburg	www.snijders-tilburg.nl
Thermocycler/Techne Progene	Techne, Cambridge	www.techne.com
Vacuum centrifuge/BaVaco-M Mini-30	Bachhofer, Reutlingen	-
Vortexing machine	Ika Labortechnik, Staufen	www.ika.de
Water baths/1004	GFL, Burgwedel	manuf.labworld-online.com/gfl
Water baths/5	Julabo, Seelbach	www.julabo.de
Water baths/M12	Lauda, Lauda-Königshofen	www.lauda.de
Weighing machine/ 2254	Sartorius, Göttingen	www.sartorius.de

5.2.3 Optics

Microscopes and accessories	Specifications	Manufacturer
Phase contrast microscope Objectives	Axiovert 25 C CP Achromat, 5x/0,12 CP Achromat, 10x/0,25 Ph1 LD Achromat, 20x/0,3 Ph1 Achromat, 40x/0,55 Ph2	Zeiss, Jena
Digital camera	Nikon N90 reflex camera equipped with a Kodak DCS 460 digital imaging device (6 Mpixel resolution)	Kodak, Stuttgart

<p>Fluorescence microscope objectives</p> <p>dichroic filter sets</p> <p>CCD-Kamera</p>	<p>Axiophot 2</p> <p>Plan-Neofluar 16×/0,5</p> <p>Fluar 40×/1,3 Oil, Ph 3</p> <p>Plan- Neofluar 40×/1,3 Oil</p> <p>Plan-Apochromat 63×/1,4 Oil</p> <p>Plan-Neofluar 100×/1,3 Oil</p> <p>DAPI (BP 365; FT 395; LP 450-490)</p> <p>FITC (BP 450-490; FT 510; LP 515-565)</p> <p>TRITC/Cy3 (BP 546; FT 580; LP 590)</p> <p>Cy5 (BP 575-625; FT 645; BP 660-710)</p> <p>Triple Filter (TBP400/495/570;FT410/505/585; TBP460/530/610)</p>	<p>Zeiss, Jena</p> <p>Coolview CCD Camera System</p>
<p>Leica Confocal Laser Scanning Microscope</p> <p>objectives</p> <p>Laser</p> <p>Beam splitters</p> <p>Emission filters</p>	<p>TCS SP</p> <p>Plan-Apochromat 100×/1,4 Oil</p> <p>Argon: 457/488/514nm laser lines</p> <p>Helium/Neon 633 nm laser line</p> <p>RSP 525: emission spectrum red</p> <p>RSP 650: emission spectrum infrared</p> <p>TD 488/568/647: for emission spectrum green and for green red combinations</p> <p>AOTF: Acousto Optical Tunable Filter</p>	<p>Leica, Heidelberg</p>
<p>Zeiss Confocal Laser Scanning Microscope</p> <p>objectives</p> <p>Laser</p> <p>Beam splitters</p> <p>Emission filters</p>	<p>LSM 410</p> <p>Plan-Neofluar 10x/0.3 Ph1</p> <p>Plan-Apochromat 63×/1.4 Oil</p> <p>Argon: 488nm</p> <p>Helium/Neon1: 543nm laser line</p> <p>Helium/Neon2: 633nm laser line</p> <p>FT 488/543</p> <p>BP 502-542: emission spectrum green</p> <p>LP 570: emission spectrum red</p> <p>BP 575-640: emission spectrum red</p> <p>LP 650: for emission spectrum infrared</p>	<p>Zeiss, Jena</p>
<p>Zeiss Confocal Laser Scanning Microscope</p> <p>objectives</p> <p>Laser</p> <p>Beam splitters</p> <p>Emission filters</p>	<p>LSM 510 Meta</p> <p>Plan-Neofluar 20x/0.5 I</p> <p>Plan-Apochromat 63×/1.4 Oil Ph3</p> <p>Argon: 488</p> <p>Helium/Neon1: 543nm laser line</p> <p>Helium/Neon2: 633nm laser line</p> <p>HFT UV/488/543/633</p> <p>BP 500-530 IR: emission spectrum yellow</p> <p>BP 565-615 IR: emission spectrum red</p> <p>LP 650 : emission spectrum infrared</p>	<p>Zeiss, Jena</p>

5.2.4 Software

Software	Manufacturer	URL
Imaging		
Adobe Photoshop® 7.0	Adobe Systems, Inc., S. Jose	www.adobe.de
Cytovision	Applied Imaging International Ltd, Newcastle Upon Tyne	www.cytovision.com
Image J (v1.29)	National Institute of Health, USA	rsb.info.nih.gov/ij
Irfan View version 3.8	Irfan Skiljan, Wiener Neustadt	www.irfanview.com
Leica-TCS NT	Leica, Heidelberg	www.leica- microsystems.com
LSM 410 software version 3.95	Zeiss, Jena	www.zeiss.de
LSM 510 software version 3.2	Zeiss, Jena	www.zeiss.de
Zeiss Image Browser	Zeiss, Jena	www.zeiss.de
Other		
3D-RRD	Developed by J. von Hase / Ruprecht-Karls-Universität Heidelberg (von Hase 2002)	-
Adobe Acrobat version 5.0	Adobe Systems, Inc., S. Jose	www.adobe.de
Adobe After Effects version 5.5	Adobe Systems, Inc., S. Jose	www.adobe.de
Amira version 3.0	TGS Europe, Merignac Cedex	www.amiravis.com
Endnote version 6.0	Thomson/ISI Researchsoft, Carlsbad	www.endnote.com
Microsoft Office 2002	Microsoft, USA	www.microsoft.com
Quicktime version 4.0	Apple, Cupertino	www.apple.com/quicktime
SPSS version 11.5	SPSS, USA	www.spss.com

	Pm128		C2C12		Lymphocytes	Fibroblasts
	myoblasts	myotubes	myoblasts	myotubes		
Source	H. Wehner, Institute for Diabetes Research, Munich		M. C. Cardoso, Max-Delbrück-Centre, Berlin		M. Moor, Department of Molecular Animal Breeding and Genetics in Munich	A. Pfeifer, Institute of Pharmacology, Munich
Medium	F10 complete medium	Differentiation medium	DMEM complete medium (20%FCS)	Differentiation medium	RPMI 1640 complete medium. Only for isolation → no stimulation	DMEM complete medium (10% FCS)
Temperature CO₂	37°C 5%	37°C 5%	37°C 5%	37°C 5%	37°C 5%	37°C 5%
Splitting rate	-1/4 every other day during the first passages, -1/10 every other day during log-phase.		1/8 every other day	-	-	1/2 every third day
Karyotype*	39, X0	See myoblasts	Hypotetraploid. Many chromosomes showed 4 or 3 copies, some 2 and only a few 1. Only a few translocations were observed.	See myoblasts	n.d.	Not karyotyped in detail, but metaphase spread showed normal number of chromosomes (2n=40) and Robertsonian translocations
Annotations	Cells were originally isolated by Irintchev et al. from hind limb musculature (Irintchev, 1997)	Cells were regarded as myotubes if they contained at least 3 nuclei in an elongated cytoplasmic body.	C2C12 cells were subcloned in Helen Blaus lab (Bains, 1984) from the C2 line of David Yaffe (Yaffe, 1977).	Myotube definition as in Pm128.	Blood drawn from male mouse-hybrids C3HeB/FeJ.	Cells were pooled from normal 14 days old male and female embryos.

Table 5.1: Table 5.1: Utilized cell lines and differentiated derivatives are shown with the most important cell culture parameters. Details on myoblast differentiation and lymphocyte isolation are described in 2.1.4. *Karyotype analysis were performed by Isabell Jentsch, Institute of Human Genetics, Munich using multiplex-FISH (Jentsch et al. 2001). See also CD-ROM for examples.

5.3 Supplementary tables

	myoblasts	myotubes	ES cells	lymphocytes	macrophages	fibroblasts
Washings/ Hypotonic treatment	rinse briefly in 1xPBS (37°C)	1' in 0.3xPBS or 0.75xPBS (37°C)	1' in 0.5xPBS (37°C)	1' in 0.3xPBS (37°C)	rinse briefly in 1xPBS (37°C)	rinse briefly in 1xPBS (37°C)
Fixation ^{1,2}	10' in 4% PFA/1xPBS ²	10' in 4% PFA/0.3xPBS or 0.75xPBS ²	10' in 4% PFA/0.5xPBS	10' in 4% PFA/0.3xPBS	10' in 4% PFA/1xPBS	10' in 4% PFA/1xPBS
After 9' a drop of 0.5% Triton X-100/1xPBS is added to the fixative to decrease the surface tension and thus to minimize the risk of cells to dry out						
Washing	3x3' in 1xPBS/0.0005% Triton X-100	3x3' in 1xPBS/0.0005% Triton X-100	3x3' in 1xPBS/0.0005% Triton X-100	3x3' in 1xPBS/0.0005% Triton X-100	3x3' in 1xPBS/0.0005% Triton X-100 ³	3x3' in 1xPBS/0.0005% Triton X-100
Permeabilization	20' in 0.5% Triton X-100 ³	20' in 0.5% Triton X-100 ³	20' in 0.5% Triton X-100 ³	20' in 0.5% Triton X-100 ³	20' in 0.5% Triton X-100	20' in 0.5% Triton X-100 ³
Glycerol incubation	30' at RT or ON at 4°C in 20% glycerol/1xPBS	30' at RT or ON at 4°C in 20% glycerol/1xPBS	30' at RT or ON at 4°C in 20% glycerol/1xPBS	30' at RT or ON at 4°C in 20% glycerol/1xPBS	30' at RT or ON at 4°C in 20% glycerol/1xPBS	30' at RT or ON at 4°C in 20% glycerol/1xPBS
freezing/ thawing	4 times repeatedly	4 times repeatedly	4 times repeatedly	4 times repeatedly	4 times repeatedly	4 times repeatedly
Washing	3x3' in 1xPBS	3x3' in 1xPBS	3x3' in 1xPBS	3x3' in 1xPBS	3x3' in 1xPBS	3x3' in 1xPBS
HCl treatment	10' in 0.1N HCl	10' in 0.1N HCl	10' in 0.1N HCl	10' in 0.1N HCl	10' in 0.1N HCl	10' in 0.1N HCl
Washing	4-5x in 2xSSC	4-5x in 2xSSC	4-5x in 2xSSC	4-5x in 2xSSC	4-5x in 2xSSC	4-5x in 2xSSC
Storage	50% Formamide/2xSSC	50% Formamide/2xSSC	50% Formamide/2xSSC	50% Formamide/2xSSC	50% Formamide/2xSSC	50% Formamide/2xSSC
Pepsinization (optional) ⁴	only for FISH using paint probes: 5'	only for FISH using paint probes: 4'30"	-	-	-	-

¹PFA solutions were prepared by dissolving the appropriate amount in 1xPBS by a magnetic stirrer and by heating at approx. 60°C. Boiling was avoided. Before use, the solution was cooled down to RT.

²For some immunofluorescence experiments, where high resolution was not needed cells were occasionally fixed using 3.7% formaldehyde/1x PBS diluted from a 37% slution containing 10-15% methanol.

³For immunofluorescence, fixation was stopped after this step and specimens were stored in 1xPBS at 4°C. In case of macrophages a permeabilization was not necessary since the visualized protein was located at the cell surface.

⁴Pepsinization was performed as described for metaphases (2.2), but using a 1/5000 dilution of pepsin in 0.01N HCl instead of 1/2000. Pepsinization was monitored under a phase microscope and immediatly stopped as the first cells started to detach from the surface.

Table 5.2: The table gives a summarized view on the different fixation steps for the various cell types.

Chromosome	Length (Ensembl)	Mapped cDNAs from the RIKEN Mouse gene Encyclopaedia project against following radiation hybrid data sets (Kawai et al., 2001):		NCBI Gene annotations (August 2002)		Ensembl Gene annotations (August 2002)				H2 isochores (Saccone et al. 1997)	Homology data: (large syntenic regions to gene poor/dense human chromosomes*)		
		Whitehead Institute genes	gene density (genes/Mb)	Jackson Laboratory genes	gene density (genes/Mb)	genes	gene density (genes/Mbp)	sum	known		novel	gene density (genes/Mb)	MG data base
1	196	174	0.89	211	1.08	3080	15.7	1312	789	523	6.7		HSA 8
2	181	239	1.32	298	1.65	3388	18.7	1795	1015	780	9.9		
3	161	159	0.99	214	1.33	2587	16.1	1028	699	329	6.4	HSA 4	HSA 4 (huge) & 8
4	153	188	1.23	237	1.55	2615	17.1	1244	765	479	8.1		HSA 8
5	150	186	1.24	200	1.33	2560	17.1	1274	826	448	8.5		HSA 4 (huge) & 3
6	150	143	0.95	183	1.22	2492	16.6	1192	776	416	7.9		
7	134	164	1.22	206	1.54	3004	22.4	1721	1019	702	12.8		HSA 19 & HSA 17
8	129	132	1.02	168	1.30	2322	18.0	1055	675	380	8.2		HSA 13, 8 (huge), 4 (huge) & 16 (huge) HSA 19
9	124	138	1.11	205	1.65	2330	18.8	1223	749	474	9.9		
10	131	120	0.92	154	1.18	2051	15.7	1021	605	416	7.8		HSA 19
11	123	168	1.37	223	1.81	2636	21.4	1661	1048	613	13.5		HSA 17
12 (NOR)	114	106	0.93	134	1.18	1861	16.3	770	464	306	6.8		
13	116	89	0.77	157	1.35	2008	17.3	804	524	280	6.9		
14	116	95	0.82	105	0.91	1796	15.5	792	472	320	6.8		HSA 13
15	104	110	1.06	146	1.40	1729	16.6	820	505	315	7.9		HSA 8
16 (NOR)	99	101	1.02	141	1.42	1509	15.2	689	449	240	7.0		HSA 22
17 (NOR)	94	112	1.19	145	1.54	1845	19.6	1052	663	389	11.2		HSA 19
18 (NOR)	91	91	1.00	97	1.07	1492	16.4	566	355	211	6.2		HSA 18
19 (NOR)	61	104	1.70	132	2.16	1225	20.1	725	462	263	11.9		HSA X
X	150	39	0.26	61	0.41	1851	12.3	848	479	369	5.7		HSA X
Y	NA	NA	NA	1	NA	N.A.	N.A.	NA	NA	NA	NA		HSA Y
∑	2577	2658	1.03	3418	1.33	44381	17.2	21592	13339	8253	8.4		

NOR=nonucleolus organizing region

HSA=Homo sapiens

*gene density of human chromosomes derived from www.ensembl.org/Homo_sapiens/: gene dense: 16,17,19 & 22. gene poor: 4,8,13,18

gene rich

gene poor

Table 5.3: The table summarizes all information that were taken into account for choosing the appropriate pair of chromosomes for the analysis of a gene density dependent radial distribution. The three most gene dense chromosomes are highlighted in red, the most gene poor in green. Most weighted decision criteria were gene annotations according to the NCBI and ENSEMBL data bases.

5.4 Supplementary CD

Karyotypes of C2C12 myoblasts EB5 embryonic stem cells and Pmi28 myoblasts:

Karyotype analyses were performed by Isabell Jentsch from the Institute of Human Genetics, Munich, using multiplex-FISH (Jentsch et al. 2001).

C2C12: Examples of three C2C12 metaphase spreads are shown. The images show an inverted DAPI staining of the metaphase chromosomes on top and a false colored picture on the bottom. Note that many chromosomes are present in a triple or quadruple number, but also monosomic chromosomes could be observed. However, no translocations could be demonstrated as discernible in these three examples. The karyotype of C2C12 cells can be considered as polyploid but without structural aberrations.

EB5: Five examples of EB5 mouse embryonic stem cell metaphases are shown. The left image depicts an inverted DAPI staining, false colored chromosomes are shown on the right. Most cells had a normal male 40, XY karyotype, although casually metaphases with numerical aberrations could be observed as “metaphase2” shown here, which is monosomic for #14 and trisomic for #15. The karyotype of EB5 can thus be classified as euploid.

Pmi28: Five analyzed metaphase spreads of Pmi28 mouse myoblasts are exemplified. Left panels illustrated the inverted DAPI staining, while the right panels show the color images of combined fluorescent signals. Note that all metaphases exhibited only one X chromosome. Since the cells were originally derived from a male mouse (Irintchev et al. 1997; Kaufmann et al. 1999), the karyotype analysis indicates a stable loss of the Y chromosome. Apart from a few sporadic trisomies (in “metaphase2” and “metaphase5”) affecting different chromosomes and one translocation (t(4;13) in “metaphase3”) the karyotype of Pmi28 myoblasts appears to be generally diploid.

Movie: Dynamic behavior of pericentric heterochromatin in a C2C12 mouse myoblast visualized in vivo. Cells were transiently transfected with MeCP2-YFP (green), thereby highlighting pericentric heterochromatin (chromocenters) and DsRed-Ligase I for cell cycle stage determination (not shown). MeCP2-YFP signals were 3 dimensionally reconstructed from confocal optical serial sections using a surface rendering approach with the software Amira 3.0 (TGS Europe). The nuclear boundaries are demarcated by a phase contrast confocal mid plane shown as transparent image (MeCP2-YFP signals beneath the phase contrast section appear in a lighter green). The time points at which the images were taken are shown in the top right corner as “hours:minutes”. Whilst during the first two hours of observation several chromocenter fusions could be traced (color-coded arrow heads), in the following two hours before mitosis signals increasingly changed their shape from ovoid/spherical to elongated irregular structures.

Moreover, abundant chromocenter splitting could be observed consequently leading to an increased chromocenter number. Confocal image stacks were aligned in the xy plane before reconstruction in order to correct for nuclear and cellular movements (therefore the phase contrast images appear tilted). **Note that the same movie is present as *.avi and *.mov format.**

6 Literature

- Abney, J. R., B. Cutler, M. L. Fillbach, D. Axelrod and B. A. Scalettar (1997): Chromatin dynamics in interphase nuclei and its implications for nuclear structure. J. Cell Biol. 137(7), 1459-68.
- Abranches, R., A. F. Beven, L. Aragon-Alcaide and P. J. Shaw (1998): Transcription sites are not correlated with chromosome territories in wheat nuclei. J Cell Biol 143(1), 5-12.
- Adkins, N. L., M. Watts and P. T. Georgel (2004): To the 30-nm chromatin fiber and beyond. Biochim Biophys Acta 1677(1-3), 12-23.
- Aguirre-Arteta, A. M., I. Grunewald, M. C. Cardoso and H. Leonhardt (2000): Expression of an alternative Dnmt1 isoform during muscle differentiation. Cell Growth Differ 11(10), 551-9.
- Ahmad, K. and S. Henikoff (2002): The histone variant H3.3 marks active chromatin by replication-independent nucleosome assembly. Mol Cell 9(6), 1191-200.
- Alami, R., Y. Fan, S. Pack, T. M. Sonbuchner, A. Besse, Q. Lin, J. M. Greally, A. I. Skoultchi and E. E. Bouhassira (2003): Mammalian linker-histone subtypes differentially affect gene expression in vivo. Proc Natl Acad Sci U S A 100(10), 5920-5.
- Alcobia, I., R. Dilao and L. Parreira (2000): Spatial associations of centromeres in the nuclei of hematopoietic cells: evidence for cell-type-specific organizational patterns [published erratum appears in Blood 2000 Aug 1;96(3):987]. Blood 95(5), 1608-15.
- Alexandrova, O., I. Solovei, T. Cremer and C. N. David (2003): Replication labeling patterns and chromosome territories typical of mammalian nuclei are conserved in the early metazoan Hydra. Chromosoma 112(4), 190-200.
- Allfrey, V. G., R. Faulkner and A. E. Mirsky (1964): Acetylation and Methylation of Histones and Their Possible Role in the Regulation of Rna Synthesis. Proc Natl Acad Sci U S A 51, 786-94.
- Allison, D. C. and A. L. Nestor (1999): Evidence for a relatively random array of human chromosomes on the mitotic ring. J. Cell Biol. 145(1), 1-14.
- Amir, R. E., I. B. Van den Veyver, M. Wan, C. Q. Tran, U. Francke and H. Y. Zoghbi (1999): Rett syndrome is caused by mutations in X-linked MECP2, encoding methyl-CpG-binding protein 2. Nat Genet 23(2), 185-8.
- Andersen, A. A. and B. Panning (2003): Epigenetic gene regulation by noncoding RNAs. Curr Opin Cell Biol 15(3), 281-9.
- Andrulis, E. D., A. M. Neiman, D. C. Zappulla and R. Sternglanz (1998): Perinuclear localization of chromatin facilitates transcriptional silencing. Nature 394(6693), 592-5.
- Arber, W. and S. Linn (1969): DNA modification and restriction. Annu Rev Biochem 38, 467-500.
- Arnoldus, E. P., I. A. Noordermeer, A. C. Peters, A. K. Raap and M. Van der Ploeg (1991): Interphase cytogenetics reveals somatic pairing of chromosome 17 centromeres in normal human brain tissue, but no trisomy 7 or sex-chromosome loss. Cytogenet Cell Genet 56(3-4), 214-6.
- Arnoldus, E. P., A. C. Peters, G. T. Bots, A. K. Raap and M. van der Ploeg (1989): Somatic pairing of chromosome 1 centromeres in interphase nuclei of human cerebellum. Hum Genet 83(3), 231-4.
- Ausio, J., D. Levin, G. De Amorim, S. Bakker and P. Macleod (2003): Syndromes of disordered chromatin remodeling. Clin Genet 64(2), 83-95.
- Avivi, L. and M. Feldman (1980): Arrangement of chromosomes in the interphase nucleus of plants. Hum Genet 55(3), 281-95.
- Baccarini, P. (1908): Sulle cinesi vegetative del "Cyonorum coccineum L." Nuovo Giornale Botanico Italiano 15(2), 189-203.
- Balmer, D., J. Goldstine, Y. M. Rao and J. M. LaSalle (2003): Elevated methyl-CpG-binding protein 2 expression is acquired during postnatal human brain development and is correlated with alternative polyadenylation. J Mol Med 81(1), 61-8.
- Barreda, D. R., P. C. Hanington and M. Belosevic (2004): Regulation of myeloid development and function by colony stimulating factors. Dev Comp Immunol 28(5), 509-54.
- Barwisch, S. (2003). Analyse altersbedingter Chromosomenveränderungen. Department Biologie II. München, Ludwig-Maximilians-Universität.

- Baylin, S. and T. H. Bestor (2002): Altered methylation patterns in cancer cell genomes: cause or consequence? Cancer Cell 1(4), 299-305.
- Beatty, B., S. Mai and J. Squire, Eds. (2001). FISH: a practical approach. A practical approach. Oxford, Oxford University Press.
- Beil, M., D. Durschmied, S. Paschke, B. Schreiner, U. Nolte, A. Bruel and T. Irinopoulou (2002): Spatial distribution patterns of interphase centromeres during retinoic acid-induced differentiation of promyelocytic leukemia cells. Cytometry 47(4), 217-25.
- Berger, S. L. (2001): An embarrassment of niches: the many covalent modifications of histones in transcriptional regulation. Oncogene 20(24), 3007-13.
- Bhattacharya, S. K., S. Ramchandani, N. Cervoni and M. Szyf (1999): A mammalian protein with specific demethylase activity for mCpG DNA. Nature 397(6720), 579-83.
- Bolzer, A. (2002). Analyse der Chromosomenverteilung in menschlichen Fibroblasten mittels 3D-Vielfarben Fluoreszenz in situ Hybridisierung. Institut für Humangenetik, Department Biologie II. Munich, Ludwig-Maximilians-Universität.
- Bolzer, A., G. Kreth, I. Solovei, D. Koehler, K. Saracoglu, C. Fauth, S. Müller, R. Eils, C. Cremer, M. R. Speicher and T. Cremer (submitted): Complete 3D-maps of chromosome positions in human male fibroblast nuclei and prometaphase rosettes demonstrate a chromosome size dependent, probabilistic arrangement.
- Borden, J. and L. Manuelidis (1988): Movement of the X chromosome in epilepsy. Science 242(4886), 1687-91.
- Boyle, S., S. Gilchrist, J. M. Bridger, N. L. Mahy, J. A. Ellis and W. A. Bickmore (2001): The spatial organization of human chromosomes within the nuclei of normal and emerin-mutant cells. Hum Mol Genet 10(3), 211-219.
- Bridger, J. M., H. Herrmann, C. Munkel and P. Lichter (1998): Identification of an interchromosomal compartment by polymerization of nuclear-targeted vimentin. J Cell Sci 111(Pt 9), 1241-53.
- Briggs, R. and T. J. King (1952): Transplantation of living nuclei from blastula cells into enucleated frogs' eggs. Proc. Natl. Acad. Sci. USA 38, 455-463.
- Broers, J. L., B. M. Machiels, G. J. van Eys, H. J. Kuijpers, E. M. Manders, R. van Driel and F. C. Ramaekers (1999): Dynamics of the nuclear lamina as monitored by GFP-tagged A-type lamins. J. Cell Sci. 112(Pt 20), 3463-75.
- Brown, D. T. (2001): Histone variants: are they functionally heterogeneous? Genome Biol 2(7), REVIEWS0006.
- Brown, K. E., S. Amoils, J. M. Horn, V. J. Buckle, D. R. Higgs, M. Merkenschlager and A. G. Fisher (2001): Expression of alpha- and beta-globin genes occurs within different nuclear domains in haemopoietic cells. Nat Cell Biol 3(6), 602-6.
- Brown, K. E., J. Baxter, D. Graf, M. Merkenschlager and A. G. Fisher (1999): Dynamic repositioning of genes in the nucleus of lymphocytes preparing for cell division. Mol Cell 3(2), 207-17.
- Brown, K. E., S. S. Guest, S. T. Smale, K. Hahm, M. Merkenschlager and A. G. Fisher (1997): Association of transcriptionally silent genes with Ikaros complexes at centromeric heterochromatin. Cell 91(6), 845-54.
- Brown, R. (1831): Observations on the organs and mode of fecundation in Orchideae and Asclepiadae. The Transactions of the Linnean Society of London 16(3), 709-737.
- Brown, S. W. (1966): Heterochromatin. Science 151(709), 417-25.
- Burgess, S. M., N. Kleckner and B. M. Weiner (1999): Somatic pairing of homologs in budding yeast: existence and modulation. Genes Dev 13(12), 1627-41.
- Burke, B. and J. Ellenberg (2002): Remodelling the walls of the nucleus. Nat Rev Mol Cell Biol 3(7), 487-97.
- Buschdorf, J. P. and W. H. Stratling (2004): A WW domain binding region in methyl-CpG-binding protein MeCP2: impact on Rett syndrome. J Mol Med 82(2), 135-43.
- Camargo, F. D., S. M. Chambers and M. A. Goodell (2004): Stem cell plasticity: from transdifferentiation to macrophage fusion. Cell Prolif 37(1), 55-65.
- Cardoso, M. C. and H. Leonhardt (1999): DNA methyltransferase is actively retained in the cytoplasm during early development. J Cell Biol 147(1), 25-32.
- Cardoso, M. C., H. Leonhardt and B. Nadal-Ginard (1993): Reversal of terminal differentiation and control of DNA replication: cyclin A and Cdk2 specifically localize at subnuclear sites of DNA replication. Cell 74(6), 979-92.

- Carlson, L. L., A. W. Page and T. H. Bestor (1992): Properties and localization of DNA methyltransferase in pre-implantation mouse embryos: implications for genomic imprinting. Genes Dev 6(12B), 2536-41.
- Celis, J. E., Ed. (1994). Cell Biology A Laboratory Handbook. San Diego, Academic Press, Inc.
- Cerda, M. C., S. Berríos, R. Fernández-Donoso, S. Garagna and C. Redi (1999): Organisation of complex nuclear domains in somatic mouse cells. Biol Cell 91(1), 55-65.
- Chadwick, B. P. and H. F. Willard (2001): A novel chromatin protein, distantly related to histone H2A, is largely excluded from the inactive X chromosome. J Cell Biol 152(2), 375-84.
- Chaly, N. and D. L. Brown (1988): The prometaphase configuration and chromosome order in early mitosis. J. Cell Sci. 91(Pt 3), 325-35.
- Chaly, N. and S. B. Munro (1996): Centromeres reposition to the nuclear periphery during L6E9 myogenesis in vitro. Exp Cell Res 223(2), 274-8.
- Chandley, A. C., R. M. Speed and A. R. Leitch (1996): Different distributions of homologous chromosomes in adult human Sertoli cells and in lymphocytes signify nuclear differentiation. J Cell Sci 109 (Pt 4), 773-6.
- Chen, W. G., Q. Chang, Y. Lin, A. Meissner, A. E. West, E. C. Griffith, R. Jaenisch and M. E. Greenberg (2003): Derepression of BDNF transcription involves calcium-dependent phosphorylation of MeCP2. Science 302(5646), 885-9.
- Cockell, M. and S. M. Gasser (1999): Nuclear compartments and gene regulation. Curr Opin Genet Dev 9(2), 199-205.
- Cohen, D. R., V. Matarazzo, A. M. Palmer, Y. Tu, O. H. Jeon, J. Pevsner and G. V. Ronnett (2003): Expression of MeCP2 in olfactory receptor neurons is developmentally regulated and occurs before synaptogenesis. Mol Cell Neurosci 22(4), 417-29.
- Comings, D. E. (1980): Arrangement of chromatin in the nucleus. Hum Genet 53(2), 131-43.
- Cook, P. R. (2001). Principles of Nuclear Structure and Function. New York, Wiley-Liss.
- Corbi, A. L., T. K. Kishimoto, L. J. Miller and T. A. Springer (1988): The human leukocyte adhesion glycoprotein Mac-1 (complement receptor type 3, CD11b) alpha subunit. Cloning, primary structure, and relation to the integrins, von Willebrand factor and factor B. J Biol Chem 263(25), 12403-11.
- Costanzi, C. and J. R. Pehrson (1998): Histone macroH2A1 is concentrated in the inactive X chromosome of female mammals. Nature 393(6685), 599-601.
- Cowell, I. G., R. Aucott, S. K. Mahadevaiah, P. S. Burgoyne, N. Huskisson, S. Bongiorno, G. Prantero, L. Fanti, S. Pimpinelli, R. Wu, D. M. Gilbert, W. Shi, R. Fundele, H. Morrison, P. Jeppesen and P. B. Singh (2002): Heterochromatin, HP1 and methylation at lysine 9 of histone H3 in animals. Chromosoma 111(1), 22-36.
- Cremer, M., K. Kupper, B. Wagler, L. Wizelman, J. Hase Jv, Y. Weiland, L. Kreja, J. Diebold, M. R. Speicher and T. Cremer (2003): Inheritance of gene density-related higher order chromatin arrangements in normal and tumor cell nuclei. J Cell Biol 162(5), 809-20.
- Cremer, M., J. von Hase, T. Volm, A. Brero, G. Kreth, J. Walter, C. Fischer, I. Solovei, C. Cremer and T. Cremer (2001): Non-random radial higher-order chromatin arrangements in nuclei of diploid human cells. Chromosome Res 9(7), 541-67.
- Cremer, T. (1985). Von der Zellenlehre zur Chromosomentheorie. Berlin, Heidelberg, Springer-Verlag.
- Cremer, T. and C. Cremer (1988): Centennial of Wilhelm Waldeyer's introduction of the term "chromosome" in 1888. Cytogenet Cell Genet 48(2), 65-7.
- Cremer, T. and C. Cremer (2001): Chromosome territories, nuclear architecture and gene regulation in mammalian cells. Nat Rev Genet 2(4), 292-301.
- Crescenzi, M., S. Soddu and F. Tato (1995): Mitotic cycle reactivation in terminally differentiated cells by adenovirus infection. J Cell Physiol 162(1), 26-35.
- Croft, J. A., J. M. Bridger, S. Boyle, P. Perry, P. Teague and W. A. Bickmore (1999): Differences in the localization and morphology of chromosomes in the human nucleus. J Cell Biol 145(6), 1119-31.
- Czermin, B. and A. Imhof (2003): The sounds of silence--histone deacetylation meets histone methylation. Genetica 117(2-3), 159-64.
- Dean, W., F. Santos, M. Stojkovic, V. Zakhartchenko, J. Walter, E. Wolf and W. Reik (2001): Conservation of methylation reprogramming in mammalian development: aberrant reprogramming in cloned embryos. Proc Natl Acad Sci U S A 98(24), 13734-8.
- DeLange, R. J. and E. L. Smith (1971): Histones: structure and function. Annu Rev Biochem 40, 279-314.

- Deng, W., S. W. Tsao, J. N. Lucas, C. S. Leung and A. L. Cheung (2003): A new method for improving metaphase chromosome spreading. *Cytometry* 51A(1), 46-51.
- Dernburg, A. F., K. W. Broman, J. C. Fung, W. F. Marshall, J. Philips, D. A. Agard and J. W. Sedat (1996): Perturbation of nuclear architecture by long-distance chromosome interactions. *Cell* 85(5), 745-59.
- Detich, N., J. Theberge and M. Szyf (2002): Promoter-specific activation and demethylation by MBD2/demethylase. *J Biol Chem* 277(39), 35791-4.
- Dev, V. G., R. Tantravahi, D. A. Miller and O. J. Miller (1977): Nucleolus organizers in *Mus musculus* subspecies and in the RAG mouse cell line. *Genetics* 86(2 Pt. 1), 389-98.
- Doerfler, W. (1983): DNA methylation and gene activity. *Annu Rev Biochem* 52, 93-124.
- Dou, Y., J. Bowen, Y. Liu and M. A. Gorovsky (2002): Phosphorylation and an ATP-dependent process increase the dynamic exchange of H1 in chromatin. *J Cell Biol* 158(7), 1161-70.
- Easwaran, H. P. (2003). A complex interplay of regulatory domains controls cell cycle dependent subnuclear localization of DNMT1 and is required for the maintenance of epigenetic information. *Mathematisch-Naturwissenschaftlichen Fakultät I. Berlin, Humboldt-Universität zu Berlin*.
- Ebbing, B. (2003). Zellkernarchitektur in Hydra: Räumliche Organisation der Centromere im Zellkern. *Institut für Zoologie, Department II. München, Ludwig-Maximilians-Universität*.
- Eggan, K., K. Baldwin, M. Tackett, J. Osborne, J. Gogos, A. Chess, R. Axel and R. Jaenisch (2004): Mice cloned from olfactory sensory neurons. *Nature* 428(6978), 44-9.
- Emmerich, P., P. Loos, A. Jauch, A. H. Hopman, J. Wiegant, M. J. Higgins, B. N. White, M. van der Ploeg, C. Cremer and T. Cremer (1989): Double in situ hybridization in combination with digital image analysis: a new approach to study interphase chromosome topography. *Exp Cell Res* 181(1), 126-40.
- Feinberg, A. P. and B. Tycko (2004): The history of cancer epigenetics. *Nat Rev Cancer* 4(2), 143-53.
- Ferreira, J., G. Paoletta, C. Ramos and A. I. Lamond (1997): Spatial organization of large-scale chromatin domains in the nucleus: a magnified view of single chromosome territories. *J. Cell Biol.* 139(7), 1597-610.
- Fisher, A. G. and M. Merckenschlager (2002): Gene silencing, cell fate and nuclear organisation. *Curr Opin Genet Dev* 12(2), 193-7.
- Flemming, W. (1882). *Zellsubstanz, Kern und Zelltheilung*. Leipzig, F.C.W. Vogel.
- Francastel, C., W. Magis and M. Groudine (2001): Nuclear relocation of a transactivator subunit precedes target gene activation. *Proc Natl Acad Sci U S A* 98(21), 12120-5.
- Francastel, C., M. C. Walters, M. Groudine and D. I. Martin (1999): A functional enhancer suppresses silencing of a transgene and prevents its localization close to centromeric heterochromatin. *Cell* 99(3), 259-69.
- Franz, P., J. H. De Jong, M. Lysak, M. R. Castiglione and I. Schubert (2002): Interphase chromosomes in Arabidopsis are organized as well defined chromocenters from which euchromatin loops emanate. *Proc Natl Acad Sci U S A* 99(22), 14584-9.
- Fraser, H. B., A. E. Hirsh, G. Giaever, J. Kumm and M. B. Eisen (2004): Noise Minimization in Eukaryotic Gene Expression. *PLoS Biol* 2(6), E137.
- Fuks, F., P. J. Hurd, D. Wolf, X. Nan, A. P. Bird and T. Kouzarides (2003): The methyl-CpG-binding protein MeCP2 links DNA methylation to histone methylation. *J Biol Chem* 278(6), 4035-40.
- Funabiki, H., I. Hagan, S. Uzawa and M. Yanagida (1993): Cell cycle-dependent specific positioning and clustering of centromeres and telomeres in fission yeast. *J Cell Biol* 121(5), 961-76.
- Garagna, S., M. Zuccotti, E. Capanna and C. A. Redi (2002): High-resolution organization of mouse telomeric and pericentromeric DNA. *Cytogenet Genome Res* 96(1-4), 125-9.
- Gaudet, F., J. G. Hodgson, A. Eden, L. Jackson-Grusby, J. Dausman, J. W. Gray, H. Leonhardt and R. Jaenisch (2003): Induction of tumors in mice by genomic hypomethylation. *Science* 300(5618), 489-92.
- Gaudet, F., W. M. Rideout, 3rd, A. Meissner, J. Dausman, H. Leonhardt and R. Jaenisch (2004): Dnmt1 expression in pre- and postimplantation embryogenesis and the maintenance of IAP silencing. *Mol Cell Biol* 24(4), 1640-8.
- Geiman, T. M. and K. D. Robertson (2002): Chromatin remodeling, histone modifications, and DNA methylation-how does it all fit together? *J Cell Biochem* 87(2), 117-25.
- Georgel, P. T., R. A. Horowitz-Scherer, N. Adkins, C. L. Woodcock, P. A. Wade and J. C. Hansen (2003): Chromatin compaction by human MeCP2. Assembly of novel secondary chromatin structures in the absence of DNA methylation. *J Biol Chem* 278(34), 32181-8.

- Gerlich, D., J. Beaudouin, B. Kalbfuss, N. Daigle, R. Eils and J. Ellenberg (2003): Global chromosome positions are transmitted through mitosis in mammalian cells. Cell 112(6), 751-64.
- Graham, F. L. and A. J. van der Eb (1973): A new technique for the assay of infectivity of human adenovirus 5 DNA. Virology 52(2), 456-67.
- Grewal, S. I. and J. C. Rice (2004): Regulation of heterochromatin by histone methylation and small RNAs. Curr Opin Cell Biol 16(3), 230-8.
- Grigoryev, S. A. (2004): Keeping fingers crossed: heterochromatin spreading through interdigitation of nucleosome arrays. FEBS Lett 564(1-2), 4-8.
- Grigoryev, S. A., J. Bednar and C. L. Woodcock (1999): MENT, a heterochromatin protein that mediates higher order chromatin folding, is a new serpin family member. J Biol Chem 274(9), 5626-36.
- Grigoryev, S. A., V. O. Solovieva, K. S. Spirin and I. A. Krasheninnikov (1992): A novel nonhistone protein (MENT) promotes nuclear collapse at the terminal stage of avian erythropoiesis. Exp Cell Res 198(2), 268-75.
- Grigoryev, S. A. and C. L. Woodcock (1993): Stage-specific expression and localization of MENT, a nuclear protein associated with chromatin condensation in terminally differentiating avian erythroid cells. Exp Cell Res 206(2), 335-43.
- Grigoryev, S. A. and C. L. Woodcock (1998): Chromatin structure in granulocytes. A link between tight compaction and accumulation of a heterochromatin-associated protein (MENT). J Biol Chem 273(5), 3082-9.
- Grogan, J. L., M. Mohrs, B. Harmon, D. A. Lacy, J. W. Sedat and R. M. Locksley (2001): Early transcription and silencing of cytokine genes underlie polarization of T helper cell subsets. Immunity 14(3), 205-15.
- Grundmann, E. and P. Stein (1961): [Studies on the nuclear structure in normal tissues and in carcinoma]. Beitr Pathol Anat 125, 54-76.
- Gurdon, J. B. and V. Uehlinger (1966): "Fertile" intestine nuclei. Nature 210(42), 1240-1.
- Haaf, T. and M. Schmid (1989): Centromeric association and non-random distribution of centromeres in human tumour cells. Hum Genet 81(2), 137-43.
- Haaf, T., C. Steinlein and M. Schmid (1990): Nucleolar transcriptional activity in mouse Sertoli cells is dependent on centromere arrangement. Exp Cell Res 191(1), 157-60.
- Habermann, F. A., M. Cremer, J. Walter, G. Kreth, J. von Hase, K. Bauer, J. Wienberg, C. Cremer, T. Cremer and I. Solovei (2001): Arrangements of macro- and microchromosomes in chicken cells. Chromosome Res 9(7), 569-84.
- Hansen, J. C. (2002): Conformational dynamics of the chromatin fiber in solution: determinants, mechanisms, and functions. Annu Rev Biophys Biomol Struct 31, 361-92.
- Harbour, J. W. and D. C. Dean (2000): Rb function in cell-cycle regulation and apoptosis. Nat Cell Biol 2(4), E65-7.
- Heidenhain, M. (1907). Plasma und Zelle. Jena, Fischer.
- Heitz, E. (1928): Das Heterochromatin der Moose. I. Jahrb. Wiss. Botanik 69, 762-818.
- Hendrich, B. and A. Bird (1998): Identification and characterization of a family of mammalian methyl-CpG binding proteins. Mol Cell Biol 18(11), 6538-47.
- Hendrich, B. and S. Tweedie (2003): The methyl-CpG binding domain and the evolving role of DNA methylation in animals. Trends Genet 19(5), 269-77.
- Henikoff, S. (1997): Nuclear organization and gene expression: homologous pairing and long-range interactions. Curr Opin Cell Biol 9(3), 388-95.
- Hens, L., M. Kirsch-Volders, L. Verschaeve and C. Susanne (1982): The central localization of the small and early replicating chromosomes in human diploid metaphase figures. Hum. Genet. 60(3), 249-56.
- Hochstrasser, M., D. Mathog, Y. Gruenbaum, H. Saumweber and J. W. Sedat (1986): Spatial organization of chromosomes in the salivary gland nuclei of *Drosophila melanogaster*. J Cell Biol 102(1), 112-23.
- Hoffmann, K., C. K. Dreger, A. L. Olins, D. E. Olins, L. D. Shultz, B. Lucke, H. Karl, R. Kaps, D. Muller, A. Vaya, J. Aznar, R. E. Ware, N. Sotelo Cruz, T. H. Lindner, H. Herrmann, A. Reis and K. Sperling (2002): Mutations in the gene encoding the lamin B receptor produce an altered nuclear morphology in granulocytes (Pelger-Huet anomaly). Nat Genet 31(4), 410-4.
- Horn, P. J. and C. L. Peterson (2002): Molecular biology. Chromatin higher order folding--wrapping up transcription. Science 297(5588), 1824-7.

- Horz, W. and W. Altenburger (1981): Nucleotide sequence of mouse satellite DNA. Nucleic Acids Res 9(3), 683-96.
- Howman, E. V., K. J. Fowler, A. J. Newson, S. Redward, A. C. MacDonald, P. Kalitsis and K. H. Choo (2000): Early disruption of centromeric chromatin organization in centromere protein A (Cenpa) null mice. Proc Natl Acad Sci U S A 97(3), 1148-53.
- Hsu, T. C. (1975): A possible function of constitutive heterochromatin: the bodyguard hypothesis. Genetics 79 Suppl, 137-50.
- Hsu, T. C., J. E. Cooper, M. L. Mace and B. R. Brinkley (1971): Arrangement of centromeres in mouse cells. Chromosoma 34(1), 73-87.
- Humpherys, D., K. Eggan, H. Akutsu, K. Hochedlinger, W. M. Rideout, 3rd, D. Biniszkiwicz, R. Yanagimachi and R. Jaenisch (2001): Epigenetic instability in ES cells and cloned mice. Science 293(5527), 95-7.
- Iizuka, M. and M. M. Smith (2003): Functional consequences of histone modifications. Curr Opin Genet Dev 13(2), 154-60.
- Imhof, A. (2003): Histone modifications: an assembly line for active chromatin? Curr Biol 13(1), R22-4.
- Irintchev, A., M. Langer, M. Zweyer, R. Theisen and A. Wernig (1997): Functional improvement of damaged adult mouse muscle by implantation of primary myoblasts. J Physiol 500(Pt 3), 775-85.
- Ijuvidin, S., O. Fuchs, U. Nudel and D. Yaffe (1990): SV40 immortalizes myogenic cells: DNA synthesis and mitosis in differentiating myotubes. Differentiation 43(3), 192-203.
- Jaenisch, R. and A. Bird (2003): Epigenetic regulation of gene expression: how the genome integrates intrinsic and environmental signals. Nat Genet 33 Suppl, 245-54.
- Jellinger, K. A. (2003): Rett Syndrome -- an update. J Neural Transm 110(6), 681-701.
- Jentsch, I., I. D. Adler, N. P. Carter and M. R. Speicher (2001): Karyotyping mouse chromosomes by multiplex-FISH (M-FISH). Chromosome Res 9(3), 211-4.
- Jenuwein, T. and C. D. Allis (2001): Translating the histone code. Science 293(5532), 1074-80.
- John, R. M. and M. A. Surani (2000): Genomic imprinting, mammalian evolution, and the mystery of egg-laying mammals. Cell 101(6), 585-8.
- Jones, P. A. and S. B. Baylin (2002): The fundamental role of epigenetic events in cancer. Nat Rev Genet 3(6), 415-28.
- Jones, P. L., G. J. Veenstra, P. A. Wade, D. Vermaak, S. U. Kass, N. Landsberger, J. Strouboulis and A. P. Wolffe (1998): Methylated DNA and MeCP2 recruit histone deacetylase to repress transcription. Nat Genet 19(2), 187-91.
- Joseph, A., A. R. Mitchell and O. J. Miller (1989): The organization of the mouse satellite DNA at centromeres. Exp Cell Res 183(2), 494-500.
- Jost, J. P., E. J. Oakeley, B. Zhu, D. Benjamin, S. Thiry, M. Siegmann and Y. C. Jost (2001): 5-Methylcytosine DNA glycosylase participates in the genome-wide loss of DNA methylation occurring during mouse myoblast differentiation. Nucleic Acids Res 29(21), 4452-61.
- Jung, B. P., D. G. Jugloff, G. Zhang, R. Logan, S. Brown and J. H. Eubanks (2003): The expression of methyl CpG binding factor MeCP2 correlates with cellular differentiation in the developing rat brain and in cultured cells. J Neurobiol 55(1), 86-96.
- Kaufmann, U., J. Kirsch, A. Irintchev, A. Wernig and A. Starzinski-Powitz (1999): The M-cadherin catenin complex interacts with microtubules in skeletal muscle cells: implications for the fusion of myoblasts. J Cell Sci 112(Pt 1), 55-68.
- Kawai, J., A. Shinagawa, K. Shibata, M. Yoshino et al. (2001): Functional annotation of a full-length mouse cDNA collection. Nature 409(6821), 685-90.
- Kernohan, N. M., H. F. Sewell and F. Walker (1990): Natural killer cells in cutaneous malignant melanoma. J Pathol 161(1), 35-40.
- Kleckner, N. and B. M. Weiner (1993): Potential advantages of unstable interactions for pairing of chromosomes in meiotic, somatic, and premeiotic cells. Cold Spring Harb Symp Quant Biol 58, 553-65.
- Klier-Choroba, A.-B. (2002). Vergleich des Replikationsmusters proliferierender und terminal differenzierter Skelettmuskelzellen der Maus. Institut für Anthropologie und Humangenetik. München, Ludwig-Maximilians-Universität.
- Knippers, R. (2001). Molekulare Genetik. Stuttgart, Georg Thieme Verlag.

- Koch, C. and W. H. Stratling (2004): DNA Binding of Methyl-CpG-Binding Protein MeCP2 in Human MCF7 Cells. Biochemistry 43(17), 5011-21.
- Kornberg, R. D. and Y. Lorch (1999): Twenty-five years of the nucleosome, fundamental particle of the eukaryote chromosome. Cell 98(3), 285-94.
- Kosak, S. T., J. A. Skok, K. L. Medina, R. Riblet, M. M. Le Beau, A. G. Fisher and H. Singh (2002): Subnuclear compartmentalization of immunoglobulin loci during lymphocyte development. Science 296(5565), 158-62.
- Koss, L. G. (1998): Characteristics of chromosomes in polarized normal human bronchial cells provide a blueprint for nuclear organization. Cytogenet Cell Genet 82(3-4), 230-7.
- Kourmouli, N., P. Jeppesen, S. Mahadevhaiah, P. Burgoyne, R. Wu, D. M. Gilbert, S. Bongiorno, G. Prantera, L. Fanti, S. Pimpinelli, W. Shi, R. Fundele and P. B. Singh (2004): Heterochromatin and tri-methylated lysine 20 of histone H4 in animals. J Cell Sci 117(Pt 12), 2491-2501.
- Kourmouli, N., P. A. Theodoropoulos, G. Dialynas, A. Bakou, A. S. Politou, I. G. Cowell, P. B. Singh and S. D. Georgatos (2000): Dynamic associations of heterochromatin protein 1 with the nuclear envelope. Embo J 19(23), 6558-68.
- Kriaucionis, S. and A. Bird (2003): DNA methylation and Rett syndrome. Hum Mol Genet 12 Suppl 2, R221-7.
- Kriaucionis, S. and A. Bird (2004): The major form of MeCP2 has a novel N-terminus generated by alternative splicing. Nucleic Acids Res 32(5), 1818-23.
- Kyba, M. and G. Q. Daley (2003): Hematopoiesis from embryonic stem cells: lessons from and for ontogeny. Exp Hematol 31(11), 994-1006.
- Lachner, M. and T. Jenuwein (2002): The many faces of histone lysine methylation. Curr Opin Cell Biol 14(3), 286-98.
- Lachner, M., D. O'Carroll, S. Rea, K. Mechtler and T. Jenuwein (2001): Methylation of histone H3 lysine 9 creates a binding site for HP1 proteins. Nature 410(6824), 116-20.
- Lachner, M., R. J. O'Sullivan and T. Jenuwein (2003): An epigenetic road map for histone lysine methylation. J Cell Sci 116(Pt 11), 2117-24.
- Ladurner, A. G. (2003): Inactivating chromosomes: a macro domain that minimizes transcription. Mol Cell 12(1), 1-3.
- LaSalle, J. M., J. Goldstine, D. Balmer and C. M. Greco (2001): Quantitative localization of heterogeneous methyl-CpG-binding protein 2 (MeCP2) expression phenotypes in normal and Rett syndrome brain by laser scanning cytometry. Hum Mol Genet 10(17), 1729-40.
- LaSalle, J. M. and M. Lalande (1996): Homologous association of oppositely imprinted chromosomal domains. Science 272(5262), 725-8.
- Lawson, M. A. and P. P. Purslow (2000): Differentiation of myoblasts in serum-free media: effects of modified media are cell line-specific. Cells Tissues Organs 167(2-3), 130-7.
- Lehnertz, B., Y. Ueda, A. A. Derijck, U. Braunschweig, L. Perez-Burgos, S. Kubicek, T. Chen, E. Li, T. Jenuwein and A. H. Peters (2003): Suv39h-mediated histone H3 lysine 9 methylation directs DNA methylation to major satellite repeats at pericentric heterochromatin. Curr Biol 13(14), 1192-200.
- Leitch, A. R. (2000): Higher levels of organization in the interphase nucleus of cycling and differentiated cells. Microbiol Mol Biol Rev 64(1), 138-52.
- Leitch, A. R., J. K. Brown, W. Mosgoller, T. Schwarzacher and J. S. Heslop-Harrison (1994): The spatial localization of homologous chromosomes in human fibroblasts at mitosis. Hum Genet 93(3), 275-80.
- Leonhardt, H., A. W. Page, H. U. Weier and T. H. Bestor (1992): A targeting sequence directs DNA methyltransferase to sites of DNA replication in mammalian nuclei. Cell 71(5), 865-73.
- Lesko, S. A., D. E. Callahan, M. E. LaVilla, Z. P. Wang and P. O. Ts'o (1995): The experimental homologous and heterologous separation distance histograms for the centromeres of chromosomes 7, 11, and 17 in interphase human T-lymphocytes. Exp Cell Res 219(2), 499-506.
- Lester, E. P. and H. L. Cooper (1985): Lymphocyte blastogenesis. Post-transcriptional controls of protein synthesis. Biochim Biophys Acta 824(4), 365-8.
- Lewin, B. (2004). Genes VIII. New Jersey, Pearson Education, Inc.
- Lewis, J. D., R. R. Meehan, W. J. Henzel, I. Maurer-Fogy, P. Jeppesen, F. Klein and A. Bird (1992): Purification, sequence, and cellular localization of a novel chromosomal protein that binds to methylated DNA. Cell 69(6), 905-14.

- Lewis, J. P., H. J. Tanke, A. K. Raap, G. C. Beverstock and H. C. Kluin-Nelemans (1993): Somatic pairing of centromeres and short arms of chromosome 15 in the hematopoietic and lymphoid system. Hum Genet 92(6), 577-82.
- Lichter, P., T. Cremer, J. Borden, L. Manuelidis and D. C. Ward (1988): Delineation of individual human chromosomes in metaphase and interphase cells by in situ suppression hybridization using recombinant DNA libraries. Hum Genet 80(3), 224-34.
- Lima De Faria, A. (1959): Incorporation of tritiated thymidine into meiotic chromosomes. Science 130, 503-4.
- Loebel, D. A., C. M. Watson, R. A. De Young and P. P. Tam (2003): Lineage choice and differentiation in mouse embryos and embryonic stem cells. Dev Biol 264(1), 1-14.
- Loidl, J. (2003): Chromosomes of the budding yeast *Saccharomyces cerevisiae*. Int Rev Cytol 222, 141-96.
- Lucifero, D., J. R. Chaillet and J. M. Trasler (2004): Potential significance of genomic imprinting defects for reproduction and assisted reproductive technology. Hum Reprod Update 10(1), 3-18.
- Mahy, N. L., P. E. Perry, S. Gilchrist, R. A. Baldock and W. A. Bickmore (2002): Spatial organization of active and inactive genes and noncoding DNA within chromosome territories. J Cell Biol 157(4), 579-89.
- Maison, C. and G. Almouzni (2004): HP1 and the dynamics of heterochromatin maintenance. Nat Rev Mol Cell Biol 5(4), 296-305.
- Maison, C., D. Bailly, A. H. Peters, J. P. Quivy, D. Roche, A. Taddei, M. Lachner, T. Jenuwein and G. Almouzni (2002): Higher-order structure in pericentric heterochromatin involves a distinct pattern of histone modification and an RNA component. Nat Genet 30(3), 329-34.
- Manuelidis, L. (1985): Indications of centromere movement during interphase and differentiation. Ann. N. Y. Acad. Sci. 450, 205-21.
- Manuelidis, L. (1985): Individual interphase chromosome domains revealed by in situ hybridization. Hum Genet 71(4), 288-93.
- Manuelidis, L. and J. Borden (1988): Reproducible compartmentalization of individual chromosome domains in human CNS cells revealed by in situ hybridization and three-dimensional reconstruction. Chromosoma 96(6), 397-410.
- Margot, J. B., A. M. Aguirre-Arteta, B. V. Di Giacco, S. Pradhan, R. J. Roberts, M. C. Cardoso and H. Leonhardt (2000): Structure and function of the mouse DNA methyltransferase gene: *Dnmt1* shows a tripartite structure. J Mol Biol 297(2), 293-300.
- Martens, U. M., E. A. Chavez, S. S. Poon, C. Schmoor and P. M. Lansdorp (2000): Accumulation of short telomeres in human fibroblasts prior to replicative senescence. Exp Cell Res 256(1), 291-9.
- Martinowich, K., D. Hattori, H. Wu, S. Fouse, F. He, Y. Hu, G. Fan and Y. E. Sun (2003): DNA methylation-related chromatin remodeling in activity-dependent BDNF gene regulation. Science 302(5646), 890-3.
- Martins, L. A.-C. P. (1999): Did Sutton and Boveri propose the so-called Sutton-Boveri chromosome hypothesis? Genet. Mol. Biol. 22(2), 261-272.
- Martou, G. and U. De Boni (2000): Nuclear topology of murine, cerebellar Purkinje neurons: changes as a function of development. Exp Cell Res 256(1), 131-9.
- Martou, G., P. C. Park and U. De Boni (2002): Intranuclear relocation of the *Plc beta3* sequence in cerebellar Purkinje neurons: temporal association with de novo expression during development. Chromosoma 110(8), 542-9.
- Matarazzo, V. and G. V. Ronnett (2004): Temporal and regional differences in the olfactory proteome as a consequence of MeCP2 deficiency. Proc Natl Acad Sci U S A 101(20), 7763-8.
- Mayer, W., A. Niveleau, J. Walter, R. Fundele and T. Haaf (2000): Demethylation of the zygotic paternal genome. Nature 403(6769), 501-2.
- Mayr, C., Z. Jasencakova, A. Meister, I. Schubert and D. Zink (2003): Comparative analysis of the functional genome architecture of animal and plant cell nuclei. Chromosome Res 11(5), 471-84.
- McGann, C. J., S. J. Odelberg and M. T. Keating (2001): Mammalian myotube dedifferentiation induced by newt regeneration extract. Proc Natl Acad Sci U S A 98(24), 13699-704.
- McKittrick, E., P. R. Gafken, K. Ahmad and S. Henikoff (2004): Histone H3.3 is enriched in covalent modifications associated with active chromatin. Proc Natl Acad Sci U S A.
- Meehan, R. R., J. D. Lewis, S. McKay, E. L. Kleiner and A. P. Bird (1989): Identification of a mammalian protein that binds specifically to DNA containing methylated CpGs. Cell 58(3), 499-507.

- Miller, O. J., W. Schnedl, J. Allen and B. F. Erlanger (1974): 5-Methylcytosine localised in mammalian constitutive heterochromatin. Nature 251(5476), 636-7.
- Mitchell, A. R. (1996): The mammalian centromere: its molecular architecture. Mutat Res 372(2), 153-62.
- Mnatzakanian, G. N., H. Lohi, I. Munteanu, S. E. Alfred, T. Yamada, P. J. MacLeod, J. R. Jones, S. W. Scherer, N. C. Schanen, M. J. Friez, J. B. Vincent and B. A. Minassian (2004): A previously unidentified MECP2 open reading frame defines a new protein isoform relevant to Rett syndrome. Nat Genet 36(4), 339-41.
- Moen, P. T., Jr., C. V. Johnson, M. Byron, L. S. Shopland, I. L. de la Serna, A. N. Imbalzano and J. B. Lawrence (2004): Repositioning of muscle-specific genes relative to the periphery of SC-35 domains during skeletal myogenesis. Mol Biol Cell 15(1), 197-206.
- Moran, J. L., Y. Li, A. A. Hill, W. M. Mounts and C. P. Miller (2002): Gene expression changes during mouse skeletal myoblast differentiation revealed by transcriptional profiling. Physiol Genomics 10(2), 103-11.
- Mosgoller, W., A. R. Leitch, J. K. Brown and J. S. Heslop-Harrison (1991): Chromosome arrangements in human fibroblasts at mitosis. Hum. Genet. 88(1), 27-33.
- Mullaney, B. C., M. V. Johnston and M. E. Blue (2004): Developmental expression of methyl-CpG binding protein 2 is dynamically regulated in the rodent brain. Neuroscience 123(4), 939-49.
- Muller, W. A. (1999): Differentiation: A central topic in developmental and cell biology. Naturwissenschaften 86(10), 457-67.
- Nagele, R., T. Freeman, L. McMorrow and H. Y. Lee (1995): Precise spatial positioning of chromosomes during prometaphase: evidence for chromosomal order. Science 270(5243), 1831-5.
- Nagele, R. G., T. Freeman, J. Fazekas, K. M. Lee, Z. Thomson and H. Y. Lee (1998): Chromosome spatial order in human cells: evidence for early origin and faithful propagation. Chromosoma 107(5), 330-8.
- Nagele, R. G., T. Freeman, L. McMorrow, Z. Thomson, K. Kitson-Wind and H. Lee (1999): Chromosomes exhibit preferential positioning in nuclei of quiescent human cells. Journal of Cell Science 112, 525-535.
- Nakano, T., H. Kodama and T. Honjo (1994): Generation of lymphohematopoietic cells from embryonic stem cells in culture. Science 265(5175), 1098-101.
- Nakayasu, H. and R. Berezney (1989): Mapping replicational sites in the eucaryotic cell nucleus. J Cell Biol 108(1), 1-11.
- Nan, X., F. J. Campoy and A. Bird (1997): MeCP2 is a transcriptional repressor with abundant binding sites in genomic chromatin. Cell 88(4), 471-81.
- Nan, X., H. H. Ng, C. A. Johnson, C. D. Laherty, B. M. Turner, R. N. Eisenman and A. Bird (1998): Transcriptional repression by the methyl-CpG-binding protein MeCP2 involves a histone deacetylase complex. Nature 393(6683), 386-9.
- Ng, H. H., D. N. Ciccone, K. B. Morshead, M. A. Oettinger and K. Struhl (2003): Lysine-79 of histone H3 is hypomethylated at silenced loci in yeast and mammalian cells: a potential mechanism for position-effect variegation. Proc Natl Acad Sci U S A 100(4), 1820-5.
- Nogami, M., A. Kohda, H. Taguchi, M. Nakao, T. Ikemura and K. Okumura (2000): Relative locations of the centromere and imprinted SNRPN gene within chromosome 15 territories during the cell cycle in HL60 cells. J Cell Sci 113 (Pt 12), 2157-65.
- O'Keefe, R. T., S. C. Henderson and D. L. Spector (1992): Dynamic organization of DNA replication in mammalian cell nuclei: spatially and temporally defined replication of chromosome-specific alpha-satellite DNA sequences. J. Cell Biol. 116(5), 1095-110.
- Olins, A. L. and D. E. Olins (1974): Spheroid chromatin units (v bodies). Science 183(122), 330-2.
- Olins, D. E. and A. L. Olins (2003): Chromatin history: our view from the bridge. Nat Rev Mol Cell Biol 4(10), 809-14.
- Orlando, V. (2003): Polycomb, epigenomes, and control of cell identity. Cell 112(5), 599-606.
- Parada, L. A., P. G. McQueen, P. J. Munson and T. Misteli (2002): Conservation of relative chromosome positioning in normal and cancer cells. Curr Biol 12(19), 1692-7.
- Parseghian, M. H., R. L. Newcomb, S. T. Winokur and B. A. Hamkalo (2000): The distribution of somatic H1 subtypes is non-random on active vs. inactive chromatin: distribution in human fetal fibroblasts. Chromosome Res 8(5), 405-24.
- Pawley, J. B., Ed. (1995). Handbook of biological confocal microscopy. New York, London, Plenum Press.

- Perez-Burgos, L., A. H. Peters, S. Opravil, M. Kauer, K. Mechtler and T. Jenuwein (2004): Generation and characterization of methyl-lysine histone antibodies. Methods Enzymol 376, 234-54.
- Peters, A. H., S. Kubicek, K. Mechtler, R. J. O'Sullivan, A. A. Derijck, L. Perez-Burgos, A. Kohlmaier, S. Opravil, M. Tachibana, Y. Shinkai, J. H. Martens and T. Jenuwein (2003): Partitioning and plasticity of repressive histone methylation States in Mammalian chromatin. Mol Cell 12(6), 1577-89.
- Peters, A. H., J. E. Mermoud, D. O'Carroll, M. Pagani, D. Schweizer, N. Brockdorff and T. Jenuwein (2002): Histone H3 lysine 9 methylation is an epigenetic imprint of facultative heterochromatin. Nat Genet 30(1), 77-80.
- Peters, A. H., D. O'Carroll, H. Scherthan, K. Mechtler, S. Sauer, C. Schofer, K. Weipoltshammer, M. Pagani, M. Lachner, A. Kohlmaier, S. Opravil, M. Doyle, M. Sibilia and T. Jenuwein (2001): Loss of the Suv39h histone methyltransferases impairs mammalian heterochromatin and genome stability. Cell 107(3), 323-37.
- Phair, R. D. and T. Misteli (2000): High mobility of proteins in the mammalian cell nucleus. Nature 404(6778), 604-9.
- Pham, A. D. and F. Sauer (2000): Ubiquitin-activating/conjugating activity of TAFII250, a mediator of activation of gene expression in Drosophila. Science 289(5488), 2357-60.
- Pirrotta, V., S. Poux, R. Melfi and M. Pilyugin (2003): Assembly of Polycomb complexes and silencing mechanisms. Genetica 117(2-3), 191-7.
- Plath, K., J. Fang, S. K. Mlynarczyk-Evans, R. Cao, K. A. Worringer, H. Wang, C. C. de la Cruz, A. P. Otte, B. Panning and Y. Zhang (2003): Role of histone H3 lysine 27 methylation in X inactivation. Science 300(5616), 131-5.
- Polioudaki, H., N. Kourmouli, V. Drosou, A. Bakou, P. A. Theodoropoulos, P. B. Singh, T. Giannakouros and S. D. Georgatos (2001): Histones H3/H4 form a tight complex with the inner nuclear membrane protein LBR and heterochromatin protein 1. EMBO Rep 2(10), 920-5.
- Prelle, K., I. M. Vassiliev, S. G. Vassilieva, E. Wolf and A. M. Wobus (1999): Establishment of pluripotent cell lines from vertebrate species--present status and future prospects. Cells Tissues Organs 165(3-4), 220-36.
- Prokhortchouk, A., B. Hendrich, H. Jorgensen, A. Ruzov, M. Wilm, G. Georgiev, A. Bird and E. Prokhortchouk (2001): The p120 catenin partner Kaiso is a DNA methylation-dependent transcriptional repressor. Genes Dev 15(13), 1613-8.
- Rabbitts, P., H. Impey, A. Heppell-Parton, C. Langford, C. Tease, N. Lowe, D. Bailey, M. Ferguson-Smith and N. Carter (1995): Chromosome specific paints from a high resolution flow karyotype of the mouse. Nat Genet 9(4), 369-75.
- Rabl, C. (1885). Über Zelltheilung. Morphologisches Jahrbuch. C. Gegenbaur. 10: 214-330.
- Rangasamy, D., L. Berven, P. Ridgway and D. J. Tremethick (2003): Pericentric heterochromatin becomes enriched with H2A.Z during early mammalian development. EMBO J. 22(7), 1599-1607.
- Redon, C., D. Pilch, E. Rogakou, O. Sedelnikova, K. Newrock and W. Bonner (2002): Histone H2A variants H2AX and H2AZ. Curr Opin Genet Dev 12(2), 162-9.
- Reik, W., W. Dean and J. Walter (2001): Epigenetic reprogramming in mammalian development. Science 293(5532), 1089-93.
- Rens, W., P. C. O'Brien, J. A. Graves and M. A. Ferguson-Smith (2003): Localization of chromosome regions in potoroo nuclei (Potorous tridactylus Marsupialia: Potoroinae). Chromosoma 112(2), 66-76.
- Rice, J. C., S. D. Briggs, B. Ueberheide, C. M. Barber, J. Shabanowitz, D. F. Hunt, Y. Shinkai and C. D. Allis (2003): Histone methyltransferases direct different degrees of methylation to define distinct chromatin domains. Mol Cell 12(6), 1591-8.
- Richmond, T. J. and C. A. Davey (2003): The structure of DNA in the nucleosome core. Nature 423(6936), 145-50.
- Riesselmann, L. and T. Haaf (1999): Preferential S-phase pairing of the imprinted region on distal mouse chromosome 7. Cytogenet Cell Genet 86(1), 39-42.
- Riggs, A. D. (2002): X chromosome inactivation, differentiation, and DNA methylation revisited, with a tribute to Susumu Ohno. Cytogenet Genome Res 99(1-4), 17-24.
- Robertson, K. D. (2002): DNA methylation and chromatin - unraveling the tangled web. Oncogene 21(35), 5361-79.
- Roix, J. J., P. G. McQueen, P. J. Munson, L. A. Parada and T. Misteli (2003): Spatial proximity of translocation-prone gene loci in human lymphomas. Nat Genet 34(3), 287-91.

- Rosania, G. R., Y. T. Chang, O. Perez, D. Sutherlin, H. Dong, D. J. Lockhart and P. G. Schultz (2000): Myo-severin, a microtubule-binding molecule with novel cellular effects. Nat Biotechnol 18(3), 304-8.
- Rouleau, M., R. A. Aubin and G. G. Poirier (2004): Poly(ADP-ribosyl)ated chromatin domains: access granted. J Cell Sci 117(Pt 6), 815-25.
- Rudert, F., S. Bronner, J. M. Garnier and P. Dolle (1995): Transcripts from opposite strands of gamma satellite DNA are differentially expressed during mouse development. Mamm Genome 6(2), 76-83.
- Sabourin, L. A. and M. A. Rudnicki (2000): The molecular regulation of myogenesis. Clin Genet 57(1), 16-25.
- Saccone, S., S. Caccio, P. Perani, L. Andreozzi, A. Rapisarda, S. Motta and G. Bernardi (1997): Compositional mapping of mouse chromosomes and identification of the gene-rich regions. Chromosome Res 5(5), 293-300.
- Sachs, L. (2002). Angewandte Statistik. Berlin, Heidelberg, NewYork, Springer Verlag.
- Sadoni, N., S. Langer, C. Fauth, G. Bernardi, T. Cremer, B. M. Turner and D. Zink (1999): Nuclear organization of mammalian genomes. Polar chromosome territories build up functionally distinct higher order compartments. J. Cell Biol. 146(6), 1211-26.
- Sambrook, J. and D. W. Russel, Eds. (2001). Molecular Cloning, A Laboratory Manual, Cold Spring Harbor Laboratory Press.
- Santos-Rosa, H., R. Schneider, A. J. Bannister, J. Sherriff, B. E. Bernstein, N. C. Emre, S. L. Schreiber, J. Mellor and T. Kouzarides (2002): Active genes are tri-methylated at K4 of histone H3. Nature 419(6905), 407-11.
- Schardin, M., T. Cremer, H. D. Hager and M. Lang (1985): Specific staining of human chromosomes in Chinese Hamster x man hybrid cell lines demonstrates interphase chromosome territories. Human Genetics 71, 281-287.
- Schermelleh, L. (2003). Dynamic organization of chromosomes in the mammalian cell nucleus. Department Biologie II. München, LMU.
- Schermelleh, L., I. Solovei, D. Zink and T. Cremer (2001): Two-color fluorescence labeling of early and mid-to-late replicating chromatin in living cells. Chromosome Res. 9, 77-80.
- Scherthan, H., S. Weich, H. Schwegler, C. Heyting, M. Harle and T. Cremer (1996): Centromere and telomere movements during early meiotic prophase of mouse and man are associated with the onset of chromosome pairing. J Cell Biol 134(5), 1109-25.
- Schlichting, C. D. (2003): Origins of differentiation via phenotypic plasticity. Evol Dev 5(1), 98-105.
- Schotta, G., A. Ebert, R. Dorn and G. Reuter (2003): Position-effect variegation and the genetic dissection of chromatin regulation in Drosophila. Semin Cell Dev Biol 14(1), 67-75.
- Schotta, G., M. Lachner, K. Sarma, A. Ebert, R. Sengupta, G. Reuter, D. Reinberg and T. Jenuwein (2004): A silencing pathway to induce H3-K9 and H4-K20 trimethylation at constitutive heterochromatin. Genes Dev.
- Schroeder, T., S. T. Fraser, M. Ogawa, S. Nishikawa, C. Oka, G. W. Bornkamm, T. Honjo and U. Just (2003): Recombination signal sequence-binding protein Jkappa alters mesodermal cell fate decisions by suppressing cardiomyogenesis. Proc Natl Acad Sci U S A 100(7), 4018-23.
- Shahbazian, M., J. Young, L. Yuva-Paylor, C. Spencer, B. Antalffy, J. Noebels, D. Armstrong, R. Paylor and H. Zoghbi (2002): Mice with truncated MeCP2 recapitulate many Rett syndrome features and display hyperacetylation of histone H3. Neuron 35(2), 243-54.
- Shahbazian, M. D., B. Antalffy, D. L. Armstrong and H. Y. Zoghbi (2002): Insight into Rett syndrome: MeCP2 levels display tissue- and cell-specific differences and correlate with neuronal maturation. Hum Mol Genet 11(2), 115-24.
- Shahbazian, M. D. and H. Y. Zoghbi (2002): Rett syndrome and MeCP2: linking epigenetics and neuronal function. Am J Hum Genet 71(6), 1259-72.
- Shelby, R. D., K. M. Hahn and K. F. Sullivan (1996): Dynamic elastic behavior of alpha-satellite DNA domains visualized in situ in living human cells. J. Cell Biol. 135(3), 545-57.
- Sheldon, C. C., E. J. Finnegan, D. T. Rouse, M. Tadege, D. J. Bagnall, C. A. Helliwell, W. J. Peacock and E. S. Dennis (2000): The control of flowering by vernalization. Curr Opin Plant Biol 3(5), 418-22.
- Shi, S. R., R. J. Cote and C. R. Taylor (2001): Antigen retrieval techniques: current perspectives. J Histochem Cytochem 49(8), 931-7.
- Shi, W., V. Zakhartchenko and E. Wolf (2003): Epigenetic reprogramming in mammalian nuclear transfer. Differentiation 71(2), 91-113.

- Shiio, Y. and R. N. Eisenman (2003): Histone sumoylation is associated with transcriptional repression. Proc Natl Acad Sci U S A.
- Shopland, L. S., C. V. Johnson, M. Byron, J. McNeil and J. B. Lawrence (2003): Clustering of multiple specific genes and gene-rich R-bands around SC-35 domains: evidence for local euchromatic neighborhoods. J Cell Biol 162(6), 981-90.
- Shultz, L. D., B. L. Lyons, L. M. Burzenski, B. Gott, R. Samuels, P. A. Schweitzer, C. Dreger, H. Herrmann, V. Kalscheuer, A. L. Olins, D. E. Olins, K. Sperling and K. Hoffmann (2003): Mutations at the mouse ichthyosis locus are within the lamin B receptor gene: a single gene model for human Pelger-Huet anomaly. Hum Mol Genet 12(1), 61-9.
- Sims, R. J., K. Nishioka and D. Reinberg (2003): Histone lysine methylation: a signature for chromatin function. Trends Genet 19(11), 629-39.
- Singh, P. B. and S. D. Georgatos (2003): HP1: facts, open questions, and speculation. J Struct Biol 140(1-3), 10-6.
- Skok, J. A., K. E. Brown, V. Azuara, M. L. Caparros, J. Baxter, K. Takacs, N. Dillon, D. Gray, R. P. Perry, M. Merkenschlager and A. G. Fisher (2001): Nonequivalent nuclear location of immunoglobulin alleles in B lymphocytes. Nat Immunol 2(9), 848-54.
- Slack, J. (2001). Essential Developmental Biology. Malden, Blackwell Science, Inc.
- Solovei, I., A. Cavallo, L. Schermelleh, F. Jaunin, C. Scasselati, D. Cmarko, C. Cremer, S. Fakan and T. Cremer (2002): Spatial Preservation of Nuclear Chromatin Architecture during Three- Dimensional Fluorescence in Situ Hybridization (3D-FISH). Exp Cell Res 276(1), 10-23.
- Solovei, I., N. Grandi, R. Knoth, B. Volk and T. Cremer (2004): Positional changes of pericentromeric heterochromatin and nucleoli in postmitotic purkinje cells during murine cerebellum development. Cytogenetics and Genome Research in press.
- Solovei, I., J. Walter, M. Cremer, F. Habermann, L. Schermelleh and T. Cremer (2001). FISH on three-dimensionally preserved nuclei. FISH: a practical approach. J. Squire, B. Beatty and S. Mai. Oxford, Oxford University Press.
- Sparvoli, E., M. Levi and E. Rossi (1994): Replicon clusters may form structurally stable complexes of chromatin and chromosomes. J Cell Sci 107(Pt 11), 3097-103.
- Spector, D. L. (1993): Macromolecular domains within the cell nucleus. Annu Rev Cell Biol 9, 265-315.
- Spector, D. L. (2003): The dynamics of chromosome organization and gene regulation. Annu Rev Biochem 72, 573-608.
- Spector, D. L., R. D. Goldmann and L. A. Leinwand, Eds. (1998). Cells A Laboratory Manual. Cold Spring Harbor, Cold Spring Harbor Laboratory Press.
- Speicher, M. R., S. G. Ballard and D. C. Ward (1996): Karyotyping human chromosomes by combinatorial multi-fluor FISH. Nature Genetics 4, 368-375.
- Srinivasan, P. R. and E. Borek (1964): Enzymatic Alteration of Nucleic Acid Structure. Science 145, 548-53.
- Stallcup, M. R. (2001): Role of protein methylation in chromatin remodeling and transcriptional regulation. Oncogene 20(24), 3014-20.
- Stancheva, I., A. L. Collins, I. B. Van den Veyver, H. Zoghbi and R. R. Meehan (2003): A mutant form of MeCP2 protein associated with human Rett syndrome cannot be displaced from methylated DNA by notch in *Xenopus* embryos. Mol Cell 12(2), 425-35.
- Strahl, B. D. and C. D. Allis (2000): The language of covalent histone modifications. Nature 403(6765), 41-5.
- Su, R. C., K. E. Brown, S. Saaber, A. G. Fisher, M. Merkenschlager and S. T. Smale (2004): Dynamic assembly of silent chromatin during thymocyte maturation. Nat Genet 36(5), 502-6.
- Sun, H. B., J. Shen and H. Yokota (2000): Size-dependent positioning of human chromosomes in interphase nuclei. Biophys. J. 79(1), 184-90.
- Suter, C. M., D. I. Martin and R. L. Ward (2004): Hypomethylation of L1 retrotransposons in colorectal cancer and adjacent normal tissue. Int J Colorectal Dis 19(2), 95-101.
- Szilvassy, S. J. (2003): The biology of hematopoietic stem cells. Arch Med Res 34(6), 446-60.
- Taddei, A., C. Maison, D. Roche and G. Almouzni (2001): Reversible disruption of pericentric heterochromatin and centromere function by inhibiting deacetylases. Nat Cell Biol 3(2), 114-20.

- Taddei, A., D. Roche, J. B. Sibarita, B. M. Turner and G. Almouzni (1999): Duplication and maintenance of heterochromatin domains. J Cell Biol 147(6), 1153-66.
- Tamaru, H. and E. U. Selker (2001): A histone H3 methyltransferase controls DNA methylation in *Neurospora crassa*. Nature 414(6861), 277-83.
- Tanabe, H., F. A. Habermann, I. Solovei, M. Cremer and T. Cremer (2002): Non-random radial arrangements of interphase chromosome territories: evolutionary considerations and functional implications. Mutat Res 504(1-2), 37-45.
- Tanabe, H., S. Muller, M. Neusser, J. von Hase, E. Calcagno, M. Cremer, I. Solovei, C. Cremer and T. Cremer (2002): Evolutionary conservation of chromosome territory arrangements in cell nuclei from higher primates. Proc Natl Acad Sci U S A 99(7), 4424-9.
- Tate, P., W. Skarnes and A. Bird (1996): The methyl-CpG binding protein MeCP2 is essential for embryonic development in the mouse. Nat Genet 12(2), 205-8.
- Telenius, H., N. P. Carter, C. E. Bebb, M. Nordenskjold, P. A. I. Ponder and A. Tunnacliffe (1992): Degenerate oligonucleotide PCR: general amplification of target DNA by a single degenerate primer. Genomics 13, 718-725.
- Telenius, H., A. H. Pelmear, A. Tunnacliffe, N. P. Carter, A. Behmel, M. A. Ferguson-Smith, M. Nordenskjold, R. Pfragner and B. A. Ponder (1992): Cytogenetic analysis by chromosome painting using DOP-PCR amplified flow-sorted chromosomes. Genes Chromosomes Cancer 4(3), 257-63.
- Teller, K. (2003). Untersuchungen zur topologischen Assoziation der paternalen und maternalen PWS/AS-Regionen auf Chromosom 15q11-13 während des Zellzyklus. Institut für Humangenetik, Department II. München, LMU.
- Thiagalingam, S., K. H. Cheng, H. J. Lee, N. Mineva, A. Thiagalingam and J. F. Ponte (2003): Histone deacetylases: unique players in shaping the epigenetic histone code. Ann N Y Acad Sci 983, 84-100.
- Tudor, M., S. Akbarian, R. Z. Chen and R. Jaenisch (2002): Transcriptional profiling of a mouse model for Rett syndrome reveals subtle transcriptional changes in the brain. Proc Natl Acad Sci U S A 99(24), 15536-41.
- Tweedie, S., J. Charlton, V. Clark and A. Bird (1997): Methylation of genomes and genes at the invertebrate-vertebrate boundary. Mol Cell Biol 17(3), 1469-75.
- Vairapandi, M. (2004): Characterization of DNA demethylation in normal and cancerous cell lines and the regulatory role of cell cycle proteins in human DNA demethylase activity. J Cell Biochem 91(3), 572-83.
- van Driel, R., P. F. Fransz and P. J. Verschure (2003): The eukaryotic genome: a system regulated at different hierarchical levels. J Cell Sci 116(Pt 20), 4067-75.
- van Holde, K., J. Zlatanova, G. Arents and E. Moudrianakis (1995). Elements of chromatin structure: histones, nucleosomes, and fibres. Chromatin Structure and Gene Expression. S. C. R. Elgin. Oxford, Oxford University Press.
- Volpi, E. V., E. Chevret, T. Jones, R. Vatcheva, J. Williamson, S. Beck, R. D. Campbell, M. Goldsworthy, S. H. Powis, J. Ragoussis, J. Trowsdale and D. Sheer (2000): Large-scale chromatin organization of the major histocompatibility complex and other regions of human chromosome 6 and its response to interferon in interphase nuclei. J Cell Sci 113(Pt 9), 1565-76.
- von Hase, J.-P. (2002). Digitale Bildanalyse der radialen Verteilung von spezifischen Subregionen im Zellkern. Naturwissenschaftlich-Mathematische Gesamtfakultät Ruprecht-Karls-Universität. Heidelberg, Ruprecht-Karls-Universität.
- von Kries, J. P., H. Buhrmester and W. H. Stratling (1991): A matrix/scaffold attachment region binding protein: identification, purification, and mode of binding. Cell 64(1), 123-35.
- Vourc'h, C., D. Taruscio, A. L. Boyle and D. C. Ward (1993): Cell cycle-dependent distribution of telomeres, centromeres, and chromosome-specific subsatellite domains in the interphase nucleus of mouse lymphocytes. Exp Cell Res 205(1), 142-51.
- Wachtler, F., A. H. Hopman, J. Wiegant and H. G. Schwarzacher (1986): On the position of nucleolus organizer regions (NORs) in interphase nuclei. Studies with a new, non-autoradiographic in situ hybridization method. Exp Cell Res 167(1), 227-40.
- Wade, P. A. (2001): Methyl CpG binding proteins: coupling chromatin architecture to gene regulation. Oncogene 20(24), 3166-73.
- Walbot, V. and N. Holder (1987). Developmental Biology. New York, Random House.

- Walter, J., L. Schermelleh, M. Cremer, S. Tashiro and T. Cremer (2003): Chromosome order in HeLa cells changes during mitosis and early G1, but is stably maintained during subsequent interphase stages. J Cell Biol 160(5), 685-97.
- Weiler, K. S. and B. T. Wakimoto (1995): Heterochromatin and gene expression in Drosophila. Annu Rev Genet 29, 577-605.
- Weimer, R., T. Haaf, J. Kruger, M. Poot and M. Schmid (1992): Characterization of centromere arrangements and test for random distribution in G0, G1, S, G2, G1, and early S' phase in human lymphocytes. Hum Genet 88(6), 673-82.
- Weitzel, J. M., H. Buhrmester and W. H. Stratling (1997): Chicken MAR-binding protein ARBP is homologous to rat methyl-CpG-binding protein MeCP2. Mol Cell Biol 17(9), 5656-66.
- West, M. H. and W. M. Bonner (1980): Histone 2A, a heteromorphous family of eight protein species. Biochemistry 19(14), 3238-45.
- White, M. J. D. (1961). The chromosomes. London, Methuen & CO LTD.
- Williams, B. J., E. Jones and A. R. Brothman (1995): Homologous centromere association of chromosomes 9 and 17 in prostate cancer. Cancer Genet Cytogenet 85(2), 143-51.
- Williams, R. R., S. Broad, D. Sheer and J. Ragoussis (2002): Subchromosomal positioning of the epidermal differentiation complex (EDC) in keratinocyte and lymphoblast interphase nuclei. Exp Cell Res 272(2), 163-75.
- Wilmut, I., K. H. Campbell and C. Tudge (2000). Dolly. München, Wien, Carl Hanser Verlag.
- Wilmut, I., A. E. Schnieke, J. McWhir, A. J. Kind and K. H. S. Campbell (1997): Viable offspring derived from fetal and adult mammalian cells. Nature 385, 810-813.
- Winking, H., K. Nielsen and A. Gropp (1980): Variable positions of NORs in Mus musculus. Cytogenet Cell Genet 26(2-4), 158-64.
- Wollenberg, C., M. P. Kiefaber and K. D. Zang (1982): Quantitative studies on the arrangement of human metaphase chromosomes. IX. Arrangement of chromosomes with and without spindle apparatus. Hum. Genet. 62(4), 310-5.
- Wollenberg, C., M. P. Kiefaber and K. D. Zang (1982): Quantitative studies on the arrangement of human metaphase chromosomes. VIII. Localization of homologous chromosomes. Hum. Genet. 60(3), 239-48.
- Wolpert, L., R. Beddington, J. Brockes, T. Jessell, P. Lawrence and Meyerowitz (1999). Entwicklungsbiologie. Heidelberg, Berlin, Spektrum Akademischer Verlag.
- Yang, A. S., M. R. H. Estecio, G. Garcia-Manero, H. M. Kantarjian and J.-P. J. Issa (2003): Comment on "Chromosomal Instability and Tumors Promoted by DNA Hypomethylation" and "Induction of Tumors in Mice by Genomic Hypomethylation". Science 302(5648), 1153b-.
- Zorn, C., C. Cremer, T. Cremer and J. Zimmer (1979): Unscheduled DNA synthesis after partial UV irradiation of the cell nucleus. Distribution in interphase and metaphase. Exp. Cell Res. 124(1), 111-9.

7 Publications

Alberio, R., A. Brero, J. Motlik, T. Cremer, E. Wolf and V. Zakhartchenko (2001): Remodeling of donor nuclei, DNA-synthesis, and ploidy of bovine cumulus cell nuclear transfer embryos: effect of activation protocol. Mol Reprod Dev **59**(4), 371-9.

Brero, A. (1999). Grössenabhängige Verteilung von Chromosomenterritorien in menschlichen Fibroblasten. Department II, Institut für Humangenetik. München, Ludwig Maximilians Universität.

Brero, A., H. P. Easwaran, D. Nowak, I. Grunewald, T. Cremer, H. Leonhardt and M. C. Cardoso (in prep): MeCP2 induces large-scale chromatin reorganization during terminal differentiation.

Cremer, M., J. von Hase, T. Volm, A. Brero, G. Kreth, J. Walter, C. Fischer, I. Solovei, C. Cremer and T. Cremer (2001): Non-random radial higher-order chromatin arrangements in nuclei of diploid human cells. Chromosome Res **9**(7), 541-67.

Netzer, C., L. Rieger, A. Brero, C. D. Zhang, M. Hinzke, J. Kohlhase and S. K. Bohlander (2001): SALL1, the gene mutated in Townes-Brocks syndrome, encodes a transcriptional repressor which interacts with TRF1/PIN2 and localizes to pericentromeric heterochromatin. Hum Mol Genet **10**(26), 3017-24.

Weierich, C., A. Brero, S. Stein, J. von Hase, C. Cremer, T. Cremer and I. Solovei (2003): Three-dimensional arrangements of centromeres and telomeres in nuclei of human and murine lymphocytes. Chromosome Res **11**(5), 485-502.

8 Curriculum vitae

Name: Alessandro Felice Francesco Brero

Geburtsdatum: 05.11.1972

Geburtsort: Turin (Italien)

Schulbildung: 1978-1983: Grundschule an der Forellenstrasse in München
1983-1992: Michaeli-Gymnasium in München

Studium: WS1992-SS1993: Studium der Musikwissenschaft an der
Ludwig-Maximilians-Universität in München
(abgebrochen)

WS1993-SS1999: Studium der Biologie an der
Ludwig-Maximilians-Universität in München
(Abschluss: Dipl. Biol.)

Seit 01-2000: Promotion am Department Biologie II der LMU
München